Removal of Inorganic and Trace Organic Contaminants by Electrodialysis

Laura Joan Banasiak

A thesis submitted for the degree of Doctor of Philosophy

The University of Edinburgh

School of Engineering

August 2009

For my dad.

Declaration

I declare that the thesis has been composed by myself and the work contained in it is my own, except where stated otherwise. Further, this work has not been submitted for any other degree or professional qualification except as specified.

Laura Joan Banasiak
September 2009

Thesis supervisor

Prof Andrea Schäfer, University of Edinburgh, School of Engineering, Edinburgh, United Kingdom

Thesis examiners

Prof Heiner Strathmann, Stuttgart University, Institute for Chemical Technology, Stuttgart, Germany

Dr Guillermo Rein, University of Edinburgh, School of Engineering, Edinburgh, United Kingdom

Abstract

With the continual concern over the presence of naturally occurring and anthropogenic *inorganic* and trace *organic* contaminants in the aquatic environment there is a growing need for the implementation of innovative treatment processes for the elimination of these contaminants from natural waters and wastewater effluents. While conventional treatment methods are ineffective in the removal of emerging contaminants such as steroidal hormones and pesticides, membrane technology, including electrodialysis (ED), has been highlighted as a potential treatment option. However, the clear lack of fundamental understanding of the behaviour of contaminants in ED is a current limitation for its extensive utilisation and is a critical issue that needs to be addressed. ED processing potentialities have not been fully exploited and more research is needed to account for all the key parameters such as contaminant physicochemical properties, solution chemistry and the presence of organic matter. The purpose of this study was to elucidate the mechanisms of inorganic and trace organic contaminant removal by ED.

The inorganic contaminants fluoride, nitrate and boron were selected due to their ubiquitous nature in the environment and public health concerns resulting from long-term exposure. The hydrated radius and strength of hydration shells played a significant role in ionic transport, whereby nitrate with a smaller hydrated radius was removed more effectively (94.1 %) than fluoride (68.3 %) with a larger hydrated radius. While fluoride and nitrate removal was pH independent, the pH dependent speciation of boron enhanced its removal with increasing pH. Territorial binding and/or complexation of the inorganics with organic matter enhanced removal.

The removal of a range of trace inorganics (e.g. arsenic, calcium, magnesium, uranium) from a brackish groundwater from a remote Australian community was investigated. Undissociated inorganics were not transported through the membranes, whereas dissociated inorganics were due to electrostatic attraction. At acidic-neutral

conditions ionic transport was the dominant removal mechanism. At neutral to alkaline conditions insoluble carbonate species precipitated and deposited as a membrane scaling layer (60 μm). This has serious implications for the long-term practical applicability of ED to treat real waters as scaling increased ED stack resistance (pH 3: 27.5 Ω, pH 11: 50 Ω) and decreased total dissolved solids removal (pH 3: 99 %, pH 11: 89.5 %).

While the treatment of trace organics by other membrane processes has been widely studied, their fate in ED and interaction with ED membranes is relatively unknown. Trace contaminant-membrane interaction studies were undertaken to quantify the partitioning of trace organics; namely steroidal hormones and the pesticide endosulfan, to ED membranes by measuring membrane-water partition coefficients (log K_M). The extremely high sorption capacity of the membranes was attributed to hydrogen bonding between the trace organic and membrane functional groups. Hormone sorption during ED was influenced by solution pH and organic matter. In the case of estrone, membrane sorption decreased at pH 11 (487 μg/cm^3) compared to pH 7 (591 μg/cm^3) due to dissociation and membrane electrostatic repulsion .At pH 11, repulsion between dissociated estrone and HA coupled with membrane electrostatic attraction resulted in increased sorption.

The findings from this study highlight that the transport of trace contaminants will depend largely on the characteristics of the membranes used in the ED process as well as the physicochemical characteristics of the contaminants, their interaction with the ED membranes and the presence of other inorganic and/or organic compounds. The knowledge gained has direct applications to current problems and uncertainties in water and wastewater treatment with regards to the fate and transport of contaminants.

Acknowledgements

Throughout my PhD I've had the opportunity to travel to several different countries and the success of this research can be partly attributed to the assistance of many people. Firstly I would like to thank my supervisors Prof Andrea Schäfer and Dr Don Glass. They have assisted me in acquiring additional skills and knowledge relating to my research and have been a source of information and their expertise has been beneficial to my progress.

Financial support for this research was provided by Australian Research Council (ARC) Linkage Project LP0454254 and Discovery Project DP0559878 in collaboration with Brisbane Water as well as a University of Edinburgh studentship. FIB-SEM/EDX analysis was funded through the Engineering and Physical Sciences Research Council (EPSRC, UK).

I began my PhD journey at the University of Wollongong, Australia. Therefore, I would like to express thanks to technical staff Joanne George, Norm Gal for their help during my time there. Special thanks to Thomas Kruttschnitt for helping with conducting experiments in Chapter 6 and for being a great friend. Also thanks to fellow students at Wollongong: Jawad Al Rifai, Melanie Werner, Marco Ahl, Philipp Sausele, Matthias Hengst, DirkVogel, Marcel Pilz and Kai Ratte. It has been great catching up with you all for our yearly German/Aussie BBQ.

In the second year of my PhD I was fortunate to spend 8 months at Katholieke Universiteit Leuven. Thank you to Prof Bart Van der Bruggen for his guidance, support and hospitality during my time there. Christine Wouters (also K.U.Leuven) is thanked for help with GC-ECD analysis. Thanks to students Kathleen Moons, Adrian Verhoef, Katleen Boussu, Stephani Arickx, Ben Bettens and Geert Cornelis for their hospitality and welcoming me into their research group.

Special thanks to my fellow membrane students at The University of Edinburgh, UK: Andrea Semiao, Peta Neale, Helfrid Rossiter, Annalisa De Munari, Molly Patrick, Ime Akanyeti and Laura Richards who have been an endless supply of support, laughs and have been willing guinea pigs for my baking experimentations. An extra special thanks to my flatmates Andrea Semiao and Colin McGill. I think our nightly de-stressing sessions over dinner have helped me to keep some semblance of sanity.

Numerous people have provided helpful advice during PhD including: Wytze Meindersma (Eindhoven University of Technology, Netherlands), Wouter Pronk and Steffen Zuleeg (Eawag, Switzerland), Ivan Kennedy (The University of Sydney, Australia), Howard Colquhoun (The University of Reading, UK), Johannes Fritsch (University of Applied Sciences, Germany), Ian Metcalf (University of Newcastle, UK), David McMullan (Scottish Water).

Many people have also assisted with sample analysis including: Peter Anderson, Tanya Peshkur, Lorna Eades (The University of Edinburgh), Michael Fay (Nottingham University, UK) for FIB-SEM and EDX analysis and Kingsley Ho (Imperial College London, UK) for zeta potential analysis. Also thanks to Alan Simm (The University of Edinburgh, UK) for lab assistance and technical support and discussions on boron chemistry.

Marian Turek (Silesian University of Technology, Poland) and Menachem Elimelech (Yale University) are thanked for review of parts of this thesis.

Most importantly, I would like to thank my family and friends for their continual support over this long journey. Special thanks to my mum and stepdad, Therese and Tony, for all their encouragement, patience, love and packages of all the food I missed while away. Our Sunday phone calls were always the highlight of my week. I can’t wait to return home to where I belong.

Publications

Accepted

Banasiak, L.J. and Schäfer, A.I. (2009). The removal of inorganic trace contaminants by Electrodialysis in Remote Australian Communities. *Desalination*, **248**(1-3), 48-57.

Banasiak, L.J. and Schäfer, A.I., (2009). Removal of boron, fluoride and nitrate by electrodialysis in the presence of organic matter. *Journal of Membrane Science*, **334**(1-2), 101-109.

Banasiak, L.J., Kruttschnitt, T.W. and Schäfer, A.I., (2007). Desalination using electrodialysis as a function of voltage and salt concentration. *Desalination*, **205**(1-3), 38-46.

Submitted and in preparation

Banasiak, L.J., Van der Bruggen, B. and Schäfer, A.I. Sorption of pesticide Endosulfan by Electrodialysis membranes. *Water Research* (Submitted June 2009).

Banasiak, L.J. and Schäfer, A.I. Sorption of steroidal hormones by Electrodialysis membranes. *Environmental Science and Technology* (Submitted July 2009).

Banasiak, L.J. and Schäfer, A.I. Inorganic Trace Contaminant Removal from a Brackish Groundwater by Electrodialysis. *Separation and Purification Technology* (In preparation June 2009).

Table of Contents

Chapter 1. Introduction

The occurrence and fate of inorganic and trace organic contaminants in the aquatic environment has long been recognised as an important health and environmental issue. A wide range of inorganic contaminants, such as fluoride, nitrate and boron, are globally ubiquitous in ground, surface and brackish water as a result of chemical weathering of rocks and anthropogenic sources such as wastewaters effluents (Einav *et al.*, 2002; Favre-Réguillon *et al.*, 2008). Concerns over inorganics range from their toxicity to their impact on process operation and product quality in industrial processes (WHO, 2006). Recent studies have shown the widespread occurrence of low-level concentrations of organic contaminants in the aquatic environment. Steroid hormones such as estrone, 17β-estradiol (natural hormone) and 17α-ethynylestradiol (the main component of the contraceptive pill), which have endocrine disrupting properties, are commonly found in municipal wastewaters and surface waters (Baronti *et al.*, 2000; Kolpin *et al.*, 2002). Endosulfan (ES), a pesticide currently banned in over 50 countries, has recently been implicated in chronic fish embryonic mutations in a river in Noosa, Australia as a result of agricultural runoff (Burke, 2009). While concern over the extreme toxic proprieties of inorganic and organic compounds has led to international efforts to control their use and disposal and to understand their global distribution and behaviours, the low removal efficiency of conventional wastewater treatment processes has meant that alternative methods of treatment are necessary. Membrane technology has been identified as a potential treatment option.

The utilisation of membrane processes such as reverse osmosis (RO) in water reuse applications is widespread. However, any contaminant that RO is designed to retain occurs in elevated concentrations in the waste stream or concentrate making its discharge to the environment questionable (Einav *et al.*, 2002). These brackish concentrates from water reuse applications contains salt, nutrients and inorganic and organic contaminants such heavy metals, endocrine disruptors (Ternes *et al.*, 1999), pharmaceutically active compounds (Daughton, 2000) and organic matter (OM) (Koprivnjak *et al.*, 2006). Currently there has been little research on the treatment of

these concentrates and what product qualities can be reached, but the treatment of this waste stream will improve the health of receiving waters and reduce the risk of increased build up of contaminants if these wastes are recycled through wastewater treatment plants.

Competing technologies for RO concentrate treatment include: high efficiency reverse osmosis (zero liquid discharge process (ZLD)); polymeric ligand exchange resins and adsorbents; ozonation; and membrane distillation. Analysis of the advantages, disadvantages, cost and energy consumption of these processes are outlined in Figure 1.1. These techniques generate solid salts and/or liquid waste streams that require special handling. In ZLD, further concentration of the concentrate must be undertaken by thermal processes, adding to the overall cost of desalination. Adsorption and ozonation processes, although able to remove trace organics, are unable to desalinate the RO concentrate. Therefore, a potential treatment option is electrodialysis (ED) (Badruzzaman *et al.*, 2009; Zhang *et al.*, 2009). Advantages of ED compared to other membrane processes include: longer membrane operation life due to higher chemical/mechanical stability; less feed water pre-treatment; higher selectivity and the option of ED reversal for membrane fouling control (Strathmann, 2004; Zagorodni, 2006). ED, which involves the preferential transport of ions across ion-exchange membranes under an electrical potential difference, was first commercially introduced in the 1960s and to date has mainly been used for the desalination of brackish and seawater sources to produce concentrated brines or salt depleted waters for industrial or potable water use (Ortiz *et al.*, 2005; Tanaka, 2003). ED has proved its feasibility and high performance in groundwater treatment (Elmidaoui *et al.*, 2002), the deacidification of organic solutions (Hábová *et al.*, 2004) and effluent treatment and recycling of industrial wastewaters (Lambert *et al.*, 2006; Marder *et al.*, 2004).

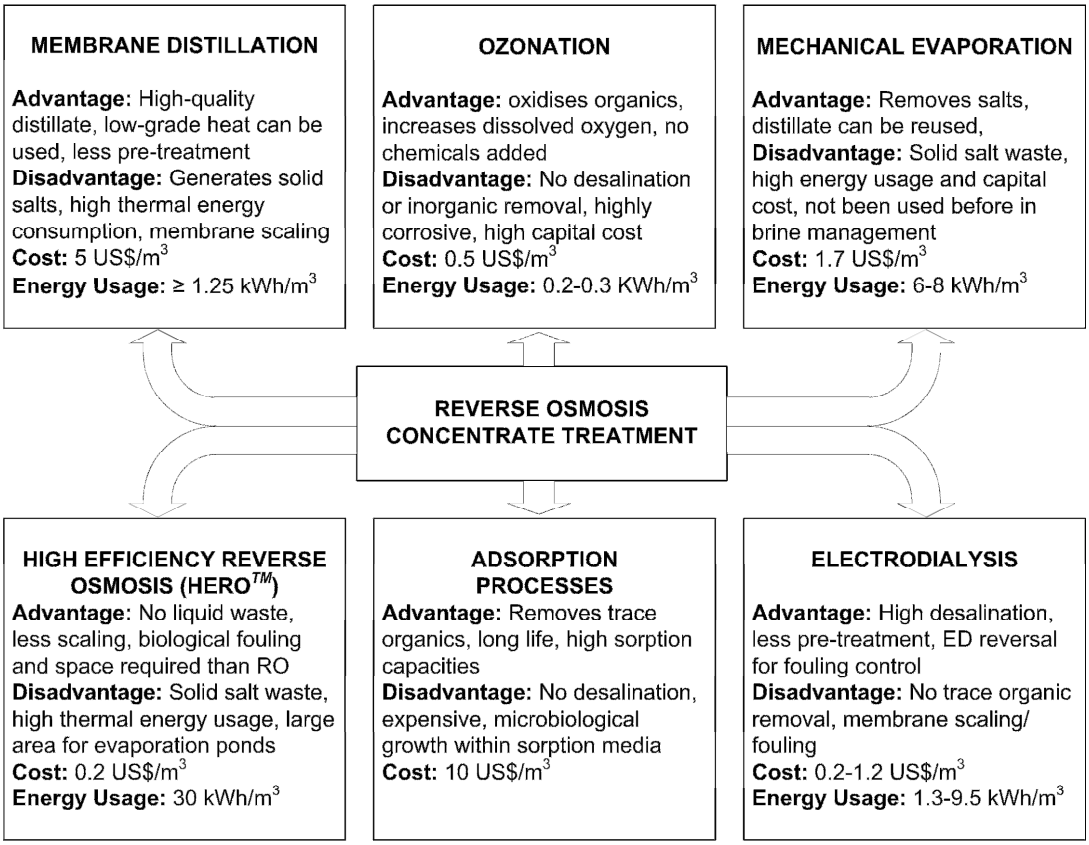

Figure 1.1. Comparison between potential treatment technologies for Reverse Osmosis Concentrate Treatment (Information sourced from Alklaibi (2008); Kumar *et al* (2007); Metcalf and Eddy *et al.* (2003); Nafey *et al.* (2008); Strathmann (2004); Schoeman and Thompson (1996)).

Despite the importance, there is a clear lack of fundamental understanding of inorganic and trace organic contaminant removal mechanisms in ED. The fate and behaviour of inorganic and trace organic contaminants in the environment is influenced by solute-solute interactions with OM (Kinniburgh *et al.*, 1999), which is ubiquitous in ground, surface and wastewater. While there have been studies on the removal of inorganic contaminants from natural and wastewaters at different conditions by ED, solute-solute interactions between inorganic contaminants and OM are not well understood. This negates the need for improved understanding of the implications of these interactions on inorganic removal by ED. While the treatment of trace organic contaminants, such as steroidal hormones and pesticides, by membrane processes such as nanofiltration (NF) and RO has been widely studied, their fate in ED is relatively unknown. ED would not be used to remove these trace organics; however, an understanding of their interaction with ED membranes is

important. Hydrophobic interactions or hydrogen bonding mechanisms between steroidal hormones, pesticides and membranes have been postulated (Kiso *et al.*, 2001; Nghiem *et al.*, 2004a). However, the quantification of such interactions to ED membranes using water-membrane partition coefficients (log K_M, L/cm^3) has not been undertaken. Therefore, the specific objectives of this thesis are to:

1. Elucidate the mechanisms of inorganic contaminant removal from model aqueous solutions and compare these results with those from a real system;
2. Undertake contaminant-membrane interaction studies to quantify the partitioning of trace organic contaminants in ED membranes; and
3. Identify the implications of solution chemistry (pH, presence of OM) and ED operational parameters (applied voltage) on these mechanisms.

This will be achieved by:

1. Determining the influence of solution pH and OM on the removal of the inorganic contaminants (fluoride, nitrate and boron) from model aqueous solutions by ED in Chapter 5;
2. Determining the influence of applied voltage and solution pH on the removal of inorganic contaminants from a brackish groundwater in Chapter 6;
3. Quantifying the interaction between the trace organic contaminants (steroidal hormones and pesticide endosulfan) by determining log K_M values to elucidate the mechanisms of trace organic-membrane interaction in Chapters 7 and 8; and
4. Determining the influence of solution pH and OM on the fate of the steroidal hormones and pesticide in ED in Chapters 7 and 8.

A schematic overview of this thesis is given in Figure 1.2. Chapter 2 describes the presence and fate of inorganic, trace organic contaminants and OM in water, their health and environmental ramifications. A review on the theoretical principles of ED and the removal mechanisms of the selected contaminants in ED is undertaken in Chapter 3 to identify gaps in current knowledge. The materials and methods are outlined in Chapter 4 including descriptions of the ED system, analytical techniques and experimental protocols utilised. Chapter 5 presents results on limiting current density determination, desalination kinetics and the removal of inorganic contaminants from model aqueous solutions. The application of ED for the treatment

of a brackish groundwater is presented in Chapter 6. Chapters 7 and Chapter 8 investigate the fate of steroidal hormones and the pesticide endosulfan, respectively, along with the interaction of these contaminants with the ion-exchange membranes. Chapter 9 provides a summary of the conclusions of this thesis and Chapter 10 outlines opportunities for further research in the light of this study.

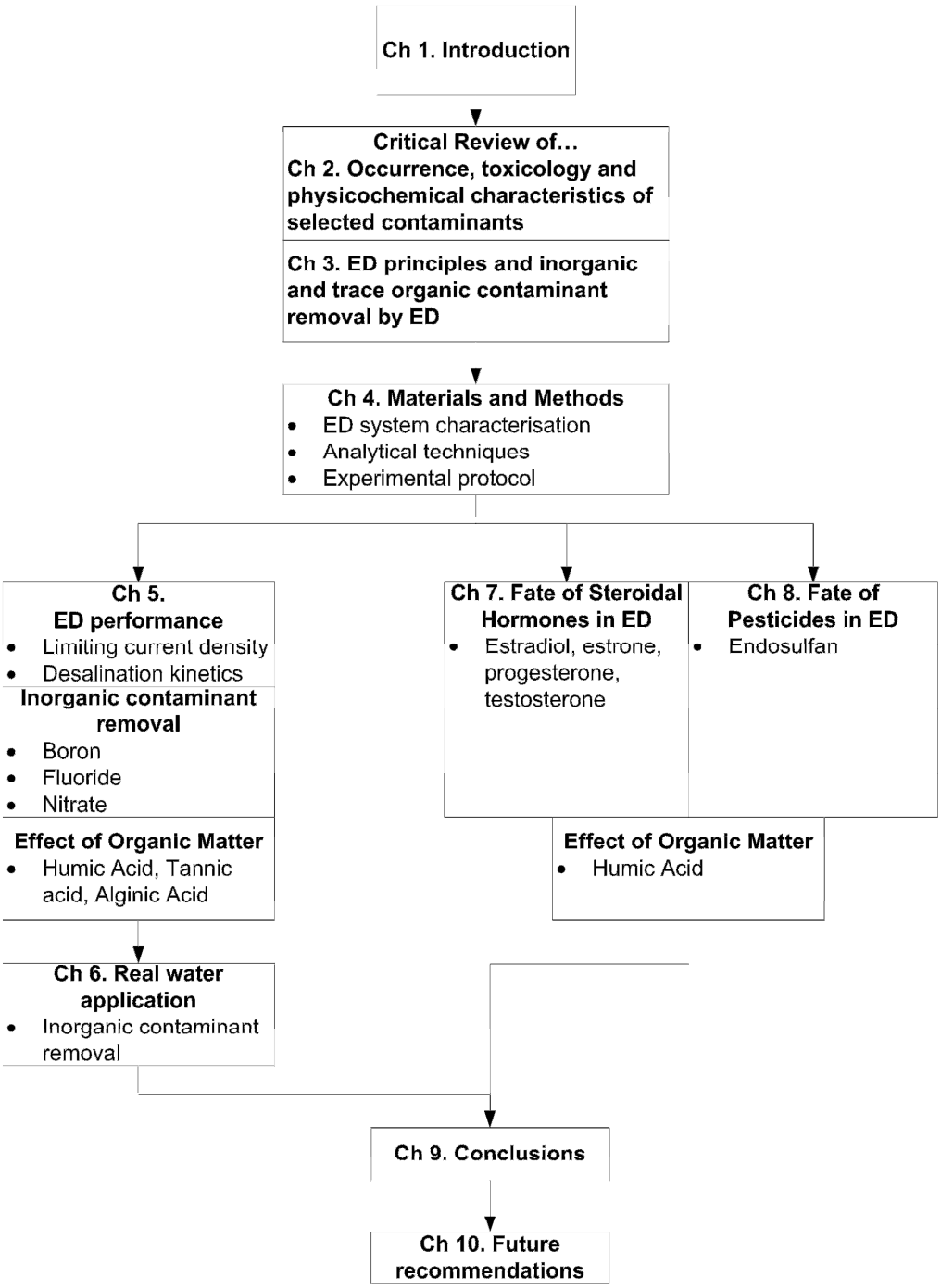

Figure 1.2. Schematic overview of thesis structure.

Chapter 2. Occurrence, Toxicology and Physicochemical Characteristics of Inorganic and Trace Organic Contaminants

Inorganic and trace organic contaminants such as metals, steroidal hormones and pesticides are ubiquitous in the aquatic environment, and are of concern due to their potential environmental and human health related impacts. In this chapter the occurrence of inorganic and organic contaminants in ground, surface, drinking and wastewater will be reviewed. The purpose of this was to identify the contaminants for use in this study. The toxicological implications associated with exposure to these contaminants will be described. Important physicochemical characteristics of the contaminants of interest in this study are summarised.

2.1 Inorganic Contaminants

Inorganic contaminants can be defined as mineral based compounds, such as metals and nutrients that typically do not contain the element carbon and can be found in the environmental either through natural or anthropogenic sources. Inorganic constituents in ground and surface waters are globally ubiquitous; mainly as a result of chemical weathering of rocks and soil ion-exchange reactions and release of (Bassett *et al.*, 1995; Favre-Réguillon *et al.*, 2008). For example, chlorides are naturally present due to leaching of chloride containing rocks and soils in contact with water and from saltwater intrusion in coastal areas. Micro- (nitrate and phosphate) and macro-nutrients (iron, copper, manganese and molybdenum) can be found in the aquatic environment as a result of the degradation of plants and animal tissue (Williamson *et al.*, 2008) and release from vegetation and soil during wildfires (Earl and Blinn, 2003).

Anthropogenic sources, including the combustion of fossil fuels and material processing, can introduce relatively large quantities of inorganic species into the environment (Nriagu and Pacyna, 1988). Other anthropogenic inputs, including the

discharging of various treated and untreated liquid wastes to receiving waters (Turek *et al.*, 2007a), the utilization of artificial fertilizers and agricultural runoff (Ritter *et al.*, 2002), domestic and industrial wastewater effluents including RO concentrates (Einav *et al.*, 2002; Marcussen *et al.*, 2008) or the contamination of the aquatic system through various construction, mining or similar activities (Braungardt *et al.*, 2003), can introduce large quantities of inorganic constituents into natural waters. The occurrence of flame retardants that contain inorganics such as bromine, and are used in conjunction with other materials to prevent fires, in the environment have recently been a serious cause for concern (Law *et al.*, 2006).

Natural background concentrations of inorganics vary according to their regional occurrence (EU, 1998; NHMRC, 2004; WHO, 2006). The majority of inorganics released into the environment are metals; for example fluoride, nitrate and boron. These inorganic contaminants were of interest in this study due to their prevalence in the environment. Table 2.1 summarises concentrations of the selected inorganics in ground, surface, drinking water and concentrates/brines from water treatment plants as well as their reported drinking water guideline values (DWG). The occurrence of contaminants in elevated concentrations in drinking waters supplied from brackish groundwater is a serious issue in developing countries and remote communities as a vast number of lives are lost annually due to lack of access to potable water (Montgomery and Elimelech, 2007; WHO, 2006). It is apparent that water treatment is necessary. While the concentration of inorganic contaminants in concentrates from water treatment plants will vary according to differences in feed concentration, this has implications for water reuse whereby those concentrates that contain contaminants above the DWG can not be used for potable use without further treatment.

Concentrations of fluoride in surface water are relatively low (<0.1–0.5 mg/L) (WHO, 2006), whereas higher concentrations have been found in groundwater's (up to 20 mg/L) (Abu and Alsokhny, 2004). Nitrate concentrations in surface water have increased significantly in almost all areas of the world, as a result of the heavy utilization of artificial fertilizers and the resultant penetration of large quantities of

nitrates into ground and surface waters (Koparal and Ogutveren, 2002). It has been estimated that 70-80 % of the nitrate in UK ground and surface waters is derived from agricultural activities (DEFRA, 2002). The proportion of groundwater bodies with an average nitrate concentration greater than 25 mg/L (DWG, Table 2.1) was reported as being approximately 50 % in the UK, 80 % in Spain, 36 % in Germany and 34 % in France (EEA, 2009). Boron is of interest due to its occurrence in seawater and difficulty of removal in desalination. While natural concentrations in surface and groundwater's are usually low, concentrations up to 100 mg/L have been found as a result of wastewater discharge (Turek *et al.*, 2007a).

Table 2.1. Concentration of selected inorganic contaminants in ground (GW), surface (SW), drinking water (DW) and water treatment plant concentrates (C) and their reported drinking water guideline values (DWG).

Inorganic	Location	Concentration (mg/L)	DWG (mg/L)		Ref.
			WHO [a]	EU [b]	
Boron	Europe	> 100 (GW)	0.5	1	1
	Worldwide	< 1 (SW)			1
	Worldwide	0.1-0.3 (DW)			1
	Australia	0.4 (C)			2
Fluoride	Worldwide	< 50 (GW)	1.5	1.5	3
	Worldwide	< 0.1-0.5 (SW)			1
	Worldwide	< 1 (DW)			4
	Australia	0.8 (C)			2
	USA	> 10 (C)			5
Nitrate	UK	5-50 (GW)	50 (25) [c]	50	6
	UK	6-69.6 (SW)			7
	Worldwide	< 10 (DW)			1
	UK	245-390(C)			8

[a] WHO (2006); [b] EU (1998); [c] Recommended value in parentheses; [d] Aesthetic guideline value; n/a Not regulated. Refs: 1. WHO (2006); 2. Al-Rifai (2008); 3. Fawell *et al*. (2006); 4. (NHMRC, 2004); 5. Malaxos and Morin (1990); 6. EEA (2009) ; 7. Neal *et al*. (2006); 8. Squire (2000).

While some inorganics are nutritionally essential for human health (e.g. copper, selenium and zinc for enzymatic reactions), there are considerable health risks, associated with the consumption of water and/or food products with elevated concentrations of some inorganics. Just as the inorganics present in the environment is highly varied, so are the associated health risks. Fluoride in drinking water can

have both negative and positive effects on health. Low concentrations are known to be negatively correlated with dental caries (tooth decay) (Clarkson and McLoughlin, 2000). The harmful effects of excess concentrations of fluoride on teeth and the skeletal system have been widely studied (Browne *et al.*, 2005; Tamer *et al.*, 2007). Dental and skeletal fluorosis is widespread in populations with drinking water directly supplied from groundwater with fluoride concentrations up to 20 mg/L (Zeni *et al.*, 2005). This concentration is significantly above the drinking water guideline value of 1.5 mg/L (Table 2.1). Deleterious health effects have been attributed to nitrate, including infantile methemoglobinaemia, also known as 'blue-baby' syndrome (Fan and Steinberg, 1996). Long term consumption of elevated levels of nitrate can affect the health of adults and older children causing cancer risks due to nitrosamines or nitrosamides (Elmidaoui *et al.*, 2002). Long-term consumption of water and food products with increased boron content results in malfunctioning of cardiac-vascular, nervous, and alimentary systems of humans (Melnyk *et al.*, 2005).

Inorganics pose a considerable environmental risk. Some animal studies have found alterations in reproductive hormone levels and fertility following exposure to relatively high doses of fluoride (> 150 mg/L) (ATSDR, 2000a). Environmental impacts of nitrate include the overproduction of algae and eutrophication of surface waters that can potentially cause the death of fish (Williamson *et al.*, 2008). Studies have identified the reproductive system of animals as the most sensitive targets of boron toxicity (ATSDR, 2000b). Certain inorganic metals are known to biomagnify (i.e. accumulate in the body tissues of organisms) in the food chain (Ikemoto *et al.*, 2008). Elevated trace metal concentrations in higher trophic groups could, owing to ingestion, pose a threat to humans.

Selected physicochemical characteristics of fluoride, nitrate and boron, are provided in Table 2.2. Their physical and chemical distribution in the environment is governed by their varying physiochemical properties (e.g. solubility, chemical speciation) as well as a number of environmental factors (e.g. pH, temperature, presence of organic matter). In aqueous environments fluoride and nitrate are both present ionic form (F^- and NO_3^-, respectively) or combined with other chemicals in minerals and other

compounds (ATSDR, 2000a; Williamson *et al.*, 2008). In aqueous environments and under acidic and near neutral conditions, boron is mainly present as boric acid ($(B(OH)_3$), a weak Lewis acid, and partially as borate ions according to the dissociation reaction in eqn (2.1) (acid dissociation constant pK_a 9.24 at 25°C; Dean (1999)). The pK_a is the parameter used to quantify the charge of an ion or compound.

$$B(OH)_3 + H_2O \rightleftharpoons B(OH)_4^- + H^+ \quad (2.1)$$

Table 2.2. Physicochemical characteristics of fluoride, nitrate and boron.

Characteristic	Unit	Fluoride	Nitrate	Boron	Ref
Molecular weight, MW	g/mol	18.99	61.97	10.81	-
pK_a		[a]	[a]	9.24	1
Crystal ionic radii, r	nm	0.116 - 0.119 0.133 - 0.135	0.179 - 0.189 0.206	0.244-0.261 [b]	2
Hydrated ionic radii, Δr	nm	0.352	0.340	[c]	3
Number of water molecules in hydration shell, n	-	2.7	2.0	[c]	4
Molar Gibbs energy of hydration, $\Delta_{hyd}G^0$	kJ/mol	-345	-275	[c]	4
Relative number of hydrogen bonds with water in ionic and pure solution, ΔG_{HB}	-	0.08	-0.68	[c]	5
Ion mobility at 25°C, u	$\times 10^{-8}$ m^2/sV	5.70	7.40	[c]	6
Jones-Dole viscosity coefficient at 25°C, B	L/mol	0.107	-0.043	0.091 [d] 0.233 [b]	7
Ion equivalent conductivity, $\lambda°$equiv	cm^2/Ωequiv	55.4	71.5	[a]	8

[a] Non-dissociable; [b] $B(OH)_4^-$ form; [c] Data not available; [d] $B(OH)_3$ form. Refs: 1. Dean (1999); 2. Collins (1995), Corti *et al*. (1980a), Kiriukhin and Collins (2002), Marcus (1991), Pauling (1960), Tansel *et al*. (2006), Volkov *et al*. (1997); 3. Volkov *et al*. (1997); 4. Marcus (1991); 5. Marcus (1994); 6. Atkins (1990); 7. Corti *et al*. (1980b), Jenkins and Marcus (1995); 8. Robinson and Stokes (1970).

2.2 Organic Trace Contaminants

Trace contaminants can be defined as carbon based natural or synthetic compounds found in the environment at low (ng/L) to very low concentrations (pg/L) (Schwarzenbach *et al.*, 2006). Over the last few decades, the detection of trace organics such as low molar mass endocrine disrupting chemicals (EDC's) including

steroidal hormones and pesticides within surface waters has been a concern in regards to the contamination of possible drinking water sources. The toxicity of these organic compounds to both humans and animals alike has added to this concern. The fate and occurrence of steroidal hormones, pesticides and OM as well as their detriment to humans and the environment are outlined.

2.2.1 Steroidal Hormones

The presence of EDC's has become a worldwide concern within the scientific community because of their ability to mimic natural hormones and inhibit the action of hormones in humans and other animals; altering the normal function of the immune, nervous, and endocrine systems (Witorsch, 2002). EDC's have been categorised in relation to their origin (natural and synthetic) and activity (estrogenic and anti-endrogenic) (Hester and Harrison, 1999). One well known example of a drug used to influence the endocrine system is the contraceptives in birth control pills (17α-ethinylestradiol). Exposure to EDC's is not confined to those of man-made origin. The natural hormones 17β-estradiol and estrone are naturally excreted by women (2-12 and 3-20 μg/day, respectively) and female animals, as well as by men (estrone 5 μg/day) (Gower, 1975) and are, therefore, ubiquitous in aquatic environments receiving sewage inputs.

For this study steroidal hormones estradiol, estrone, progesterone and testosterone were selected due to their environment ubiquity and toxicology. While estrogenic compounds excreted from humans, and therefore released into sewers, are in biologically less active conjugated forms (glucuronides and sulphates), studies have shown the widespread occurrence of low-level concentrations (ng/L) of EDC's in the aquatic environment (Belfroid *et al.*, 1999; Boyd *et al.*, 2004; Rodriguez-Mozaz and Barceló, 2004; Ternes *et al.*, 1999b; Urase and Kikuta, 2005) as a result of industrial activities (Cui *et al.*, 2006; Matthiessen *et al.*, 2006) and effluent from sewage treatment plants (STPs) (Baronti *et al.*, 2000; Kolpin *et al.*, 2002; Williams *et al.*, 2003). This indicates the conversion of the conjugated estrogens back into active form (Desbrow *et al.*, 1998; Johnson and Sumpter, 2001; Ternes *et al.*, 1999a). While many factors have been thought to influence the distribution, fate and removal

efficiency of steroidal hormones in wastewater treatment, *Escherichia coli*, which is eliminated in large quantities in faeces has been suggested to be responsible for the above conversion (D'Ascenzo *et al.*, 2003; Dray *et al.*, 1972). Table 2.3 summarises concentrations of the selected steroidal hormones detected in surface, drinking water, STP effluents and concentrates/brines from water treatment plants. While studies on the concentration of steroidal hormones in drinking water are limited (Halling-Sørensen *et al.*, 1998) the concentrations depend on the treatment technologies implemented. Steroidal hormones have been found in RO concentrates (Snyder *et al.*, 2007) and the effluents from water recycling treatment plants (Khan *et al.*, 2004). The concentration of hormones in RO concentrates has serious implications for water reuse; thus further treatment is necessary.

Table 2.3. Concentration of steroidal hormones in surface water (SW), sewage treatment plant effluent (STP) and water treatment plant concentrates (C).

Steroidal hormone	Location	Concentration (ng/L)	Refs.
Estradiol	USA	< 2-9.3 (SW)	1
	Europe	2.7-94 (STP)	2
	Australia	< 4.7 (C) [a]	3
	USA	< 1 (C) [a]	4
Estrone	Europe	< 0.1-4.1 (SW)	5
	UK	1.4-76 (STP)	2
	Australia	< 92 (C) [a]	3
	USA	< 78 (C) [a]	4
Progesterone	USA	0.72-199 (SW)	1
	USA	< 1 (C) [a]	4
Testosterone	USA	214 (SW)	1
	USA	≤ 6.1 (STP)	4
	USA	< 1 (C) [a]	4

[a] RO concentrates. Refs: 1. Kolpin *et al*. (2002); 2. Ying *et al*. (2002); 3. Khan *et al*. (2005); 4. Snyder *et al*. (2007); 5. Belfroid *et al*. (1999), Kuch and Ballschmiter (2001).

A number of steroidal hormones have a considerably high biological potency down to the μg/day doses, therefore it is highly likely that they cause effects at low concentrations in the environment (Ternes, 2001). Possible human health effects include breast, prostrate and testicular cancer (Boulay and Perdiz, 2005; Joffe, 2000), and abnormal sexual development and reduced male fertility (Hess *et al.*, 1997;

Sharpe and Skakkebaek, 1993). Steroidal hormones pose widespread and severe physiological and morphological threats to fish, amphibians, birds, reptiles and mammals (Carey and Bryant, 1995; Ottinger *et al.*, 2002; Thorpe *et al.*, 2003). Most produce effects on non-target animals as a by-product of other functions. Biomagnification within animal body tissues leads to increases in the concentration of these chemicals at higher trophic levels (Clotfelter *et al.*, 2004). The effects of steroidal estrogens, especially to fish, have been widely investigated at the level of individual (Lange *et al.*, 2001; Routledge *et al.*, 1998). Effluents from STPs have been shown to induce the production of plasma vitellogenin (VTG), a female specific egg-yolk protein precursor, in male fish (Jobling *et al.*, 1998; Rodgers-Gray *et al.*, 2001; Thorpe *et al.*, 2001). A study by Purdom *et al*. (1994) investigated the effects of estrogenic STP effluent on the production of rainbow trout and found that the degree of VTG in the exposed fish ranged from 500 to 50,000-fold increase. Exposure to 10 ng/L 17α-ethinylestradiol for a period of 3 weeks resulted in maximal concentrations of VTG. Behavioural measures have been used as bio-indicators of endocrine disruption (Clotfelter *et al.*, 2004). It is, however, unknown whether EDC's have consequences on a population scale (Sumpter, 2005).

Physicochemical characteristics of the selected steroidal hormones are given in Table 2.4. While structurally similar, they vary in terms of functional group content, hydrogen bonding ability, hydrophobicity and solubility. Estradiol and estrone with pK_a values of 10.23 and 10.34, respectively, dissociate at high pH due to the phenolic hydroxyl functional group in the C-3 position. Progesterone and testosterone are both neutrally charged from pH 3 to 12. Hydrophobicity, as indicated by the octanol-water partition coefficient values (log K_{ow}), varies for the studied hormones. Hormones can be either hydrogen-donors (i.e. contain phenolic hydroxyl groups, OH) or hydrogen acceptors (i.e. contain carbonyl groups, C=O). The hydrophobicity and hydrogen bonding of a compound would influence its fate in water treatment processes as well as interactions with other contaminants. This will be discussed further in Chapters 3, 7 and 8.

Table 2.4. Physicochemical characteristics of the steroidal hormones studied.

Characteristic	Estradiol	Estrone	Progesterone	Testosterone	Ref
Molecular formula	$C_{18}H_{24}O_2$	$C_{18}H_{22}O_2$	$C_{21}H_{30}O_2$	$C_{19}H_{28}O_2$	-
Molecular weight, MW (g/mol)	272.4	270.4	314.5	288.4	-
Solubility in water at 25°C (mg/L)	1.51-13	1.3-30	8.81	24-30	1
Log K_{ow} [a]	4.01 (3.94)	3.13 (3.43)	3.87 (3.67)	3.32 (3.27)	2
pK_a	10.23	10.34	n/a	n/a	3
Polarity	Bipolar	Bipolar	Monopolar	Bipolar	-
Dipole moment, μ (debye)	1.409	3.695	3.501	3.530	4
Hydrogen donors	2	1	0	1	-
Hydrogen acceptors	2	2	2	2	-
Structure [b]	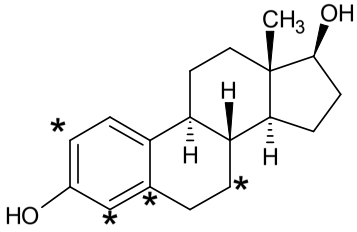	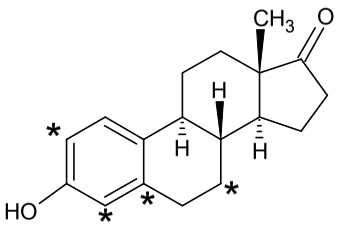	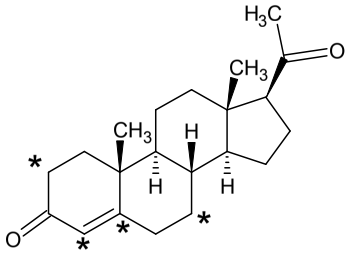	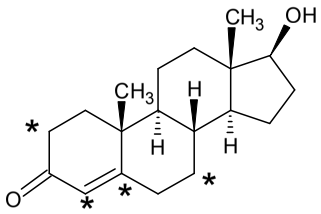	5

[a] Values inside parentheses are estimated using KowWin Log P software (Syracuse Research Corporation, 2009); [b] Asterix on hormones indicate location of radiolabel. Refs: 1. Lai *et al.* (2000), Lide (2008), SIS (2009); 2. Hansch *et al.* (1995); 3. Kwon *et al.* (2006); 4. Nghiem (2005); 5. ACD (2007).

2.2.2 Pesticides

Due to the extensive use of pesticides, herbicides and other agricultural chemicals, large amounts of these compounds have been introduced into the aquatic environment as a result of drift from aerial spraying, discharge from pesticide production plants and surface runoff from agricultural fields into adjacent waterways. Significant concentrations of these compounds and their metabolites have been detected in the environment. Widespread public concerns with pesticides and pollution of the aquatic environment were brought about by the publication of the *Silent Spring* (Carson, 1962). This in effect brought about the ban of the pesticide DDT in 1972 in the USA. The European Union Directive on the Quality of Water Intended for Human Consumption (EEC) sets a maximum admissible concentration (MAC) of 0.1 μg/L per individual pesticide in drinking water and 0.5 μg/L for the sum of all pesticides detected (EU, 1998). The justification for these guidelines is that pesticides should not be present within drinking water. WHO (2006) has derived drinking water guideline values for 31 pesticides. The concentrations of many pesticides in surface and groundwater, however, exceed these guidelines. In 2006 about 6.5 % of surface water samples in the UK contained pesticide concentrations above 0.1ug/L (Environment Agency, 2006).

Endosulfan (ES), a synthesised cyclodiene organochlorine pesticide, was selected for use in this study due to its environmental and health impacts and occurrence on numerous priority lists published to protect the quality of drinking and surface waters (Barceló, 1993). ES has been used extensively in agriculture for the control of insect pests of field crops such as cotton, vegetables, fruit and tobacco (Antonius *et al.*, 1998). The movement of ES via runoff and spray drift can lead to contamination of aquatic environments and ES and its isomers and degradation products have been found in a number of environmental samples. Table 2.5 summarises concentrations of ES detected in ground, surface, and wastewater and STP effluents. Although ES has been found at low concentration in surface and groundwater, little information was found in the available literature regarding current concentrations of ES in domestic and industrial wastewater and STP effluents. Surface water samples in the US generally contain less than 1 μg/L (WHO, 2003). A survey of 80 surface water

sites in the UK revealed only two samples greater than 10 ng/L (German Federal Environment Agency, 2004). However, in areas of application ES has been found in brackish groundwater at 4.2 µg/L (Gonçalves *et al.*, 2007) and up to 1700 µg/L in surface water (Ernst *et al.*, 1991). ES usually occurs at concentrations in drinking water below those at which toxic effects are expected to occur (Fielding *et al.*, 1992). However, drinking water sourced from ES contaminated water poses a considerable health hazard and has implications for water reuse applications.

Table 2.5. Concentration of endosulfan in ground (GW), surface (SW) and wastewater (WW) and sewage treatment plant effluent (STP).

Pesticide	Location	Concentration (µg/L)	Ref.
Endosulfan	Portugal	4.2 (GW)	1
	UK	0.02 (SW)	2
	Australia	< 70 (SW)	3
	Canada	40-1700 (SW)	4
	Canada	0.09 (WW)	5
	Greece	0.003 (STP)	6

[a] DWG in parentheses (WHO, 2006). Refs: 1. Gonçalves *et al*. (2007); 2. Wenzel *et al*. (2000); 3. Edge *et al*. (1999); 4. Ernst *et al*. (1991); 5. Luek Wong *et al*. (1995); 6. Katsoyiannis and Samara (2007).

Pesticides have significant environmental and human and animal health risks. Non-target pesticide poisoning has been identified as a cause of illnesses in humans, either through occupational exposure or from the ingestion of contaminated food (Eddleston *et al.*, 2002). Some pesticides can be categorised as EDCs as they disturb the endocrine processes in humans and invertebrates at concentrations below those which are metabolically toxic. Exposure to pesticides of an endocrine disrupting nature has been linked to cancer (Mathur *et al.*, 2002), reproductive disorders and birth defects (Schreinemachers, 2003). Potential human health impacts of exposure to ES include cardiovascular, endocrine, gastrointestinal, kidney toxicity and respiratory, immunotoxicity, neurotoxicity and skin sensitivity (ATSDR, 2000c). Numerous studies have shown the toxicity of ES to fish and aquatic invertebrates (Hose *et al.*, 2003; Naqvi and Vaishnavi, 1993). A study by Capkin *et al*. (2006) found that concentrations of ES > 1.7 µg/L killed 50 % of rainbow trout within 96 hours.

The threat of pesticides to human and animal health is exacerbated by their long-term environmental persistence long after initial application. Pesticides that have been banned for over 20 years and no longer employed in agriculture, particularly organochlorine pesticides, are still detected in the environment (Verliefde *et al.*, 2007). These pesticides are predominantly associated with soil. Their persistence and mobility is, therefore, dependent on the mechanisms and kinetics of their adsorption and desorption from soil particles (Moorman *et al.*, 2001). Adsorption of pesticides to soil particles are due to a range of interactions including ionic, covalent and hydrogen bonding, hydrophobic interactions and ligand exchange (Gevao *et al.*, 2000). A number of pesticides banned in developed countries are still being widely used in developing countries. For example, ES is widely used in developing countries because of its effectiveness and low application cost (Siang *et al.*, 2007).

Important physicochemical properties of α-ES, β-ES, ES sulfate and ES diol are outlined in Table 2.6. The physical and chemical properties of ES are sufficiently well characterised to enable assessment of the environmental fate of the compound (Budavari, 1996; Coleman and Dolinger, 1982). ES is a mixture of two stereoisomers, α-endosulfan (α-ES) and β-endosulfan (β-ES) in the range of 64-70 % and 29-32 %, respectively (Cerrillo *et al.*, 2005; Rice *et al.*, 1997) and may contain up to 2 % endosulfan diol (ES diol) and 1 % endosulfan ether (ES ether) (ATSDR, 2000c). ES sulfate is more stable in the environment and has similar toxicological properties as ES (Ali *et al.*, 1984; Kullman and Matsumura, 1996). The α-isomer has been shown to be about three times as toxic as the β-isomer. Previous studies have reported that isomerisation can occur between the isomers in aqueous systems, with the reaction favouring α-ES formation (Schmidt *et al.*, 1997; Schmidt *et al.*, 2001). The primary degradation product of environmental concern is endosulfan sulfate (ES sulfate), which is formed in the environment via microbial degradation in soils and organisms as a result of oxidation, biotransformation and photolysis (Coleman and Dolinger, 1982). The cyclic sulfite group of ES can be hydrolysed to form the less toxic endosulfan diol (ES diol) (Goebel *et al.*, 1982).

Table 2.6. Physicochemical characteristics of the endosulfan compounds studied.

Characteristic	α-endosulfan	β-endosulfan	Endosulfan sulfate	Endosulfan diol	Ref
Molecular formula	$C_9H_6Cl_6O_3S$	$C_9H_6Cl_6O_3S$	$C_9H_6Cl_6O_4S$	$C_9H_8Cl_6O_2$	
Molecular weight, MW (g/mol)	406.93	406.93	422.9	360.88	
Solubility in water at 20°C (mg/L)	0.51	0.45	0.48	300	1
pK_a	n/a	n/a	n/a	14.62-15.22	2
Log K_{ow}	3.83 (3.50)	3.83 (3.50)	3.66 (3.64)	(3.68)	3
Polarity	Monopolar	Monopolar	Monopolar	Bipolar	-
Dipole moment, μ (debye)	1.02	3.18	4.10	-	4
Hydrogen acceptors	3	3	4	2	-
Hydrogen donors	0	0	0	2	-
Structure [b]	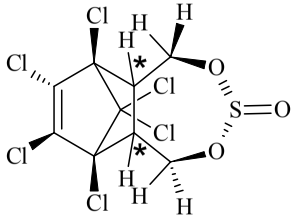	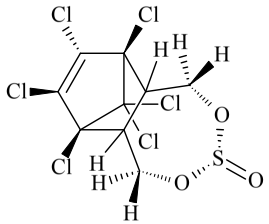	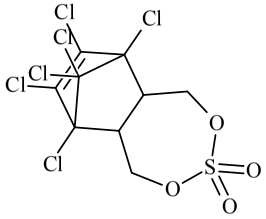	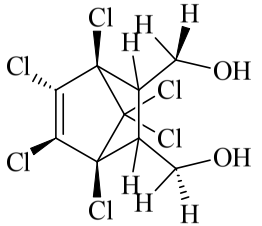	2

[a] Values inside parentheses are estimated using KowWin Log P software (Syracuse Research Corporation, 2009); [b] Asterix on α–ES indicates location of radiolabel within ES structure. Refs: 1. Lide (2008), SIS (2009); 2. ACD (2007), Kwon *et al*. (2006); 3. Hansch *et al*. (1995) ; 4. Forman *et al*. (1965).

2.3 Organic Matter

The presence of OM, categorised as high molar mass particles, is ubiquitous in the aquatic environment and is of prime concern for drinking water production. OM can be found in most natural waters at concentrations of 0.1-100 mgC/L (Frimmel, 1998) and in domestic wastewater above 20 mgC/L (Metcalfe and Eddy *et al.*, 2003) and RO concentrates (Koprivnjak *et al.*, 2006). Humic substances (HS) are the dominant fraction of OM in waters. HS are composed of humin (insoluble), humic acid (HA) (insoluble at pH 1) and fulvic acid (FA) (soluble at any pH). Although OM is not considered harmful to human health, the formation of carcinogenic disinfection-by-products (DBPs) such as trihalomethanes (THMs), chlorophenols and halacetic acids (Chang and Juang, 2004) during pre-oxidation with chlorine in the presence of OM is a serious issue in the treatment of water by conventional treatment processes.

Dissolved OM have the ability to interact with metal ions, oxides hydroxides, minerals and organics including toxic pollutants such as pesticides and hormones, to form water-soluble and water-insoluble complexes of widely differing chemical and biological stabilities (Hayes *et al.*, 1995). These interactions include ion-exchange, chelation, surface adsorption and coagulation (Schulten, 1994) and significantly enhance the solubility and transport of contaminants in the environment. Therefore, these interactions would have implications for inorganic and trace organic contaminant removal during water treatment. This will be discussed further in Chapter 5, 7 and 8.

Three types of OM were selected for use in this study; namely HA, tannic acid (TA) and alginic acid (AA). HA is a degradation product of lignin, carbohydrate and protein (Hanna et al., 1991) with major functional groups of carboxylic, phenolic, alcohol/aldehyde acids, and methoxyl. Carboxylic functional groups account for 60-90 % of all functional groups (Hong and Elimelech, 1997) and they are largely ionized at pH above 6 (Collins *et al.*, 1986), while the phenolic groups dissociate at pH above 8 (Hong and Elimelech, 1997). Therefore, HA acquires a negative charge that increases with increasing pH independently of ionic strength (Avena *et al.*, 1999; Chin *et al.*, 1994). Although HAs are defined as insoluble at pH < 2 (Hayes, 1989)

their solubility decreases at low pH due to the poor dissociation of carboxylic acid groups (Shin *et al.*, 1999). Soil HA behaves like rigid spherocolloids at low pH or high ionic strength (50-100 mM NaCl) and as flexible linear colloids at high pH and low ionic strength (1 mM NaCl) (Ghosh and Schnitzer, 1980). This is believed to be applicable to aqueous HA and Aldrich HA (Avena *et al.*, 1999). Aldrich HA used in this study is peat-derived and is larger than typical aquatic HA (Tang et al., 2007).

As a plant polyphenol, present in surface waters due to leaching from vegetation (Cruz *et al.*, 2000), TA can form inter- and intramolecular hydrogen bonds and often exists in solution as loosely bound complexes of molecules (Shutava and Prouty, 2005). At acidic pH TA is neutrally charged, however as pH increases the charge becomes negative (An and Dultz, 2007).

AA is a naturally occurring hydrophilic colloidal polysaccharide, is obtained from brown seaweed and exhibits negatively charged carboxylate and neutral hydroxyl groups at pH 7 (Coradin and Livage, 2003). AA is composed of mannuronic (~ 60 %) and guluronic (~ 40 %) acids (De Stefano *et al.*, 2006). Below pH 4, the charge density decreases causing increased aggregation, whereas above pH 8 dissociation has been observed and a pK_a of approximately 3.4 has been reported (Avaltroni *et al.*, 2007).

Selected physiochemical characteristics of HA, TA and AA are presented in Table 2.7. Variations in solution chemistry, particularly ionic strength and solution pH, have implications for the charge of OM, as mentioned above. Therefore, the implications of solution chemistry on the interaction of inorganic and trace organics with OM needs consideration.

Table 2.7. Physicochemical characteristics of Aldrich humic acid, tannic acid and alginic acid.

Organic Matter	Category	Origin	Molecular formula	Molecular Weight, MW (g/mol)	Carbon (%)	pK_a	Total acidity (meq/g)	Carboxylic groups (meq/g)	Hydroxyl groups (meq/g)	Ref
Aldrich Humic Acid	OM surrogate	Soil	$C_{342}H_{388}O_{124}N_5$ [a]	60-60000	56	4.3	7.06	4.80	2.26	1
Tannic Acid	Polyphenol	Plants	$C_{76}H_{52}O_{46}$	1701	54	8.5	8.65	7.20	1.63	2
Alginic Acid	Polysaccharide	Brown seaweed and algae	$[C_6H_7NaO_6]_n$	21000	36	3.4	11.4	1.88	9.55	3

[a] Based on model by Schulten (1994). Refs: 1. Davis *et al*. (2003), Kim *et al*. (1990), Shin *et al*. (1999), Simpson (2002); 2. Flores-Céspedes *et al*. (2006), Kraal *et al*. (2006), Shutuva and Prouty (2005), Yamamoto *et al*. (2003); 3.Avaltroni *et al*. (2007), Jeon *et al*. (2002).

2.4 Summary

Inorganic and organic contaminants that are of concern in ground, surface, drinking as well as reclaimed wastewater have been selected carefully to cover a range of ionic and neutral compounds. These contaminants are ubiquitous in ground and surface waters, while the concentration of such contaminants are sometimes present in greater quantities in wastewater and RO concentrates given the origin of the water and the purpose of RO to remove such contaminants. This has serious implications for water reuse applications. The occurrence and fate of both inorganic and organic contaminants in the aquatic environment is, therefore, a significant concern in regards to human and environmental health.

The treatment of water and wastewater containing these contaminants will improve the health of receiving waters and reduce the risk of increased build up of contaminants if the water is recycled through wastewater treatment plants. ED, as a potential treatment option, and the removal mechanisms of contaminants are discussed in Chapter 3. The changes in physicochemical characteristics of the inorganic and organic contaminants in relation to solution chemistry has highlighted the need to considered the implications of solution chemistry on their removal and fate in ED.

Chapter 3. Removal of Inorganic and Trace Organic Contaminants by Electrodialysis

In this chapter, the membrane process Electrodialysis (ED) is reviewed. The theoretical principles of ED including ionic transport in solutions and within ion-exchange membranes and the issue of concentration polarisation and limiting current density are outlined. Membrane obstructions such as fouling, scaling and poisoning has serious implications for the performance of ED and its potential as a water treatment method, thus the physical and chemical factors affecting these obstructions are addressed.

The dominant mechanisms controlling the removal of inorganic and organic trace contaminants during ED are reviewed; namely migration-diffusion, charge interactions, solute-solute interactions and membrane deposition/sorption. The varying compound and membrane specific physiochemical properties influencing the removal mechanism are acknowledged. This review highlights the gaps in knowledge in the current literature and the weaknesses and uncertainties in both conventional water and wastewater treatment processes and more advanced processes such as membrane technology.

3.1 Introduction to Electrodialysis

ED has been used in the desalination of natural occurring surface and groundwater's since the 1950's (Allison, 1995). The desalination of saline solutions either to produce concentrated brines or salt depleted waters for industrial use or potable water mainly from brackish water sources is the largest application of ED (Demircioglu *et al.*, 2003; Lee *et al.*, 2002d; Ortiz *et al.*, 2005; Turek and Dydo, 2008). ED is competitively more economical than RO for the desalination of water with relatively low salt concentrations (< 5 g/L NaCl) and the costs of potable water are in the range of US$0.2-1.2/m^3 (Strathmann, 2004). In brackish water desalination,

more than 2000 plants with a total capacity of greater than 1 million m^3/day product water are installed (Veza, 2001). Due to water shortages, particularly in the arid coastal areas of India and the Middle East, the desalination of seawater by ED has been extensively utilised (Sadrzadeh and Mohammadi, 2008; Tanaka, 2003).

Although ED was the first membrane process to have a large-scale commercial impact, other membrane processes, such as RO, continue to attract more research. According to the International Desalination Association there were 13,869 desalination plants worldwide, producing 62.8 million cubic metres per day (m^3/d) as of June 2008 (International Desalination Association, 2008-2009). Of this total, ED makes up only 4 % compared to RO (59 %). However, ED has been applied to a number of other applications including the treatment of industrial wastewaters for the separation of metal ions, amino acids, proteins and organic acids from fermentation broths, the desalination of process streams in the food, biotechnology and pharmaceutical industry.

3.2 Principles of Electrodialysis

ED involves the separation of charged ionic species across charged anion- and cation-exchange membranes (AEMs and CEMs, respectively). The driving force for the transport of certain components in an ED system from a feed solution to a receiving solution is an electrical potential difference (electrical voltage) across a membrane separating the two solutions. As a result of the driving force of the electric field, anions in a solution permeate the AEMs and cations permeate the CEMs, resulting in concentrated (concentrate) and diluted (diluate) solutions in adjoining compartments, as illustrated in Figure 3.1.

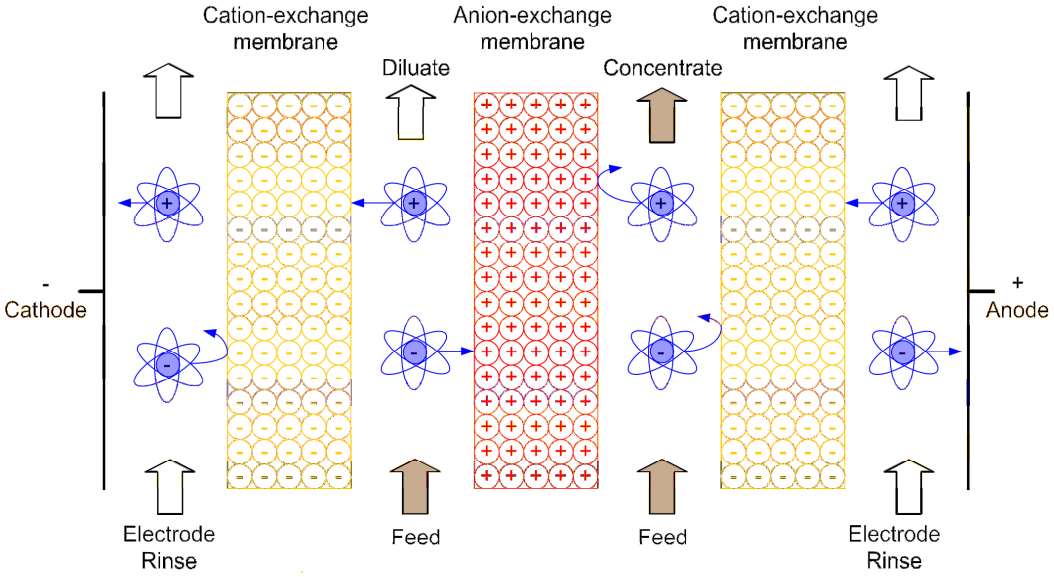

Figure 3.1. Schematic diagram illustrating the principle of electrodialysis and the transport of ionic species across the cation- and anion-exchange membranes.

3.2.1 Mass Transport and Balance in an Electrodialysis System

The mass transport in an ED cell pair composed of two compartments bounded by an AEM and CEM, as shown in Figure 3.2, is determined by a mass balance, which hypothesises that all components removed from the feed will be transferred to the concentrate. A concentration gradient develops in the x-direction while the solution flows through the compartments in the direction of the x-coordinate. The flux in the x-direction is determined by convection due to a hydrostatic pressure gradient. The flux in the z-direction is determined by migration and diffusion due to an electrical potential gradient and concentration differences between the diluate and concentrate. The diluate and concentrate are assumed to have identical geometry and hydrodynamic conditions so as to obtain identical pressure losses and to avoid osmotic pressure differences between the concentrate and diluate (Strathmann, 2004).

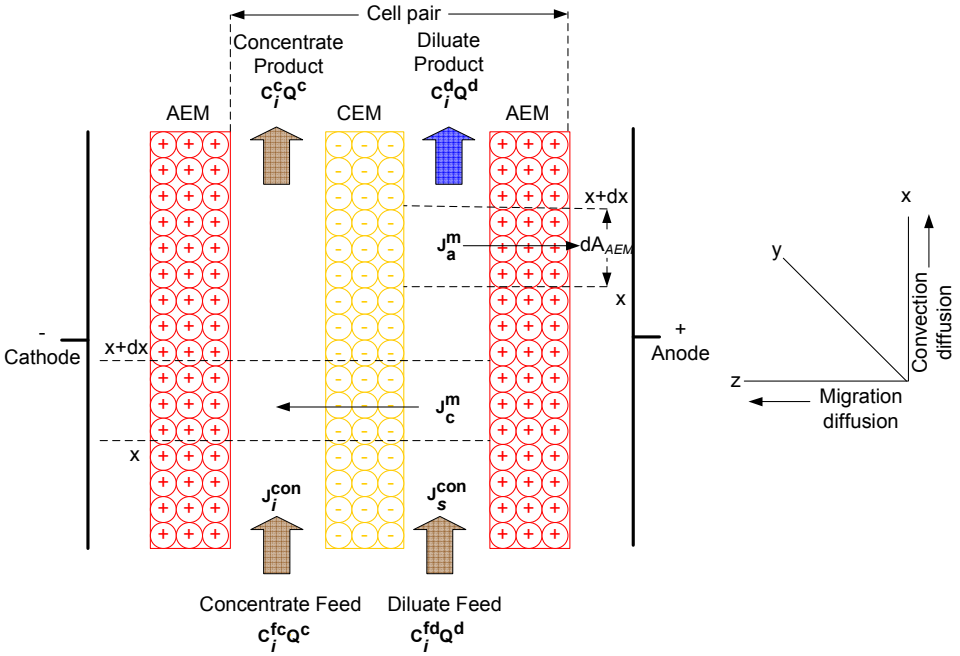

Figure 3.2. Schematic illustrating mass transport in an electrodialysis cell pair (Adapted from Rautenbach and Albrecht (1989) and Strathmann (2004)).

A material balance of mass transport within an ED stack which takes into account the flow rates within the diluate and concentrate as well as current utilisation is given in eqn (3.1).

$$\left(C_i^{\mathrm{fd}} - C_i^{\mathrm{d}}\right)Q^{\mathrm{d}} = \left(C_i^{\mathrm{c}} - C_i^{\mathrm{fc}}\right)Q^{\mathrm{c}} = \frac{\xi I}{\sum_{\mathrm{c}} z_{\mathrm{c}} \nu_{\mathrm{c}} F} \tag{3.1}$$

where C_i^{fd} and C_i^{fc} are the diluate (superscript d) and concentrate (superscript c) feed concentrations (mol/m^3) of a component subscript *i*, C_i^{d} and C_i^{c} are the diluate and concentrate product concentrations (mol/ m^3), Q^{d} and Q^{c} are the flow rates of the diluate and concentrate parallel to the membrane surface (m^3/s), I is the total current passing through a cell pair (A), ξ is the current utilisation (-), z is the cation (subscript c) valence (C/mol), ν is the stoichiometric coefficient (-), F is the Faraday constant (96485 C/mol).

The current efficiency (usually $\xi < 1$) is a measure for the amount of total current passing through an ED stack that can be utilised for the removal of the ions from the

feed (Strathmann, 2004). This is dependent on current leakages across the stack, transport of H^+ and OH^- instead of salt ions, the transport of water and membrane selectivity according to eqn (3.2).

$$\xi = n \cdot \text{electrical efficiency} = n \cdot \eta_s \cdot \eta_w \cdot \eta_m \tag{3.2}$$

where n is the number of cell pairs within a ED stack, η_s is the membrane selectivity, η_w is the water transport efficiency and η_m is the membrane manifold efficiency.

Deficiencies in current utilisation may arise from not entirely selective membranes and water transport across the ion-exchange membranes due to osmosis and electroosmosis. However, water transport by osmosis is relatively slow at low osmotic pressure and is only considered notable at very high osmotic pressure (200-400 atm) (Korngold, 1975). For the range of NaCl concentrations used in this study (1-35 g/L), the osmotic pressure difference between the diluate and concentrate solutions ranged from approximately 1.2 to 58.2 atm.

The ionic material balance can be used to estimate the required membrane surface area. This membrane area is proportional to the amount of ions removed from the feed solution (eqn (3.3).

$$A_{eff} = \frac{Q^{\mathrm{d}}\left(C_i^{\mathrm{fd}} - C_i^{\mathrm{d}}\right) zFn}{i\eta} \tag{3.3}$$

where A_{eff} is the effective membrane area (m^2) and i is the current density (A/m^2) which should be approximately 80 % of the limiting current density (LCD) (Strathmann, 2004) (described in Section 3.2.3).

3.2.2 Transport of Ions in Solution and through Ion-exchange Membranes

Mass transport within ionic solutions and the transport in ion-exchange membranes are governed by two principles: the Nernst-Planck equation and Donnan equilibrium. When an electrical potential difference is established between a cathode and anode during ED, the transport of ions in solution is a result of diffusion due to

concentration differences and migration as a result of the established electrical potential difference, as previously demonstrated in Figure 3.2. The ionic flux in solution (J_i, mol/m^{2}s) and in a membrane (J_i^m, mol/m^{2}s) is represented by the Nernst-Planck equations (eqn (3.4) and eqn (3.5).

Solution: $$J_i = -D_i\left(\frac{\mathrm{d}C_i}{\mathrm{dx}} + \frac{z_i F C_i}{RT}\frac{\mathrm{d}\varphi}{\mathrm{dx}}\right) \quad (3.4)$$

Membrane: $$J_i^m = -D_i^m\left(\frac{\mathrm{d}C_i^m}{\mathrm{dx}} + \frac{z_i F C_i^m}{RT}\frac{\mathrm{d}\varphi}{\mathrm{dx}}\right) \quad (3.5)$$

where D_i is the diffusion coefficient (m^2/s), C_i is the concentration (mol/m^3), R is the gas constant (8.314 J/molK), T is the absolute temperature (K), φ is the electrical potential/applied voltage (V) and the superscript m refers to the membrane phase.

The Donnan equilibrium describes the idea that at equilibrium, the electrochemical potential of a component is equal in both the solution and membrane phase i.e. electroneutrality. Considering Na^+ and Cl^- ions in solution, electroneutrality is expressed as:

Solution: $$[Na^+] = [Cl^-] \quad (3.6)$$

Membrane: $$[Na^+]^m = [Cl^-]^m + [R^-]^m \quad (3.7)$$

where R^- is the fixed charge of the ion-exchange membrane (in this case a negatively charged CEM).

The amount of NaCl transferred through the ion-exchange membrane is given by eqn (3.8).

$$C_{NaCl} = [Cl^-]^m = [Na^+]^m - [R^-]^m \quad (3.8)$$

Quantitative expressions of the Donnan potential i.e. electrochemical potentials in each phase, are given in eqn 3.9 and eqn 3.10 (Mulder, 1996; Zagorodni, 2006).

Solution: $$\mu_i = \mu_i^\circ + RT\ln \mathrm{m}_i + RT\ln\gamma_i + z_i F\varphi \quad (3.9)$$

Membrane: $$\mu_i^m = \mu_i^{m\circ} + RT\ln \mathrm{m}_i^m + RT\ln\gamma_i^m + z_i F\varphi^m \quad (3.10)$$

where μ_i is the electrochemical potential (J/mol), $\mu_i°$ is the electrochemical potential of a pure component under standard temperature and pressure conditions (J/mol), m_i is the mobility coefficient (mol m/Js) and γ is the activity coefficient (-).

When equilibrium is attained, the electrochemical potential between the solution and membrane phase are equal i.e. $\mu_i = \mu_i^m$. The Donnan potential (φ_{don}, V) is found by combining eqn 3.9 and 3.10 (Mulder, 1996; Strathmann, 2004):

$$\varphi_{don} = \varphi^m - \varphi = \frac{RT}{z_i F} \ln\left(\frac{\gamma_i^m m_i^m}{\gamma_i m_i}\right) \tag{3.11}$$

The principle of Donnan exclusion in ion-exchange membranes is illustrated in Figure 3.3. Fixed ions are those fixed functional groups fixed on the polymer backbone of the ion-exchange membranes. Counter-ions are mobile ions of opposing charge, while co-ions are mobile ions present of the same charge as the fixed ions. Under ideal conditions, membranes only contain counter-ions. However in real membranes, co-ions can be found within the membrane, thus decreasing membrane permselectivity. Donnan exclusion occurs when ions with the same charge as the fixed ions in the membrane are excluded and are not transported through the ion-exchange membrane. Donnan exclusion and, therefore, membrane permselectivity, depend on the concentration of the fixed ions and electrolyte solute, the valence of the co-ions and counter-ions and the affinity of the membrane with respect to the counter-ions (Nagarale *et al.*, 2006).

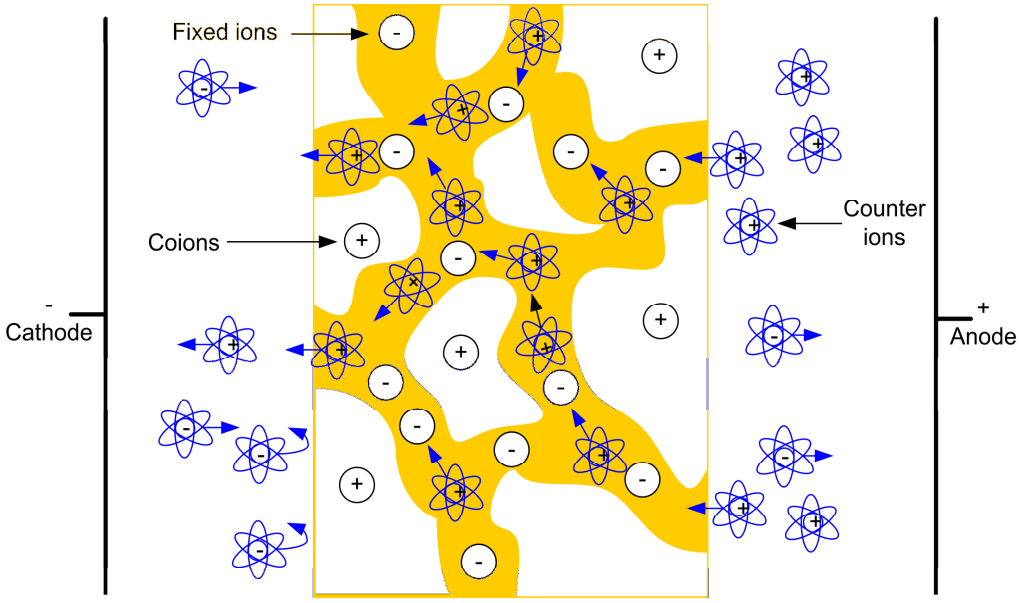

Figure 3.3. Transport of ions through a cation-exchange membrane illustrating the principle of Donnan Exclusion (Adapted from Strathmann (2004)).

3.2.3 Concentration Polarisation and Limiting Current Density

The transport of charged species to the anode or cathode through a set of ion-exchange membranes leads to a concentration decrease of counter-ions in the boundary layer at the membrane surface facing the diluate and an increase at the surface facing the concentrate. This concentration polarisation, as it is known, on both sides of the ion-exchange membrane needs to be taken into account and is illustrated in Figure 3.4. Concentration polarisation in the diluate compartment is of particular importance in an ED system and, therefore, this study in view of the fact that the concentration of the ions decreases towards the membrane surface as a consequence of ionic membrane permeation. A drop in the diluate pH level, an increase in electrical resistance and an increase in the concentrate pH or a drop in current efficiency is an indication that no ions are available for current transport. Water dissociation (usually an undesirable condition) and transport occurs in this situation. The ED system in this study needs to be operated under conditions whereby the effects of concentration polarisation are minimised. This is achieved by reducing the current density and operating below the LCD.

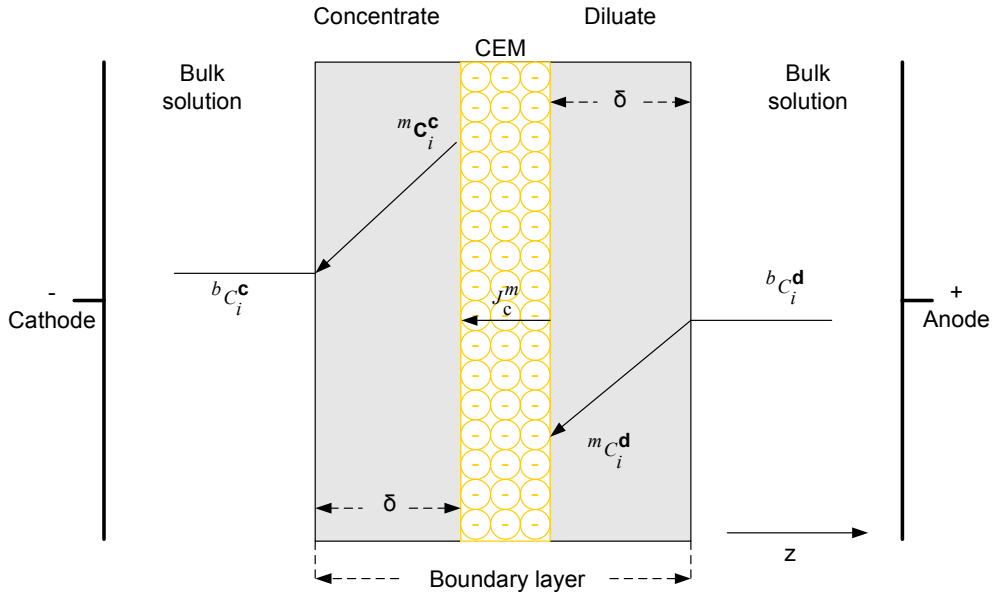

Figure 3.4. Schematic illustrating concentration polarisation in the electrodialysis of a solution of component *i* (Adapted from Rautenbach and Albrecht (1989) and Strathmann (2004)).

In an ED stack under idealised conditions by assuming that only the lateral concentration gradient is significant and that steady-state conditions apply, the counter-ion flux through the membrane can be calculated from an equivalent mass balance in the boundary layer at the diluate side of the CEM. As fractions of the current carried by a certain ion within solution are expressed by the ion transport number, which is the number of moles of the ionic species transported by 1 Faraday of electricity, the total flux of counter-ions through the boundary layer and membrane is calculated by eqn (3.12) and eqn (3.13), respectively (Rautenbach and Albrecht, 1989).

Boundary layer: $$J_i = -D_i \frac{\mathrm{d}C_i^{\mathrm{d}}}{\mathrm{dz}} + T_i \frac{i}{z_i F} \tag{3.12}$$

Membrane: $$J_i^m = T_i^m \frac{i}{z_i F} \tag{3.13}$$

where J_i is the flux in the boundary layer δ, J_i^m is the flux in the membrane, dz is the directional coordinate, T_i is the transport number of the counter-ion within the boundary layer, T_i^m is the transport number of the counter-ion within the membrane.

Combining eqn (3.12) and eqn (3.13) and considering the flux of cations at the diluate side of the CEM gives the current density through an ion-exchange membrane as a function of the component concentrations within the bulk solution (eqn (3.14).

$$i = \frac{FD_i}{z_i\left(T_i^m - T_i\right)}\frac{\mathrm{d}C_i^{\mathrm{d}}}{\mathrm{d}z} = \frac{FD_i}{z_{\mathrm{c}}\left(T_{\mathrm{c}}^m - T_{\mathrm{c}}\right)}\frac{\left({}^bC_{\mathrm{c}}^{\mathrm{d}} - {}^mC_{\mathrm{c}}^{\mathrm{d}}\right)}{\left(\Delta z\right)} \tag{3.14}$$

where Δz is the thickness of the membrane boundary layer (m).

When the concentration within the membrane boundary ($^mC_{\mathrm{c}}^{\mathrm{d}}$) tends towards zero the limiting current density (i_{lim}) for a salt solution (subscript *s*) can be described by eqn (3.15).

$$i_{\mathrm{lim}} = \frac{Fk_s^{\,s}\,{}^bC_s^{\mathrm{d}}}{z_{\mathrm{c}}\left(T_{\mathrm{c}}^m - T_{\mathrm{c}}\right)} \tag{3.15}$$

This takes into account the influence of hydrodynamics, geometry and material properties, which is described by the mass transfer coefficient $k_s^s = D_i / \Delta z$.

The mass transfer coefficient is related to the Sherwood Number (*Sh*) (eqn (3.16), which is determined from a relationship between the Reynolds number (Re) and the Schmidt number (*Sc*) (eqn (3.17). The Sherwood Number is difficult to define in ED stack due to the spacers used to promote turbulence (Isaacson and Sonin, 1976).

$$Sh = \frac{k_s^{\,s}\,2h}{D_i} \tag{3.16}$$

$$Sh \sim Sc^{1/2}\left(\frac{h}{\Delta L}\right)^{1/2}\mathrm{Re}^{1/2} \tag{3.17}$$

where *h* is the membrane spacer distance/hydraulic diameter (m) and Δ*L* is the spacer mesh width (m).

The Schmidt number is calculated from the kinematic viscosity (υ, m^2/s) and diffusion coefficient (eqn 3.18).

$$Sc = \frac{\nu}{D_i} \tag{3.18}$$

Reynolds number is calculated using the linear flow velocity (v, m/s), the hydraulic diameter and the kinematic viscosity (eqn (3.19).

$$\mathrm{Re} = \mathrm{v}\frac{h}{\nu} \tag{3.19}$$

Operation of an ED system below the LCD places boundaries on the arrangement of cell pairs within an ED stack, seeing as the current density which can be applied to the whole stack is ascertained by the diluate compartment with the lowest mean ionic concentration (dependent on ED system operating parameters). Experimental determination of the LCD, as illustrated in Figure 3.5, is presented in Chapter 5.

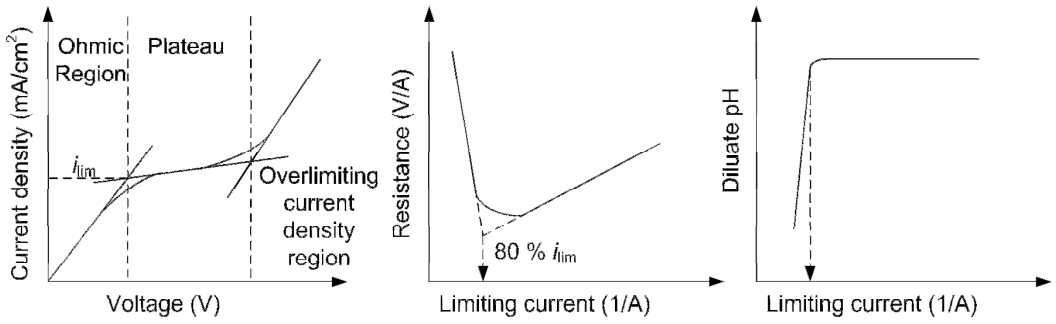

Figure 3.5. Experimental determination of the limiting current density (LCD).

3.3 Energy Requirements in Electrodialysis

Energy consumption within an ED stack is directly proportional to the salt concentration and is a function of the voltage drop in a stack. The energy requirement for ED can be expressed by eqn (3.20).

$$E_{stack} = I^2 R_{stack} t \tag{3.20}$$

where E_{stack} is the energy requirement (Wh/L), R_{stack} is the electrical resistance of the ED stack (Ω), t is the time (h).

Power consumption (Wh) during ED is expressed by eqn (3.21), while specific energy consumption (SEC, Wh/L) during ED is expressed by eqn (3.22).

. $$P = U \cdot I \tag{3.21}$$

$$\text{SEC} = \frac{\sum P}{V_D} \tag{3.22}$$

where V_D is the volume of the diluate (L).

The electric resistance of a cell pair (R_{cell}) is the sum of the resistances of the membranes and the diluate and concentrate streams (eqn 3.23).

$$R_{\text{cell}} = R_{AEM} + R_D + R_{CEM} + R_C \tag{3.23}$$

where R_{AEM}, R_D, R_{CEM}, and R_C are the resistances of the AEM, diluate stream, and CEM and concentrate stream, respectively, as specified below.

$$R_{AEM} = \frac{r_{AEM}}{A_{eff}} \tag{3.24}$$

$$R_{CEM} = \frac{r_{CEM}}{A_{eff}} \tag{3.25}$$

where r_{AEM} and r_{CEM} are the specific resistances of the AEMs and CEMs, respectively (Ω cm^2).

The resistances of the diluate (R_D) and concentrate (R_C) are inversely proportional to the mean conductivity and hence to the mean salt concentration of the solution (Rautenbach and Albrecht, 1989), where:

$$R_D = \frac{h}{(\kappa A_{eff})} \tag{3.26}$$

$$R_C = \frac{h}{(\kappa A_{eff})} \tag{3.27}$$

where κ is the specific conductivity (S/m).

The electric resistance of the ED stack (R_{stack}) is calculated by eqn (3.28).

$$R_{\text{stack}} = nR_{\text{cell}} \tag{3.28}$$

The total energy used for the actual ion transfer from a feed to a concentrate is theoretically the same for a system in which the required membrane area is installed in a one cell pair between two electrodes as for a system in which the membrane area

is installed in a multitude of cell pairs since the energy consumption is the product of current and voltage drop. As current density increases, energy consumption and cost increases while the required membrane area decreases. Therefore, the total desalination cost is a sum of the membrane, energy and operating costs and will reach a minimum or optimum at a certain current density, as shown in Figure 3.6.

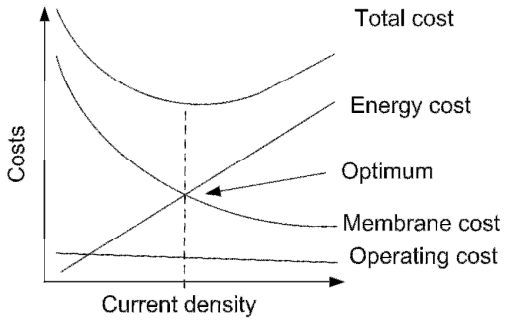

Figure 3.6. Schematic of Electrodialysis process costs as a function of applied current density (Adapted from Strathmann (2004)).

3.4 Membrane Performance Inhibitors

The performance of an ion-exchange membrane and, therefore, the ED process can be inhibited by membrane obstructions. Table 3.1 outlines the different types of membrane obstructions. The typical categories of membrane obstructions are fouling, scaling and poisoning. These obstructions are further described in the following sections and are of particular importance in this study as presence of the selected contaminants in water and wastewater can hamper ion-exchange membrane performance. For example, the inorganics and trace organics can lead to scaling and poisoning, respectively. While numerous efforts have been undertaken to minimise the problems of membrane fouling, scaling and poisoning via different approaches such as pre-treatment there is still a need for additional research on the mechanisms involved so that the performance of ED systems can be optimised.

Table 3.1. Types of membrane obstructions and corresponding examples.

Membrane Obstruction Type	Example
Fouling	Accumulation of particulate and OM
Scaling	$CaCO_3$, $MgCO_3$, $Mg(OH)_2$ and $CaSO_4$
Poisoning	Mass penetration by multivalent ions

3.4.1 Membrane Fouling

Fouling of ion-exchange membranes can be defined as the accumulation of particulates, trace organic compounds and OM that adhere to the membrane surface and/or within the membrane through hydraulic or other physical or electrical forces (Grebenyuk *et al.*, 1998; Lindstrand *et al.*, 2000b). Generally, the AEM is more sensitive to organic fouling than CEM due to electrostatic attraction between negative charged organics and the positively charged AEM (Kim *et al.*, 2002). Ion-exchange membranes are also attacked by strong oxidising agents (Rautenbach and Albrecht, 1989). This can result in membrane deterioration and a decrease in the performance of ED system. Membrane fouling is characterised by a decrease in the selectivity of the membrane, an increase in the voltage drop during the ED process and a decrease in the electrical conductance of the membranes.

Membrane fouling in ED is influenced by a number of electrochemical and physical properties of both the membrane (e.g. resistance, zeta potential) and the foulants in question (e.g. charge, molecular size), along with the operational parameters of the ED system (e.g. current density, frequency, solution pH). The concentration and the solubility of trace organic foulants in a study by Lindstrand *et al*. (2000b) controlled AEM fouling and the extent of the increase in the membrane resistance. Prominent fouling of larger acid molecules can be expected to be due not only to their lower mobility in the membrane, but to their lower solubility, and hence greater sorption affinity to the membrane.

The fouling characteristics of the ion-exchange membranes are related to their electric resistances, hydrophobicities, exchange capacities and zeta potentials. The zeta potential, related to the surface charge properties of the foulants and membrane,

is thought of as one of the key properties to predict the fouling tendencies. The zeta potential of a membrane gives an indication of the amount of electrical surface charges interacting with their surroundings. Lee *et al*. (2002a) compared fouling potentials of 100 mgC/L sodium humate in ED, as indicated by resistance and NaCl removal, at pH values below and above the membrane isoelectric point (IEP, pH 5.1-5.4) i.e. the pH where membrane surface carries no charge. The AEM fouling potentials were linked more to the sorption of anions rather than the chemistry of the functional groups themselves. The zeta potentials of humate were more positive under acidic conditions but still had highly negative values (-18 and -25 mV over the entire pH range). The removal rate of NaCl at pH 4.8 was higher than that of pH 5.8, implying that the attractive force between the membrane and foulant may have little effect on AEM fouling during ED. This was substantiated by Kim *et al*. (2002) where the amount of OM on a membrane surface at pH 10 was three times greater than the amount at pH 4 as a result of an increase in the charge of the OM due to carboxylic and phenolic groups. This increase in charge enhances the interaction between the negatively charged OM and positively charged AEM.

Several approaches to mitigate membrane fouling have been examined through pre-treatment of the feed solution, optimization of operating conditions, the modification of the membrane properties and cleaning methods. The use of pre-treatment will represent an extra operating cost, but will be effective if membrane fouling is reduced. The removal of insoluble particulate matter present in the feed water can be achieved by filtration, as is applied in almost all ED systems. Chlorination of the feed water reduces organic fouling but care needs to be taken so as not to oxidise the anionic resin itself which could thereby acquire –COOH groups and lose part of its selectivity (Korngold *et al.*, 1970). Pre-treatment procedures can be reduced by using ED reversal (EDR). The cleaning of membranes can be categorised as hydraulic, mechanical and chemical cleaning. Hydraulic cleaning includes alternate pressurising and depressurising and by changing the flow direction at a given frequency. Hydraulic and chemical cleaning methods require additional chemicals or instruments resulting in an increase in the installed cost of the ED system as well as the operating/maintenance cost. If the ion-exchange membranes have become

severely fouled it may be necessary to dismantle the stack and clean the membranes individually. This process is, however, time consuming. Membrane cleaning only has a temporary impact on membrane resistance and, therefore, is not an ideal method for the treatment of fouled membranes. Chemical cleaning of membranes results in an additional waste stream.

3.4.2 Membrane Scaling

Scaling is a complex process involving both crystallisation and hydrodynamic transport mechanism in which the precipitation of sparingly soluble inorganic salts on the concentrate of the CEM, and to a lesser extent on the AEM occurs (Korngold *et al.*, 1970). The salts that cause scale formation are ubiquitous in most water environments. Precipitation of suspended matter, silicates, and salts with low solubility such as calcium sulfate ($CaSO_4$), calcium carbonate ($CaCO_3$) or iron hydroxides (FeOH) may occur within the actual flow channels resulting in high hydrodynamic pressure losses and non-uniform flow distribution in the stack (Strathmann, 2004). The treatment of seawater by ED results in membrane scaling as a result of limited solubility of salt species (Elleuch *et al.*, 2006b).

Solution chemistry for example solution pH (Ayala-Bribiesca *et al.*, 2006b) and inorganic concentration (Kabay *et al.*, 2008) as well as ED operation parameters such as flow rate and the occurrence of concentration polarisation have implications for the scale formation process. Precipitation on the membranes is governed by the solubility of the scalant, which is influence by solution pH. Ayala-Bribiesca *et al.* (2006b) identified scaling of a CEM under mineral conditions with $CaCl_2$ at alkaline conditions (pH 12). The presence of scaling on the CEM surface indicated that pH conditions on the other side of the membrane actively affect the local pH conditions at the membrane-solution interface on the opposite side, precipitating calcium as a carbonate or hydroxide at the membrane interface with the concentrate.

Methods for preventing scaling include adjustments to the feed solution pH and physical, mechanical and chemical cleaning of the membranes. The precipitation of soluble salts on the membranes can be minimised by ion-exchange softening or by

the addition of a precipitation inhibiting agent i.e. acid addition. Injection of anti-scalants such as polyacrylates, polyacrylic acids, or polyphosphates within the concentrate can be used to inhibit the precipitation of sparingly soluble salts in an ED stack (Elleuch *et al.*, 2006b).

3.4.3 Membrane Poisoning

The most severe of the membrane obstructions is poisoning of ion-exchange membranes by trace organic compounds that are small enough to penetrate the membranes but whose mobility is so low that they virtually remain inside the membrane. This poisoning could also be due to the sorption of organics on the membranes and the mass penetration by multivalent ions, which tend to neutralise the fixed charges within the membranes (Grossman and Sonin, 1973). A portion of OM may also penetrate the membranes leading to membrane poisoning (Park *et al.*, 2003a). When membrane poisoning takes place, the transport of salt ions through the membrane is hindered by organic molecules in the membrane and/or the sorption or precipitation of organic molecules in the membrane restricting salt transport (Lee *et al.*, 2002c). This leads to a drastic increase in the membrane resistance and a significant reduction in the efficiency of the membranes as well as the ED stack as a whole (Strathmann, 2004). Lindstrand *et al*. (2000b) studied the influence of various kinds of organic compounds (sodium dodecylbenzene sulfonate (SDBS), octanoic acid, sodium octanoate, decanoate and propanoate) on AEM and CEM fouling (Selemion AMV and CMV). The AEM showed a severe increase in resistance in the presence of sodium octanoate and sodium decanoate, but a small decrease when sodium propanoate was present. Therefore, sodium octanoate and sodium decanoate restricted the movement of the inorganic ions through the membrane. Only a minor increase in membrane resistance was observed for the CEM.

Methods for preventing membrane poisoning include the use of pre-treatment process such as microfiltration (MF) or ultrafiltration (UF), activated carbon and membrane cleaning with concentration acids or bases (e.g. HCl, NaOH) (Korngold *et al.*, 1970).

3.5 Contaminant Removal using Membrane Technology

The removal of inorganic and trace organics from water and wastewater is important due to possible exposure from drinking water, their production in water treatment and the relevance of this to water reuse. This following section outlines the capacity of ED for the treatment of contaminated water. Where ED has not been applied i.e. for steroidal hormones and pesticides the inadequacies of conventional treatment processes are summarised to highlight the need for further treatment.

While a number of inorganics, such as chloride and sulphate, cannot be removed from aqueous solution by conventional water treatment processes, membrane technology such as ED and RO have successfully been applied (Mariñas and Selleck, 1992; Turek *et al.*, 2007b). Table 3.2 summarises the removal of the selected inorganics investigated in this study by ED. As can be seen, the removal is highly variable and dependent on the feed concentration, solution pH and the membrane utilised. While in some cases, removal by membrane processes in comparison to conventional treatment is advantageous, membrane scaling by inorganic complexes is a serious issue in the application of membrane technology in water and wastewater treatment (Lee and Lee, 2000; Shih *et al.*, 2005).

Given the inadequate performance of conventional treatment processes for the removal of steroidal hormones from water and wastewater, numerous studies have studied the effectiveness of membrane processes such as RO and NF. Near complete retentions have been reported (Nghiem *et al.*, 2004a; Schäfer *et al.*, 2003). Koyuncu *et al*. (2008) investigated the retention of estrone, progesterone, testosterone, 17α-ethinylestradiol, estriol and estradiol using NF membranes and the largest retentions observed were 90 % (17α-ethinylestradiol) and 98 % (progesterone). Chang *et al*. (2003) reported 95 % retention of estrone using MF hollow fibre membranes. Sorption of estrone to the MF membranes was noted. This mechanism of sorption will be further discussed in detail in Section 3.6. While these studies demonstrate the high levels of removal, it is highly dependent on the hormone type, the membrane used and the operating conditions. As will be further discussed in Section 3.6.3, the

treatment of water and wastewater containing steroidal hormones has been generally neglected. Therefore, the fate of steroidal hormones in ED is unknown.

Table 3.2. Removal (%) of inorganic contaminants from water by electrodialysis.

Inorganic	Feed (mg/L)	Removal (%)	Membranes	Notes	Refs.
Boron	64-77	97	Neosepta ® AMX and CMX	pH 9-10	1
	64	12 25	Neosepta ® AMX and CMX	pH 8.3 pH 9.4	2
	1.5	33	Ionics anion-204-8XZL-388 and CR67-HMR-6712	pH 5.5	3
Fluoride	3	79	Neosepta ® CMX, CMS, ACS, AFN	pH 6.5 Brackish water	4
	3.3	80	Neosepta ® ACS and CMX	pH 7.9	5
	10	40 97	Selemium ® MZA Selemium ® AMP	Groundwater	6
Nitrate	90	73-83	Neosepta ® ACS and CMX	pH 8.1 Groundwater	7
	210	90	Neosepta ® ACS and CMX	pH 7.7 Groundwater	8
	133	75 68	Neosepta ® ACS and CMX	pH 7.4 Groundwater	9

Refs: 1. Turek *et al*. (2007a); 2. Turek *et al.* (2005); 3. Melnik *et al.* (1999); 4. Amor *et al*. (2001); 5. Menkouchi Sahli *et al*. (2007); 6. Zeni *et al*. (2005); 7. Elmidaoui *et al*. (2002); 8. Menkouchi Sahli *et al*. (2008); 9. Elmidaoui *et al*. (2001).

The removal of pesticides from water by traditional water treatment methods, commonly powdered or granulated activated carbon (PAC, GAC) and oxidation by ozone or hydrogen peroxide is difficult due to the extensive range of compounds with varying physicochemical characteristics as well as the low concentrations in which they are present in natural water. Coagulation/flocculation, sedimentation, and filtration processes in conventional water treatment are not effective in removing certain pesticides belonging to triazine, acetanilide, carbamate, and urea derivative classes (Hetrick *et al.*, 2000). A study by Ormad *et al*. (2008) compared the effectiveness of different traditional treatments, namely pre-oxidation by chlorine or

ozone, chemical precipitation with aluminium sulphate and activated carbon adsorption, for the removal of 44 organic pesticides detected in the Ebro River Basin (Spain). While standard coagulation was not sufficient for removal, coagulation with pre-oxidation by chlorine increased removal to 60 % as a result of pesticide degradation. Pre-oxidation with ozone was efficient for removing 70 % of the pesticides. A combination of coagulation with activated-carbon absorption enhanced this removal to 90 %.

Certain pesticides are susceptible to transformation to during chlorination. Magara *et al*. (1994) demonstrated that organophosphate pesticides containing S=O bonds, diazinon and thiobencarb, were degraded and produced oxons (P=S) as primary by-products. The production of such by-products during conventional treatment of pesticides is a serious concern to water recycling; thus alternative treatment methods are needed. Among the possible alternatives of treatment, membrane technology would offer many advantages. Much attention has been given to the use of NF and RO membranes for pesticide treatment with variable retention of uncharged pesticides (Berg *et al.*, 1997; Berg, 2002; Kiso *et al.*, 2000; Van der Bruggen *et al.*, 2001), while ED has remained neglected due to the inability of ED to separate uncharged compounds. Therefore, the fate of pesticides in ED is unknown.

OM has traditionally been removed from water by coagulation and flocculation, followed by chlorination or ozonation disinfection, as well as granular activated carbon and ion exchange resins. Conventional water treatment processes, however, are ineffective in the removal of OM with molecular weight less than 500 daltons (Collins *et al.*, 1986). Although OM is not considered harmful to human health, the formation of carcinogenic disinfection-by-products (DBPs) such as trihalomethanes (THMs), chlorophenols and halacetic acids (Chang and Juang, 2004) during pre-oxidation with chlorine in the presence of OM is a serious issue in the treatment of water by conventional treatment processes. The removal of OM in membrane processes is a challenge, particularly owing to the occurrence of membrane fouling (Fan *et al.*, 2001; Hong and Elimelech, 1997; Seidel and Elimelech, 2002).

3.6 Contaminant Removal Mechanisms in Electrodialysis

The mechanisms of contaminant removal are complex and a clear lack of fundamental understanding of inorganic and trace organic contaminant removal mechanisms is a current limitation; thus greater understanding will open up new avenues for the application of ED. The following section reviews the dominant removal mechanisms of inorganic and organic trace contaminants in ED.

3.6.1 Transport and Electrostatic Interaction

The prevailing mechanisms of ionic transport during ED can be separated into those that determine transport within solution and those that determine transport within the ion-exchange membranes. Within solution, migration is predominantly dependent on the applied electrical potential and the resultant current, ionic mobility and competition with other ions, while diffusion is resultant from concentration differences between the bulk solution and the membrane boundary layer. Transport within the ion-exchange membranes is a result of ionic charge and electrostatic repulsion between the ion and the membranes. The physicochemical characteristics of contaminants themselves strongly influence their transport and removal during ED. These characteristics include charge, mobility, concentration and speciation. ED operating conditions such as applied electrical potential and the resultant current, hydrodynamic conditions within the ED stack (e.g. flow rate), solution pH and temperature play a role.

Electrostatic repulsion is important in the case of both charged inorganic and organic molecules. Electrostatic repulsion between counter-ions and specific ion-exchange membranes depend on the charge of the ions or other charged molecules and the charge of the ion-exchange membrane surface, as described by the principle of Donnan exclusion (Section 3.2.2). In order to reach an equilibrium state in an ion-exchange membrane, the number of positive ions should be equal to that of negative ions based on the Donnan equilibrium and electroneutrality rule i.e. a divalent positive ion (cation) is accompanied by a divalent negative ion (anion). Therefore,

monovalent ions competitively equilibrate with the ion-exchange membranes and pass through them with less difficulty than divalent ions.

The influence of ionic charge and valence state on the removal of inorganic contaminants in ED is well established (Firdaous *et al.*, 2007; Kabay *et al.*, 2003; Oldani *et al.*, 1992). Sadrzadeh et al. (2007) showed that the separation of monovalent ions from wastewater was larger than the separation of divalent and trivalent ions in the following order $Na^{+} > Cu^{2+}$, Zn^{2+}, $Pb^{2+} > Cr^{3+}$. It was thought that the monovalent ions occupy more surface active sites within the ion-exchange membranes, which restrict the passage of competitive ions. The number of membrane surface active sites occupied by trivalent ions is three times more than that occupied by monovalent ions. Since the amount of these sites is constant, it was concluded that separation decreases with increasing valence.

The separation of ions with the same charge and same valence using ion exchange membranes is an important but difficult process. For ions of similar valence, separation has been found to be restricted by molecular weight. Sadrzadeh *et al*. (2007) attributed the separation of multivalent ions from wastewater to molecular weight (e.g. $Pb^{2+} < Cu^{2+} < Zn^{2+}$). The transport of ions through an ion-exchange membrane is dependent upon their permselectivity. Permselectivity between ions with the same charge is evaluated by the equivalence of specific ions permeated through the membrane when one equivalent of a standard cation or anion, such as Na^{+} or Cl^{-} permeates. This permselectivity is proportional to the transport numbers of the ions and the concentration of the ions within solution. The permselectivity among, for example, cations in solution through ion-exchange membranes is governed by differences in affinity of the cations and the membrane and differences in their mobility or migration speed within the membranes (Sata *et al.*, 2002). The permselectivity of anions in relation to chloride ions (permselectivity) is decided by not only the size of hydrated radius but the affinity of anions onto the membrane surface. This affinity is influenced by membrane characteristics such as hydrophobicity as emphasized by Sata *et al*. (1995; 1997) and Li and Xu (2008).

While the model describing ionic transport within solution in ED i.e. the Nernst equation is simple and may be sufficient for strong electrolyte ions, it is much more complicated when considering weak electrolyte ions due to the fact that transport depends strongly on ionic mobility. The mobility of ions in solution is directly related to their hydration energy and thus hydration ability. The hydration ability of ions or the hydrophilicity of ions is expressed by their standard molar Gibbs free energies ($\Delta_{hyd}G^0$, kJ/mol). Gibbs free energy (G) is the maximum amount of energy which may be obtained from a system (Smith, 2004). The Gibbs free energy of interaction of the ion with its surroundings is the sum of the contributions of the Gibbs free energy of the electrostatic interactions in the hydration shell and the interactions in the bulk water beyond the shell. Therefore, the hydration of an ion influences its interaction with its surroundings including other ions (e.g. trace contaminants) and surfaces (e.g. membranes). Table 3.3 shows the mobility and molar Gibbs free energy of hydration of several cations and anions. The mobility of Li^+ and Na^+ ions are lower than that of Ca^{2+} and SO_4^{2-} because of the higher hydration shell and lower charge of the former. Li and Xu (2008) indicated that anions with lower Gibbs hydration energies permeated a hydrophobic AEM more easily. In the case of anions with similar Gibbs hydration energies (F^-, Cl^-, Br^-), membrane permeation ($Br^- > Cl^- > F^-$) was favoured in anions with smaller hydrated radii ($F^- > Cl^- > Br^-$). The relationship between hydrated radii and the transport of monovalent ions during ED is not understood. Therefore, the relationship between hydrated radii and the transport and removal of inorganic contaminants from model aqueous solutions and a brackish groundwater will be investigated in Chapters 5 and 6.

Table 3.3. Ion mobility (*u*) in water at 25°C and Gibbs energy of hydration of several cations and anions.

Ion	Mobility [a] u ($\times 10^{-8}$ m^2/sV)	Molar Gibbs energy of hydration [b] $\Delta_{hyd}G^0$ (kJ/mol)	Crystal ionic radius [c] r (nm)	Hydrated ionic radius [c] (nm)
Li^+	4.01	-510	0.094	0.382
Na^+	5.19	-385	0.117	0.358
K^+	7.62	-305	0.149	0.331
Ca^{2+}	6.17	-1515	0.100	0.253 [d]
Cl^-	7.91	-270	0.164	0.332
Br^-	8.09	-250	0.180	0.330
SO_4^{2-}	8.29	-1145	0.215 [d]	0.300 [d]

[a] Atkins (1990); [b] Marcus (1991); [c] Volkov *et al*. (1997); [d] Kiriukhin and Collins (2002).

Some studies have linked the separation of monovalent and multivalent ions in ED to the mobility of ions and thus their migration rates within ion-exchange membranes (Ayala-Bribiesca *et al.*, 2006a; Van der Bruggen *et al.*, 2004). Van der Bruggen *et al*. (2004) studied the separation of monovalent (Na^+, Cl^-, NO_3^-) and divalent (SO_4^{2-}, Mg^{2+}) ions from single model salt solutions (NaCl, Na_2SO_4, $MgCl_2$, $MgSO_4$ and $NaNO_3$) by ED and NF using selective ACS AEMs and CMS CEMs (Astom Corporation, Japan). Removal of NaCl was faster than that of $NaNO_3$, $MgCl_2$ and Na_2SO_4, $MgSO_4$, where both the cation and anion are divalent, removal was the slowest. While the differences in separation were attributed to selectivity of the membranes for different ions, ionic size was thought to have an additional impact. It was postulated that the larger the hydrated ion, the more sterically hindered its transport through the membrane i.e. multivalent ions are more strongly retained in the membrane matrix and thus transported more slowly. This steric hindrance occurs when the size of groups within a particular molecule prevents chemical reactions that are otherwise observed in related smaller molecules. While this study was undertaken on single salt solutions of mixed monovalent/multivalent solutions with specific affinity for the selected membranes, the influence of hydrated radius on the separation or removal of ions during ED of multiple salt solutions is still not thoroughly understood.

Sata (2000) and Sata *et al*. (1996) reviewed and studied the permselectivity of specific anions (I^-, NO_3^-, Br^-, Cl^-, F^- and SO_4^{2-}) through AEMs cross-linked with methylene groups of diamines and found that that transport numbers of the anions and thus separation was mainly governed by a balance of the Gibbs hydration energy of the anions with the hydrophilicity of the membranes, and partly by hydrated ionic radius of the anions, except with membranes having an oppositely charged layer on the membrane surface. The permeation of anions with a higher transport number (e.g. SO_4^{2-}) through the ion-exchange membranes was reduced in comparison to those with a lower transport number (e.g. I^-). While the permeation through membranes with high cross-linkage was reduced, the number of methylene groups of the diamines increased the hydrophobicity of the anion-exchange groups within the membranes and affected the relative transport number between two anions. The lower the hydration of anions, the higher the relative transport number of the anions through the membranes with the hydrophobic anion-exchange groups. This shows that the permeation of anions is not only dependent on the mobility through the membranes but on the affinity between the anions and the AEM.

Operating conditions influence the transport mechanisms of inorganics during ED. For example, Sadrzadeh et al. (2007) investigated the effect of a range of contaminant physicochemical properties (concentration) and ED operating conditions (temperature, flow rate and applied electrical potential) on the separation of monovalent (Na^+), divalent (Cu^{2+}, Zn^{2+}, Pb^{2+}) and trivalent (Cr^{3+}) ions from wastewater. The results showed that increasing feed concentration, applied electrical potential and temperature improved separation. Separation, however, decreased with increasing flow rate. It was found that all factors had significant effect on the separation with flow rate having the largest effect. Increasing the flow rate of solutions through the diluate and concentrate decreases their residence time within the ED stack. Therefore, in the treatment of a solution containing inorganic or organic contaminants contact time between the contaminants and the ion-exchange membranes and thus migration diffusion within the diluate and diffusion through the membranes would be reduced.

Ions or compounds exist in solution as different chemical forms or species. Their distribution in solution is termed chemical speciation and is dependent on solution conditions (e.g. pH, temperature and ionic strength). Inorganic and organic contaminants can be neutrally, positively or negatively charged in accordance to their pK_a, which varies with solution pH. Speciation of a particular contaminant significantly affects its behaviour in regards to transport and bioavailability by determining charge and solubility. The formation of inorganic and organic complexes is dependent on speciation. Therefore, speciation has implications for the removal of inorganic contaminants in ED and will be studied in Chapter 5 and 6.

3.6.2 Solute-Solute Interactions

Some inorganics may interact with other solutes or components present in water and wastewater, such as dissolved organic and inorganic molecules or organic and inorganic particulates. OM is known to form complexes with inorganics, such as metal ions and this complexation influences their mobility and transport in the environment (Kinniburgh *et al.*, 1999; Merdy *et al.*, 2006). The extent of metal-OM binding varies with size, composition and configuration of the OM, solution pH and ionic strength and the chemical properties of the metal (Ritchie and Perdue, 2003; Tipping, 2002). Some inorganic trace contaminants may act independently of each other, while others may have additive effects. Studies addressing the possible interdependence of these inorganics on their removal during ED have, however, received limited attention in the literature. Knowledge of such solute-solute interactions is crucial for assessing their transport in the environment as well as the removal capabilities of different water treatment processes. Many published works describe the removal of inorganics and OM from natural and wastewaters at different conditions. However, solute-solute interactions (such as complexation) of OM with inorganic compounds (such as boron, fluoride and nitrate) during ED have not been investigated. The impact of these interactions in complex groundwater systems has received limited research attention with research mainly focusing on the treatment of simple systems of one or two trace contaminants at a time (Elmidaoui *et al.*, 2001; Kabay *et al.*, 2006).

Interactions between organic trace contaminants, specifically steroidal hormones and pesticides, and OM are not well understood; nor are the influence of OM on the fate of these organic contaminants in ED. The complexation of organic molecules with OM has previously been reported (Neale *et al.*, 2009; Ohlenbusch *et al.*, 2000; Rebhun *et al.*, 1998). This interaction can be quantified by OM-water partition coefficients (K_{OM}, L/kg), which relates the concentration of contaminant sorbed to OM to the freely dissolved concentration of contaminant in solution (Schwarzenbach *et al.*, 2003). Ohlenbusch *et al*. (2000) showed that either hydrophobic or specific interactions between phenolic compounds and OM depended on the physicochemical characteristics of both the contaminant and the OM. Interactions increased with both the molecular weight and the number of functional groups of the OM and therefore the ability to facilitate specific interactions with the phenolic compounds. Hydrophobicity is quantified as the relative partitioning between the liquid octanol and water i.e. by the octanol-water partition coefficient (K_{ow}) and has been used as an indication of interaction between OM and trace organics. Those organic compounds with a higher log K_{ow} indicate higher hydrophobicity. The value of K_{ow} is commonly expressed in a log scale as defined in eqn (3.29) (Schwarzenbach *et al.*, 2003).

$$\log K_{ow} = \log \frac{C_{oc}}{C_w} \tag{3.29}$$

where C_{oc} is the concentration of the solute in octanol and C_w is the concentration of the solute in water at equilibrium.

However, Neale *et al*. (2009) quantified the interaction between HA and the steroidal hormones estradiol and estrone and found that partitioning was due to specific hydrogen bonding between the phenolic hydroxyl groups in the steroidal hormones and the carboxylic functional groups of HA. Strong interactions between OM and the mobility of pesticides have also been reported (Agbedoko *et al.*, 1996; Gao *et al.*, 1998; Kumar and Philip, 2006) with pesticide sorption to OM influencing the transport and final fate of the pesticide compounds (Kumar and Philip, 2006). The influence of OM on the removal of steroidal hormones during other membrane processes is variable with trace organic-OM complexation, membrane electrostatic repulsion and sorption determined as the principle mechanisms for removal

(Agbedoko *et al.*, 1996; Comerton *et al.*, 2009; Schäfer *et al.*, 2002; Yoon *et al.*, 2006). The fate of trace organics freely dissolved in solution would be different to those sorbed to OM. The complexation of OM and hydrophobic organic contaminants could either enhance or reduce their removal during ED. Therefore, it is important to study the implication of OM on the fate of steroidal hormones and pesticides in ED.

Variations in solution chemistry, namely pH and ionic strength, can have implications for the charge, conformation and solubility of OM (Avaltroni *et al.*, 2007; Ghosh and Schnitzer, 1980). However, very few studies have considered the implications of solution chemistry on the interaction of inorganic and organic trace contaminants with OM. Therefore, the influence of solution chemistry on the mechanisms of inorganic and organic trace contaminants removal during ED will be considered in this study.

3.6.3 Membrane Deposition and Sorption

Though membrane deposition and sorption of inorganic and trace organic contaminants to ion-exchange membranes can not technically be termed a 'removal' mechanism due to the fact that the contaminant is not transported through the membranes, they are indeed important mechanisms that need to be considered. The deposition of inorganics on ion-exchange membranes can also be referred to as scaling, as discussed in Section 3.4.2. An inorganic contaminant can precipitate out of solution and be deposited on an ion-exchange membrane if its concentration exceeds its solubility (Turek and Dydo, 2003). Research on the scaling of CEMs in ED has focused on the formation of calcium and magnesium hydroxide as well as calcium carbonate and its influence on membrane morphology (Ayala-Bribiesca *et al.*, 2006b; Casademont *et al.*, 2008b). There have been few reports on scaling treatment of groundwater (Shaposhnik *et al.*, 2002; Turek and Dydo, 2003) and its influence on inorganic contaminant removal and desalination (Casademont *et al.*, 2008a). As scaling is likely to affect the removal of inorganic contaminants, the evaluation of ED for desalination and the removal of a range of inorganic contaminants from a brackish groundwater will investigated in this study in Chapter

6. The implication of solution pH, an influencing factor in membrane scaling, will also be investigated.

The mechanism of sorption is crucial as it may significantly affect the fate of molecules in both the environment and in water treatment processes. Two possible mechanisms for the sorption (partitioning) of organic molecules to membranes have been suggested, both of which are based on intermolecular forces between functional groups of molecules and the membranes. These interactions are namely: hydrophobic interaction between the organic molecules (e.g. organic acids, hormones and pesticides) and the membrane surface (Kiso *et al.*, 2000; Kiso *et al.*, 2001; Lindstrand *et al.*, 2000a; Lindstrand *et al.*, 2000b; Pronk *et al.*, 2006; Yoon *et al.*, 2003) and hydrogen bonding between the functional groups within the organic molecules and the membrane active layer (Chian *et al.*, 1975; Ng and Elimelech, 2004; Nghiem *et al.*, 2002; Nghiem *et al.*, 2004c).

Organic compounds that are more hydrophobic are expected to sorb more readily on a membrane surface, especially on hydrophobic membranes. Lindstrand *et al*. (2000a; 2000b) investigated the sorption of ion-exchange membranes by three organic acids (propanoic, octanoic and decanoic acid) and two anionic surfactants (sodium octanoate and SDBS) as a function of solution pH and with and without an applied voltage. Sorption due to electrostatic interactions been sodium octanoate and SDBS and the AEM was identified while interaction between the acid compounds and AEM was attributed to hydrophobicity. Quantification of these interactions was, however, neglected. Pronk *et al*. (2006) reported that both molecular size and hydrophobic interaction with the ion-exchange membranes played a role in the sorption and permeation (diffusion) behaviour of organic compounds during ED. It was assumed that acidic compounds (ibuprofen and diclofenac) i.e. those with a higher log K_{ow} sorb mainly to the AEMs while basic compounds (propanolol) sorb mainly to the CEMs. Neutral compounds (17α-ethinylestradiol and carbamazepine) sorb to both types of membranes but 17α-ethinylestradiol with the highest log K_{ow} value (3.67) exhibited stronger sorption (carbamazepine log K_{ow} 2.45).

Hydrogen bonding is a specific intermolecular interaction with a hydrogen atom being present in an intermolecular bond and is referred to as an electrostatic dipole-dipole interaction. Dipole-dipole interactions occur between two molecules with permanent dipoles. An example of hydrogen bonding is illustrated in Figure 3.7. A hydrogen atom is covalently (chemically) bound in one molecule, which acts as the hydrogen donor (δ^+), while the other molecule acts as the hydrogen acceptor (δ^-) (e.g. O). Other chemical groups which can take part in hydrogen bonding include –OH, C=O, -NH_2, =NH and =N. The permanent dipole moment reflects the charge distribution within a dissolved molecule and may thus be a measure for interactions between a molecule and membrane. A high dipole moment (μ), measured in debye units (D), causes a more intense interaction with the membrane by the preferential orientation of the dipoles towards the membrane with the opposite charge of the membrane charge in the direction of the membrane surface (Mukhopadhyay and Law, 2001). The strength of the dipole moment of a molecule may influence both electrostatic interactions and sorption of organic contaminants with the ion-exchange membranes.

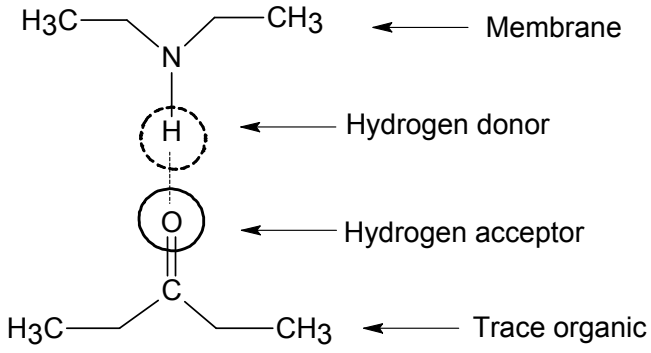

Figure 3.7. Example of hydrogen bonding between dipoles of an organic contaminant and a membrane showing hydrogen donor (H) and acceptor groups (O).

While the treatment of steroidal hormones by membrane processes such as MF, NF, and RO has been widely reported (Chang *et al.*, 2003; Koyuncu *et al.*, 2008; McCallum *et al.*, 2008; Nghiem *et al.*, 2004c), studies on the fate of steroidal hormones in ED are limited (Escher *et al.*, 2006; Pronk *et al.*, 2006). Pronk *et al.*

(2006) investigated the removal of organic compounds diclofenac, carbamazepine, propranolol, ibuprofen and the steroidal hormone 17α-ethinylestradiol from urine using batch and continuous ED. Considerable sorption of 17α-ethinylestradiol (75 %) to the ion-exchange membranes was observed during the batch experiments. This sorption was attributed to hydrophobic interaction. Jansen *et al*. (1996) reported sorption of progesterone and testosterone to polystyrene particles; which are a component of the polymer matrix of the ion-exchange membranes used in this study. The mechanisms of sorption to the polystyrene particles were, however, not identified.

The treatment of pesticides by other membrane processes have also been widely studied and their removal was found to be enhanced by membrane sorption (Berg *et al.*, 1997; Chian *et al.*, 1975; Hofman *et al.*, 1997; Kiso *et al.*, 2000; Kiso *et al.*, 2001; Van der Bruggen *et al.*, 1998; Van der Bruggen *et al.*, 2001; Verliefde *et al.*, 2007). ED, however, has so far been neglected as a possible treatment process. While ED is not expected to removal uncharged trace organics the motivation for this study is to investigate their behaviour in treatment. The quantification of sorption of steroidal hormones and pesticides to ion-exchange membranes has not been undertaken nor have the mechanisms involved in this process been thoroughly identified. A thorough understanding of the partitioning of both steroidal hormones and pesticides between water and ion-exchange membranes, via membrane-water partition coefficients (log K_M, L/cm^3), would be important for the prediction of their fate during ED. Therefore, this study aims to address this issue and the fate of steroidal hormones and pesticides in ED is investigated in Chapter 7 and 8. Solution chemistry would have implications for sorption of trace organics to the ion-exchange membranes. The pH can influence the charge of the trace organic and this has implications for the interaction between the trace organic and the membrane i.e. reduced sorption when the organic is dissociated (> pK_a). Therefore, the influence of solution pH on trace organic sorption will be investigated.

Deposition of OM on ion-exchange membranes occurs during ED, as discussed in Section 3.4.1. Minimal deposition of OM is expected to occur on CEMs due to the

electrostatic repulsion between the membrane surface and the negatively charged functional groups of the OM. Negatively charged OM moves toward the AEMs due to electrostatic attractive forces. OM with large molecular weights do not pass through the ion-exchange membrane but deposit on the membrane surface due to the steric effect and the electrostatic interaction rather than penetration into the membranes (Korngold *et al.*, 1970; Lindstrand *et al.*, 2000b). However, Park *et al.* (2003a) found that a small fraction of HS may permeate through the AEM indicating that organic molecules may be removed during ED.

The interaction of OM with ion-exchange membranes can be directly related to OM functional group content. Many studies indicate that the number-average molecular weight of OM is around 103 and that 50 % or more of its acidic functional groups are dissociated at pH > 4 (Nyström *et al.*, 1996; Ritchie and Perdue, 2003). This combination of large size and negative charge accounts for its selective retention by ED membranes (Kim *et al.*, 2002; Lee *et al.*, 2002b).

Conformational changes may have implications for the behaviour of OM in ED as changes in organic concentration, ionic strength and solution pH, particularly within the ion-exchange membrane boundary layers may induce charge interactions and promote membrane fouling (Kim *et al.*, 2002). Therefore, investigations into the influence of solution conditions are crucial for determining the effectiveness of ED in the treatment of water containing OM. Korngold *et al*. (1970) found that an alkaline pH decreased humate fouling, especially in buffered solutions. Although it is clear that deposition of OM on ion-exchange membranes depends on numerous factors including the physicochemical characteristics of the OM and membranes and the operation conditions of the ED process, the mechanisms underlying such principles are poorly understood. The implication of solution pH on the deposition of the selected OM in this study (HA, TA and AA) on the ion-exchange membranes will be evaluated in Chapter 5.

3.7 Summary

Incomplete knowledge of the removal mechanisms in ED makes it difficult to design and implement large-scale ED systems. This needs to be addressed in this study, as the lack of fundamental understanding of inorganic and trace organic contaminant transport is a current limitation for ED. The transport and removal of such contaminants are dependent on the physicochemical characteristics of the membranes (e.g. charge, hydrophobicity, membrane polymer type and functional groups) and contaminants (e.g. charge, functional groups, molecular size, log K_{ow}, pK_a) solution chemistry (e.g. pH, ionic strength) as well as possible solute-solute interactions (e.g. complexation with OM) and interactions between the contaminants and membranes (e.g. electrostatic attraction, hydrogen bonding).

This study will lead to an improved understanding of theoretical principles that will fill significant knowledge gaps. The knowledge gained in this study will have direct applications to current problems and uncertainties in water and wastewater treatment. It is this area that requires a substantial contribution to lift the ED process into a new application that will increase water efficiency. Solute-solute interactions such as complexation of OM with the selected inorganic contaminants are not understood. Therefore, the mechanisms of inorganic contaminant removal in model aqueous and brackish groundwater solutions will be elucidated in Chapters 5 and 6, respectively. While hydrophobic interactions or hydrogen bonding mechanisms between steroidal hormones and pesticides and the ion-exchange membranes have been postulated for their removal in ED, the quantification of such interactions have not been undertaken. Therefore, this study aims to address this issue through the determination of log K_M values and an investigated into the fate of steroidal hormones and pesticides during ED in Chapters 7 and 8.

Chapter 4. Materials and Methods

In this chapter the materials used (chemicals, inorganics, organics, membranes and ED equipment) are described. Solution preparation, analytical methods and experimental protocols employed during this work are presented. A detailed description of the ED lab-scale system (system schematics, operation modes) along with characteristics of the ion-exchange membranes is given in this chapter.

Some methods requiring considerable attention such as analytical instrument calibration can be found in Appendix 1.

4.1 Chemicals and Background Solution

All experiments were conducted in a background buffer solution, unless stated otherwise, made up with ultrapure water (UW) (18.2MΩ/cm; Elga PURELAB Ultra (High Wycombe, UK)), which was selected as simple representative model of brackish waters. The composition of this background buffer solution is outlined in Table 4.1. The concentration of NaCl (5g/L) was chosen to represent brackish water. $NaHCO_3$ was used to allow pH adjustment without significantly changing the ionic strength (Schäfer, 2001). The chemicals outlined in Table 4.1 were analytical grade and purchased from Sigma-Aldrich (Australia) or Fisher Scientific (Loughborough, UK).

Table 4.1. Background buffer solution composition.

Chemical	Molecular weight, MW (g/mol)	Concentration (mM)	Concentration (g/L)
$NaHCO_3$	84	1	0.084
NaCl	58.5	85.5	5

In some experiments, analytical grade 1 M NaOH and/or HCl, were used to adjust the diluate and concentrate or feed solution pH. Na_2SO_4 (99 % purity) was used in the electrode rinse solution in all ED experiments (both from Fisher Scientific, Loughborough, UK).

4.2 Inorganic Contaminants

For ED experiments with fluoride, nitrate and boron, the feed solutions (diluate and concentrate, 4 L each) were prepared by dissolving NaF (5 mg/L as fluoride; total mass 2.1 mmol), $NaNO_3$ (100 mg/L as nitrate; total mass 57 mmol) and $B(OH)_3$ (10 mg/L as boron; total mass 7.4 mmol) (Sigma Aldrich, Gillingham, UK) in the background buffer solution. The concentrations of fluoride, nitrate and boron were selected within the range found in brackish waters (Koparal and Ogutveren, 2002; Melnik *et al.*, 1999). Additional experiments with an identical concentration of 10 mg/L for the inorganic trace contaminants were carried out.

4.3 Organic Trace Contaminants

The radiolabeled steroidal hormones [2,4,5,7-^{3}H] 17β-estradiol (3.15 TBq/mmol), [2,4,5,7-^{3}H] estrone (3.55 TBq/mmol), [2,4,5,7-^{3}H] progesterone (3.52 TBq/mmol) and [2,4,5,7-^{3}H] testosterone (2.70 TBq/mmol) were supplied in toluene-ethanol by GE Healthcare (Little Chalfont, UK). The radioactive concentration of each hormone was 37 MBq/mL and had radiochemical purity greater than 98.5 %. Radiolabeled hormones were specifically used due to ease of detection and quantification using liquid scintillation counting (LSC).

Non-labelled estradiol, estrone, progesterone and testosterone (≥ 98 % purity) were purchased from Sigma Aldrich (Gillingham, UK). Stock solutions of the radiolabeled (100 µg/L) and non-labelled (990 mg/L and 1000 mg/L) hormones were prepared in analytical grade methanol (CH_3OH) (Fisher Scientific, Loughborough, UK). All trace organic stock solutions were stored in the dark < 4°C.

Radiolabeled ES was provided in solid form by Izotop (Budapest, Hungary). A stock solution (10 mg/L) was prepared in analytical grade ethanol (C_2H_5OH) (≥ 99.8 % purity; Fisher Scientific, Loughborough, UK). Intermediate stock solutions (100 µg/L) were prepared in CH_3OH. Radiolabeled ES was used due to ease of detection and quantification using LSC and the fact that an extraction prior to analysis was not needed. Non-labelled α-ES (99.6 % purity), β-ES (99.4 % purity), ES sulfate (97.3 % purity) and ES diol (99.8 % purity), used in experiments undertaken at Katholieke Universiteit Leuven (K.U. Leuven), were supplied in powder form from Sigma

Aldrich (Seelze, Germany). Stock solutions (100 mg/L) were made up in analytical grade CH_3OH obtained from Chem-Lab (Zedelgem, Belgium).

Non-labelled ES compounds used in experiments conducted at The University of Edinburgh were purchased from Sigma Aldrich (Gillingham, UK) but the different stock solutions (990 mg/L and 1000 mg/L) were prepared in analytical grade CH_3OH purchased from Fisher Scientific (Loughborough, UK).

Analytical grade dichloromethane (CH_2Cl_2), stabilised with amylene for residue analysis, and anhydrous Na_2SO_4, used in the extraction of the ES compounds from the samples, were obtained from Acros Organics (Belgium). Trifluralin (5 μL of 75 mg/L; 99.1 % purity), the extraction internal standard, was purchased from Reidel-de-Haën (Germany).

4.4 Organic Matter

Three different types of OM were selected for use; namely humic acid sodium salt (HA), tannic acid (TA) and alginic acid sodium salt (AA) were obtained from Sigma Aldrich (Gillingham, UK). Stock solutions (1L) of 100 mgC/L of HA, TA and AA were prepared in ultrapure water. The stock solutions were stored in the dark < 4°C. While the concentration of OM in treated wastewater and surface water is highly variable and can range from 0.2 to 30 mgC/L (Chefetz *et al.*, 2006; Frimmel, 1998), 12.5 mgC/L was used in all experiments containing OM.

4.5 Analytical Techniques

4.5.1 pH, Conductivity and Temperature

pH, electrical conductivity (EC, mS/cm) and temperature of feed and experimental samples were measured using a pH/Conductivity meter (Multiline P4 epoxy gel combination pH electrode, automatic temperature compensation immersion probe, WTW Germany). Conductivity readings that were taken during the desalination experiments, outlined in Section 4.9.1, were converted to NaCl concentration from eqn (4.1). Further details of this relationship are given in Appendix 1.

$$\mathrm{NaCl\,(mg/L)} = 1.87 \times \mathrm{EC\,(mS/cm)} \tag{4.1}$$

4.5.2 Ion-selective Electrodes

Fluoride and nitrate were potentiometrically determined using ion-selective electrodes (ISE's) in conjunction with a reference electrode (Ag/AgCl) connected to a Metrohm 781 Ion Meter (UK). Calibration standards of 0.1, 1, 5, 10, 25, 50, 100 and 150 mg N/L as nitrate were prepared from a 200 mg/L nitrate stock solution. Calibration standards of 0.1, 1, 5, 10, 25 and 50 mg/L fluoride were prepared from a 50 mg/L stock solution. The ISE's were regularly calibrated, with and without OM, and cleaning using standard methods. These standard methods and changes in ISE performance in the presence of OM are further described in Appendix 1. Standards and samples were mixed with a total ionic strength adjustment buffer (TISAB) to avoid possible interferences resulting from changes in solution pH and conductivity.

4.5.3 Nutrient Analysis

Nitrate sample analysis using a QuickChem 8500 FIA Nutrient analyser (Lachat Instruments, Colorado, USA), whereby nitrate was reduced to nitrite through a cadmium column, was utilised to cross check and analyse experimental samples for nitrate. Further details of this method are given in Appendix 1. Calibration standards of 0.2, 0.4, 1, 4, 8 and 20 mg N/L as nitrate were prepared from a 200 mg N/L stock solution. The detection limit was 0.01 mg N/L. Samples were chilled to 4°C and analysed within 48 hours.

4.5.4 Ion Chromatography

Anion analysis of samples taken during experiments outlined in Section 4.9.2 was undertaken using Ion chromatography (IC) (DX-500 ion chromatograph (DIONEX, USA). Separation was achieved using an IonPac AS4A-5C analytical column and a mobile phase composed of 1.7 mM sodium bicarbonate/1.8 mM sodium carbonate delivered at a flow rate of 2 mL/min. Post-column eluent suppression was achieved using an anion self-regenerating suppressor (ASRS-1) operated at a current of 50 mA. Detection was via an ED40 electrochemical detector set at an output range of 30 μS. Instrument control and data collection were accomplished using PeakNet software. Calibration standards of 1, 5, 10 and 25 mg/L were prepared from a multi-element stock solution of 100 mg/L.

4.5.5 Inductively-coupled Plasma Optical Emission Spectroscopy

Analysis of samples taken during experiments outlined in Section 4.9.2 were performed with Inductively-coupled Plasma Optical Emission Spectroscopy (ICP-OES) (Perkin Elmer Optima 5300 DV, Waltham, USA) to determine the concentration of cations in the mg/L concentration range. Calibration standards of 0.1, 1, 5 and 10 mg/L were prepared from a 1000 mg/L multi-element stock solution (Merck, Darmstadt, Germany). Samples were collected in polyethylene centrifugal tubes instead of borosilicate glassware sample bottles because of possible leaching of boron from the glassware. Prior to analysis samples were acidified with 1 % Aristar nitric acid (BDH Chemicals, supplied by VWR, Lutterworth, UK).

4.5.6 Inductively-coupled Plasma Atomic Mass Spectroscopy

Analysis of samples taken during experiments outlined in Section 4.9.2 were performed with Inductively-coupled Plasma Atomic Mass Spectroscopy (ICP-MS) (Agilent 7500ce, USA) to determine the concentration of cations in the μg/L concentration range. Sample collection and preparation prior to analysis was the same as employed for ICP-OES. Calibration standards of 0.5, 1, 2.5, 5, 10 and 100 μg/L were prepared from a 1 mg/L multi-element stock solution (Merck, Darmstadt, Germany).

4.5.7 Chemical Speciation Modelling

Speciation modeling of selected trace inorganic contaminants studied during real water experiments was conducted using the Visual MINTEQ (version 2.53) software package. Groundwater parameters were entered and 'sweep tests' were run based on component activity to determine the chemical speciation of the dominant ionic species over the studied solution pH range. Assumptions made include: a fixed carbonate concentration (partial pressure of 3.8×10^{-4} atm) and temperature (25°C), set valence states based on groundwater information and phase diagrams, and a charge difference between cations and anions ≤ 5 % (Richards *et al.*, 2009).

4.5.8 UV Absorbance and SUVA

OM absorbance was measured using a Cary 100 Scan UV-Visible spectrophotometer (UV-Vis) (Palo Alto, USA). Specific OMs show definitive UV absorbance bands reflecting their particular saturation pattern and aromatic components. Absorbance of HA and TA were analyzed at wavelengths of 254 and 275 nm, respectively. AA absorbance measurements by UV-Vis were not possible due to its lack of aromatic functional groups. Calibration standards of 0.1, 0.5, 1, 5, 7, 10, 12.5, 20, 50, 70, 80 and 100 mgC/L were prepared from 100 mgC/L stock solutions of each OM studied. Experimental samples were measured immediately after collection and prior to refrigeration to avoid possible changes due to coagulation or precipitation. For each sample (3.5 mL), 4 replicate measurements were performed. Further details of the measurement parameters and calibration of OM by UV-Vis are given in Appendix 1.

Specific UV absorbance (SUVA), which is an indication of aromaticity (Wang and Hsieh, 2001), was calculated for HA. SUVA values correspond to the ratio between UV absorbance at 254 nm and dissolved organic carbon (DOC) concentration as given by eqn (4.2).

$$\text{SUVA (L/mg.m)} = \frac{\text{UV Abs (1/cm)}}{\text{DOC (mgC/L)}} \tag{4.2}$$

4.5.9 Total Organic Carbon Analysis

OM concentrations in samples containing HA, TA and AA were determined using a total organic carbon (TOC) analyser (Shimadzu TOC-VCPH, Milton Keyes, UK). Analysis was conducted in non-purgeable organic carbon mode (NPOC) and the samples were acidified using 2 M HCl acid and sparged for 2 min to remove inorganic carbon prior to injection. TOC analysis is not without its limitations (e.g. oxidation efficiency of different OM), which are further discussed in Appendix 1.

4.5.10 Liquid Scintillation Counting

Radiolabeled hormone concentration in samples and calibration standards were analysed using a Beckman Coulter scintillation counter (LS 6500, Fullerton, USA). A 0.5 mL sample was added to scintillation vials along with 3.5 mL Ultima Gold® scintillation cocktail (Perkin Elmer, Waltham, USA). Each sample and/or standard was shaken to allow complete mixing and then counted for 10 minutes (3 replicates).

Calibration standards of 0.01, 0.1, 1, 10, 100 and 1000 ng/L were prepared from a 100 μg/L radiolabeled hormone stock solution. The detection limits for estradiol, estrone, progesterone and testosterone were 1.02, 1.11, 1.03 and 1.07 ng/L.

Radiolabeled ES was analysed using a Beckman Coulter scintillation counter (LS 6500, Fullerton, USA). A 1 mL sample was added to scintillation vials along with 7 mL Ultima Gold® scintillation cocktail (Perkin Elmer, Waltham, USA). Each sample was shaken to allow complete mixing and then counted for 20 minutes (3 replicates). Calibration standards of 0.01, 0.1, 1, 10, 100, 1000, 2000 and 5000 ng/L were prepared from a 100 μg/L radiolabeled ES stock solution. The detection limit of radiolabeled ES was 100 ng/L. Further details regarding LSC and the analysis of steroidal hormones and ES are given in Appendix 1.

4.5.11 Gas Chromatography-Electron Capture Detection

Pesticide experiments undertaken at K.U. Leuven used unlabeled ES. The trace analysis of ES in water required sample pre-treatment which consisted of an extraction, isolation, and concentration step (liquid-liquid extraction, LLE), before quantitative analysis and determination via chromatographic analysis using Gas-Chromatography-Electron Capture Detection (GC-ECD), which is a widely used analytical technique for determining low μg/L and ng/L levels of ES. Further details of the LLE procedure are outlined in Appendix 1. A Perkin Elmer Autosystem XL gas chromatograph equipped with an electron-capture detector (ECD) was used for the determination of ES compounds in the extracted samples. Quantitation of the ES compounds was made from the injection of standard solutions (10-2500 μg/L). Further details of gas chromatographic analysis including details on the column used, determined extraction efficiencies and interferences are given in Appendix 1.

4.5.12 Contact Angle Measurement

The contact angle (θ) of a membrane gives an indication of the hydrophobicity and wettability of the membrane. The greater the contact angle the more hydrophobic the membrane (Nghiem, 2005), as shown in Figure 4.1. Surface structural characteristics of the membranes (e.g. roughness) as well as hydration will influence the contact angle. Contact angle measurements of an unused AEM and CEM (given in Section

4.7) were undertaken using an FM40 EasyDrop Contact Angle measuring instrument (Krüss, Hamburg, Germany). The medium used was ultrapure water. The method employed was the sessile drop method whereby the angle between the water droplet surface and the membranes was measured using a light microscope. The contact angles of the AEM and CEM were 69.9 ± 3.4º and 61.8 ± 5.1º, respectively. The AEM contact angle found in this study is in good agreement with those reported by Lee *et al*. (2002a) (66-70º). No studies have been published on the contact angle for the CEM. Further details of this method are outlined in Appendix 1.

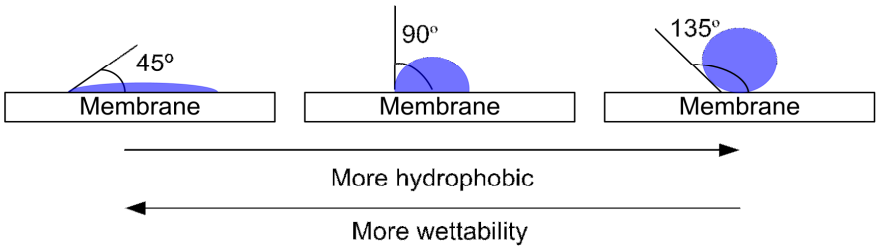

Figure 4.1. Contact angle (θ) and membrane hydrophobicity and wettability (adapted from (Nghiem, 2005).

4.5.13 Membrane Zeta Potential Measurement

The isoelectric points of the ion-exchange membranes was undertaking by measuring the streaming potential with an electrokinetic analyser EKA (Anton Paar KG, Gratz, Austria) equipped with an autotitrator for pH adjustment (VWR, Germany), rectangular measuring cell and Ag/AgCl-electrodes (SE 4.2, Sensortechnik Meinsburg, Waldheim, Germany). The membranes were rinsed and soaked in ultrapure water 24 hours prior to measurement. The membranes were soaked in the electrolyte solute (1mM $NaHCO_3$, 20 mM NaCl) for 30 minutes. The pH of the electrolyte solution was adjusted automatically with 1 M HCl or KOH. Six measurements were taken for each pH value and all measurements were performed at room temperature (approximately 21°C).

4.5.14 Optical Microscopy

Photographs of used and unused membranes were taken at a range from 100× to 200× magnification on an Axioskop 2 MAT optical microscope equipped with a colour camera (AxioCam MRc5) (Zeiss Optical, Thornwood, USA). The images were processed with Axiovision Rel. 4.7 image capture software. The microscope

light source was placed under the membrane. Due to the translucent nature of the membranes, both sides of the used membrane could be seen simultaneously on the same photograph.

4.5.15 Focused Ion Beam–Scanning Electron Microscopy and Energy Dispersive X-Ray Spectroscopy

Used and unused membranes were analysed using focused ion beam-scanning electron microscopy coupled (FIB-SEM) coupled with energy dispersive x-ray spectroscopy (EDX). Membrane samples were mounted edge on an aluminium stub using a "Tissue-Tek" low temperature-mounting compound mixed with colloidal graphite. Samples were cryogenically fixed by plunging into "slushed" nitrogen (liquid nitrogen that was first pumped under vacuum until solidifying) and then vented under dry nitrogen. Frozen samples were transferred to a PP2000T cryo-transfer system (Quorum Technologies, Ringmer, UK) for initial observation and cryo-fracture where appropriate. Initial samples were freeze fractured, but this resulted in a very shattered edge rather than a clean break. Therefore, samples were cut with a scalpel before mounting. Analysis in the FIB-SEM (FEI Quanta 2003D, Hillsboro, USA) was carried out on a sample stage cooled to -140 ºC. Secondary electron imaging was carried out at 1kV, 3.1nA and 15kV, 3.9nA. Elemental analysis of the membrane surface and cross-sections using EDX (Oxford Instruments INCAx-sight, Abingdon, UK) was carried out at 15kV, 3.9nA. Ion beam-induced secondary electron imaging was carried out with a 30kV with a 10 pA incident beam. Ion beam milling at high current (30kV, 20nA) was found to be insufficient to remove significant amounts of membrane material at the 100+ μm scale.

4.5.16 Solid-State Nuclear Magnetic Resonance

Membranes exposed to OM were analysed using solid-state ^{13}C cross-polarisation magic-angle spinning (CPMAS) nuclear magnetic resonance (NMR) (Durham University, Department of Chemistry). Solid-state ^{13}C NMR is a spectroscopic technique which can quantify carbon functional groups (e.g. aromatic, carbohydrate and aliphatic). A Varian VNMRS spectrophotometer (Palo Alto, USA) was operated at 100.56 MHz with a 6 mm rotor probe to obtain the ^{13}C spectra. Membrane samples were selected from the AEM and CEM positioned closest to the cathode within the

ED stack. Each membrane sample was cut into small 1-2mm squares before adding to the rotor. Spectral referencing was with respect to tetramethylsilane (internal standard).

4.6 Electrodialysis System and Stack

All ED experiments were carried out using a commercial laboratory ED stack (BEL-500 unit, Berghof, Germany). A photograph of the ED system is shown in Figure 4.2. The ED stack was connected to a DC electric potential (GW Instek DC Power supply Model GPR-1810HD, Taiwan) through TiO_2-coated titanium electrodes. The diluate, concentrate and electrode rinse streams were recirculated through the ED stack using peristaltic pumps (Diluate and concentrate: Masterflex 77601-10 Easy-load I/P pump heads; Electrode rinse: Masterflex 77800-62 Easy-load L/S pump head, Cole Palmer, USA). Recirculation flow rates in all compartments were set at the necessary rate, as specified in experimental protocol (Section 4.9) (Diluate and concentrate: Masterflex I/P Variable speed pump system; Electrode rinse: Masterflex L/S economy analogue pump drive, Cole Palmer, USA).

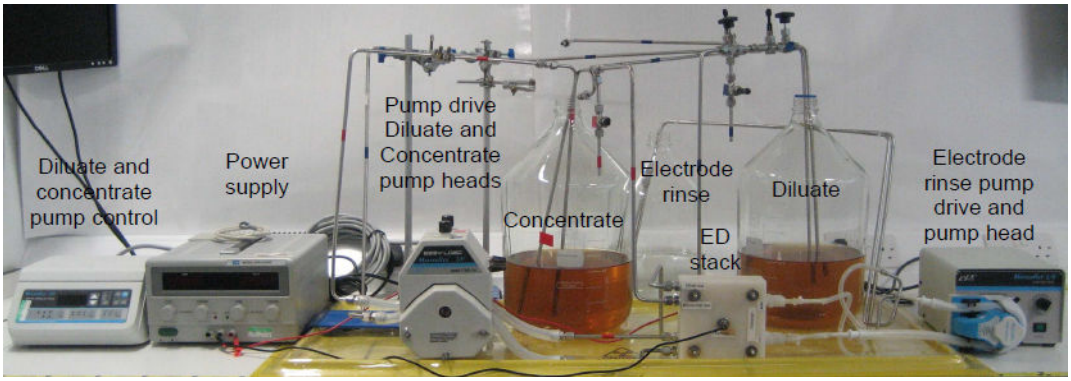

Figure 4.2. Electrodialysis system layout with pump control, power supply, pump, ED stack and three containers with diluate, concentrate and electrode rinse.

Figure 4.3 is a schematic representation of the ED system showing batch (A) and continuous (B) operation modes. The diluate, concentrate and electrode rinse lines were originally silicon tubing (Masterflex L/S 96410-16); however, these were changed to stainless steel to avoid possible sorption of trace organics. Silicon (platinum-cured) tubing was used in the pump heads (Diluate and concentrate: Masterflex L/S 96410-73; Electrode rinse: Masterflex L/S 96410-36, Cole Palmer,

USA). In batch ED experiments, the feed solution was added to the diluate and concentrate borosilicate glass containers (4L each). The diluate, concentrate and electrode rinse were pumped through the ED stack using peristaltic pumps until the desired product (0.5 g/L NaCl) within the diluate was achieved. During continuous ED experiments, the feed solution (diluate and concentrate combined, 4L) was recirculated through the stack into a single container. Samples were taken from the diluate and concentrate outlets as well as from within the diluate and concentrate containers.

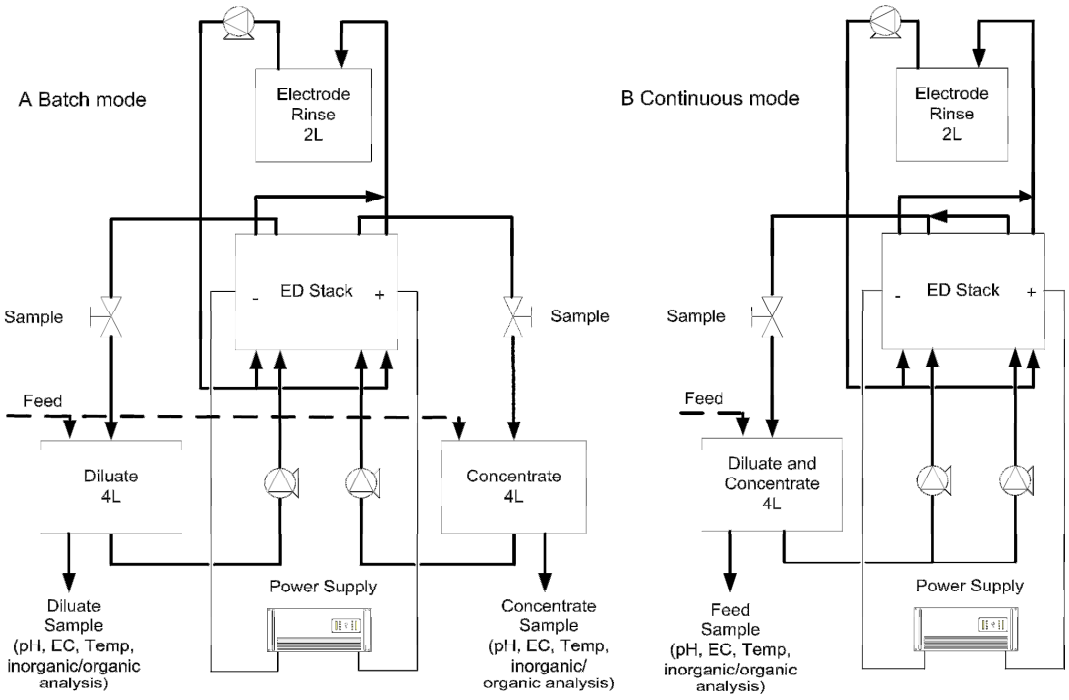

Figure 4.3. Schematic of Electrodialysis System and (A) batch and (B) continuous operation modes.

The ED stack was equipped with six Neosepta® AMX-SB AEMs and seven Neosepta® CMX-SB CEMs (i.e. 6 cell pairs) as further described in Section 4.7. The different components of the ED stack are shown in Figure 4.4. Spacers (Berghof, Germany) were used to provide the pathway for solution flow. They aid in keeping even velocity distribution within the ED system and promote turbulence, which reduces concentration polarisation. Spacer thickness is typically between 0.5 to 2 mm (Strathmann, 2004). In a sheet-flow ED stack the solution flow is approximately in a straight path from the entrance of the stack to the exit ports, which are located on

opposite sides in the spacer gasket (Figure 4.4D). It is recommended that the distance between each membrane, i.e. the cell thickness, should be as small as possible to maintain energy consumption due to electrical resistance of the solutions within the ED stack as low as possible. The most serious design problem for an ED stack is that of assuring uniform flow distribution in the various compartments and good mixing of the solutions in the stack at low pressure losses.

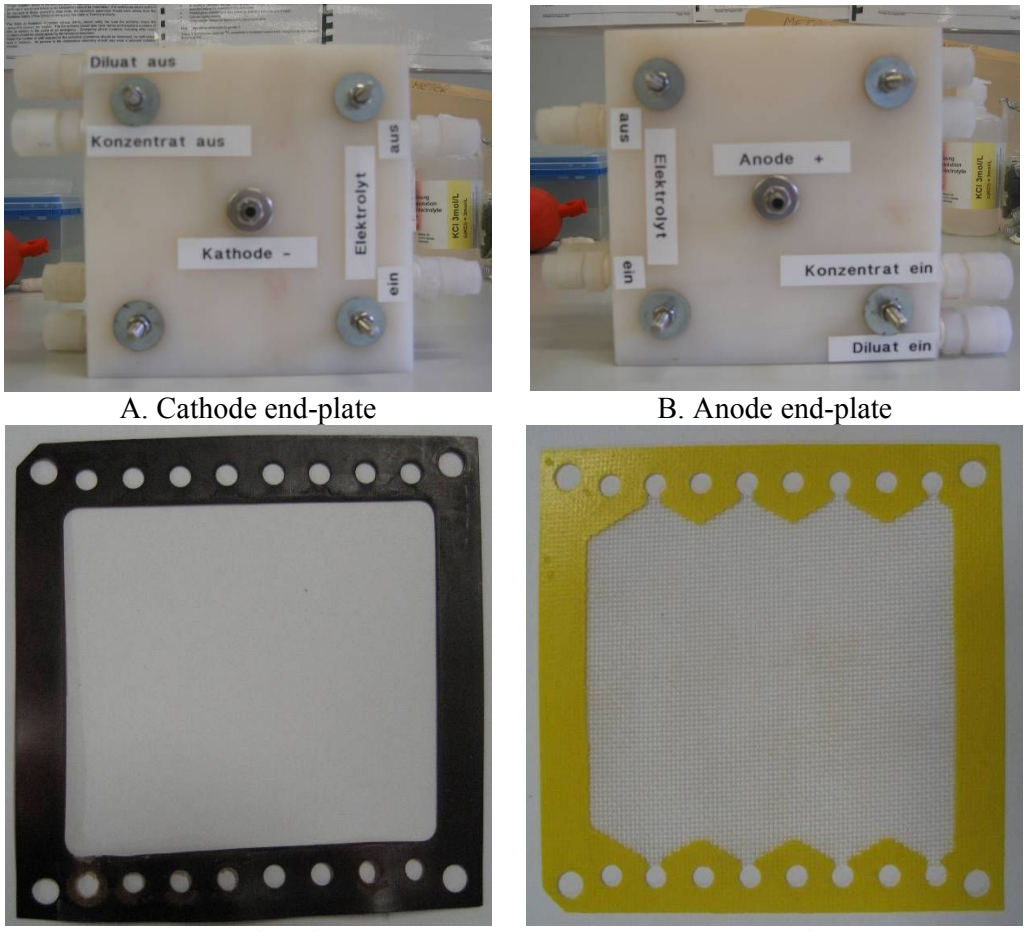

A. Cathode end-plate B. Anode end-plate

C. End seal D. Integrated spacer

Figure 4.4. Electrodialysis stack components (cathode and anode end-plates, end seal and integrated spacer gasket).

Figure 4.5 shows a schematic diagram of the ED stack arrangement consisting of the series of AEMs and CEMs arranged in an alternating pattern between the anode and a cathode to form individual cells. The ED stack is composed of two end-plates containing the negative cathode (A) and positive anode (B). Insulated pilot pins were placed through the cathode end-plate along with an end seal (C). The first membrane

was added (CEM) followed by an integrated silicone and polyester mesh spacer (D) and AEM and another integrated spacer. The total space occupied between two adjoining membranes next to the diluate compartment, and the two adjoining AEM and CEM make up a cell pair. This step was repeated until the appropriate amounts of cation- and anion-exchange membranes were added. The stack ends with a CEM adjacent to the anode to provide protection of the electrodes and prevent ions migrating into the diluate stream. The electrode rinse provides protection to the membranes from precipitation. Sodium sulphate (Na_2SO_4) is used as an electrode rinse instead of NaCl so that Cl^- gas is not generated during the ED process. Another end seal was added before the anode end-plate. The insulated pilot pins were tightened uniformly crosswise using calipers so that the end-plates were parallel to each other. This was an important step to reduce any possible leakage currents within the stack.

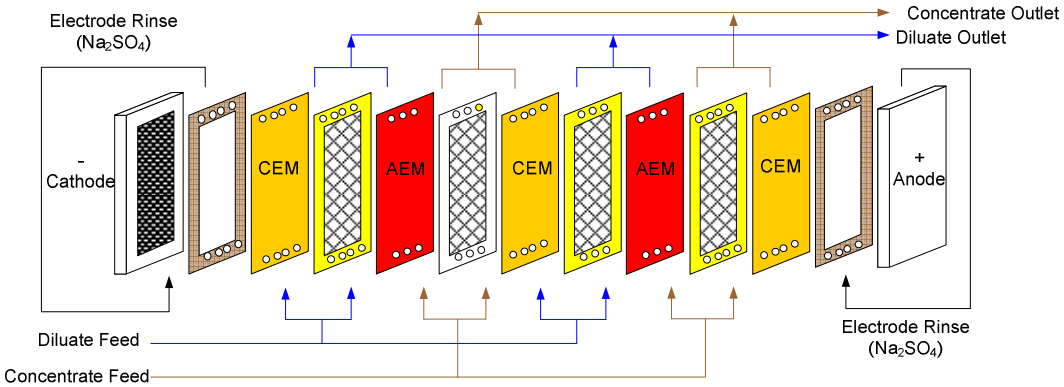

Figure 4.5. Schematic drawing of an electrodialysis stack arrangement with cation- and anion-exchange membranes in alternating series between two electrodes (Adapted from Strathmann (2004)).

Recirculation flow rates in the diluate, concentrate and electrode rinse streams were checked before each ED experiment. Each stream was collected in a graduated cylinder. The time t (s) needed to obtain 1L volume was measured and the flow rate Q (L/min) was calculated using eqn (4.3).

$$Q = \frac{1}{\left(t/60\right)} \tag{4.3}$$

If the recorded flow rates were too fast or slow, pump head occlusion pressure adjustments (tighten or loosen) were made to obtain the correct flow rate. Occlusion controls the squeezing of the peristaltic pump tubing between the pump head rollers and the tubing. The ED stack was periodically dismounted and the integrated spacers were cleaned with ultrapure water to remove any built-up residues within the mesh near the inlet and outlet holes.

4.7 Electrodialysis Membranes

While the first use of ED as a separation process occurred in 1903 (Morse and Pierce, 1903), early membranes used in ED systems were uncharged and therefore not selective (Prausnitz and Reiststotter, 1931). The first studies on ion-exchange membranes were conducted in 1925 by Michaelis *et al*. (1925). It wasn't until after the 1940s that interest in the development of more sophisticated and effective membranes occurred (Haagen and Helfferich, 1959). The development of high-productivity, temperature and chemically stable membranes has created greater opportunities to remove different substances from a solution, as well as selective separation of single components from a mixture (Grebenyuk *et al.*, 1998).

The membranes used in an ED stack are either made from a 50-75 % by volume mixture of a powdered ion-exchange resin (size of particles dependent on manufacturer) and a polymer matrix such as polypropylene or polystyrene or by block polymerisation/block condensation of polyelectrolytes. A common example of an ion-exchange membrane is sulfonated polystyrene cross-linked with divinylbenzene. The utilisation of polystyrene divinylbenzene copolymers (PS-DVB) as starting materials for ion-exchange membranes lies in the reactivity of the aromatic rings for the reactions of sulfonation, nitration and chloromethylation which leads to either strong acids and strong and weak bases (Kesting, 1985). Since a sufficient capacity for membrane swelling in water is essential for the ion transfer, the degree of polymer cross-linking in the polymerisation/polycondensation process has to be carefully controlled (Rautenbach and Albrecht, 1989). Membranes with high cross-linking are harder and more stable, however, the diffusion within these membranes tend to be slower (Zagorodni, 2006).

Functional groups (or ion-transfer sites) are added to the membranes with the site charge differing between AEMs and CEMs to allow each type to selectively pass either anions or cations. There is a diverse range of functional groups with differing exchanging properties that can be attached to a membrane depending on the application the membrane is utilised for. Common anionic functional groups include weak and strong base nitrogen containing groups such as strong-base quaternary ammonium ($-N^{+}(CH_3)_3$), tertiary sulphonium ($-S^{+}$) and quaternary phosphonium ($-P^{+}$). Common cationic functional groups are sulphonic ($-SO_3^{-}$), carboxylic ($-COO^{-}$), phosphoric ($-PO_3H_2$) and carboxylic acid ($-COO^{-}$) (Xu, 2005; Zagorodni, 2006). Ion-exchange membranes are categorised as either homogenous or heterogeneous, with homogenous the most widely used (Kariduraganavar *et al.*, 2006). In homogenous membranes the functional groups are chemically bonded to and distributed uniformly throughout the membrane matrix, whereas in heterogeneous membranes the functional groups are mixed with and dispersed at distinct points within the membrane matrix.

Table 4.2 outlines a number of current major manufacturers of ion-exchange membranes available worldwide. The major commercially used membranes are Nafion® (Dupont), Aciplex (Asahi Kasei Chemicals Co.) and Flemion (Asahi Glass Co. Ltd.) (Savari *et al.*, 2008). Typically each ED system membrane manufacturer produces membranes tailored to a specific application and equipment utilised.

Two types of commercially available ion-exchange membranes were selected for use in this study: Neosepta® AMX-SB (AEM) and Neosepta® CMX-SB (CEM) (supplied by Eurodia, Germany; manufactured by ASTOM Corporation, Japan). The membranes contain sulfonic acid (SO_3H, CEM) and alkylammonium ($N(CH_3)_3$, AEM) ion-exchange groups attached to the aromatic rings of a PS-DVB matrix on a microporous polyvinyl chloride (PVC) gel supported by plasticized PVC cloth (Krol, 1997; Park *et al.*, 2006). A polymer mesh additionally reinforces the membranes. PS-DVB membranes are classified according to their mechanisms: sieving of ions with changing cross linking, the effect of charge and resultant electrostatic repulsion on ion permselectivity, and specific interaction between the specific ion-exchange groups, membrane matrix and ions (Kariduraganavar *et al.*, 2006). The chemical structure of the ion-exchange membranes is illustrated in Figure 4.6.

Table 4.2. Manufacturers of commercially available ion-exchange membranes and relevant membrane information.

Manufacturer	Membrane	Type	Polymer	Application
Asahi Glass Co. Ltd., Japan	Selemion®: AMV, ASV, DSV	AEM	Polystyrene-divinylbenzene	ED, diffusion dialysis
	CMV	CEM	Polystyrene-divinylbenzene	
	Flemion	-	Polytetrafluorethylene	Fuel cells
Asahi Kasei Chemicals Co., Japan	Aciplex®: A192, 501SB, A201, A221	AEM	Polytetrafluorethylene	Desalination, Diffusion dialysis
	K-192, 501SB	CEM	Polytetrafluorethylene	
Astom Corporation, Japan	Neosepta® Standard Grade: AMX	AEM	Polystyrene-divinylbenzene	Concentration, desalination
	CMX	CEM	Polystyrene-divinylbenzene	
	Neosepta® Special Grade: AHA, ACM, ACS, AFN, AFX	AEM	Polystyrene-divinylbenzene	Diffusion dialysis, ED, alkali removal, pharmaceutical purification
	CIMS, CMB	CEM	Polystyrene-divinylbenzene	
	Neosepta® Bipolar Membrane: BP-1E	BP		
Dupont, Worldwide	Nafion®: 112, 115, 117	CEM	Polytetrafluorethylene	Chloro-alkali production, fuel cells
Fumatech, Germany	Fumasep: FAS, FAB, FAN, FAA, FAD	AEM	Polytetrafluorethylene	ED, acid concentration, fuel cells
	FKS, FKB, FK-40, FKD	CEM	Polytetrafluorethylene	
Ionics Inc., USA (now part of GE Water)	AR103QDP, AR204SZRA, AR112-B	AEM	Polystyrene-divinylbenzene	ED, whey purification
	CR61-CMP, CR67-HMR	CEM	Polystyrene-divinylbenzene	EDR, whey purification
Mega a.s., Czech Republic	Ralex®: AM(H), AMH5E-HD	AEM	Polyethylene	ED, EDI, Cataphoresis
	CM(H), CMH5E-PM	CEM	Polyethylene	ED, EDI, Anaphoresis
Solvay S.A., Belgium	Morgane®: ADP, ADW	AEM	Fluorinated	ED, acid concentration
	CDS, CRA	CEM		Concentration, desalination
Sybron Chemicals Inc., USA	Ionac®: MA-3475, MA-7500	AEM	Polystyrene-divinylbenzene	Acid concentration, metal recovery
	MC-2470	CEM	Polystyrene-divinylbenzene	

Refs: Asahi Glass Co Ltd (2009), Asahi Kasei Chemicals Co. (2009), Astom Corporation (2009), Ge Water (2009), Mega (2009), Solvay S.A. (2009), Sybron Chemicals Inc (2009) and Xu (2005).

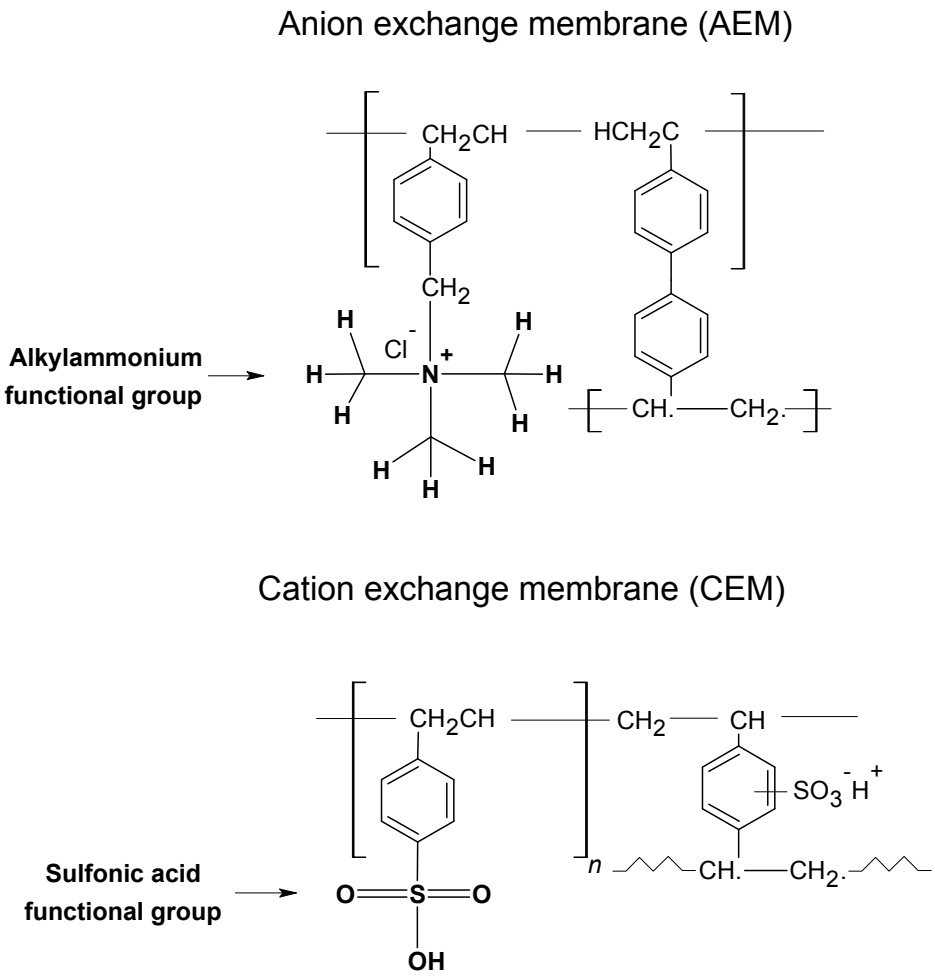

Figure 4.6. Chemical structure of the Neosepta® AMX-SB anion- and CMX-SB cation-exchange membranes.

The Neosepta® ion-exchange membranes are prepared from a paste that consists of a monomer with the appropriate functional group, DVB as the cross-linking agent, a polymerisation initiator and powdered PVC. This paste is coated onto a PVC cloth as reinforcing material, the monomers are copolymerised and either sulfonated or aminated to produce the ion-exchange membranes with sulfonic acid (SO_3H) or alkylammonium groups ($N(CH_3)_3$) (Kariduraganavar *et al.*, 2006). Sulfonation is primarily in the para position (tied to a benzene ring in the position 1 and 4). After displacement of excess acid, the membranes are converted to sodium form by neutralisation with a slight excess of alkali (Kesting, 1985). Photographs (Figure 4.7) taken using optical microscopy and focused ion beam–scanning electron microscopy (FIB-SEM) (described in Sections 4.5.13 and 4.5.15, respectively) show the

characteristic woven structure of the membranes with approximately 15 µm membrane fibres observed (Figure 4.7D inset).

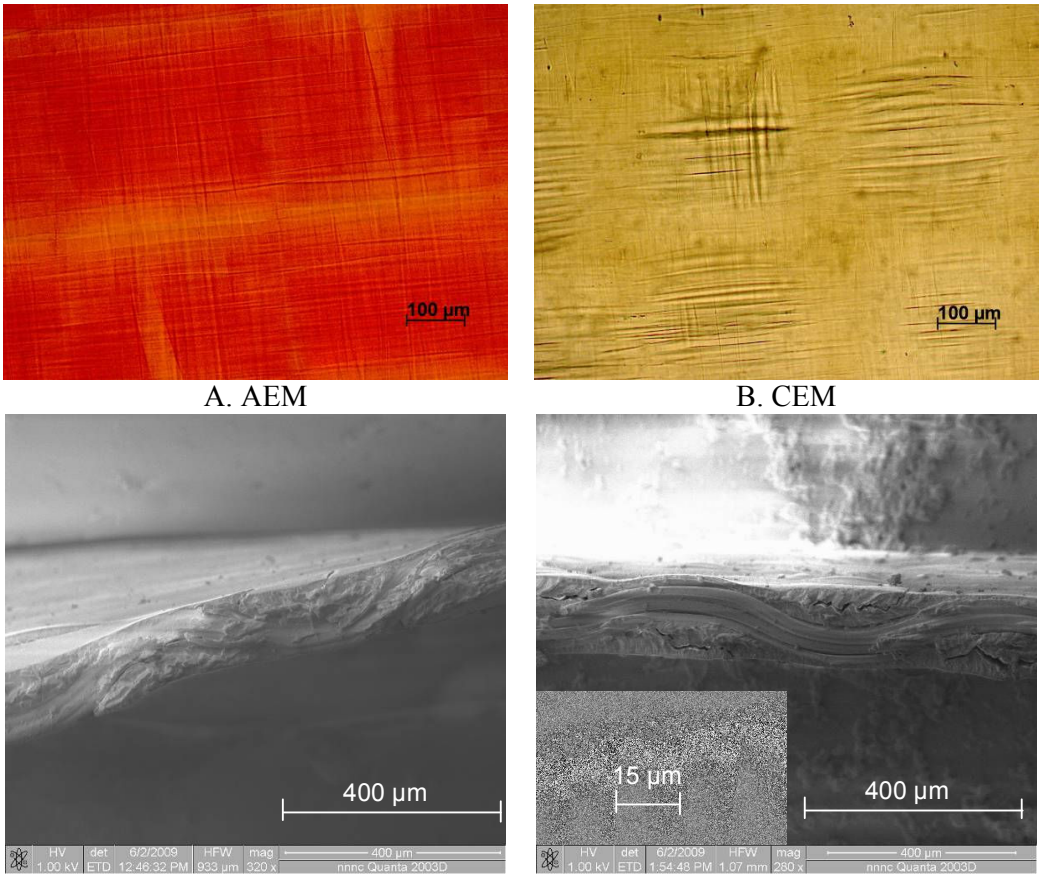

A. AEM B. CEM

C. AEM D. CEM

Figure 4.7. Top view of an unused (A) AMX-SB AEM and (B) CMX-SB CEM (Axioskop 2 MAT, Zeiss Optical, UK, Optical zoom 100×) and cross-section view of (C) AMX-SB AEM and (D) CMX-SB CEM (FEI Quanta 2003D, USA).

Elemental analysis of the unused ion-exchange membranes using FIB-SEM coupled with Energy dispersive x-ray spectroscopy (EDX) was undertaken. The peak of chloride (Cl) on both sides of the AEM (Figure 4.8A) corresponds to the chloromethylation of the benzene rings on the linear PS membrane matrix. The presence of sulfur (S) through the CEM (Figure 4.8B) corresponds to the SO_3H functional group.

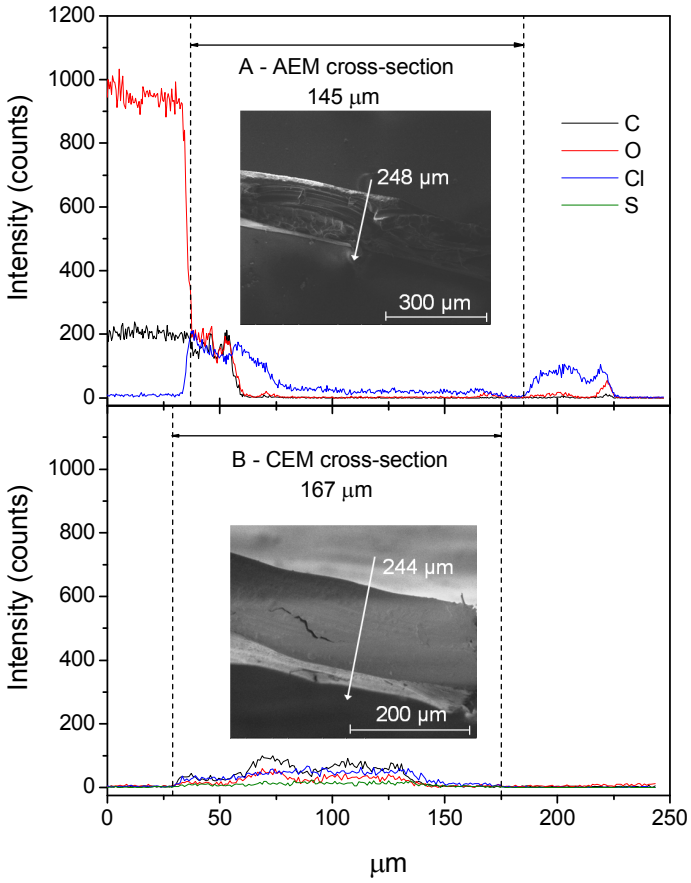

Figure 4.8. Cross-sectional EDX profile of unused (A) AEM and (B) CEM (15 kV beam energy). Inset cross-section FIB-SEM images of (A) AEM and (B) CEM (15 and 1 kV beam energy, respectively; 200 and 700 × magnification, respectively; white arrow indicates direction of EDX profile).

Essential requirements for ion-exchange membranes are a high permselectivity, low electrical resistance and high chemical, thermal, mechanical stability and form stability, low cost and low diffusion of water. In regards to permselectivity, a membrane must be permeable to counter-ions and impermeable to co-ions. Good mechanical and form stability means that the membrane has a low degree of swelling and/or shrinking. To minimize electrical energy requirements, the membranes should have the lowest possible electrical resistances possible. Thin membranes with high water contents are desirable to achieve low electrical resistances; however, in the development and/or the selection of ion-exchange membranes compromises are essential. The Neosepta AMX-SB and CMX-SB membranes have excellent characteristic properties, namely good low electric resistance, high permselectivity,

high ion-exchange capacity compared to other available membranes (e.g. meq/g dry membrane: 0.9 (MA-3475, Sybron Chemicals), 0.8-1.0 (Nafion-112)), dimensional, thermal and chemical stability in a wide range of pH with resistance against many aggressive chemicals as well as easy handling. The most important characteristics and properties of the membranes are summarised in Table 4.3.

Table 4.3. Characteristics and properties of the anion (AEM) and cation (CEM) exchange membranes as specified by the membrane manufacturer.

Grade	AMX-SB (AEM)	CMX-SB (CEM)
Type	Strongly basic Anion permeable	Strongly acidic Cation permeable
Polymer material	Polystyrene divinylbenzene	Polystyrene divinylbenzene
Functional group	$N(CH_3)_3$	SO_3H
Characteristics	High mechanical strength (Cl-form)	High mechanical strength (Na-form)
Electric Resistance [a] (Ω cm^2)	2.0-3.5	1.8-3.8
Burst Strength (MPa) [b]	0.30	$\geq$ 0.40
Thickness (mm)	0.14	0.17
Volume during ED (cm^3)	4.9	6.9
Exchange capacity (meq/g dry membrane)	1.4-1.7	1.5-1.8
Transport number for Na^+	0.98 <	0.98 <
Water content [a] (g H_2O/g dry membrane)	0.25-0.30	0.25-0.30
Contact angle (θ) [c]	69.9 ± 3.4	61.8 ± 5.1
Chemical Resistance (slightly attacked)	Caustic soda, Ammonia, dioxane	Acetone, dioxane, phenol
Chemical Resistance (attacked)	strong oxidising agent	strong oxidising agent

[a] Equilibrated with 0.5 M-NaCl solution at 25°C; [b] Burst strength measured by a Mullen Burst Strength device; [c] Determined in this study using sessile-drop technique (Section 4.5.12). Data derived from manufacturer fact sheet (Astom Corporation, 2009) and Park *et al*., (2006).

Zeta potential analysis undertaken on the membranes is shown in Figure 4.9. The isoelectric points of the membranes were determined to be 3.35 and 3.12 for the AEM and CEM, respectively.

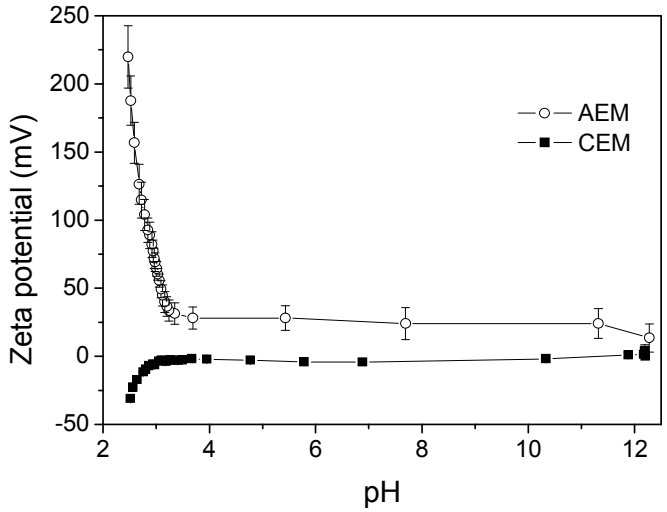

Figure 4.9. Zeta potential of the ion-exchange membranes (Background electrolyte: 1mM $NaHCO_3$, 20 mM NaCl).

To reduce the impacts of membrane fouling and, therefore, maintain the performance of the ED stack and the ion-exchange membranes, it should be flushed regularly with a solution of about 0.1 M alkali (1.0 wt % NaOH), acid solution (0.35 wt % HCl), and distilled water. The rinses are preferably performed under an electric current in the direction opposite to that used in ED. If the stack has been operated under daily current reversal, the current for de-fouling should be applied in both directions.

The dimensions of the membranes used in the ED stack were 10 × 10 cm with an A_{eff} of 58 cm^2 each. The total area and volume of membrane used in the ED stack was 1392 cm^2 and 11.8 cm^3, respectively. The ion-exchange membranes were provided in individual 0.5 × 0.5 m sheets. Each sheet was cut into 10 × 10 cm pieces. A stainless steel template (manufactured by the engineering workshop) and sharp pilot pins (Figure 4.10) were used to make holes in the membranes corresponding to the inlet and outlet holes on the ED stack end-plates. The membranes were handled carefully, kept flat, stored in a solution of 0.5 M NaCl and refrigerated according to manufacturers instructions (Astom Corporation, 2009). Before use, each membrane was washed briefly with ultrapure water.

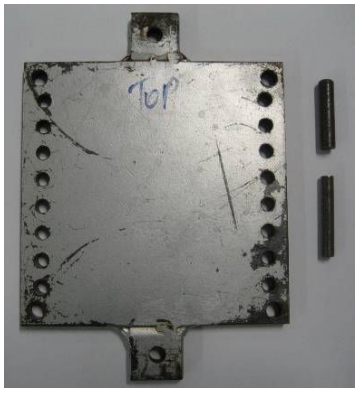

Figure 4.10. Stainless steel template used for cutting inlet and outlet holes in ion-exchange membranes.

4.8 Limiting Current Density Determination

ED systems are operated under limiting current conditions because operating above the LCD (i_{lim}, mA/cm^2) can lead to energy losses within the system along with water dissociation, resultant pH changes and membrane damage. It is, therefore, essential to assess the LCD for an individual ED stack to maximise the overall current efficiency. LCD depends on membrane and solution properties as well as operational parameters such as flow rate. Therefore, two LCD experiments corresponding to the flow rates used during this study (1.5 and 3 L/min) were undertaken. As LCD is usually determined for the conditions at the end of the process i.e. lowest product concentration, a feed concentration of 0.5 g/L NaCl was used.

For the determination of the LCD of the BEL-500 ED stack, the ED system was run in continuous operation mode (Figure 4.3). The purpose of this was to keep a constant feed NaCl concentration and to allow accurate voltage drop readings. The flow rate for the electrode rinse was 1.5 L/min in all ED experiments undertaken during this study. The applied current was increased incrementally (30 mA). After each increase in the current, the system was allowed to reach steady-state conditions (approximately 1 minute) before the voltage was recorded. The pH of the diluate, concentrate and electrode rinse was continuously monitored for changes. For each LCD experiment, the theoretical LCD was determined using eqn (2.23), eqn (2.25), and the diluate NaCl concentration in each experimental sample and the parameters given in Table 4.4.

Table 4.4. Parameters used in the theoretical determination of the limiting current density (LCD).

Parameter	Unit	Stack flow rate (L/min)	
		1.5	3
Linear flow velocity, v	m/s	0.08	0.16
Valence, *z*	equiv/mol	1	1
Kinematic viscosity, ν	m^2/s	9.4×10^{-7}	9.4×10^{-7}
Faraday constant, *F*	C/mol	96500	96500
Diffusion coefficient, D_s	m^2/s	1.67×10^{-9}	1.67×10^{-9}
Membrane spacer distance, *h*	cm	0.06	0.06
Spacer mesh width, ΔL	cm	0.24	0.24
Reynolds number, *Re* [a]	-	52.1	104.3
Schmidt number, *Sc* [a]	-	562.9	562.9
Sherwood number, *Sh* [a]	-	29.8	42.1

[a] Reynolds, Schmidt and Sherwood number calculated using eqn (2.27), eqn (2.26) and eqn (2.25) respectively.

4.9 Experimental Protocols

4.9.1 Desalination Kinetics

Desalination experiments were undertaken to determine the optimum operating conditions of the ED system. Applied voltage and feed salt concentration were varied to determine the performance of the ED system as a function of applied voltage and to investigate the scope of ED for a range of groundwater salinities, as outlined in Table 4.5. The ED system was operated in batch mode (Figure 4.3) whereby the diluate and concentrate were recirculated through the ED stack at a flow rate of 3 L/min until the desired diluate product was achieved (0.5 g/L NaCl). The pH, EC and temperature of the diluate and concentrate were continuously monitored throughout each experiment at 10 minute intervals.

Table 4.5. Desalination kinetics experimental outline.

Applied Voltage (V)	Feed NaCl concentration (g/L)
9	5, 10
12	1, 5, 10, 20, 25, 35
18	5, 10

Removal of NaCl (R_D, %) from the diluate was calculated using eqn (4.4).

$$R_D = \left(1 - \frac{C_D^t}{C_D^0}\right) \times 100 \tag{4.4}$$

where C_D^0 is the initial (superscript 0) diluate concentration (mg/L) and C_D^t is the diluate concentration (mg/L) in the ED time period *t* (h).

Standard deviation (S.D.) of R_D was calculated using eqn (4.5) and presented as ± S.D.

$$s = \sqrt{\sum_i \left(x_i - \bar{x}\right)^2 / \left(n-1\right)} \tag{4.5}$$

where *s* is the standard deviation, x_i is the sample value, $\bar{x}$ is the sample mean and *n* is the number of samples taking during experiments.

The flux of NaCl (g/m^{2}h) across the membranes was calculated using eqn (4.6).

$$J = \frac{1}{A_{\text{trans}}} \frac{\mathrm{d}m_C}{\mathrm{d}t} \tag{4.6}$$

where m_C is the concentrate mass (g) in the time period *t* (h) and A_{trans} is the ED stack membrane area (m^2) used in the transport of NaCl (i.e. $A_{trans} = A_{eff} \times 6$ AEMs and 7 CEMs = 0.0754 m^2).

4.9.2 Inorganic Contaminant Removal

The removal of the inorganic trace contaminants boron, fluoride and nitrate from aqueous solutions in the absence and presence of OM (12.5 mgC/L) using ED was investigated as a function of solution pH. The ED system was operated in batch desalination mode and the diluate and concentrate were recirculated through the ED stack at a flow rate of 1.5 L/min until the desired diluate product was achieved (0.5 g/L NaCl; 140 min). Concentrate and diluate pH was maintained constant (see Section 4.1). EC of both solutions were continuously monitored and samples (50 mL) were collected at the beginning and at 20 minute intervals for analyses of boron, fluoride and nitrate. Confirmation of the concentration of OM in the diluate and concentrate was undertaken by UV-Vis absorbance and TOC analysis.

ED experiments with an identical concentration of 10 mg/L for boron, fluoride and nitrate as well as detailed investigation of the pH range 8.5 to 9.5 for the initial diluate and concentrate NaCl concentrations of 5 g/L and 20 g/L were undertaken.

This was to determine if increasing NaCl concentration influenced the dissociation of boron.

After the completion of each experiment, the following membrane cleaning protocol was carried out:

1. Ultra-pure water rinsing (1 L diluate and concentrate, 20 min);
2. Acid washing (0.1 M HCl, 1 L diluate and concentrate, 20 min);
3. Ultra-pure water rinsing (2 L, 20 min);
4. Alkaline washing (0.01 M NaOH, 1L diluate and concentrate, 20 min); and
5. Ultra-pure water rinsing (1 L diluate and concentrate, 20 min);

The procedure took a total of 1 hour and 40 minutes. Samples (13.5 mL) taken from the cleaning solutions were analysed for UV-Vis absorbance and TOC analysis. After each set of experiments with OM, the ED stack was dismounted and photographs were taken of the AEMs and CEMs.

The influence of applied voltage (12 and 18 V) and solution pH (3-11) on inorganic trace contaminant removal from a brackish groundwater from a remote Australian community by ED was investigated. An applied voltage of 12 V was fixed for all pH experiments. The ED system was operated in batch desalination mode and the diluate and concentrate were recirculated through the ED stack at a flow rate of 1.5 L/min for 110 minutes. EC and pH of the diluate and concentrate was continuously monitored and samples (50 mL) were collected at the beginning and at 10 minute intervals for cation and anion analysis. After each pH experiment, the diluate and concentrate were mixed and returned to the diluate and concentrate containers for the next experiment. The experiment undertaken at pH 11 was completed twice.

EC in samples taken from ED experiments undertaken on the brackish groundwater was converted to total dissolved solids (TDS, mg/L) using a conversion factor k = 0.64 for Australian groundwater with high sodium content (McNeil and Cox, 2000). It is important to note that this conversion is dependent on feed water characteristics and will vary if the ionic composition changes.

EC, TDS and trace inorganic removal from the diluate in the model aqueous and groundwater experiments was determined using eqn (4.4), however, the units for C_D^t and C_D^0 were mS/cm, mg/L and mg/L, respectively. OM removal from the diluate and concentrate (R_C, %) was determined using eqn (4.4), however, the unit for $C_{D/C}^t$ and $C_{D/C}^0$ was mgC/L. Note that trace inorganic and OM removal includes deposit formation. Standard deviation (S.D.) of R_C was calculated using eqn (4.5) and presented as ± S.D.

The flux of EC, TDS and inorganics was calculated using eqn (4.5), however, the units for m_C were mS/cm, g and mg, respectively, and A_{trans} is the ED stack membrane area (m^2) used in the transport of the respective contaminant (i.e. A_{trans} for EC and TDS 0.0754 m^2, A_{trans} for anions or cations = A_{eff} × 6 CEMs or AEMs = 0.0348 m^2).

The mass of each inorganic contaminant deposited per unit volume of membrane (m_{DEP}, mg/cm^3) was calculated using eqn (4.7).

$$m_{DEP} = \frac{C_{FD}V_{FD} - C_D^t V_D^t - C_C^t V_C^t}{V_{trans}} \tag{4.7}$$

where C_{FD} is the feed concentration (mg/L), C_D^t and C_C^t are the diluate and concentrate concentration (mg/L) at time t (h), V_{FD} is the volume of the feed (L), V_D^t and V_C^t are the diluate and concentrate volume (L) at time t (h) and V_{trans} is the membrane volume (cm^3) used in the transport of the respective contaminant (i.e. V_{trans} for anions = (A_{eff} × AEM thickness) × 6 AEMs = 4.9 cm^3; V_{trans} for cations = (A_{eff} × CEM thickness) × 6 CEMs = 5.9 cm^3).

4.9.3 Water-membrane Partition Coefficients for Trace Organic Contaminants

Partition coefficients are used to relate the concentration of a particular contaminant sorbed to a material to the freely dissolved concentration of the contaminant in solution. An understanding of the partitioning of the steroidal hormones and ES between water and the CEMs and AEMs (log $K_{AEM/CEM}$, L/cm^3) is important for the prediction of their fate during ED.

To determine the water-membrane partition coefficients for the steroidal hormones and ES, batch sorption experiments were undertaken. Radiolabeled (100 ng/L) and non-labelled hormones or ES (70α-ES:30β-ES mix) were added to 100 mL glass bottles of background buffer solution (adjusted to pH 7) to make the following concentrations: 0.1, 0.5, 1, 10, 100 and 2500 μg/L for hormones and 1, 2, 10, 100 and 2500 μg/L for ES. A 2 cm^2 segment of AEM or CEM (3 replicates per membrane type) was added to each bottle and shaken on an incubator shaker (Certomat BS-1, Sartorius, Göttingen, Germany) at 200 revolutions per minute (RPM) and a temperature of 25 ± 1°C. A sample (hormones: 0.5 mL; ES: 1 mL) was taken from each bottle before membrane addition and periodically during each experiment for hormone and ES analysis by liquid scintillation counting (LSC) (Section 4.5.10).

As ES is known to form complexes with OM batch isotherm experiments with ES were undertaken with HA (12.5 mgC/L). For these experiments the sample bottles were shaken for 24 hours prior to membrane addition to allow for ES-HA equilibrium. Samples (3.5 mL) were taken from each bottle before membrane addition and periodically during each ES-HA batch sorption experiment for HA analysis (UV-Vis spectroscopy).

Control hormone or ES solutions with the addition of a biocide (0.5 % sodium metabisulfite ($Na_2S_2O_5$)) and without membrane addition were shaken to eliminate possible hormone degradation and determine hormone sorption to the glass bottles. Hormone and ES desorption from the membranes used in the 1 μg/L batch sorption experiment was determined by the addition of a AEM or CEM in 100 mL solutions of 0.002 mol/L NaOH, HCl and ultrapure water and shaken until steady-state was reached. Samples were taken from each bottle before membrane addition and periodically during each desorption experiment for hormone analysis.

While sorption kinetics showed that a constant mass of hormone or ES sorbed was not reached, t = 170 hours was arbitrarily chosen for the determination of the log $K_{AEM/CEM}$ values. The mass of hormone or ES sorbed to each membrane at 170 hours ($m_{AEM/CEM}$, μg or ng) was calculated using a mass balance (eqn (4.8)).

$$m_{AEM/CEM} = m_w^0 - m_w^t = C_w^0 V_w^0 - C_w^t V_w^t \quad (4.8)$$

where m_w^0 and m_w^t are the initial and 170 h mass of hormone or ES freely dissolved in aqueous solution (subscript *w*) (μg or ng), C_w^0 and C_w^t are the initial and 170 h hormone or ES concentration (μg/L or ng/L), V_w^0 and V_w^t are the initial and 170 h solution volume (L).

The concentrations of the hormones and ES sorbed per unit area of membrane ($C_{AEM/CEM}$, μg/cm^3 or ng/cm^3) were calculated using eqn (4.9).

$$C_{AEM/CEM} = \frac{m_{AEM/CEM}}{V_{AEM/CEM}} = \frac{C_w^0 V_w^0 - C_w^t V_w^t}{V_{AEM/CEM}} \quad (4.9)$$

where $V_{AEM/CEM}$ is the AEM or CEM volume (cm^3).

The partition coefficient, log $K_{AEM/CEM}$ (L/cm^3) for each hormone and ES between the respective membrane (AEM or CEM) and the bulk solution was evaluated using eqn (4.10).

$$K_{AEM/CEM} = \frac{C_{AEM/CEM}}{C_w^t} = \frac{m_{AEM/CEM}}{V_{AEM/CEM}} \cdot \frac{V_w^t}{m_w^t} \quad (4.10)$$

Due to the error associated with the individual $K_{AEM/CEM}$ measurements it was necessary to determine $K_{AEM/CEM}$ over the entire concentration range. Log $K_{AEM/CEM}$ can be derived from the slope (n_i) of the linear regression of $C_{AEM/CEM}$ as a function of C_w^t if the sorption isotherms (plotted on a log scale) are linear (Schwarzenbach *et al.*, 2003). Since the hormone and ES concentration range was several orders or magnitude, the sorption isotherms were plotted on a log scale according to eqn (4.11) and the slope of the linear regression indicates the sorption isotherm deviation from linearity. When $n_i = 1$, the sorption isotherm is linear and sorption affinity remains the same over the concentration range. When $n_i < 1$, the sorption isotherm is concave downward and it can be inferred that as concentration increases it becomes more difficult to sorb additional molecules.

$$\log C_{AEM/CEM} = \log K_{AEM/CEM} + n_i \log C_w^t \quad (4.11)$$

S.D. associated with the $K_{AEM/CEM}$ values was calculated using eqn (4.5) and presented as ± S.D. Confidence intervals (± C.I.) of the mean associated with the $K_{AEM/CEM}$ values and partition coefficients were calculated using eqn (4.12) because as the number of sample points on the linear isotherms is low (n = 5 for hormones; n = 4 for ES) S.D. becomes less reliable as an estimate of the mean (Miller and Miller, 2000).

$$\bar{x} \pm t_{n-1} s / \sqrt{n} \tag{4.12}$$

where t is the degrees of freedom (95 %).

4.9.4 Trace Organic Contaminant Sorption during Electrodialysis

ED experiments with hormones and ES were undertaken because the sorption of hormone and ES to the ion-exchange membranes is likely to be different during ED due to different hydrodynamic and electrochemical conditions within the ED stack channels in comparison to those conditions within the shaker sample bottles. The influence of solution pH (pH 7 and 11) and the presence of HA (12.5 mgC/L) on hormone sorption during continuous and batch desalination ED experiments was evaluated to identify differences in sorption between undissociated and dissociated species and to determine the influence of possible trace organic-HA complexation on membrane sorption.

4.9.5 Steroidal Hormones

For the ED experiments with steroidal hormones, the feed solutions (2500 µg/L mixed radiolabeled and non-labelled progesterone or estrone, 4 L total) were prepared in background buffer solution (adjusted to pH 7 and 11 or 12.5 mgC/L HA). These specific hormones were selected due to their high sorption affinity noted in the batch sorption isotherm experiments. Feed hormone concentrations in the ED experiments were much greater than concentrations usually found in natural waters because saturation of the membranes with hormones would be much slower at a lower concentration. The hormone concentration was selected due to the high sorption capacity of the membranes observed during the sorption isotherm experiments. The ED system was operated in continuous mode (Figure A1.1 B) whereby the feed (diluate and concentrate combined) was recirculated through the

ED stack at a flow rate of 1.5 L/min. Continuous ED experiments were firstly undertaken to evaluate hormone membrane sorption. For this objective, if the ED system had been operated in batch desalination mode it could not have been operated continuously due to a decrease in diluate NaCl concentration. An applied voltage of 10 V was fixed for all ED experiments with hormones. In the continuous ED experiments in the presence of HA the feed solutions were stirred for 24 hours prior to starting the experiment to allow for hormone-HA equilibrium.

EC and pH was continuously monitored and samples were collected at the beginning and periodically for the duration of the experiments for hormone (0.5 mL) and HA (3.5 mL) analysis using LSC and UV-Vis spectroscopy, respectively. The experimental duration of the continuous experiments was 14 hours. A new set of membranes was used in each continuous ED experiment to avoid the hormone sorbed by previous experiments. After the continuous ED experiments were undertaken, differences in sorption within the diluate and concentrate were evaluated in batch desalination experiments. The experimental duration of the batch desalination experiments for hormones was 1.25 hours; required to achieve desalination from 5g/L to 0.5 g/L NaCl. In order to test of desorption of estrone could be achieved during ED, the diluate and concentration was filled with background buffer solution (adjusted to pH 7) and the ED system was rerun (batch desalination mode) for 2 hours. Due to estrone dissociation at pH 11 extended batch ED desalination experiments (total duration 15 hours) were undertaken to evaluate possible membrane permeation of negatively charged estrone from the diluate into the concentrate. The feed solution (4L) was prepared by adding 2500 μg/L estrone (mixed radiolabeled and non-labelled) to the background buffer solution.

Using the determined log $K_{AEM/CEM}$ values, a prediction of the mass of progesterone, estrone and ES sorbed to the membranes within the ED stack (m_{stack}, μg) was made. Due to the fact that the ED stack is composed of both AEMs and CEMs, the mass predicted to sorb to the AEMs and CEMs separately was calculated using eqn (4.13), which is essentially a rearrangement of eqn (4.10), and multiplied by the total membrane volume within the stack (V_{stack}, cm^3) divided by the volume of membrane used in the isotherm experiments (eqn (4.14).

$$m_{AEM/CEM} = m_{FD}^{t} \cdot \frac{K_{AEM/CEM}}{V_{w}^{t}} \cdot V_{AEM/CEM} \tag{4.13}$$

$$m_{stack} = m_{AEM/CEM} \cdot \left(\frac{V_{stack}}{V_{AEM/CEM}} \right) \tag{4.14}$$

The mass of hormone freely dissolved in the ED feed solution at 170 hours (m_{FD}^{t}, μg), respectively, was calculated by multiplying the initial mass of hormone within the feed (m_{FD}^{0}, μg) by the fraction of hormone freely dissolved at 170 hours (f_w, %) determined experimentally in the isotherm experiment with an initial feed hormone concentration of 2500 μg/L (eqn (4.15).

$$m_{FD}^{t} = m_{FD}^{0} \cdot f_{W} \tag{4.15}$$

The mass of hormone and ES sorbed per unit volume of membrane during ED experiments (C_{stack}, μg/cm^3) were calculated using eqn (4.16).

$$C_{stack} = \frac{C_{FD/D/C}^{0} V_{FD/D/C}^{0} - C_{FD/D/C}^{t} V_{FD/D/C}^{t}}{V_{stack}} = \frac{m_{FD/D/C}^{0} - m_{FD/D/C}^{t}}{V_{stack}} \tag{4.16}$$

where $C_{FD/D/C}^{0}$ and $C_{FD/D/C}^{t}$ are the initial and final concentration of hormone or ES in the feed, diluate or concentration (μg/L), respectively, $V_{FD/D/C}^{0}$ and $V_{FD/D/C}^{t}$ are the initial and final volumes (L), $m_{FD/D/C}^{0}$ and $m_{FD/D/C}^{t}$ are the initial and final mass of hormone or ES within the feed, diluate and concentrate (μg).

Hormone and ES removal as a result of membrane sorption within the feed (R_{FD}, %), diluate or concentrate (R_C, %) was determined using eqn (4.4), however, the unit for $C_{FD/D/C}^{t}$ and $C_{FD/D/C}^{0}$ was μg/L.

4.9.6 Endosulfan

Preliminary ED experiments were undertaken at K.U. Leuven to study the removal of α-ES, β-ES and ES sulfate during batch desalination. These were carried out before membrane sorption was postulated as a possible removal mechanism and before membrane-water partition coefficients for ES were determined. The influence

of solution pH (pH 3 and 7) on the behaviour of ES compounds during ED was evaluated. The feed solutions (100 μg/L α-ES, β-ES and ES sulfate (non-labelled), 4L, separate diluate and concentrate) were prepared in background buffer solution (pH and feed NaCl adjusted). Samples (100 mL) were collected at the beginning and periodically for the duration of the pH experiments (140 min, required to achieve desalination from 5g/L to 0.5 g/L NaCl.).

ES sorption as a function of solution pH (7 and 11) and the presence of HA during continuous ED experiments was evaluated. The feed solutions (2500 μg/L radiolabeled and non-labelled mixed 70α-ES:30β-ES, 4L) were prepared in background buffer solution (adjusted to pH 7 and 11 or 12.5 mgC/L HA). EC and pH was continuously monitored and samples were collected at the beginning and periodically for the duration of the experiments for ES (1 mL) and HA (3.5 mL) analysis using LSC and UV-Vis spectroscopy, respectively. The experimental duration of the continuous experiments was 4 hours. A new set of membranes was used in each continuous experiment to avoid the ES sorbed by previous experiments. After the continuous ED experiments were undertaken, differences in sorption within the diluate and concentrate were evaluated in batch desalination experiments. The experimental duration of the batch desalination experiments with ES was 1.25 hours.

A mixed ES and estrone (2500 μg/L each) continuous ED experiment was undertaken to evaluate competitive sorption between compounds exhibiting similar behaviour (dissociated). Samples were collected at the beginning of each ED experiment and periodically for ES and/or estrone (1 mL) and UV-Vis absorbance (3 mL) analysis.

4.9.7 Solute-Solute Interactions during Electrodialysis

The implication of solute-solute interactions between the selected steroidal hormones progesterone and estrone and HA on membrane sorption during ED could be estimated. Using experimental OM-water partition coefficients (log K_{OM}, L/kg), f_w (%) values for progesterone (69 %) and estrone (43 %) determined by Neale (2009), eqn (4.15) and eqn (4.18), the mass sorbed to HA ($m_{ADS\text{-}HA}$, μg) was calculated.

$$m_{ADS-HA} = m_{FD}^{e} \cdot \frac{K_{OM}}{V_{FD}} \cdot m_{HA} \qquad (4.18)$$

where $m_{ADS\text{-}HA}$ is the mass of hormone sorbed to HA (μg), m_{FD}^{e} is the mass of hormone freely dissolved in the feed at hormone-HA equilibrium (μg), V_{FD} is the feed volume (L) and m_{HA} is the mass of HA (kg).

Using $m_{ADS\text{-}HA}$ it was possible to predict hormone sorption to the membranes during ED due to hormone-HA interactions (PR_{FD}, %) using eqn (4.19).

$$PR_{FD} = \frac{m_{ADS-HA} \cdot R_{FD}}{m_{FD}^{0}} \times 100 \tag{4.19}$$

where R_{FD} is the removal of HA from the feed (%) calculated using eqn (4.4).

4.10 Electrodialysis Parameters and Performance

Current density (i, mA/cm^2) of the ED stack during all ED experiments was calculated using eqn (4.20).

$$i = \frac{I}{A_{eff}} \tag{4.20}$$

The electrical resistance (R_{stack}, Ω) across the ED stack in all ED experiments was calculated using Ohms law (eqn (4.21).

$$R_{stack} = \frac{U}{I} \tag{4.21}$$

where U is the electrical potential/applied voltage (V).

Power consumption (P, Wh) between each sample time period and cumulative (duration of experiment) was calculated using eqn (2.29).

SEC (Wh/L), which increases with experimental duration, was calculated for all ED experiments using eqn (2.30).

Chapter 5. Desalination and Inorganic Contaminant Removal from Aqueous Model Solutions

Desalination kinetics and performance parameters (electrical resistance, power and specific energy consumption) of the ED system are investigated in the first part of this chapter.

In the second part of this chapter, the removal of the inorganic contaminants F^-, NO_3^- and $B(OH)_4^-$ from synthetic aqueous solutions containing OM, specifically HA, TA and AA, using ED is investigated. Due to its high selectivity and low chemical demand, ED has proved an efficient method for desalination and the removal of F^- and NO_3^- (Kabay *et al.*, 2008; Kesore *et al.*, 1997; Ortiz *et al.*, 2005). $B(OH)_4^-$ removal using ED has previously been studied and is capable of removing 42-75 % of $B(OH)_4^-$, with removal efficiency dependent on solution pH (97 % at pH 9-10) and the degree of desalination (Melnik *et al.*, 1999; Turek *et al.*, 2007a; Yazicigil and Oztekin, 2006).

As most OM is negatively charged at neutral pH, deposits form predominantly on the AEM. The impact of such deposits on removal of specific contaminants is not well understood. Further, solute-solute interactions (such as complexation) of OM with the selected inorganic compounds has to date not been investigated. As mentioned in Chapter 2, the extent of inorganic-OM complexation is influenced by the chemical composition and configuration of the OM, physicochemical characteristics of the inorganics and solution pH. As such interactions are likely to affect removal the main objective of this chapter was to examine the influence of pH and three types of OM on the removal of F^-, NO_3^- and $B(OH)_4^-$ during ED systematically. The purpose of this was to elucidate the mechanisms of inorganic contaminant removal including membrane deposition and solute-solute interactions. In order to achieve this goal the study was conducted in five stages, namely (1) mechanisms of inorganics removal in the absence of OM, (2) OM removal, (3) impact of OM on inorganics removal, (4) inorganic membrane deposit formation, and (5) organic deposit formation.

5.1 Limiting Current Density

In ED, concentration polarisation limits the amount of current that can pass through the cells within the ED stack. This concentration polarisation is influenced by the applied current density, stack dimensions, the linear flow velocity within the stack channels and properties of the membranes (e.g. resistance) (Tanaka, 2004). Therefore, the LCD needed to be experimentally determined for the ED stack used in this study to decide on the maximum voltage that can be applied without exceeding the LCD. The LCD drops during an experiment because of the decrease in electron carriers in the diluate; however, the LCD is determined using a diluate concentration based on the final product concentration. Figure 5.1 shows the current-voltage curves (*I-U*) obtained for the BEL-500 ED stack in the 0.5 g/L NaCl solution (final diluate product concentration) for 1.5 and 3 L/min flow rates (linear flow velocity through ED stack 0.08 and 0.16 m/S, respectively calculated using the cross-sectional area of flow within the stack). The shapes of these curves are influenced by concentration, flow rate and physicochemical conditions at the membrane surface. Both curves show that voltage initially increased proportionally with the current density, following Ohm's law ($U = IR$). The second phase in typical *I-U* curves is characterised by a plateau in which concentration polarisation manifests as a rapid change in slope (inflexion). This is the region of the LCD where the concentration of NaCl at the membrane interface on the diluate side approaches zero. Measurements in ED stacks with multiple cell pairs often do not show clear indication of resistance change when the LCD is exceeded (Strathmann, 2004). Slight decreases in slope were noted above 11 and 14 V for 1.5 and 3 L/min, respectively. However, the smoothness of the curves, particularly the curve corresponding to the 1.5 L/min flow rate, caused difficulties in accurately differentiating inflexions in the curve. Thus, characterisation of the plateau phase and the LCD's was difficult using these *I-U* curves.

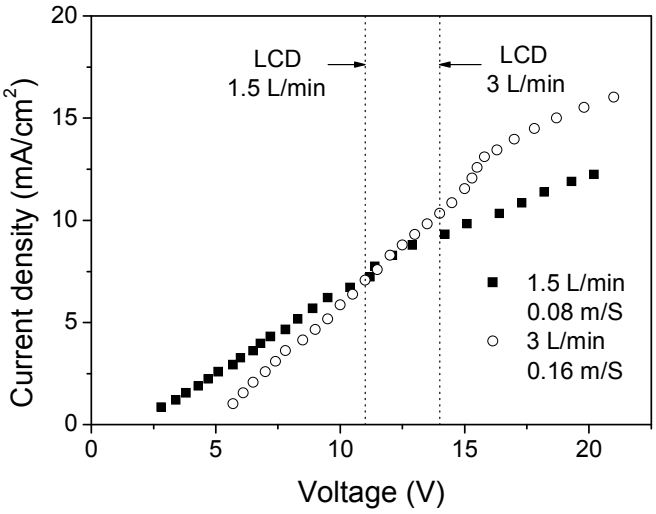

Figure 5.1. Current-voltage curves for the BEL-500 ED stack at flow rates 1.5 and 3 L/min (Feed solution: 0.5 g/L NaCl, 6 cell pairs, linear flow velocities: 0.08 m/s, 0.16 m/s; vertical dotted lines indicated theoretical LCD).

The LCD was subsequently determined from Cowan plots (Cowan and Brown, 1959) showing the reciprocal of the current versus the stack resistance (Figure 5.2). The resistance across the ED stack rises sharply once the LCD has been reached. The point at which the resistances increased sharply at 1.5 and 3 L/min (vertical dotted lines on Figure 5.2) corresponded to reciprocal current values of 2.22 and 1.32 1/mA. Changes in the solution pH of the diluate were used as an approximation of the LCD. The pH of the diluate alters near where the slope of the resistance changes and decreases as the current density increases because of water dissociation between the membranes and the boundary layer.

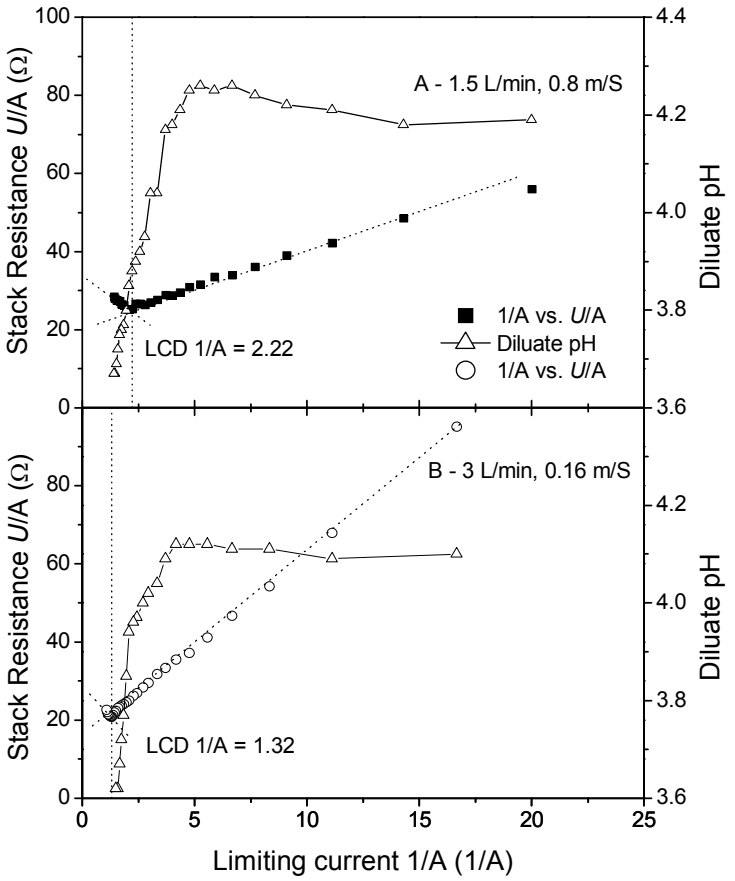

Figure 5.2. Reciprocal current vs. stack resistance at flow rates 1.5 and 3 L/min (Feed solution: 0.5 g/L NaCl, 6 cell pairs, linear velocities: 0.08 m/s, 0.16 m/s).

A comparison between the experimental and theoretical LCD values for the different flow rates is shown in Table 5.1, along with the corresponding maximum applied voltage allowed before the LCD is reached. The experimental LCD at 3 L/min (13.1 mA/cm^2) was greater than the LCD at 1.5 L/min (7.8 mA/cm^2). This is in agreement with other studies (Lee *et al.*, 2006; Tanaka, 2005) and is a result of changes in the thickness of the membrane boundary layer (δ). The faster the linear flow velocity within the ED stack channels the thinner the boundary layer and the distance over which concentration polarisation can occur is reduced. With a slower linear flow velocity, the natural ionic convection-diffusion within this boundary layer is enhanced. To ensure that the ED system was operated at a current density below the LCD, applied voltages of 10 and 12 V (unless otherwise stated) were chosen for the ED experiments with flow rates of 1.5 and 3 L/min, respectively.

Table 5.1. Comparison between experimental and theoretical limiting current density (LCD) for the flow rates 1.5 and 3 L/min (Feed solution: 0.5 g/L NaCl).

Flow rate (L/min)	Theoretical LCD (mA/cm^2)	Experimental LCD (mA/cm^2)	Maximum applied voltage (V)
1.5	6.8 ± 0.1	7.8 ± 0.2	11.4 ± 0.3
3	9.7 ± 0.2	13.1 ± 0.3	15.8 ± 0.3

5.2 Desalination Kinetics

5.2.1 Influence of Applied Voltage

The desalination kinetics of the ED stack used in this study was evaluated as a function of applied voltage (9, 12 and 18 V). These particular voltages where chosen to make a comparison between results below and above the experimental LCD (13.1 mA/cm^2). The concentration of NaCl in the diluate and concentrate streams as a function of time, applied voltage and feed NaCl concentration is shown in Figure 5.3. As the applied voltage was increased, the electrochemical potential within the ED stack thus increased and the time it took to produce 4L of water with NaCl below the drinking water guideline (DWG, 0.5 g/L NaCl) was reduced.

With a higher feed NaCl concentration, the mass of NaCl within the diluate to be transported through the ion-exchange membranes is greater and thus the time to reach the DWG increases (t_{DWG}, 5 g/L NaCl: 9 V-70 min, 12 V-50 min, 18 V-27 min; 10 g/L NaCl: 12 V-73 min, 18 V-37 min). The DWG was attained in all experiments except at an applied voltage of 9 V and feed salt concentration of 10 g/L NaCl.

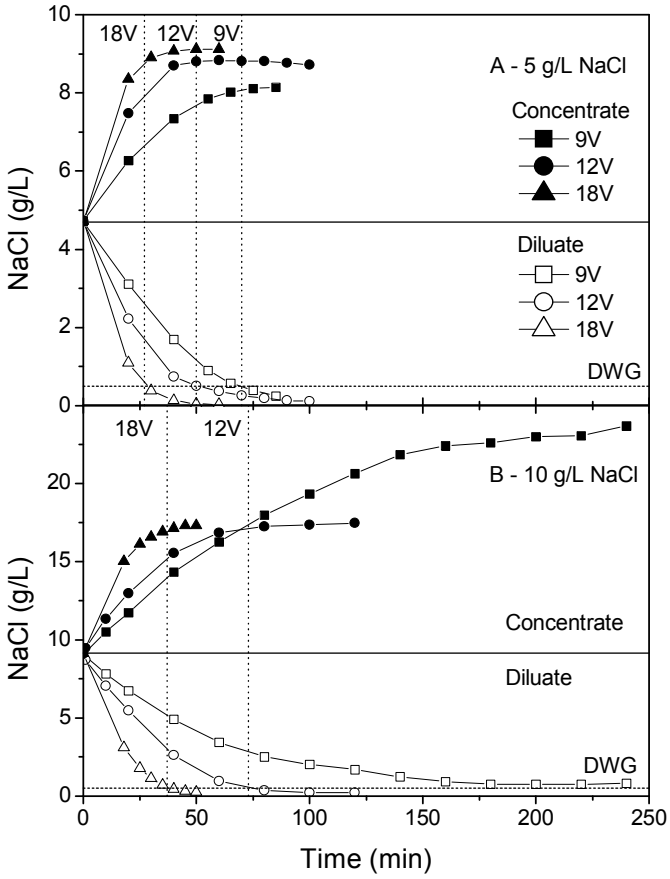

Figure 5.3. NaCl concentration within the diluate and concentrate as a function of time, applied voltage and feed NaCl concentration (A) 5 g/L NaCl and (B) 10 g/L NaCl (3 L/min, 12 V; horizontal dotted line indicates DWG 0.5 g/L NaCl; vertical dotted lines indicate time when DWG is reached).

In all experiments, the NaCl concentration within the diluate and concentrate rapidly decreased and increased, respectively, within the first 30 minutes. Figure 5.4 demonstrates the decrease in NaCl flux from the diluate through the ion-exchange membranes to the concentrate. At both feed salt concentrations, the flux of NaCl is significantly greater at 18 V (5 g/L: 589.9 g/m^{2}h; 10 g/L: 922.6 g/m^{2}h) compared to 9 V (5 g/L: 229.4 g/m^{2}h; 10 g/L: 196.0 g/m^{2}h) and 12 V (5 g/L: 409.5 g/m^{2}h; 10 g/L: 273.0 g/m^{2}h). The initial NaCl flux was greater in the 10 g/L NaCl experiment compared to the 5 g/L experiment due to the higher initial concentration of electron carriers within the diluate.

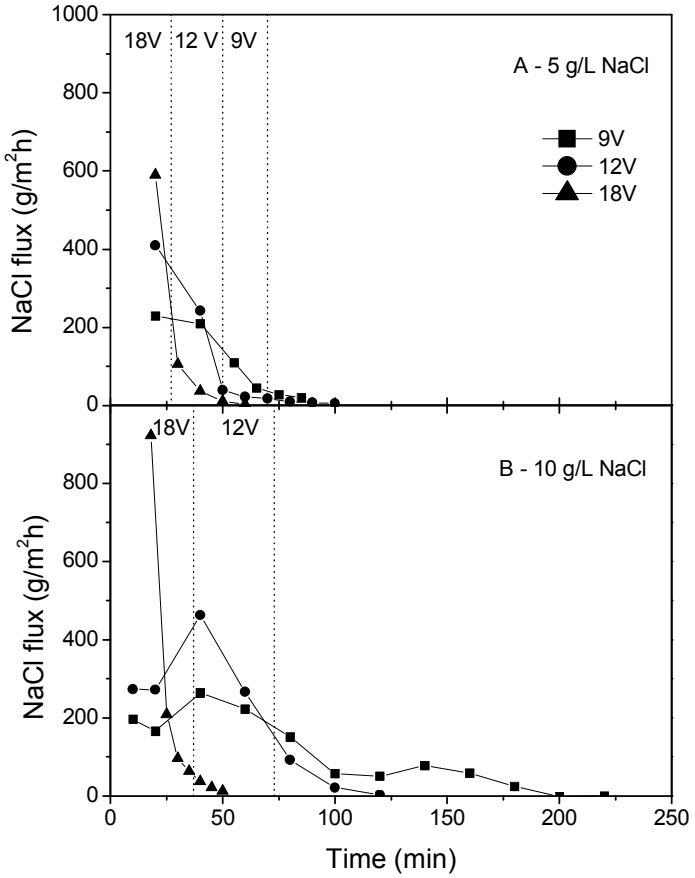

Figure 5.4. NaCl flux (g/m^{2}h) from the diluate to the concentrate as a function of time, applied voltage and feed NaCl concentration (A) 5 g/L NaCl and (B) 10 g/L NaCl (3 L/min, 12 V; vertical dotted lines indicate time when DWG 0.5 g/L NaCl is reached).

After 30 minutes, NaCl flux decreased and was accompanied by a smaller incremental decrease in the current density between the two electrodes within the stack (Figure 5.5). The increase in NaCl flux between 30 and 40 minutes in the 10 g/L NaCl experiment at 9 and 12 V is a result of an increase in current (9 V: 2.50 to 2.55 A; 12 V: 3.60 to 3.76 A). This slight increase in current was regularly noted in the initial stages (10-20 min) of the ED experiments performed during this study and is a result of hydrodynamic conditions (diluate and concentrate mixing) within the ED system. This indicates a strong dependence between the current and NaCl flux. The fastest NaCl flux during the early stage of the ED process can be attributed to the initial availability of the Na^+ and Cl^- ions serving as current carriers, as noted by

the higher current density in the initial ED stages. The rapid depletion of these current carriers within the diluate contributes to the lower current density across the ED stack and this in turn reduces the ionic flux. The current across the stack in the final stages of the ED process in the 9 V and 10 g/L NaCl experiment may have been insufficient and could explain why the DWG was not reached.

Figure 5.5 illustrates when the current density across the stack was above the theoretical and experimental LCD. At 9 V, the theoretical LCD was exceeded only after the NaCl concentration within the diluate dropped below the DWG in the 5g/L NaCl experiment (85 min, 0.25 g/L NaCl diluate). A similar trend was noted in the 12 V and 10 g/L NaCl experiment. Although the initial current density across the stack was below the theoretical LCD in both the 18 V experiments, the theoretical LCD was exceeded after 10 minutes. This is due to operation above the experimental LCD (13.1 mA/cm^2) and the corresponding maximum allowable applied voltage (15.8 V, Table 5.1).

Operation above the LCD and a decrease in the ions available for current transport is indicated by an increase in the electrical resistance (Ω) across the stack. Operation above the LCD correlated with increases in resistance (Figure 5.6). Resistance was initially relatively stable. However, a dramatic increase in resistance was noted during the 18 V experiments after 20 minutes due to operation above the theoretical LCD. Although the LCD was not exceeded in the 9 V and 10 g/L NaCl experiment the resistance increased (3.6 to 10.7 Ω) due to the depletion of current carriers within the diluate in the final stages of the ED process.

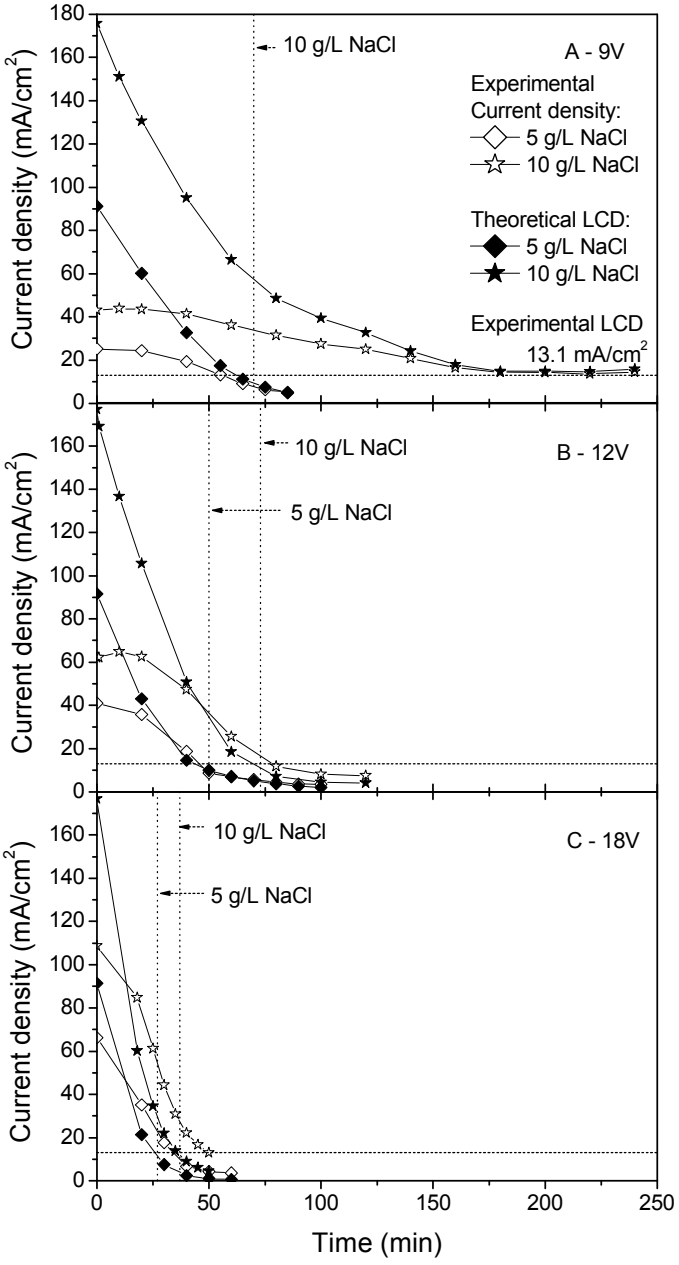

Figure 5.5. Comparison between the current density (mA/cm^2) within the ED stack and the experimental and theoretical LCD (9, 12 and 18 V; 5 and 10 g/L NaCl; 3 L/min; horizontal dotted line indicates experimental LCD 13.1 mA/cm^2; vertical dotted line indicates time when DWG 0.5 g/L NaCl was reached).

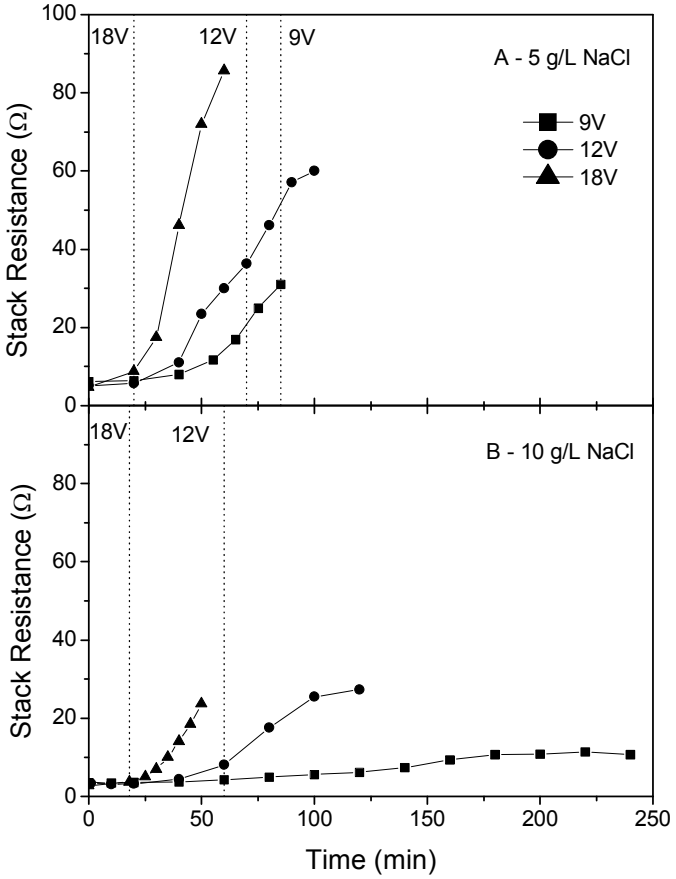

Figure 5.6. Electrical resistance (Ω) as a function of a function of time, applied voltage and feed NaCl concentration (A) 1 g/L NaCl and (B) 5 g/L NaCl (3 L/min; vertical dotted line indicates time when theoretical LCD was exceeded).

Table 5.2 outlines the power (Wh) and specific energy consumed (Wh/L) in the production of drinking water (0.5 g/L NaCl) for each experiment. When the DWG was not reached (9V and 10 g/L NaCl experiment) the power and energy consumed at experimental completion is given. With a feed salt concentration of 5 g/L NaCl, power consumption and SEC within the ED stack was proportional to the applied voltage i.e. power consumption and SEC increased with increasing voltage. However, at 10 g/L NaCl, power consumption and SEC at 9 V was greater than at 12 V because the DWG was not reached. Therefore, 12 V appears as the optimum operating condition concerning energy consumption during the 10 g/L NaCl experiment. When power consumed and SEC for each experiment was compared at the same experimental time (50 min, Table 5.2) they were proportional to applied voltage at both 5 and 10 g/L NaCl. The SEC for the 5 g/L NaCl experiment (2.8-5.7

Wh/L) is less than SEC (9.6-11.4 Wh/L; applied voltage 16-24 V) reported for the desalination of brackish waters (Schoeman, 2008).

Table 5.2. Power consumption (Wh) and specific energy consumption (SEC, Wh/L) of the ED stack in production of drinking water (DWG 0.5 g/L NaCl).

Feed NaCl concentration (g/L)	Applied voltage (V)	Power consumption (Wh) at time (min)		SEC (Wh/L) at time (min)	
		t_{DWG} [a]	50 [b]	t_{DWG} [a]	50 [b]
5	9	9.5 ± 0.2	11.5 ± 0.3	2.8 ± 0.1	3.4 ± 0.1
	12	16.8 ± 0.4	16.8 ± 0.4	4.4 ± 0.1	4.4 ± 0.1
	18	20.9 ± 0.5	25.3 ± 0.6	5.7 ± 0.1	7.0 ± 0.2
10	9	54.6 ± 1.2 [c, d]	18.2 ± 0.4	11.9 ± 0.3 [c, d]	4.5 ± 0.1
	12	38.8 ± 0.6	31.7 ± 0.7	9.9 ± 0.2	8.3 ± 0.2
	18	48.2 ± 1.1	52.3 ± 1.2	13.1 ± 0.3	14.3 ± 0.3

[a] Determined when the drinking water guideline was reached (0.5 g/L NaCl); [b] Determined at common time (50 min) during each experiment; [c] Power consumption and SEC at completion of experiment presented since the DWG was not reached; [d] Final NaCl concentration and experimental duration: 0.8 g/L at t = 240 min.

Figure 5.7 shows the costs of the ED stack as a function of applied voltage. As the applied voltage increases, energy consumption and cost increases while the required membrane area decreases. Membrane costs decrease with increasing applied voltage. Total membrane costs were calculated using a membrane cost per unit area of 150 $/m^3, an ED stack operating period of 24 h/d and a membrane life of 340 d/yr.

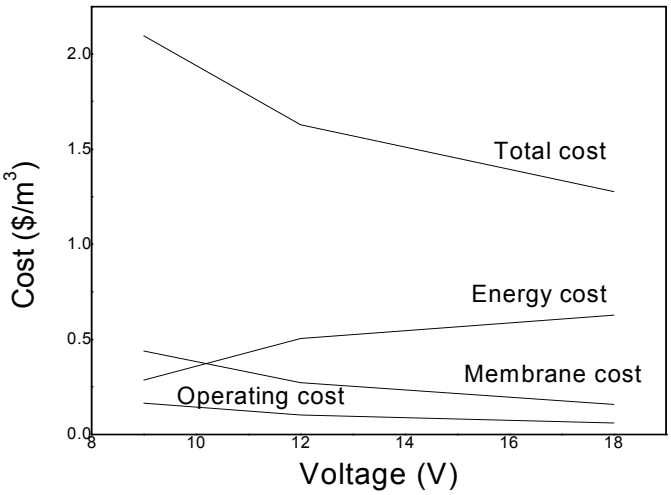

Figure 5.7. Electrodialysis process costs as a function of applied voltage.

5.2.2 Influence of Feed Salt Concentration

ED is applicable for the desalination of waters with higher concentrations of dissolved solids (up to 35 g/L of seawater) (Tanaka *et al.*, 2003). The performance of the ED stack was evaluated as a function of feed salt concentration (1-35 g/L NaCl) in order to determine the scope of ED for a range of salinities. The concentration of NaCl within the diluate and concentrate as a function of time and feed salt concentration is shown in Figure 5.8. The DWG was only reached in the experiments with a feed salt concentration of 1 g/L NaCl (17 min, R_D 50 %), 5 (60 min, R_D 90 %) and 10 g/L NaCl (115 min, R_D 95 %). For feed salt concentrations greater than 10 g/L NaCl, desalination was marginal after 90-120 minutes due to the depletion of current carriers within the diluate. This can also be attributed to the decrease in ion-exchange membrane permselectivity with increasing feed salt concentration (Strathmann, 2004).

NaCl removal as a function of feed salt concentration is summarised in Table 5.3. NaCl removal decreased as feed salt concentration increased. In the 35 g/L NaCl experiment NaCl removal at t = 40 min was 42.1 % compared to 85.7 % in the 1 g/L NaCl experiment. A similar trend was observed at other periods, except after 80 minutes when NaCl removal in the 25 g/L NaCl experiment was slightly lower than removal in the 35 g/L NaCl experiment.

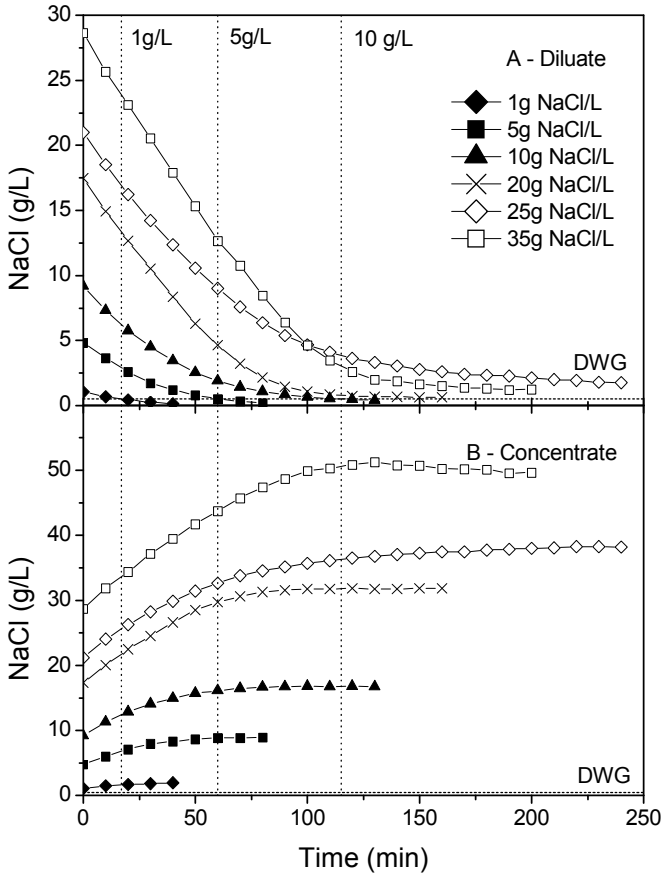

Figure 5.8. NaCl concentration within the diluate (A) and concentrate (B) as a function of time and feed NaCl concentration (1-35 g/L NaCl) (3 L/min; 12 V; horizontal dotted line indicates DWG 0.5 g/L NaCl; vertical dotted lines indicate time when DWG is reached).

Table 5.3. Desalination kinetic results as a function of feed NaCl concentration (1-35 g/L NaCl, 3 L/min, 12V).

Feed NaCl concentration (g/L)	Time to reach DWG, t_{DWG} (min)	NaCl removal (R_D, %) at time (min)					
		40	80	130	160	200	240
1	17	85.7	-	-	-	-	-
5	60	75.5	96.0	-	-	-	-
10	115	64.2	89.6	96.3	-	-	-
20	-	54.4	89.2	96.7	96.9	-	-
25	-	43.7	72.6	86.7	89.6	91.8	93.5
35	-	42.1	74.1	94.3	95.9	97.8	-

Current density across the stack, and thus NaCl flux is related to the concentration of current carriers within the diluate. NaCl flux from the diluate to the concentrate increased with increasing feed salt concentration (Figure 5.9). Initial NaCl flux (t = 10 min) in the 1 g/L NaCl experiment was 68 g/m^{2}h compared to 484 g/m^{2}h in the 35 g/L NaCl experiment. The fluctuations in flux in the 35 g/L NaCl experiment correspond to fluctuations in the measured current. Between 20 and 30 minutes the current increased from 7.2 to 7.4 A and consequently NaCl flux increased from 390 to 498 g/m^{2}h. Similarly, in the 25 g/L NaCl experiment the current increased from 5.4 to 5.5 A between 10 and 20 minutes and NaCl flux increased from 405 to 474 g/m^{2}h.

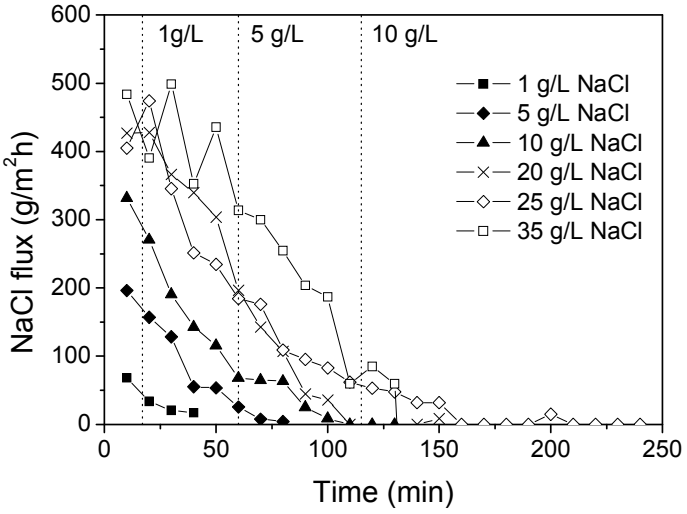

Figure 5.9. NaCl flux (g/m^{2}h) from the diluate to the concentrate as a function of time and feed NaCl concentration (1-35 g/L NaCl) (3 L/min; 12 V; vertical dotted lines indicate time when DWG 0.5 g/L NaCl is reached).

Current density only exceeded the theoretical LCD after the DWG was reached at feed salt concentrations of 1, 5 and 10 g/L NaCl (Figure 5.10). Initial current density increased with increasing salt concentration (1 g/L NaCl: 12.6 mA/cm^2; 35 g/L NaCl: 120 mA/cm^2). Operation of the ED stack above the LCD corresponded to an increase in electrical resistance across the stack (Figure 5.11); the same trend observed in the applied voltage experiments. While the initial increase in resistance was due to the depletion of ions within the diluate the rapid increase in resistance, for example in the 1 g/L NaCl experiment after 30 minutes (35 to 52 Ω) is result of concentration

polarisation and water dissociation between the membranes and membrane boundary layer. The increase in resistance in the 20 g/L NaCl (2.3 to 14.0 Ω), 25 g/L NaCl (2.2 to 9.9 Ω) and 35 g/L NaCl experiments (1.7 to 10.8 Ω) was similar to that noted in the 9 V and 10 g/L NaCl experiment.

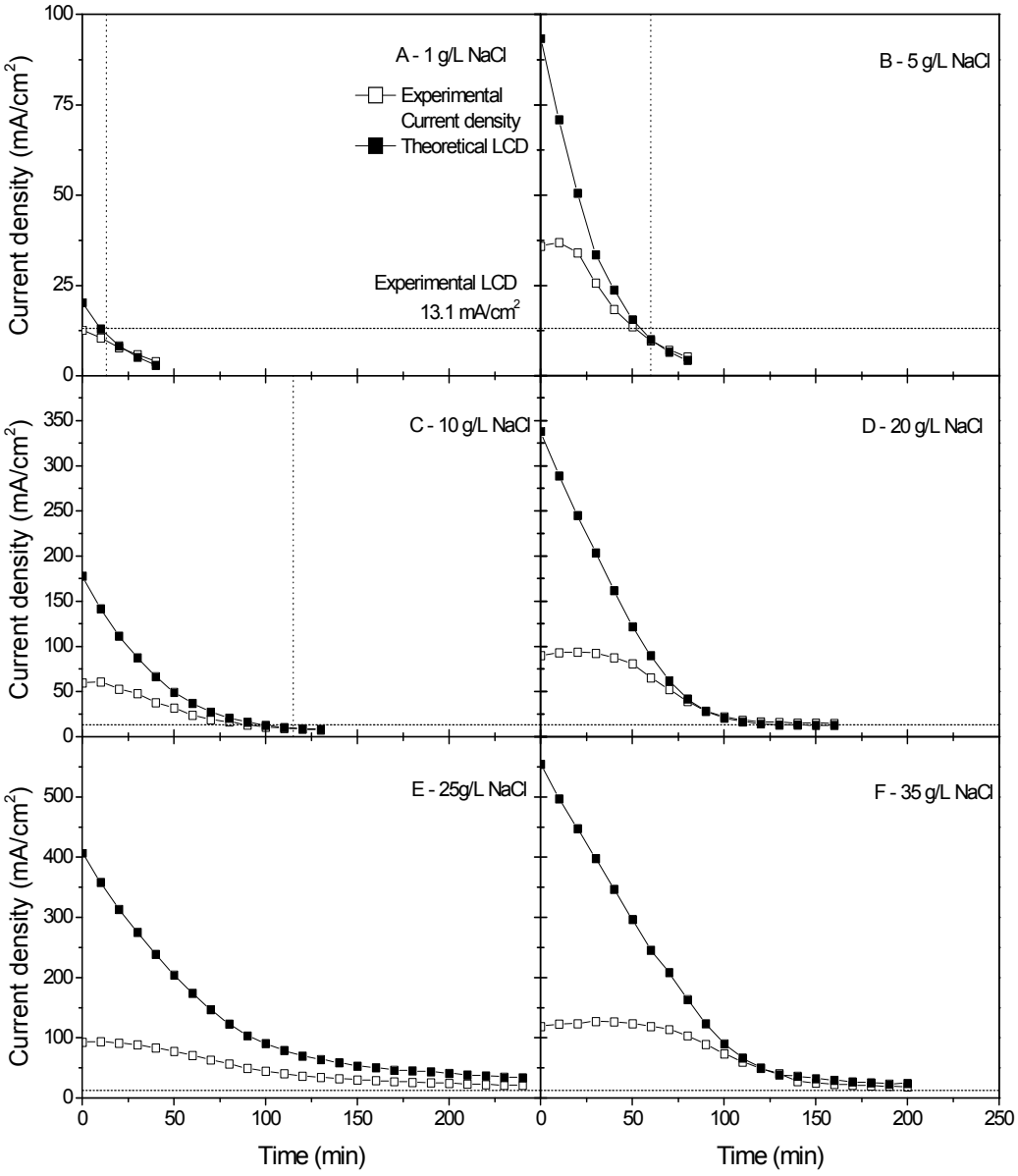

Figure 5.10. Comparison between the current density (mA/cm^2) within the ED stack and the experimental and theoretical LCD (3 L/min, 12 V; horizontal dotted line indicates experimental LCD 13.1 mA/cm^2; vertical dotted line indicates time DWG 0.5 g/L NaCl is reached).

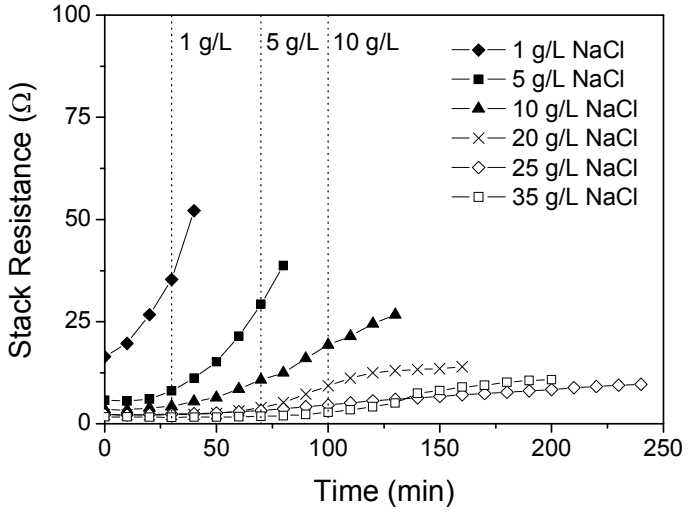

Figure 5.11. Electrical resistance (Ω) as a function of a function of time and feed NaCl concentration (1-35 g/L NaCl) (3 L/min, 12 V; vertical dotted line indicates time when theoretical LCD 13.1 mA/cm^2 was exceeded).

Power consumption and SEC increased as a function of feed salt concentration (Table 5.4). Power consumption increased linearly with feed salt concentration ($R > 0.99$), while SEC increased exponentially ($R > 0.99$).

Table 5.4. Power (Wh) and Specific Energy Consumption (Wh/L) of the ED stack in the production of drinking water (DWG 0.5 g/L NaCl, 3 L/min, 12 V).

Feed NaCl Concentration (g/L)	Power Consumption (Wh)	SEC (Wh/L)
1	2.1 ± 0.1	0.5 ± 0.1
5	17.6 ± 0.4	5.0 ± 0.1
10	41.1 ± 0.9	12.6 ± 0.3
20 [a, b]	91.6 ± 2.0	29.1 ± 0.6
25 [a, c]	133.8 ± 2.9	49.6 ± 1.1
35 [a, d]	172.2 ± 3.8	88.3 ± 1.9

[a] Power consumption and SEC at completion of experiment presented since the DWG was not reached, Final NaCl concentration and experimental duration: [b] 0.6 g/L at t = 160 min, [c] 1.7 g/L at t = 240 min, [d] 1.3 g/L at t = 200 min.

5.3 Implications of Solution Chemistry on Inorganic Contaminant Removal

5.3.1 Influence of Solution pH

As a first stage the removal (R_D, %) of F^-, NO_3^- and $B(OH)_4^-$ in the absence of OM was determined to establish a baseline. The removal of F^- from the diluate is shown in Figure 5.12A. The removal of F^- was independent of pH, which is due to the pH independence of F^- speciation (Richards *et al.*, 2009). The average removal of F^- was 68.3 ± 4.5 %, while flux was approximately 0.02 mg/cm^{2}h (see Figure 5.13A). F^- was removed below the DWG at pH 6, 8, 10 and 12 in the absence of OM (R_D needed to reach DWG of 1.5 mg/L was 70 %).

Removal of NO_3^- was higher than that of F^- but equally pH independent (Figure 5.12B), again because NO_3^- speciation does not vary over the pH range studied (Richards *et al.*, 2009). The average removal of NO_3^- was 94.1 ± 1.3 % while NO_3^- flux was significantly higher than for F^- and decreased gradually from 1.16 to 0.57 mg/cm^{2}h (Figure 5.13B). The DWG of 25 mg/L (R_D 75 % needed) was achieved in each experiment over the pH range.

$B(OH)_3$ does not dissociate between pH 3 and 8 and in consequence is not transported effectively through the AEMs (Figure 5.12C). Above pH 9 removal increased to 61.2 % at pH 12 due to $B(OH)_3$ dissociation; hence speciation plays an important role. While Yazicigil and Oztekin (2006) determined that pH 9 was the optimal point for boron removal, in this study it was only 13.7 % at pH 9. $B(OH)_4^-$ flux is in the same order of magnitude as F^- but increased during experiments (Figure 5.13C), which confirms the findings of Yazicigil and Oztekin (2006) who attributed this to the increase in electrochemical potential gradient between the diluate and concentrate (i.e. larger difference in salt concentration). $B(OH)_4^-$ was not removed below the 0.5 mg/L DWG (R_D of 97 % needed).

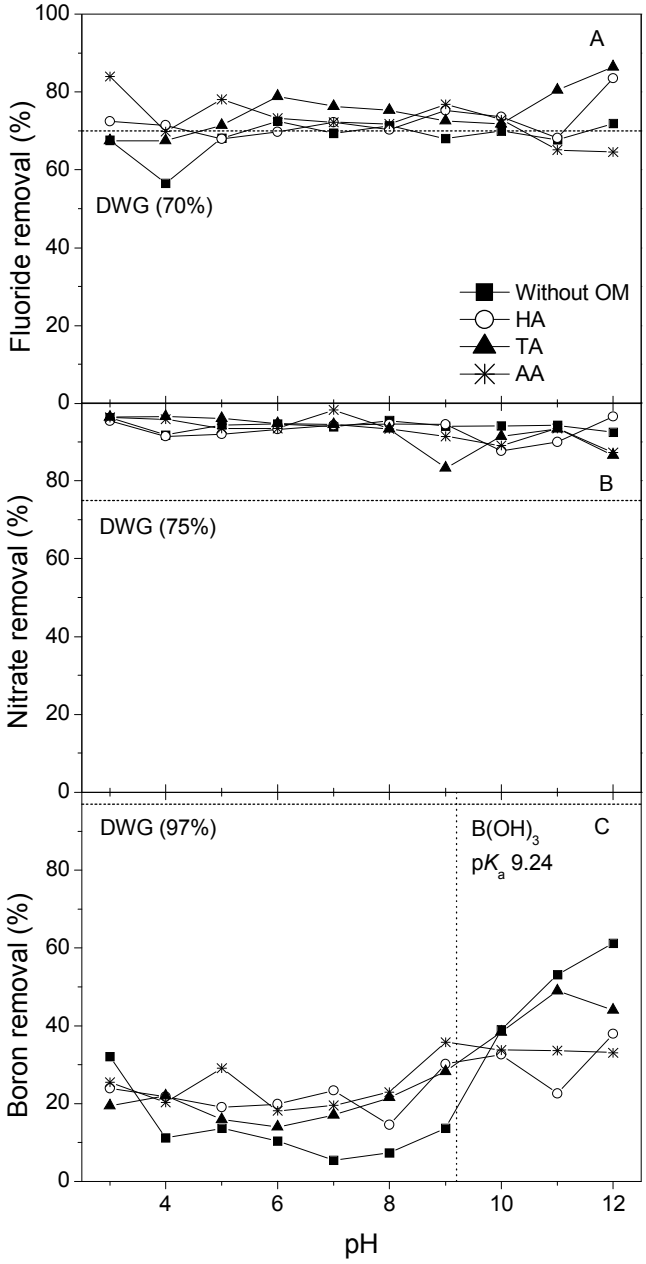

Figure 5.12. The removal of (A) F^-, (B) NO_3^- and (C) $B(OH)_4^-$ from the diluate as a function of solution pH (3-7) (Initial feed concentration: 5 mg/L F^-, 100 mg/L NO_3^-, 10 mg/L $B(OH)_4^-$; experimental duration 140 min; horizontal dotted lines indicate R_D % needed to reach DWG; vertical dotted line indicates $B(OH)_3$ pK_a 9.24).

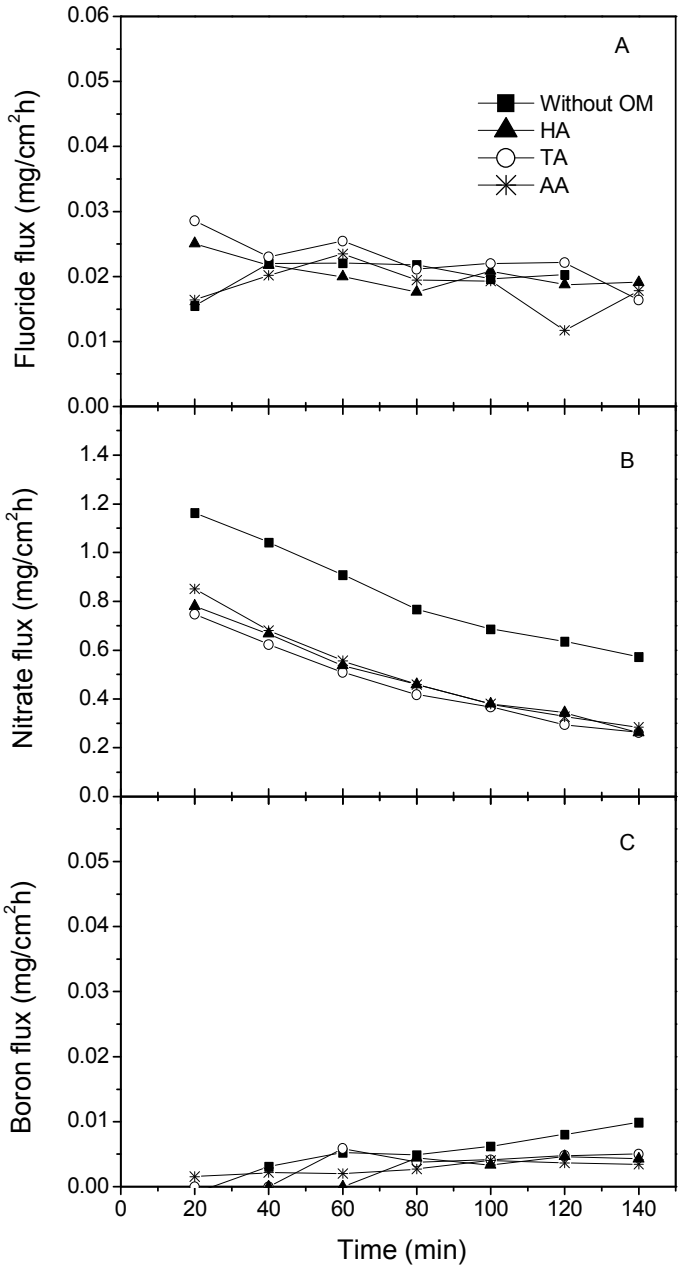

Figure 5.13. Flux (mg/cm^{2}h) of (A) F^-, (B) NO_3^- and (C) $B(OH)_4^-$ (Initial feed mass (diluate and concentrate combined): 39.9 mg F^-, 3532.3 mg NO_3^-, 78.0 mg $B(OH)_3$).

The dissociation constant of $B(OH)_3$ decreases with increasing NaCl concentration (Owen and King, 1943). Further ED experiments were undertaken to examine this effect with a solution pH range between 8.5 and 9.5 (Figure 5.14) at two feed salt

concentrations of 5 and 20 g/L NaCl. In the 5 g/L experiment $B(OH)_4^-$ removal ranged from 6.1 % at pH 8.5 to 29.4 % at pH 9.5. $B(OH)_4^-$ was not removed over this pH range in the 20 g/L experiment presumably due to the higher concentration of competitive ions within the diluate. In consequence, no discernable shift in the dissociation constant of $B(OH)_3$ was observed. The results demonstrate, however, that NaCl concentration affects removal of other ions.

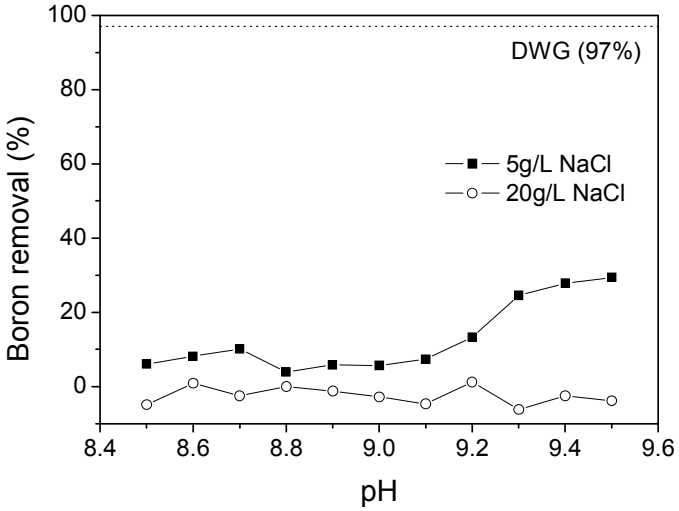

Figure 5.14. Removal of $B(OH)_4^-$ from the diluate as a function of solution pH (8.5-9.5) and feed salt concentration (5 and 20 g/L NaCl) (horizontal dotted line indicates R_D % needed to reach DWG; experimental duration 140 min).

5.3.2 Ionic Hydration and Mobility

Physicochemical characteristics of ions have a significant role in aqueous chemical land biological systems (Conway, 1981) and, therefore, influence their transport and removal behaviour in membrane processes. The ionic characteristics given in Table 2.2 can be used to explain differences in the transport (removal and flux) of F^- and NO_3^- through the ion-exchange membranes. As no data was available on the hydrated radius of $B(OH)_4^-$, comparison of $B(OH)_4^-$ removal and ionic characteristics is not discussed. Ions with smaller intrinsic crystal radii have higher hydration numbers, larger hydrated radii and hold their hydration shells more strongly (Tansel *et al.*, 2006), as illustrated in Figure 5.15. The crystal ionic radius of F^- is 0.116 nm

compared with 0.179 nm for NO_3^-. The larger the crystal ionic radius the more diffuse the electric charge and the fewer water molecules surround the ion (Volkov *et al.*, 1997). Therefore, NO_3^- ions are less hydrated than F^- ions and may separate from their hydration layer (Tansel *et al.*, 2006) and transport through the ion-exchange membranes more easily.

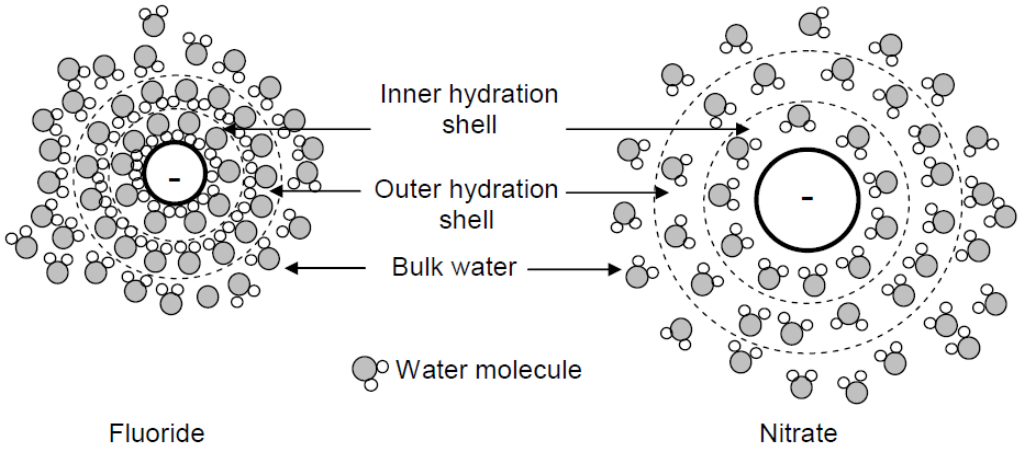

Figure 5.15. Schematic representation of hydration shells around F^- and NO_3^- ions (Adapted from Tansel *et al.* (2006)).

Hydration strength influences the mobility of F^- and NO_3^-. The strength of hydration is influenced by ionic structure and concentration, ionic strength, solution pH and temperature. Thermodynamic parameters such as entropy of hydration, the Jones-Dole viscosity coefficient *B* and electrostriction pressure can be used to assess the strength of the hydration shells around ions. Jones-Dole *B* viscosity coefficients provide information concerning the hydration of F^- and NO_3^- and their effects on the structure of the surrounding water molecules. The viscosity of a salt solution (η) varies with concentration (c, up to 0.1 M) according to the Jones–Dole expression (eqn 5.1) (Collins, 1997):

$$\eta / \eta_0 = 1 + Ac^{1/2} + Bc \qquad (5.1)$$

where η_0 is the viscosity of water (mPa.s) at the same temperature, A is an electrostatic constant (measure of ion-ion interactions) that is solute and temperature dependent and neglected at moderate concentrations and B is a measure of ion-water

interactions. Weakly hydrated ions exhibit a smaller change in viscosity with concentration and have negative *B* coefficients (NO_3^- -0.043 L/mol, Table 2.2) in comparison to strongly hydrated ions that have positive *B* coefficients (F^- 0.107 L/mol) (Jenkins and Marcus, 1995).

Hydration strength is also quantified by the Gibbs energy of hydration and the number of water molecules within their hydration shells. Ions within solution are surrounded by a hydration shell, where water is immobilised and electrostricted, and the bulk water, which is under the influence of the electric field of the ion. The change in Gibbs free energy (ΔG) is related to the driving forces behind a chemical reaction (entropy and enthalpy) within a system and is defined as (eqn (5.2)):

$$\Delta G = \Delta H - \Delta(TS) \tag{5.2}$$

where ΔH is the enthalpy (Joule), ΔT is the temperature (K) and ΔS is the entropy (Joule/K).

The average number of hydrogen bonds in which water molecules participates in an ionic solution relative to that of pure water (ΔG_{HB}) is given by eqn (5.3) (Marcus, 1994):

$$\Delta G_{HB} = \left(\frac{\Delta_{tr} G^*}{-0.929 \text{ kJ/mol}} \right) \tag{5.3}$$

where $\Delta_{tr}G^*$ is the Gibbs free energy of transfer of ions from heavy to light water ($H_2O \rightarrow {}^2H_2O$) and - 0.929 kJ/mol is the difference in hydrogen bonding energies of light and heavy water.

The ΔG_{HB} values for F^- and NO_3^- (0.08 and -0.68, respectively; Table 2.2) determine whether they are classified as water structure-making or structure-breaking ions (Marcus, 1994). In pure water solutions at 25°C each water molecule is hydrogen bonded to an average 1.55 other water molecules (Marcus and Ben-Naim, 1985). Near F^- ions 1.55 + 0.08 = 1.47 hydrogen bonds are available and F^- is defined as being water structure-making; thus more strongly hydrated. Near NO_3^- ions 1.55 - 0.68 = 0.87 hydrogen bonds are available and thus NO_3^- is a structure-breaking ion. NO_3^- has a lower Gibbs free energy ($\Delta_{hyd} G^0_{calc}$, -275 kJ/mol compared to -345 kJ/mol

for F^-, Table 2.2). While it is to date not understood if water molecules separate from their ions during transport through ion-exchange membranes, it is hypothesised that separation is possible if the 'transport energy' is greater than the Gibbs free energy that bonds the hydrated shell to the ion.

Ion mobility and ionic permeability (Strathmann, 2004) further influences transport through ion-exchange membranes. The ionic mobility of NO_3^- in solution (7.4×10^{-8} m^2/sV) solution is greater than the ionic mobility of F^- (5.7×10^{-8} m^2/sV) (Atkins, 1990). The current passing through an ionic solution in ED and the resultant transport of ions is related to the conductivity of the ionic solutions. The ion equivalent conductivity of NO_3^- (71.5 $cm^2/\Omega.equiv$) is greater than that of F^- (55.4 $cm^2/\Omega.equiv$), all factors contributing to higher flux of NO_3^- than F^-. To confirm those results independent of their concentration, an experiment with the same initial mass concentration for boron, F^- and NO_3^- (10 mg/L at pH 10) was carried out. The removal of NO_3^- was 95.3 % compared with 76.2 % for F^-, further indicating that NO_3^- with the smaller hydrated radius is removed more efficiently than F^- with the larger hydrated radius.

5.4 Implications of Organic Matter on Inorganic Contaminant Removal

Figure 5.16 shows the removal of OM as a function of solution pH from the diluate and concentrate. The fact that OM was removed from both compartments indicates that this removal was from deposition on the membranes rather than transport through the membranes. However, staining of the membranes indicates that membrane penetration occurs. Removal of AA from the diluate was low with an average of 9.2 ± 1.6 % and was independent of pH given its negative charge at pH 3-12. The removal of HA and TA from the diluate was higher with an average removal of 19.1 ± 3.7 % and 19.8 ± 9.5 %, respectively. While HA removal is pH independent, the removal of TA increased with pH to 44.3 % at pH 12 due to its increasing negative charge. Removal of OM from the concentrate was less than OM removal from the diluate due to electrostatic repulsion with the negatively charged functional groups in the CEMs adjacent to the concentrate compartment. This

confirms the results of Park *et al*. (2003a) who found that deposits occur mostly on the diluate side of AEMs.

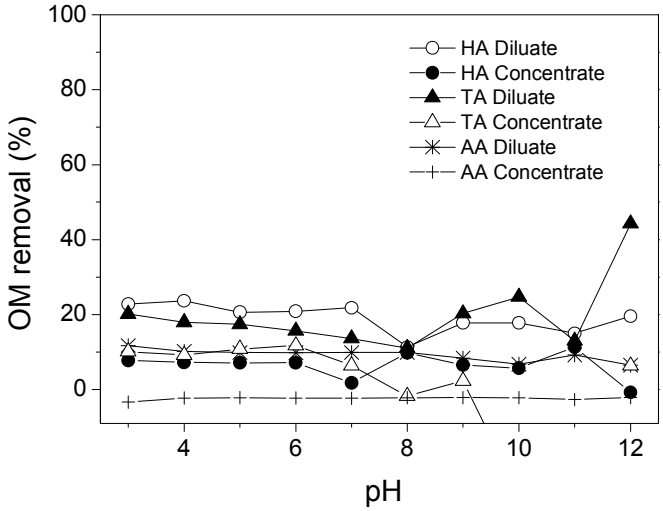

Figure 5.16. OM removal from the diluate and concentration as a function of solution pH (12.5 mgC/L OM; experimental duration 140 min).

Table 5.5 compares the removal of F^-, NO_3^- and $B(OH)_4^-$ in experiments with and without OM. OM deposits on the membranes and interacts with inorganic contaminants. The removal of F^- was greater in the presence of OM (Figure 5.12A), which can be attributed to the binding of F^- to the OM (Hayes *et al.*, 1995). The average percentage of F^- removed with TA was 74.8 ± 5.7 %, followed by AA and HA with 72.9 ± 5.8 % and 72.5 ± 4.5 % respectively. The flux of F^- was reduced in the presence of OM. The final flux (after 140 minutes) was 0.019 mg/cm^{2}h, 0.016 mg/cm^{2}h and 0.018 mg/cm^{2}h with HA, TA and AA, respectively compared to 0.020 mg/cm^2.h in the absence of OM. Combined increase in removal and reduced flux indicates F^- membrane deposition.

No significant difference in NO_3^- removal due to OM was observed (Table 5.5). For experiments with TA, NO_3^- removal was highest under acidic-neutral pH conditions (R_D 95.2-93.2 % at pH 3-7). In HA experiments, NO_3^- removal was pH independent

while the flux of NO_3^- (Figure 5.13B) was reduced in the presence of OM. This again demonstrated some degree of membrane deposition.

The presence of OM enhanced boron removal between pH 3 and 8 (Figure 5.12C) while above pH 9, the removal of $B(OH)_4^-$ in the presence of OM was lower. $B(OH)_4^-$ flux at high pH was lower in the presence of OM (Figure 5.13C), and again results indicate $B(OH)_4^-$-OM complexation and $B(OH)_4^-$ membrane deposition. The S.D. associated with the removal of $B(OH)_4^-$ presented in Table 5.5 is high due to the pH dependent removal of $B(OH)_4^-$.

Table 5.5. Comparison between the average removal (R_D ± S.D.) of F^-, NO_3^- and $B(OH)_4^-$ in the presence and absence of OM.

Experiment	Removal (R_D, %)		
	F^-	NO_3^-	$B(OH)_4^-$
Without OM	68.3 ± 4.5	94.1 ± 1.3	24.7 ± 20.3
Humic Acid	72.5 ± 4.5	92.9 ± 2.7	24.6 ± 7.0
Tannic Acid	74.8 ± 5.7	92.5 ± 4.4	27.9 ± 12.5
Alginic Acid	72.9 ± 5.8	93.2 ± 3.3	27.2 ± 6.7

5.5 Inorganic Contaminant Membrane Deposition

The deposit formation can be quantified using mass balance. The mass of F^- deposited on the membranes is shown in Figure 5.17A, with negligible deposition in experiments without OM. In the presence of OM the mass of F^- deposited was between 0.4 and 2.3 mg/cm^3 (4.7 and 28.8 % initial mass); with a greater amount deposited with HA and TA. HA contains voids which can trap inorganic compounds (Schulten and Schnitzer, 1995) and binding of F^- has been shown to be pH dependent (Hayes *et al.*, 1995). Hayes *et al*. (1995) studied the binding of F^- to HA as a function of solution pH (5.0-6.6) and in this narrow pH range F^- was being trapped within the large structure of HA rather than bound to a particular functional group. As solution pH increases HA deprotonates and the negative charge on the carboxylates repels the F^- ion. This phenomenon was not observed in this current study because the

adsorption of F^- in ED would be governed by several other factors (e.g. presence of other contaminants).

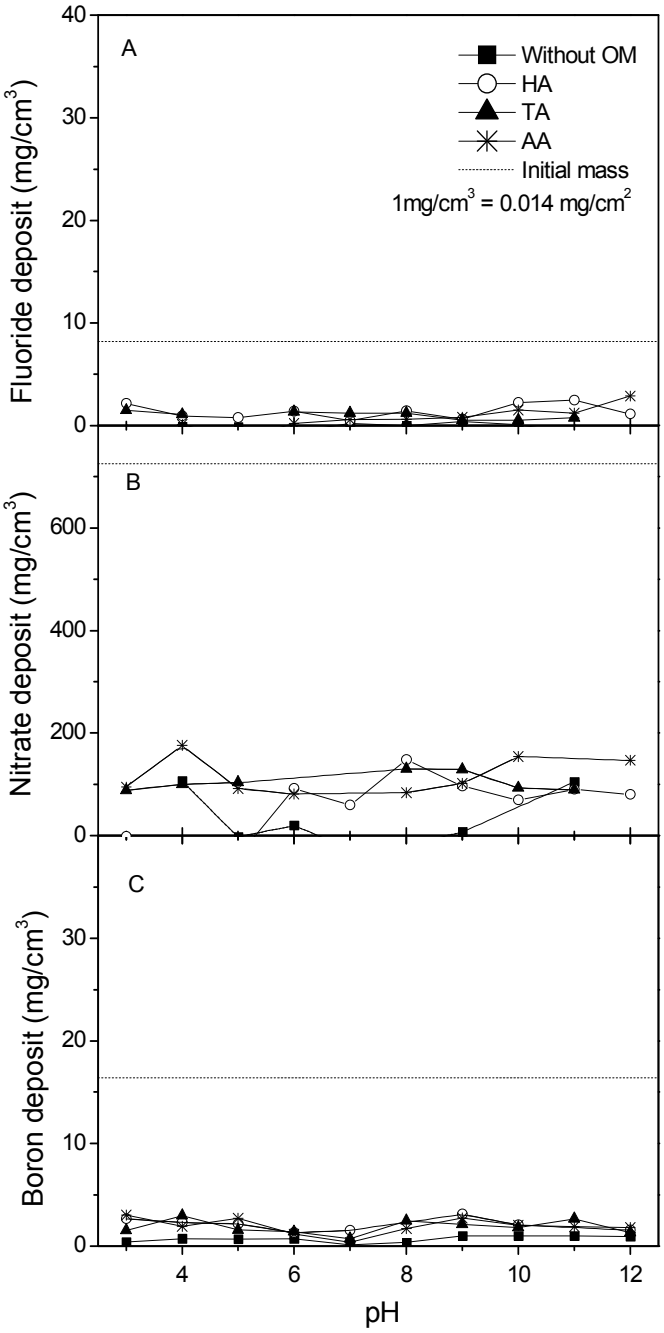

Figure 5.17. Membrane deposit of (A) F^- (B) NO_3^- and (C) $B(OH)_4^-/B(OH)_3$ as a function of solution pH (3-12) (Initial feed concentration (diluate and concentrate combined): 8.2 mg/cm^3 F^-, 725.0 mg/cm^3, NO_3^-, 16.4 mg/cm^3 $B(OH)_3$; experimental duration 140 min).

The mass of NO_3^- deposited on the membranes was greater in experiments with OM (Figure 5.17B) with values of between 58.5 and 175.5 mg/cm^3 (8.1 and 24.2 % initial mass). Contrary to the negative charge of HA above pH 5 (Table 2.7) the mass of NO_3^- adsorbed to the membranes in the presence of HA increased above pH5. Adsorption of NO_3^- in experiments with TA was independent of pH. In the presence of AA, the mass of NO_3^- adsorbed was lower at pH 6 - 8 because repulsion between the negatively charged AA and NO_3^- would be expected.

The mass of $B(OH)_4^-$ deposited on the membranes is greater in experiments with OM (Figure 5.17C) with values of between 0.7 and 3.1 mg/cm^3 (4.0 and 19.0 % initial mass). Removal of $B(OH)_3$ between pH 3 and 8 (Figure 5.12C) may be the result of $B(OH)_3$ complexation with polar organic compounds (Chauveheid and Denis, 2004; Lemarchand *et al.*, 2005), such as HA. Schmitt-Kopplin *et al*. (1998) postulated that $B(OH)_3$ binds to carboxylate groups (COO^-) within HA where it forms a transient hydrogen bonded structure with the HA. A schematic of this complexation mechanism is shown in Figure 5.18. Due to the transport direction of the negatively charged HA, $B(OH)_4^-$ is deposited on the AEMs. The decrease in removal of $B(OH)_3$ above pH 9 in the presence of OM can be attributed to electrostatic repulsion between negatively charged $B(OH)_4^-$ and OM.

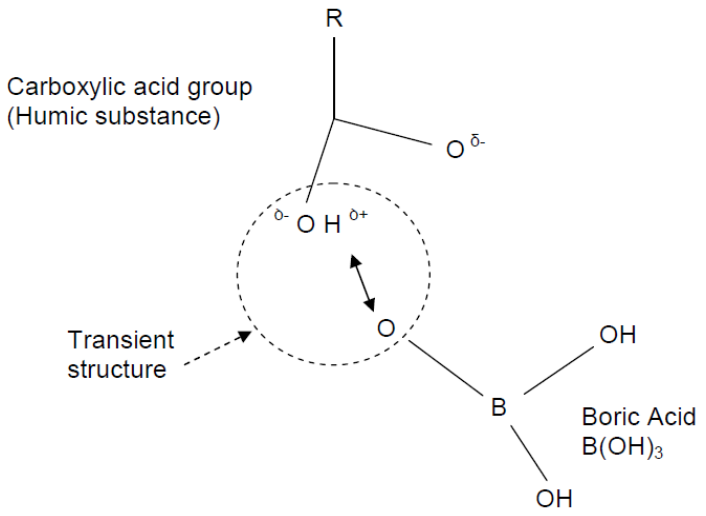

Figure 5.18. Schematic of $B(OH)_3$ complexation with humic substances.

5.6 Organic Matter Membrane Deposition

UV-Vis and NPOC measurements showed a decrease in OM within the ED system over the duration of each experiment. The reduction of OM in both diluate and concentrate indicates that the OM is deposited. Minimal deposition of OM is expected to occur on the CEMs due to electrostatic repulsion between the membrane surface and the negatively charged functional groups of the OM. Figure 5.19 shows that the mass of OM (mgC) deposited on the AEMs was greater than the mass deposited on the CEMs, which confirms results Lee *et al.* (2002a). The negatively charged HA deposits more readily on the positively charged AEMs in experiments with a higher solution pH. However, Park *et al*. (2003a) showed that HA has a negative zeta potential in a wide pH range, so that it can foul AEMs in almost the entire pH range. In this study the amount of HA deposited on the AEMs showed a slight decrease with increasing solution pH (from pH 6) (Figure 5.19A) which cannot be explained by repulsive forces. The macromolecular structures of HS influences the properties and affinities of these materials (Ghosh and Schnitzer, 1980). According to Chen and Schnitzer (1976), HS behave like uncharged (spherical) polymers at very low pH whereas at high pH, they exhibit polyelectrolytic character of linear shape. Lee *et al*. (2002b) postulated that the fouling of an AEM is related more to the properties of the foulant (humate) than the electrostatic force between the foulant and the membrane.

Unlike HA, the mass of TA deposited on the AEM was pH independent (Figure 5.19B), with an exception (decrease) at neutral pH. As large molecular weight organics have more difficulty in permeating the AEMs (Park *et al.*, 2003a), TA, with its lower molecular weight, has increased potential for transportation through the AEM compared to HA. The mass of AA deposited on the AEMs was lower than HA and TA over the studied pH range (Figure 5.19C). Avaltroni *et al*. (2007) found that the structure of AA follows three pH dependent trends (1) increased aggregation below pH 4 due to a decrease in charge density, (2) molecular expansion between pH 4 and 8 and (3) dissociation above pH 8. The variability seen in the mass above pH 8 could be attributed to AA dissociation.

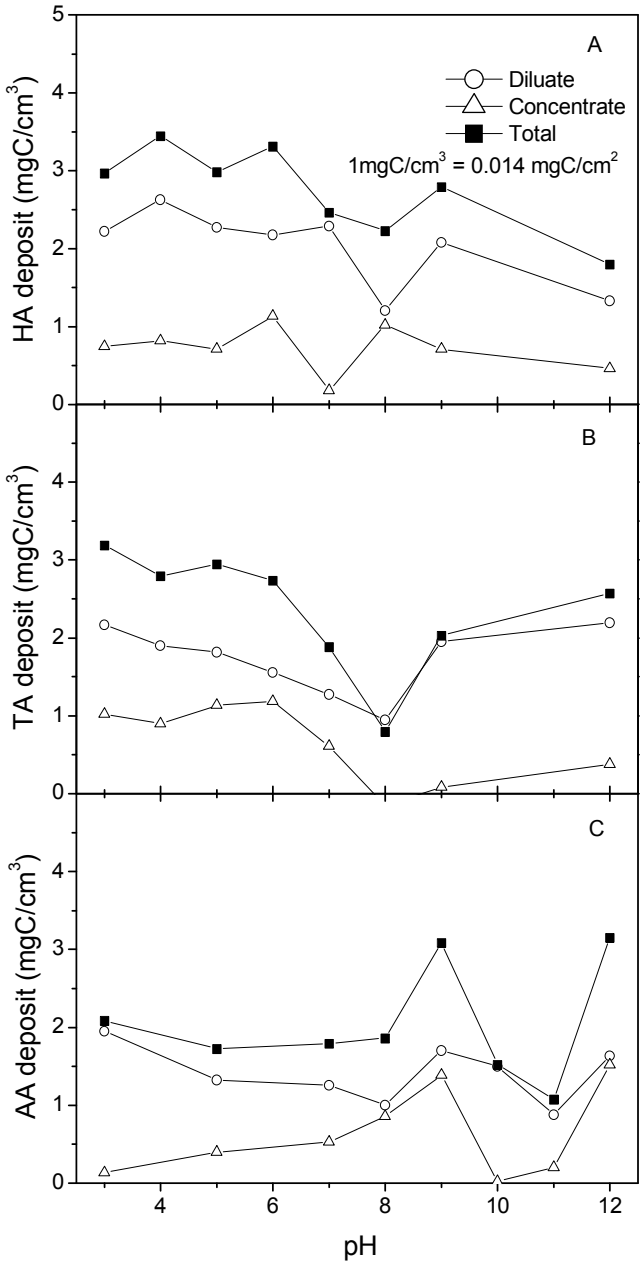

Figure 5.19. Membrane deposit of (A) Humic acid (B) Tannic acid and (C) Alginic acid as a function of solution pH (3-12) (Initial feed mass (diluate and concentrate combined) of OM was 100 mgC (20.5 mgC/cm^3); experimental duration 140 min).

SUVA (L/mg.m) values for HA experiments are shown in Figure 5.20. SUVA is used as an indicator for the aromatic content of carbon within a water sample (Croué *et al.*, 1999). SUVA values in the diluate and concentrate for the HA experiments

were pH and time independent with a values between 2.6 and 5.6 L/mg.m. Shin *et al*. (1999) stated that the non-aromatic (aliphatic nature) fractions of HA have a larger molecular size in comparison to the aromatic and carboxylate groups of smaller size fractions. Results from this study, therefore, indicate that ED does not separate the aromatic and non-aromatic fractions of HA.

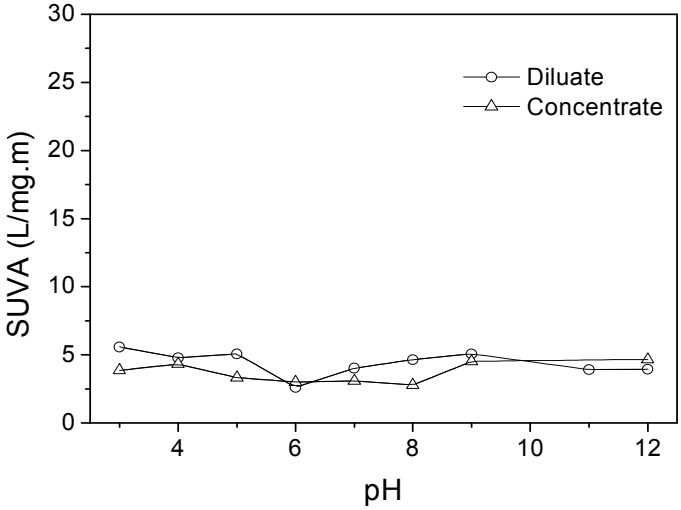

Figure 5.20. SUVA (L/mg.m) as a function of pH (3-12) (Initial mass of HA 100 mgC; experimental duration 140 min).

5.7 Analysis of Membrane Fouling

The AEM surface in contact with the diluate showed visible fouling with HA and TA. Photographs of the membranes used in experiments with HA are shown in Figure 5.21. Membranes exposed to TA were visibly similar to those exposed to HA This fouling was not reversed by chemical cleaning indicative of strong binding of the OM to the AEM functional groups and penetration into the membrane. The observed colour change was more pronounced on the area of membranes in contact with ED stack inlets. The fouling of the AEMs was accompanied by visible swelling. The hydrophobic and hydrophilic acids contained in OM cannot pass through the membranes due to their high molecular weight and it is thought that a fraction of the OM is transported through the membranes as a result of their negative charge density and molecular structure (Kim *et al.*, 2002; Lee *et al.*, 2002b; Park *et al.*, 2003a).

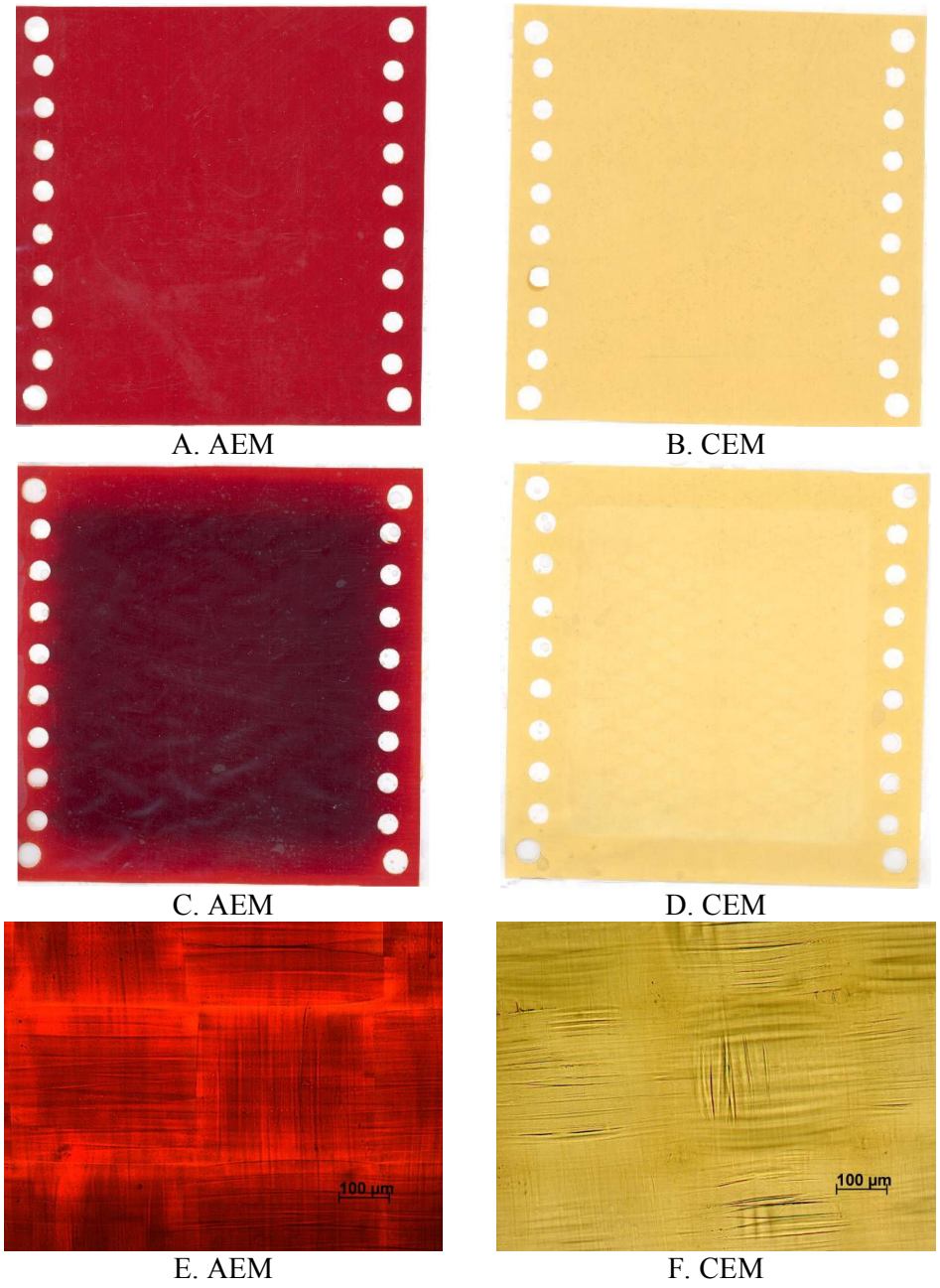

Figure 5.21. Top view of (A, B) unused AEM and CEM (C, D, E, F) AEM and CEM exposed to HA (12.5 mgC/L) (A, B, C, D: Canon IXUS 65; E, F: Axioskop 2 MAT, Zeiss Optical, UK, Optical zoom 100×).

The surface of the CEMs in contact with both the concentrate and diluate presented little visible evidence of fouling, due to electrostatic repulsion of the negatively charged functional groups within the CEM. Although visible fouling was noted on the AEM, no major difference in spectra was observed in the presence of HA using

^{13}C NMR spectroscopy (Figure 5.22). This, however, does not mean that fouling had not occurred as the detection limit of ^{13}C NMR is ~ 1% wt of a particular carbon-rich OM component in another component (e.g. membrane) (Apperley, 2009) and greater than the mass of HA sorbed to the membrane sample analysed.

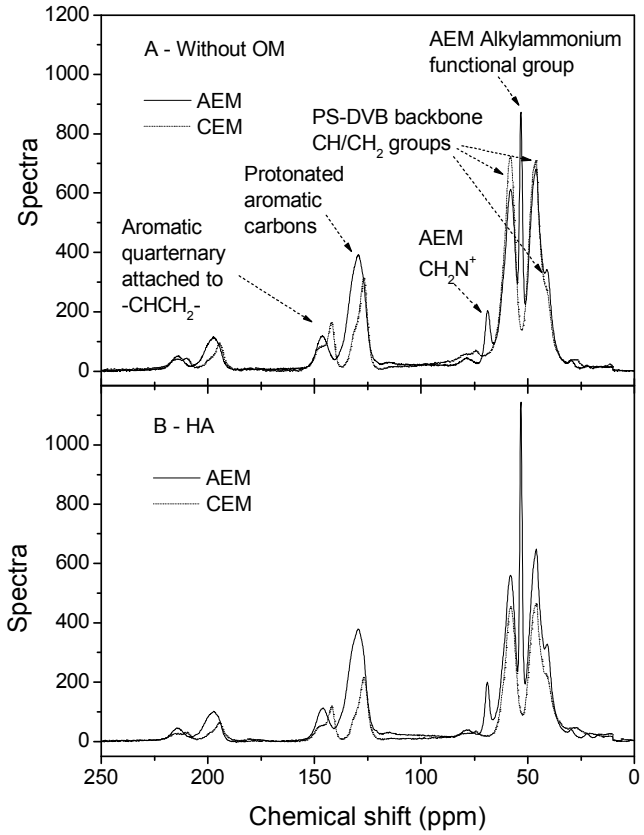

Figure 5.22. Solid state ^{13}C NMR spectra for an AEM and CEM (A) unused and (B) exposed to HA (1mM $NaHCO_3$, 5 g/L NaCl, 12.5 mgC/L HA).

The surface morphology of an AEM exposed to TA was studied using FIB-SEM coupled with EDX. No distinguishing features to indicate fouling were observed (Figure 5.23A). The small particles on the AEM surface are ice crystals due to the low temperature of the membrane sample. EDX spectral analysis of the membrane surface (Figure 5.23B, C, E) showed no distinct pattern in the distribution of carbon (C), chloride (Cl) and boron (B). The aggregation of oxygen (O) on the membrane surface (white dots in Figure 5.23D) further indicates the presence of ice crystals. F^- was not detected above the background noise of the spectral signal (Figure 5.23F).

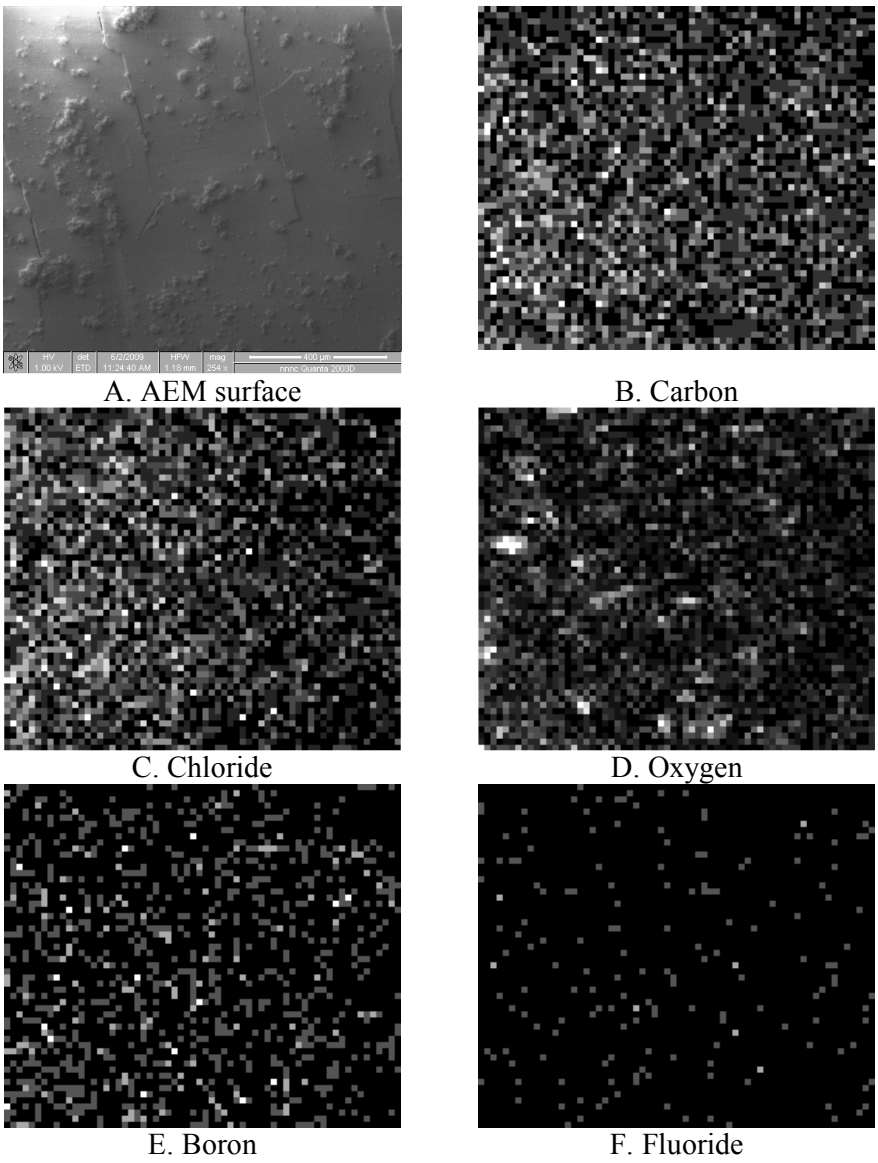

Figure 5.23. (A) FIB-SEM surface image of AEM exposed to TA during ED experiments (FEI Quanta 2003D, USA, 1 kV beam energy) and (B-F) EDX elemental maps of AEM surface (Oxford Instruments INCAx-sight, UK, 15 kV beam energy).

Elemental analysis of the cross section of the AEM, however, facilitated the understanding of the modification of the membrane structure due to the presence of OM. EDX undertaken on cross-sections of an AEM exposed to HA and TA (Figure 5.24A and B, respectively) showed the presence of C, O and Cl through the membrane, in contrast to the peaks of C, O and Cl within the top and bottom 30-50

μm of the unused AEM (Figure 4.6). B was detected slightly above the background spectra within the AEM exposed to HA. While the presence of Cl and B can be attributed to the transport of Cl^- through the AEM from NaCl and $B(OH)_4^-$ in the ED feed solution, the presence of C and O indicates the penetration of OM.

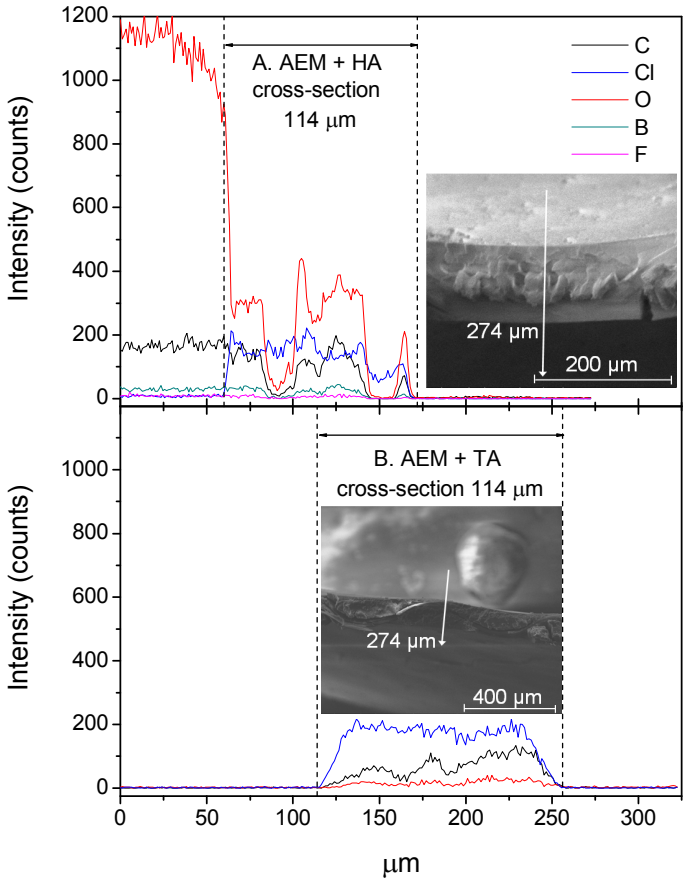

Figure 5.24. Cross-sectional EDX line profile of AEM exposed to (A) HA and (B) TA during ED experiments (15 kV beam energy). Inset FIB-SEM cross-section images of AEM exposed to (A) HA and (B) TA (15 kV beam energy, 802 and 280× magnification).

5.8 Electrodialysis Parameters and Performance

The evolution of electrical resistance during the ED experiments with and without OM is shown in Figure 5.25. An increase in resistance was observed at the beginning of the ED process in all experiments because of ion depletion within the diluate and membrane boundary layer. An increase in resistance observed at the end of the ED experiments without OM is attributed to the higher demineralization rate in the

diluate solution. However, the deposition of inorganic contaminants and OM on the membranes has implications for ED performance. ED stack resistance as a function of solution pH is shown in Figure 5.26. OM deposition as a foulant layer on and/or inside the membranes increases the resistance at the membrane surface (Lindstrand *et al.*, 2000b; Park *et al.*, 2006). Between pH 3 and 8 the average stack resistances were indeed greater in the presence of OM; HA (46.3 ± 2.2 Ω), TA (51.3 ± 5.0 Ω) and AA (44.5 ± 1.6 Ω), due to enhanced OM deposition within this pH range (Figure 5.19). Above pH 8, resistance decreased due to decreased OM membrane deposition.

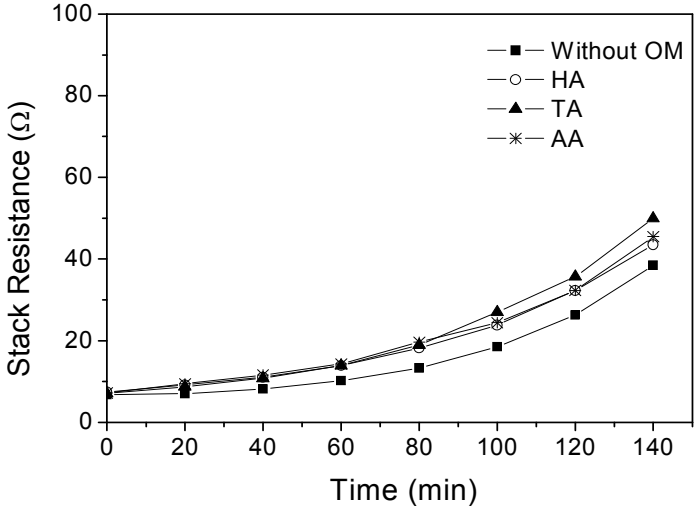

Figure 5.25. Electrical resistance (Ω) as a function of time (Solution pH 7).

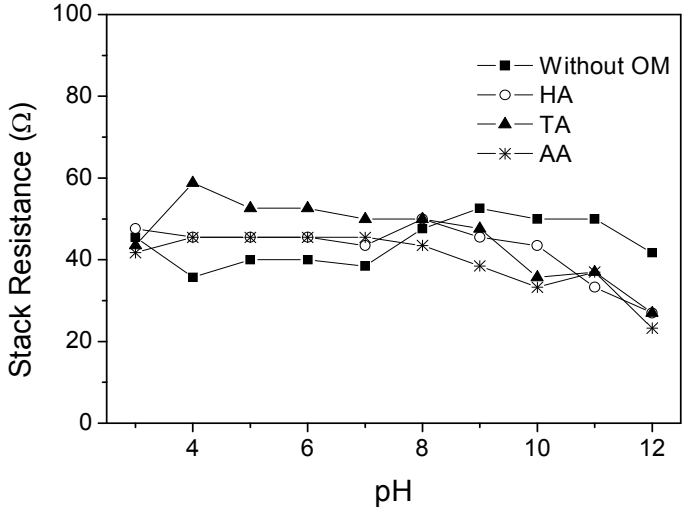

Figure 5.26. Electrical resistance as a function of solution pH (3-12) (Experimental duration 140 min).

The current density across the stack for the duration of each experiment (with and without OM) was below the theoretical LCD (Figure 5.27). Although the presence of NaF, $NaNO_3$ and $B(OH)_3$ within the feed solution would contribute to the measured EC, it was converted using eqn (4.2) to estimate when the NaCl DWG was reached and to calculate the theoretical LCD. The theoretical LCD presented in Figure 5.27 represents the minimum calculated LCD. After the NaCl DWG was reached (between 131 and 138 min) the current density was still below the experimental LCD.

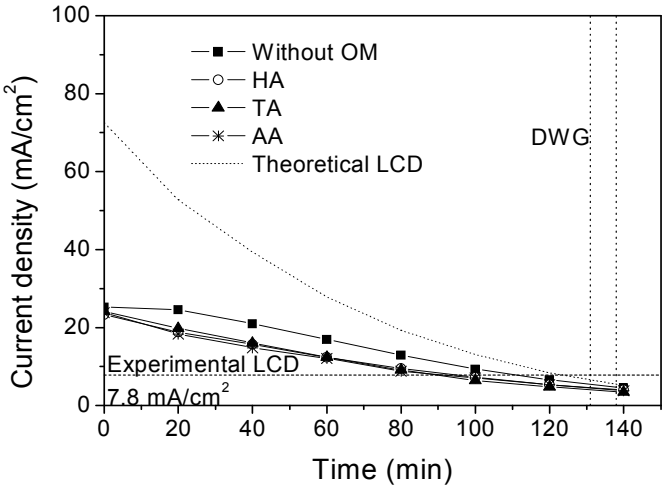

Figure 5.27. Current density (mA/cm^2) as a function of time (Solution pH 7; vertical dotted lines indicate time period in which the DWG was reached).

As the concentration of NaF, $NaNO_3$ and $B(OH)_3$ and OM within the diluate decreases with time and as the electrical resistance increases, the current needed to keep the applied voltage constant decreases exponentially (Figure 5.28, $R > 0.99$). The decrease in current density was more pronounced in the experiments with OM due to the membrane deposition of the OM. Numerous studies have reported decreases in current density as a result of membrane fouling during ED (Audinos, 1989; Mondor *et al.*, 2009). Similarly, power consumption and SEC decreased in the presence of OM (Table 5.6).

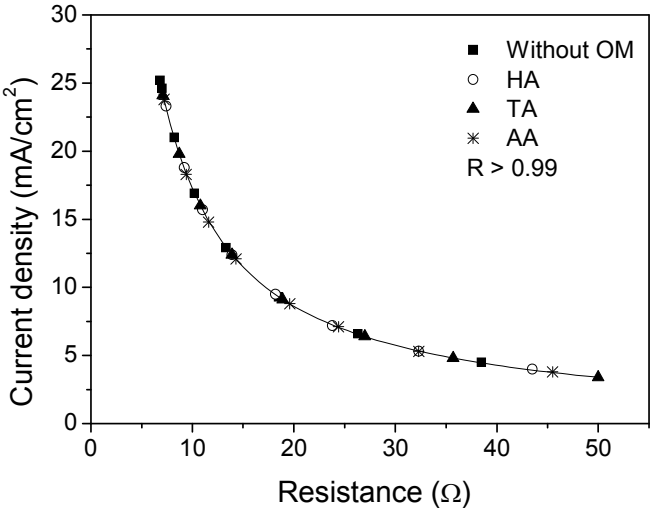

Figure 5.28. Electrical resistance (Ω) vs. current density (mA/cm^2) at pH 7.

Table 5.6. Power consumption (Wh) and specific energy consumption (SEC, Wh/L) of the ED stack in the production of drinking water (DWG 0.5 g/L NaCl) in the presence and absence of OM at pH 7.

Experiment [a]	Power consumption (Wh)	SEC (Wh/L)
Without OM	20.5 ± 0.5	5.7 ± 0.1
Humic Acid	16.0 ± 0.4	4.8 ± 0.1
Tannic Acid	15.9 ± 0.3	4.7 ± 0.1
Alginic Acid	15.5 ± 0.3	4.7 ± 0.1

[a] New membranes used for each set of experiments.

The performance of the ED process can be evaluated by the removal of EC (Figure 5.29). The average percentage of EC removed without OM was 93.0 ± 2.1 % compared with 91.7 ± 2.5 %, 92.6 ± 3.0 % and 89.4 ± 4.8 % with HA, TA and AA respectively. The presence of OM on the membranes did not significantly lower EC removal. It is possible the OM was loosely packed on the AEM still allowing for the migration of salt ions through the membrane; though at a slightly decreased initial flux (Figure 5.30; Without OM: 1.02 × 10^{-2} mS/cm/cm^{2}h; HA: 0.96 × 10^{-2} mS/cm/cm^{2}h; TA: 0.90 × 10^{-2} mS/cm/cm^{2}h; AA: 0.84 × 10^{-2} mS/cm/cm^{2}h).

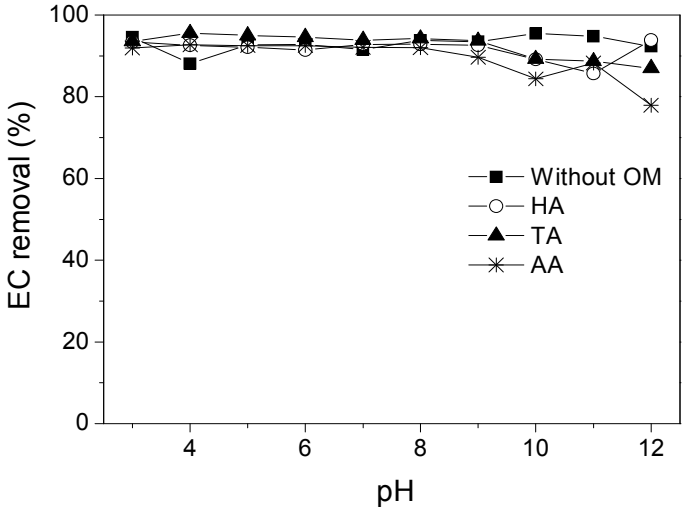

Figure 5.29. The removal of EC (%) from the diluate as a function of solution pH (3-12) (5 g/L NaCl feed concentration; experimental duration 140 min).

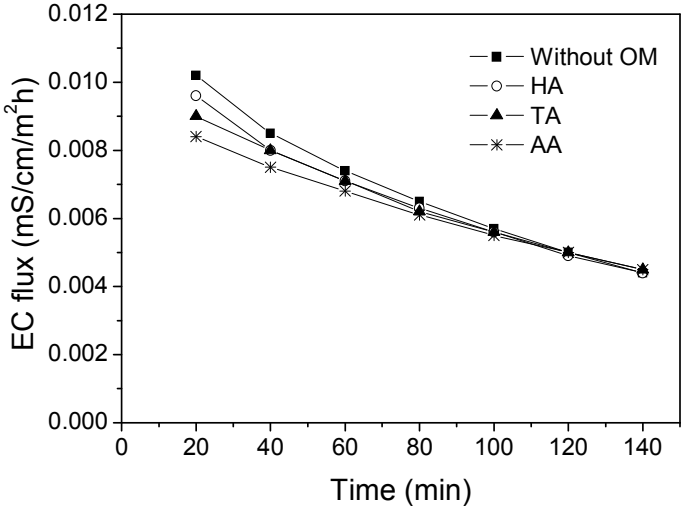

Figure 5.30. Flux of EC (mS/cm/cm^{2}h) (Initial feed EC: 9900 mS/cm).

5.9 Summary

The purpose of the first section of this chapter was to determine the LCD and investigate the desalination kinetics of the ED stack. Results from the experimental determination of the LCD were consistent with a range of published studies, particularly with regards to increase in LCD with linear flow velocity. In the practical application of ED, the ED system should be operated below the theoretical LCD to minimise concentration polarisation. Therefore, the ED system used in this

study was operated at an appropriate voltage (Experimental conditions during this study: 10 V at 1.5 L/min or 12 V at 3 L/min). While NaCl removal increased with applied voltage due to higher initial flux, it decreased as feed salt concentration increased. Power consumption and SEC increased with applied voltage and feed concentration due to the higher concentration of current carriers within the diluate. The consequence of operation above the theoretical LCD was a significant increase in stack resistance, which thus hampered NaCl flux, and the overall removal achieved. Operation over the LCD resulted in higher energy consumption (9 V: 31.0 Ω, 18 V: 85.7 Ω).

The second purpose of this chapter was to understand the mechanisms of inorganic contaminant removal during ED in the absence and presence of OM. The removal of the contaminants followed the order NO_3^- > F^- > $B(OH)_4^-$. Their transport through the ion-exchange membranes was evaluated in relation to hydrated ionic radius and subsequent strength of hydration shells. A positive correlation was found in the absence of OM. NO_3^-, with the smaller hydrated radius and weaker hydration shell, was removed more effectively than F^-, which has a larger hydrated radius and stronger hydration shell. The removal of F^- and NO_3^- was not significantly influenced by solution pH due to their pH independent speciation. The removal of $B(OH)_4^-$ was dependent on increasing solution pH and the degree of demineralisation.

The removal of the inorganic contaminants F^- and $B(OH)_4^-$ was enhanced by the presence of dissolved OM (HA, TA and AA) while the flux decreased indicating mutual dependence of inorganic and organic contaminants in ED. The mechanism for this involves the possible territorial binding of F^- within the negatively charged OM structure and complexation of $B(OH)_3$ with carboxylate groups in the OM and the subsequent OM deposition on the positively charged AEMs. This membrane deposition led to an increase in stack electrical resistance and a slight reduction in initial EC flux. Although OM fouling during the experiments was less than that experienced under real conditions, it is important to study the behaviour of these contaminants with OM to better understand the feasibility and applicability of ED for the treatment of real waters.

Chapter 6. Inorganic Contaminant Removal from a Real Brackish Groundwater

The presence and fate of contaminants in groundwater is a serious issue and the increase in concern means that the problem requires increased attention from within the scientific community. Therefore, in this chapter the removal of inorganic contaminants from a brackish groundwater using ED is investigated.

As shown in Chapter 5, a higher applied voltage increased NaCl flux and thus removal. The transport of contaminants during ED is also highly dependent on the applied voltage. Changes in solution pH within the brackish groundwater will have implications for chemical form, contaminant solubility, solute-solute interactions and thus inorganic removal and membrane deposition in ED. The influence of solution pH on membrane scaling during the ED of groundwater has not been investigated. Therefore, the main objective of this chapter was to evaluate the influence of applied voltage and solution pH on inorganic contaminant removal during ED. The rationale of this was to identify the mechanisms of inorganic contaminant removal from groundwater including membrane deposition in the form of scaling and the influence of solute-solute interactions. To achieve this, the study was conducted in five stages, specifically (1) mechanisms of inorganics removal from groundwater as a function of applied voltage (12 and 18 V), (2) impact of applied voltage on inorganic membrane scaling, (3) mechanisms of inorganics removal from groundwater as a function of solution pH (3-11), (4) impact of solution pH on inorganic membrane scaling and (5) impact of scaling on ED system operation parameters (TDS removal and flux, stack resistance).

6.1 Groundwater Origin and Characteristics

In Australia, approximately 67 % of indigenous communities with a population less than 100 people use groundwater for their supply (ABS, 2002). In these remote communities, drinking water is generally sourced from groundwater bores of varying quality. The ED experiments were performed on groundwater (bore number

RN13693) sourced from Pine Hill Station, a cattle farm approximately ~140 km northwest of Alice Springs, Northern Territory, Australia (Werner and Schäfer, 2007) (Figure 6.1). This bore was chosen due to its high salinity, hardness and elevated contaminant content. The concentrations of inorganic contaminants of interest within the groundwater along with their respective drinking water guideline levels are outlined in Table 6.1. The concentrations presented were specifically measured in the groundwater and relate to an average feed concentration for the ED experiments. The inorganic contaminants above the DWG values were boron, chloride, fluoride, nitrate, sodium, sulphate, uranium and selenium. While there are no set guidelines for calcium and magnesium, concentrations within the groundwater were high.

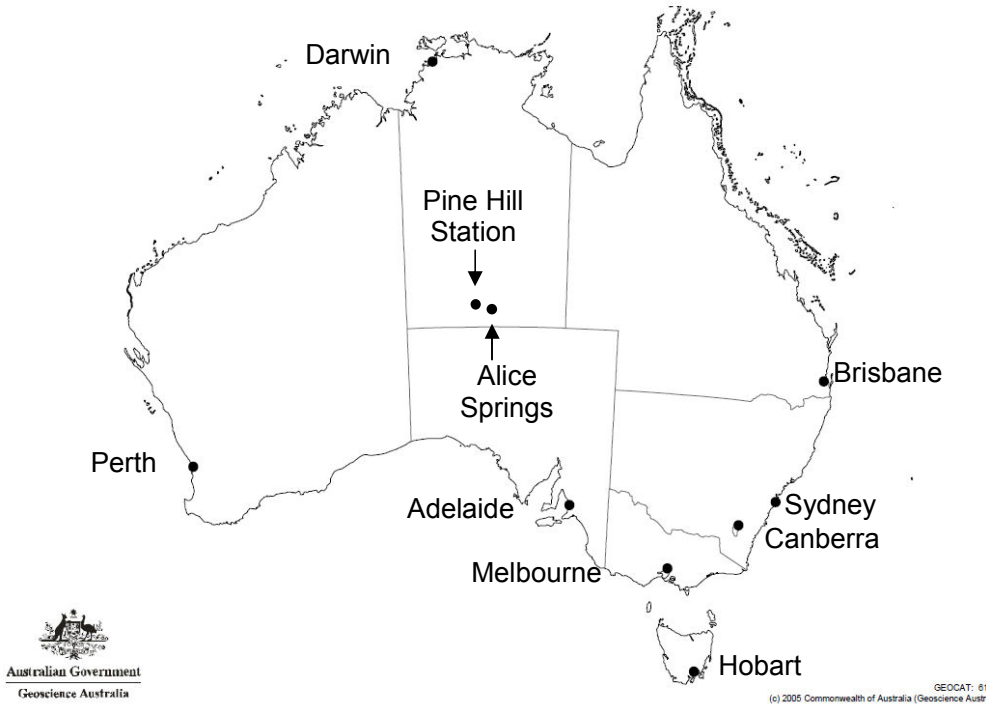

Figure 6.1. Location of Pine Hill Station, Northern Territory, Australia (Map sourced from Geoscience Australia (2005).

Table 6.1. Water quality at Pine Hill Station in comparison with drinking water guideline values (DWG).

Inorganic	Symbol	Unit	Groundwater concentration	ADWG [a]	DWG WHO [b]	EU [c]
Monovalent ions						
Boron	B	mg/L	1.30	0.3	0.5	1
Bromide	Br^-	mg/L	10.6	n/a	n/a	n/a
Chloride	Cl^-	mg/L	2000	250 [e]	n/a	250
Fluoride	F^-	mg/L	5.82	1.5	1.5	1.5
Nitrate	NO_3^-	mg/L	31.1	50	50 (25) [d]	50
Lithium	Li^+	mg/L	0.04	n/a	n/a	n/a
Potassium	K^+	mg/L	35.4	n/a	n/a	n/a
Sodium	Na^+	mg/L	1650	180 [e]	200 [e]	200
Multivalent ions						
Sulphate	SO_4^{2-}	mg/L	717	500 [e]	n/a	250
Uranium	U	mg/L	0.26	0.02	0.015	n/a
Calcium	Ca^{2+}	mg/L	105	n/a	n/a	n/a
Magnesium	Mg^{2+}	mg/L	172	n/a	n/a	n/a
Strontium	Sr^{2+}	mg/L	2.30	n/a	n/a	n/a
Zinc	Zn^{2+}	mg/L	0.22	3 [e]	3	n/a
Arsenic	As(V)	mg/L	0.006	0.007	0.01	0.01
Selenium	Se(VI)	mg/L	0.02	0.01	0.01	0.01
General water quality parameters						
TDS [f]		g/L	5.3	0.5	n/a	n/a
pH		-	8.4	6.5-8.5	n/a	6.5-9.5
EC		µS/cm	8290 [g]	n/a	n/a	n/a

[a] Australian Drinking Water Guideline (ADWG) (NHMRC, 2004); [b] World Health Organization (WHO, 2006); [c] European Union Directive (EU, 1998); [d] Recommended value in parentheses; [e] Aesthetic guideline value; [f] Calculated using TDS = 0.64 × EC (McNeil and Cox, 2000); [g] Average of feed conductivity throughout field testing at Pine Hill Station (Schäfer *et al.*, 2007)); n/a Not regulated.

In Australian remote communities water hardness due to high concentrations of calcium (Ca^{2+}) and magnesium (Mg^{2+}) is a widespread issue (Werner and Schäfer, 2007). Ca^{2+} is a major constituent in most surface and groundwater. Common mineral forms of Ca^{2+} are calcite and aragonite (carbonate mineral, $CaCO_3$), gypsum ($CaSO_4.H_2O$), anhydrite ($CaSO_4$), and fluorite (CaF_2) (Cockell, 2003). Sources of Mg^{2+} include ferromagnesium minerals in igneous and metamorphic rocks and Mg^{2+} carbonate ($MgCO_3$) in limestone and dolomite (WHO, 2009). High levels of Ca^{2+} and Mg^{2+} can reduce the palatability of water and also lead to the blocking of water

distribution pipes by the precipitation of $CaSO_3$ scale (Montgomery, 1985). At high concentration in drinking water, Mg^{2+} salts may have laxative effects (WHO, 2009).

Potassium (K^+) is less abundant than sodium (Na^+) in natural waters but runoff from agricultural regions may contribute to temporary high concentrations in nearby surface water as a result of vegetative decay. In regards to drinking water and human health, K^+ generally creates no adverse effects. Sulphate (SO_4^{2-}) is a dominant sulphur species in the aquatic environment and its level is greatly elevated in polluted groundwater as direct result of acidic deposition due to the use of coal, oil and other sulphur-containing fuel (Nriagu and Hem, 1978). The presence of SO_4^{2-} in drinking water does not pose a health threat but affects its aesthetic quality (WHO, 2006) and is an indicator for the acidification of water, which in turn is a considerable health concern.

Uranium (U) is a naturally occurring element that is present in nearly all rocks and soils and is redistributed in the environment by weathering, volcanic eruptions and also released by the operation of coal-burning power plants (ATSDR, 2000d; Lide, 2008). U, which was significantly above the DWG values in the Pine Hill groundwater, is of principal health concern because soluble U compounds lead to damage to renal tissue. U toxicity is however dependent upon chemical and physical form and route of intake. The water-soluble compounds (uranyl nitrate hexahydrate ($UO_2(NO_3)_2$), uranium hexafluoride, uranyl fluoride (UF_6), uranium tetrachloride (UCl_4), uranium pentachloride (UCl_5)) have been found to be the most toxic in regards to renal function (ATSDR, 2000d).

Although selenium (Se) is an essential trace element, it is toxic if taken in excess and can lead to selenosis. Symptoms of selenosis include gastrointestinal disorders, hair loss, fatigue and neurological damage. Extreme cases of selenosis can result in cirrhosis of the liver, pulmonary oedema and death (Bertolino *et al.*, 2006; Tinggi, 2003). The toxicity of Se in the environment depends on its concentration and also on its chemical form. Selenite (SeO_3^{2-}, Se(IV)) is more toxic than selenate (SeO_4^{2-}, Se(VI)) (Pitts *et al.*, 1995).

Bromide (Br^-) is naturally present in raw water, especially in groundwater and surface water in coastal regions. Industrial activities, such as pest control (Ge *et al.*, 2007), has led to elevated concentrations in natural waterways. Br^- is considered non-toxic at concentrations found in most drinking water sources; however, it reacts with commonly used disinfectants, most notably ozone, chlorine and chloramine, to produce bromo-disinfection by-products (Richardson et al 2003), which are highly toxic for human health.

6.2 Chemical Speciation of the Groundwater

It is important to quantitatively predict the chemical speciation of the inorganic contaminants as changes in solution pH, and thus speciation and solubility, will influence inorganic contaminant removal during ED. The modelling of this speciation can aid in explaining the occurrence of solute-solute interactions and trends in removal. Chemical speciation modelling of the selected inorganic contaminants in the groundwater was conducted using Visual MINTEQ (Version 2.53). For further details including input parameters refer to Chapter 4.

A number of assumptions on arsenic speciation were made based on groundwater conditions (Rossiter, 2008). Approximate redox values (Eh) for groundwater in general are +0.2 at pH 8 (aerobic) (Langmuir, 1997). While reducing environments generally occur in waterlogged areas, arid and oxidising conditions persist in Australia. High levels of dissolved manganese (Mn) and iron (Fe) are expected if the environment is reducing (Thayalakumaran *et al.*, 2008). High levels of SO_4^{2-} present at pH 8.4 indicate aerobic conditions (Morel and Hering, 1993). The groundwater has very low (close to detection limit) concentrations of Mn and Fe, indicating that redox conditions of the water was not Mn or Fe reducing. High SO_4^{2-} concentrations indicate SO_4^{2-} reduction did not occur. There were high concentrations of U, which is generally immobilised as uranium dioxide (UO_2) in reducing conditions. Thus, it was assumed that the groundwater is aerobic. Under these conditions, arsenic is present as As(V) at pH 8.4 (Xie *et al.*, 2009). While under mixed conditions As(III) and As(V) might be present, the arsenic species present was assumed to be As(V).

Figure 6.2 shows the predicted speciation of the selected inorganic contaminants within the groundwater and Table 6.2 outlines the predominant species present during the ED experiments undertaken to investigate the influence of applied voltage. Species that were above their saturation index, a measure of precipitation and scaling potential (Ω), are labelled as solid (s). Dissolved uncharged species are labelled as aqueous (aq).

Br^-, Cl^-, NO_3^-, SO_4^{2-}, Na^+ and Se^{6+} are all generally pH independent with Br^-, Cl^-, NO_3^-, SO_4^{2-} and SeO_4^{2-} the predominant species over the studied pH range (pH 3-11), respectively. B, F^-, Li^+, K^+, Na^+ and As(V) exhibit one significant switch in chemical species, which corresponds to their respective pK_a values. Neutral $B(OH)_3$ transitions to dihydrogen borate ion ($H_2BO_3^-$) at pH 9.24. At pH 3, hydrogen fluoride (HF (aq)) dissociates and F^- is the predominant ion from pH 3 to 11. Li^+, K^+ and Na^+ form complexes with SO_4^{2-} at pH 11 to form $LiSO_4^-$, KSO_4^- and $NaSO_4^-$, respectively. The dihydrogen arsenate ion ($H_2AsO_4^-$) transitions to hydrogen arsenate ($HAsO_4^{2-}$) at a solution pH of 6.94. In the groundwater Ca^{2+}, Mg^{2+} and Sr^{2+} are predominantly present in ionic form and all exhibit major changes to precipitated carbonate species $CaCO_3$ (s), $MgCO_3$ (s) and $SrCO_3$ (s), respectively, above pH 9.

The chemical speciation of U and Zn^{2+} is more complicated than the other inorganics. U can exist in five oxidation states: 2+, 3+, 4+, 5+, and 6+ (Lide, 2008). However, only the 4+ and 6+ states are of practical importance. Major compounds of U include oxides, fluorides, carbides, nitrates, chlorides and acetates (ATSDR, 2000d). In the groundwater at high pH both U and Zn^{2+} form carbonate salt species $(UO_2)_2CO_3(OH)^-$, $UO_2(CO_3)_3^{4-}$ and $Zn(CO_3)_2^{2-}$, respectively. However, below pH 9 they undergo a number of transitions. Between pH 3 and 6, freely dissolved UO_2F^+ and uranyl fluoride UO_2F_2 (aq) dominate. Between pH 7 to 10 U forms the $CaCO_3$ complex dicalcium uranyl tricarbonate ($Ca_2UO_2(CO_3)_3$ (aq)). Between pH 3 and 8, ionic Zn^{2+} predominates; followed by a transition to zinc hydroxide ($Zn(OH)_2$ (aq)) and zinc carbonate ($ZnCO_3$ (aq)) between pH 8 and 10.

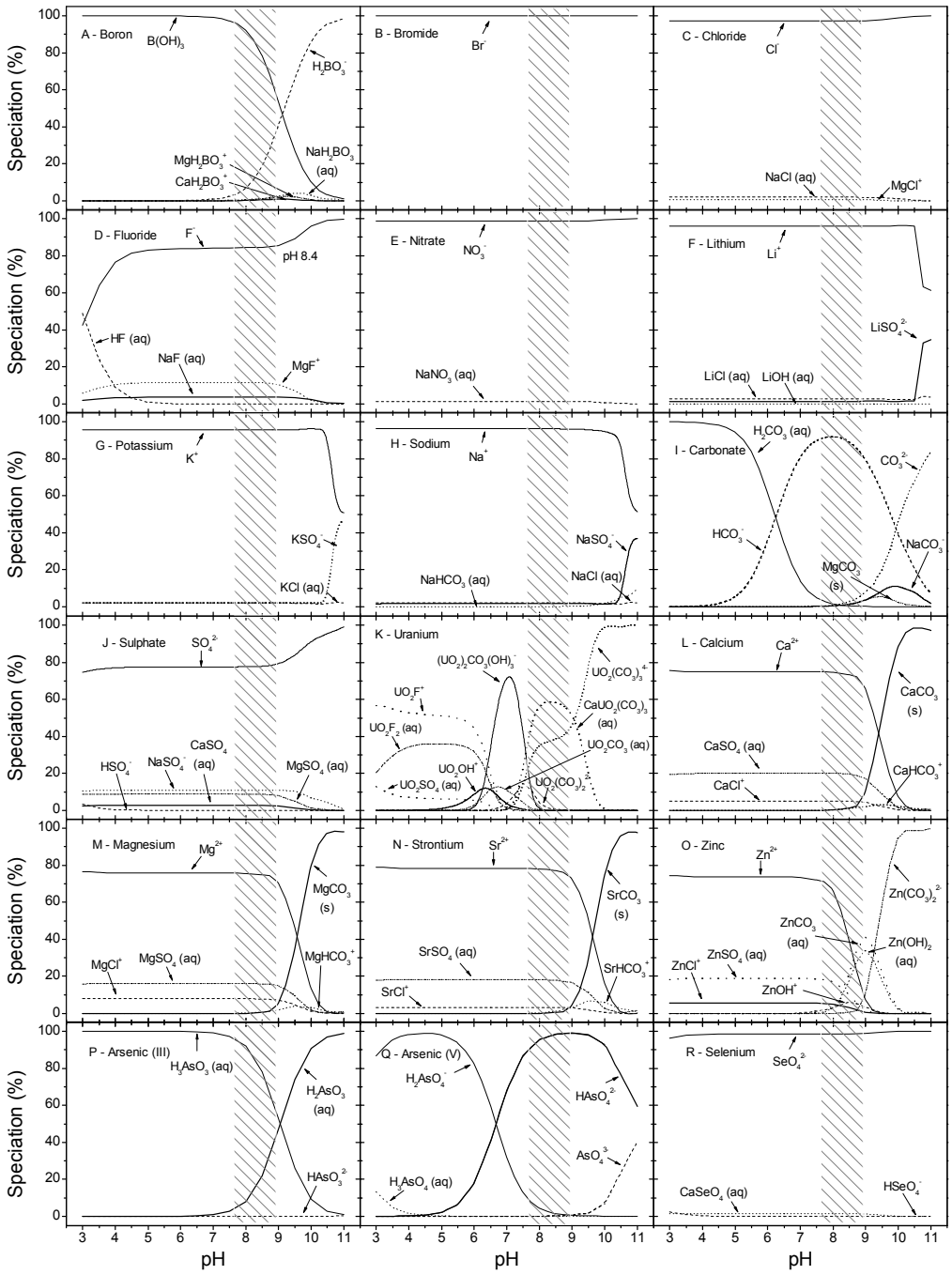

Figure 6.2. Predicted speciation of the inorganic contaminants in the Pine Hill groundwater: (A) boron, (B) bromide, (C) chloride, (D) fluoride, (E) nitrate, (F) lithium, (G) potassium, (H) sodium, (I) carbonate, (J) sulphate, (K) uranium, (L) calcium, (M) magnesium, (N) strontium, (O) zinc, (P) arsenic (III), (Q) arsenic (V), (R) selenium ('aq' and 's' indicates dissolved and precipitated complexes; Shaded region indicates pH range (7.64-8.92) during voltage experiments).

Table 6.2. Predominant inorganic species present within the Pine Hill groundwater during the ED experiments as a function of applied voltage (12 and 18 V, pH 7.64-8.92).

Inorganic	Species		
	Ionic	Dissolved (aq) [a]	Solid (s) [b]
Boron	$H_2BO_3^-$	$B(OH)_3$	-
Bromide	Br^-	-	-
Chloride	Cl^-	-	-
Fluoride	F^-, MgF^+	-	-
Nitrate	NO_3^-	-	-
Lithium	Li^+	-	-
Potassium	K^+	-	-
Sodium	Na^+	-	-
Sulphate	SO_4^{2-}, $NaSO_4^-$	$MgSO_4$	-
Uranium	$UO_2(CO_3)_3^{4-}$, $(UO_2)_2CO_3(OH)^-$, $UO_2(CO_3)_2^{2-}$	$Ca_2UO_2(CO_3)_3$, UO_2CO_3	-
Calcium	Ca^{2+}, $CaCl^+$	$CaSO_4$	$CaCO_3$
Magnesium	Mg^{2+}, $MgCl^+$	$MgSO_4$	$MgCO_3$
Strontium	Sr^{2+}, $SrCl^+$	$SrSO_4$	-
Zinc	Zn^{2+}, $ZnCl^+$, $ZnOH^+$, $Zn(CO_3)_2^{2-}$	$Zn(OH)_2$, $ZnSO_4$, $ZnCO_3$	-
Arsenic (V)	$HAsO_4^{2-}$, $H_2ASO_4^-$	-	-
Selenium (VI)	SeO_4^{2-}	$CaSeO_4$	-

[a] Aqueous (aq) indicates dissolved complexes; [b] Solid (s) indicates precipitated complexes.

6.3 Implications of Applied Voltage

6.3.1 Inorganic Contaminant Removal

The removal of the inorganics from the groundwater as a function of applied voltage is shown in Figure 6.3 and Table 6.3. The removal of B was minimal and voltage independent (12 V: 3.2 %, 18 V: 4.4 %) (Figure 6.3A). B was present as undissociated $B(OH)_3$ in the experiments (speciation: $B(OH)_3$ 53.5-97.3 %; $H_2BO_3^-$ 2.3-40.9 %, Figure 6.2A); thus accounting for the low removal and negligible flux (Figure 6.4A). B was not removed below the 0.5 mg/L DWG (final diluate concentrate: 12 V: 1.41 mg/L; 18 V: 1.32 mg/L).

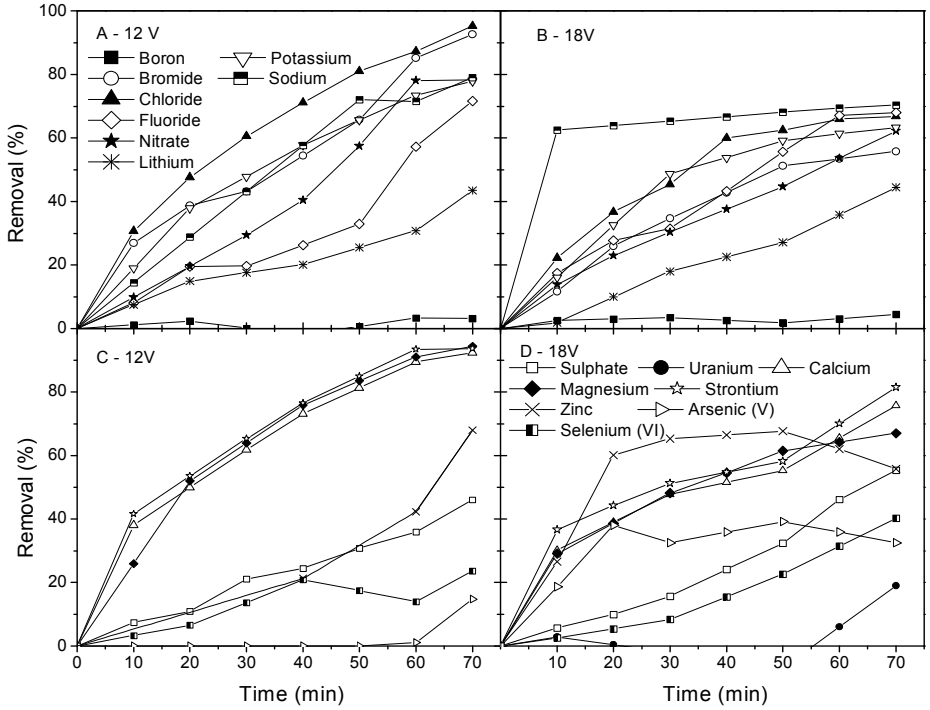

Figure 6.3. Removal (R_D, %) of contaminants from the groundwater (A, B) Monovalent ions, (C, D) Multivalent ions ('apparent' removal includes membrane deposition).

Table 6.3. Removal (R_D, %) of inorganic contaminants from the diluate as a function of applied voltage.

Inorganic	Removal (R_D, %)	
	12 V	18 V
Boron	3.2	4.4
Bromide	100	55.8
Chloride	95.8	67.6
Fluoride	71.7	68.1
Nitrate	78.3	62.3
Lithium	50.6	51.4
Potassium	77.9	63.3
Sodium	79.0	70.3
Sulphate	52.7	55.3
Uranium	0	29.0
Calcium	92.4	75.6
Magnesium	94.4	66.9
Strontium	93.6	81.5
Zinc	67.9	55.7
Arsenic (V)	25.3	40.9
Selenium (VI)	33.1	47.6

Br^- was removed to a greater extent that the other inorganic contaminants at 12 V (R_D 100 %, Figure 6.2B) due to the presence of Br^- in uncomplexed ionic form within the groundwater (speciation: 99.9 %, Figure 6.2B). Enhanced Br^- flux in the early stages of the 18 V experiment (0.5 mg/cm^{2}h) compared to the 12 V experiment (0.2 mg/cm^{2}h) (Figure 6.4A and B) is due to the higher driving force and resultant increase in migration towards the AEM and diffusion within the membrane boundary layer (Strathmann, 2004). While 'apparent' removal of Br^- was observed in the 18 V experiment after 50 minutes, there was no flux. Membrane deposition was postulated as possible removal mechanism thus accounting for the lower removal at 18 V (55.8 %). The quantification of this mass deposited will be further discussed in Section 6.3.2. While there is DWG for Br^-, the final diluate concentration (12 V: 1.0 mg/L, 18 V: 5.6 mg/L) was greatly reduced compared to the initial concentration (10.6 mg/L).

The removal of Cl^-, F^-, NO_3^-, K^+ and Na^+ (95.8, 71.7, 78.3, 77.9 and 79.0 %, respectively) was slightly less than removal of Br^- at 12 V (Figure 6.3A, Table 6.3) due to their lower percent in ionic form (Cl^-: 97.3 %, F^-: 84.4-85.3 %, MgF^+: 10.6-11.5 %, NO_3^-: 98.9 %, K^+: 95.8 %, Na^+: 96.3 %). The trend of higher removal at 12 V and higher initial flux followed by negligible or no flux at 18 V was observed for these inorganics (Figure 6.4B). For example, K^+ flux decreased from 1.6 mg/cm^{2}h to no flux at 12 V (t = 50 min) compared to a decrease from 4.8 mg/cm^{2}h to no flux (t = 30 min) at 18 V. 'Apparent' removal of Cl^-, F^-, NO_3^-, K^+ and Na^+ coupled with negligible or significantly reduced flux from 30 minutes at 12 and 18 V indicated membrane deposition. Cl^-, F^-/MgF^+ and NO_3^- were successfully reduced below the DWG (Table 6.1) in the diluate at 12 V (Cl^-: 96.5 mg/L; F^-/MgF^+: 1.4 mg/L; NO_3^-: 1.9 mg/L). Cl^-, F^- and Na^+ were not removed below the DWG at 18 V (750, 2.1 and 224 mg/L, respectively), whereas NO_3^- was (5.2 mg/L). There is no DWG for K^+, however, the final diluate concentration (12V: 3.7 mg/L; 18 V: 20.2 mg/L) was significantly reduced from its initial concentration (35.4 mg/L).

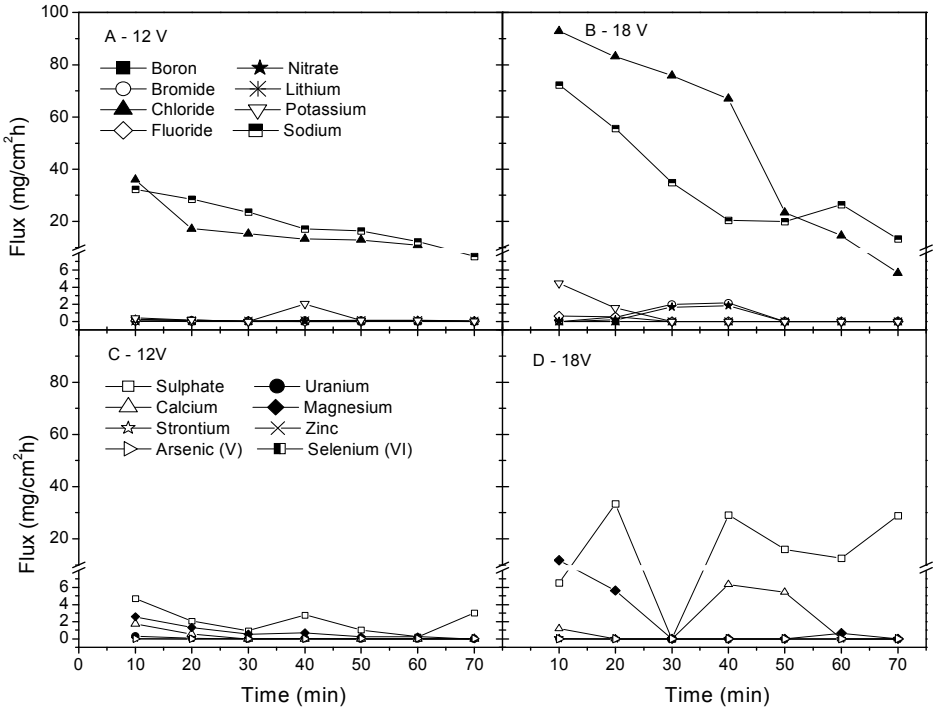

Figure 6.4. Flux (mg/cm^{2}h) of contaminants from the groundwater as a function of applied voltage. (A, B) Monovalent ions, (C, D) Multivalent ions.

The removal of multivalent inorganics was greater at 12 V, excluding SO_4^{2-}, U, As(V) and Se(VI). SO_4^{2-} removal at 18 V (55.3 %) was only slightly higher than removal achieved at 12 V (52.7 %) (Figure 6.3C and D, Table 6.3). The initial SO_4^{2-} flux was greater at 18 V (6.5 mg/cm^{2}h) compared to 12 V (4.7 mg/cm^{2}h) (Figure 6.4C and D) due to enhanced ionic migration. However, unlike the monovalent inorganics, SO_4^{2-} flux at 18 V fluctuated and increased to 28.9 mg/cm^{2}h. SO_4^{2-} was reduced below the 500 mg/L aesthetic ADWG (final diluate concentration: 12 V-392.3 mg/L, 18 V-365.2 mg/L).

The removal of Ca^{2+}, Mg^{2+}, Sr^{2+} and Zn^{2+} was greater at 12 V (Figure 6.3C and D, Table 6.3). However, initial flux was greater at 18 V (e.g. Mg^{2+}: 12 V-2.6 mg/cm^{2}h, 18 V-11.8 mg/cm^{2}h; Figure 6.4D). Apparent removal coupled with negligible flux in the final stages of the 18 V experiment indicates membrane deposition. While no

DWG has been established for Ca^{2+} and Mg^{2+}, they were significantly reduced (12V: Ca^{2+} 4.7 mg/L, Mg^{2+} 9.4 mg/L; 18 V: Ca^{2+} 25.2 mg/L, Mg^{2+} 68.0 mg/L) from their initial concentration (Ca^{2+} 105 mg/L, Mg^{2+} 172 mg/L; Table 6.1).

While U was not removed at 12 V, removal at 18 V was 29.0 %. Flux of U was negligible at 12 and 18 V, therefore, indicating the contribution of membrane deposition to apparent removal. Molecular weight has implications on the flux and removal of ions in ED, with those ions of higher molecular weight removed less efficiently (Sadrzadeh *et al.*, 2007). The speciation of U in the groundwater is complex with various ionic species and complexes present. The predominant ionic species were $UO_2(CO_3)_3^{4-}$ (11.5-45.1 %), $(UO_2)_2CO_3(OH)_3^-$ (0-37.6 %) and $UO_2(CO_3)_2^{2-}$ (0-12.9 %). U and its complexes have a significantly larger molecular weight (e.g. $UO_2(CO_3)_3^{4-}$ 330 g/mol) than the other inorganic contaminants present in the groundwater. U was not removed to below the DWG (12 V: 0.3 mg/L; 18 V: 0.2 mg/L).

Like SO_4^{2-} and U, the removal of As(V) (speciation: $HAsO_4^{2-}$ 87.2-98.9 %, $H_2ASO_4^-$ 0.5-12.8 %) and Se(VI) (speciation: SeO_4^{2-} 98.5-98.7 %; insoluble $CaSeO_4$ 1.3-1.5 %) was greater at 18 V. Flux of As(V) and Se(VI) was negligible indicating membrane deposition. Se(VI) was not reduced below the 0.01 mg/L DWG (12 V: 0.013 mg/L, 18 V: 0.01 mg/L).

While previous studies have reported enhanced inorganics removal during ED with a higher applied voltage (Kabay *et al.*, 2003; Kabay *et al.*, 2008), results from this study varied. In summary, the dominant inorganic removal mechanisms were found to be ionic transport coupled with membrane deposition. A higher applied voltage, and thus higher driving force, initially enhanced ionic transport towards and through the ion-exchange membranes. While apparent inorganic removal occurred in the final stages of the 18 V experiment, flux was minimal and in some cases negligible. This is attributed to inorganic membrane deposition, which is further discussed in Section 6.3.2.

6.3.2 Inorganic Contaminant Membrane Deposition

The mass of inorganics deposited on the ion-exchange membranes (m_{DEP}) was quantified by a mass balance using eqn (4.7), as represented in Figure 6.5 and Table 6.4. The mass of multivalent inorganics deposited, especially SO_4^{2-}, Ca^{2+} and Mg^{2+}, was higher than the monovalent inorganics (excluding Cl^-). This is related to their higher initial groundwater concentration (mg/L range). The lower mass of As(V) and Se(VI) deposited on the membranes correlates with their low initial concentration (μg/L range).

Greater inorganic membrane deposition of SO_4^{2-}, Ca^{2+}, Mg^{2+} and Sr^{2+} was observed at 18 V (180, 107, 68.6 and 2.3 mg/cm^3, respectively) compared to 12 V (139, 72, 57.7 and 1.0 mg/cm^3, respectively). This is due to enhanced migration towards the ion-exchange membranes and diffusion within the membrane boundary layer. While flux of these inorganics was initially high at 18 V; due to the increase in membrane deposition with experimental duration, flux through the membranes is hampered; thus accounting for the lower apparent removal (Section 6.3.1). For example, a decrease in SO_4^{2-} flux from 30 minutes at 18 V (Figure 6.4D) corresponds to an increase in membrane deposition (Figure 6.5D).

A similar trend of enhanced U deposition at 18 V (0.15 mg/cm^3) compared to 12 V (0.04 mg/cm^3) was observed. However, contrary to Ca^{2+}, Mg^{2+} and Sr^{2+}, removal of U was greater at 18 V. The presence of Ca^{2+} and CO_3 influences U speciation and increase its mobilization through the formation of $Ca(UO_2)(CO_3)_3$ (Fox *et al.*, 2006) and UO_2CO_3 complexes (Figure 6.2K). While $Ca(UO_2)(CO_3)_3$ and UO_2CO_3 complexes are present in both the 12 and 18 V experiment (speciation: $Ca(UO_2)(CO_3)_3$: 18.5-51.9 %; UO_2CO_3: 0-3.7 %), greater U membrane deposition at 18 V as a result of enhanced migration. The higher apparent removal of U at 18 V compared to Ca^{2+}, Mg^{2+} and Sr^{2+} at 12 V can be attributed the higher speciation of $Ca(UO_2)(CO_3)_3$ and UO_2CO_3 complexes presented in the groundwater compared to the carbonate ($CaCO_3$: 0-10.5 %; $MgCO_3$: 0-5.6 %; $SrCO_3$: 0-4.5 %; $ZnCO_3$: 0.4-41.2 %), sulphate ($CaSO_4$: 17.4-20.1 %; $MgSO_4$: 14.8-16.2 %; $SrSO_4$: 16.8-18.3 %) and hydroxide complexes ($Zn(OH)_2$: 0.3-33.8 %). Therefore, the formation of

inorganic-inorganic complexes coupled with membrane deposition contributes to apparent removal and in turn a reduction in flux.

The speciation of complexes with monovalent inorganics within the groundwater was relatively low (insoluble species: 0.2-2.6 % NaH_2BO_3, 1.1 % $NaNO_3$) compared to that of the multivalent inorganics. This accounts for their lower membrane deposition. The complexation of monovalent inorganic contaminants with Ca^{2+}, Mg^{2+} and SO_4^{2-} to form ionic species, although low ($CaH_2BO_3^+$ 0-0.8 %, $MgH_2BO_3^+$ 0.1-2.2 %, $MgCl^+$ 0.6-0.7 %, CaF^+ 0.4-0.5 %, MgF^+ 10.6-11.5 %, $LiSO_4^-$ 1.3 %, KSO_4^- 2.2 %), may have contributed to membrane deposition.

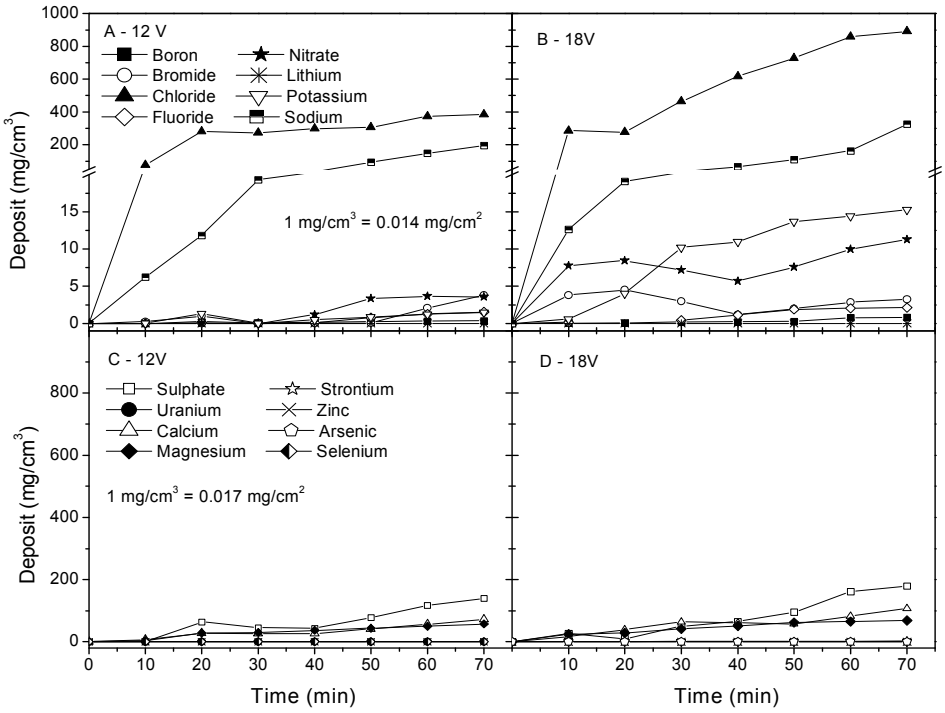

Figure 6.5. Membrane deposition (m_{DEP}, mg/cm^3) of the contaminants as a function of applied voltage. (A, B) Monovalent ions, (C, D) Multivalent ions.

Table 6.4. Membrane deposition (m_{DEP}, mg/cm^3 and % of initial feed mass) of the contaminants (pH 8.4, experimental duration 70 min).

Inorganic	Mass deposit, m_{DEP} (mg/cm^3)		Mass deposit (% initial feed mass)	
	12 V	18 V	12 V	18 V
Boron	0.3	0.8	15.9	38.1
Bromide	3.8	3.2	21.8	18.6
Chloride	383	891	11.7	27.1
Fluoride	1.5	2.1	16.0	22.1
Nitrate	3.5	11.3	6.9	22.1
Lithium	0.01	0.006	20.2	11.0
Potassium	1.5	15.3	3.1	32.0
Sodium	195	326	8.7	14.6
Sulphate	139	180	11.8	15.3
Uranium	0.04	0.15	10.0	41.9
Calcium	72.0	107	71.1	75.8
Magnesium	57.7	68.6	31.8	29.5
Strontium	1.0	2.3	32.9	74.6
Zinc	0.02	0.02	6.6	6.6
Arsenic (V)	1.5×10^{-5}	7.2×10^{-5}	0.2	0.9
Selenium (VI)	1.4×10^{-3}	2.2×10^{-3}	1.7	2.7

At 18 V the current density across the stack was above the experimental (i_{lim} 13.1 mA/cm^2; Chapter 4) and theoretical LCD before the DWG was reached (Figure 6.6). Therefore, concentration polarisation on both side of the ion-exchange membranes is enhanced at 18 V due to the greater decrease in inorganic concentration within the boundary layer at the membrane surface facing the diluate and in turn the high concentration at the surface facing the concentrate. Above the LCD electrogenerated OH^- promotes the formation of precipitation on the CEM (Strathmann, 2004). Therefore, the precipitation of insoluble multivalent inorganics within the groundwater would be deposited on the CEMs as a scaling layer. A number of authors have reported the formation of $CaOH_2$, $MgOH_2$ and $CaCO_3$ at the surface and within ion-exchange membranes (Araya-Farias and Bazinet, 2006; Ayala-Bribiesca *et al.*, 2006b; Bazinet and Araya-Farias, 2005). Chemical analysis of the membrane deposit i.e. scaling layer is presented in Section 6.5.

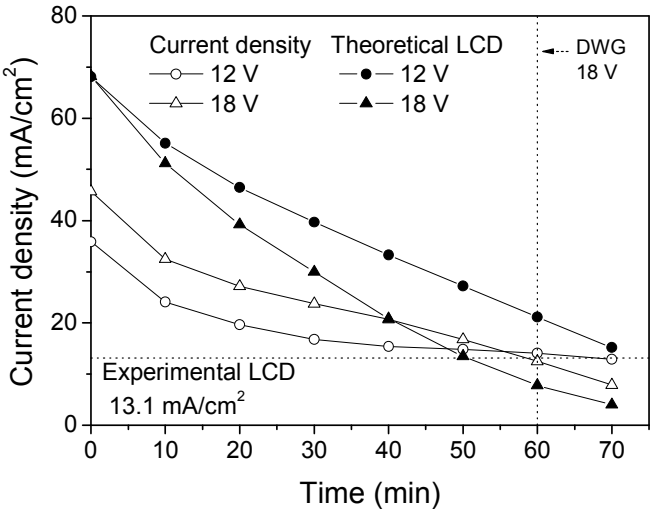

Figure 6.6. Comparison between the current density (mA/cm^2) within the ED stack and the experimental and theoretical LCD during ED experiments with Pine Hill groundwater (Vertical dotted line indicates time when DWG 0.5 g/L TDS is reached).

In summary, the apparent removal of the inorganic contaminants B, Li^+, SO_4^{2-}, U, As(V) and Se(VI) from the groundwater was enhanced at 18 V, while the apparent removal of Br^-, Cl^-, F^-, NO_3^-, K^+, Ca^{2+}, Mg^{2+}, Sr^{2+} and Zn^{2+} was greater at 12 V. Ionic transport coupled with solute-solute interactions such as the complexation and membrane deposition are the predominant mechanisms of inorganic contaminant removal. At 12 V inorganic removal is due to ionic transport, electrostatic interactions with the membranes coupled with minor contribution from membrane deposition. While removal at 18 V was relatively high, flux from the diluate into the concentrate was low and in some cases negligible, indicating a strong contribution of membrane deposition to 'apparent' removal. An increase in deposition of the inorganics on the membranes at 18 V reduced flux through the membranes and in turn reduced removal from the groundwater. No membrane fouling protocols were employed during this study and the results demonstrate the complexity of the treatment of groundwater compared to model aqueous solutions.

6.3.3 Ionic Hydration and Mobility

The higher flux of the multivalent inorganics through the ion-exchange membranes compared to the monovalent inorganics (except for Cl^-) (Figure 6.4) is contradictory to results from the study by Van der Bruggen (2004), whereby the transport of multivalent ions through the ion-exchange membranes was hindered due to larger ionic size (indicated by hydrated radius) and stronger retention within the membrane matrix. The removal and flux of inorganic contaminants from model aqueous solutions in Chapter 5 were positively correlated with hydrated radius. Crystal and hydrated ionic radii of the inorganic contaminants along with their mobility and removal achieved during the voltage experiments is given in Table 6.5.

Table 6.5. Ionic radii (crystal and hydrated) (nm), ion mobility ($\times 10^{-8}$ m^2/sV) and removal of inorganic contaminants (%).

Inorganic	Crystal ionic radii, *r* (nm) [1]	Hydrated ionic radii, Δ*r* (nm) [2]	Mobility at 25°C, *u* ($\times 10^{-8}$ m^2/sV) [3]	Removal (R_D, %)	
				12 V	18 V
Boron	[a]	0.244-0.261	[a]	3.2	4.4
Bromide	0.180-0.196	0.330	8.09	100	55.8
Chloride	0.164-0.198	0.195-0.332	7.91	95.8	67.6
Fluoride	0.116-0.135	0.352	5.70	71.7	68.1
Nitrate	0.179-0.206	0.340	7.40	78.3	62.3
Lithium	0.059-0.092	0.155-0.382	4.01	50.6	51.4
Potassium	0.133-0.164	0.201-0.331	7.62	77.9	63.3
Sodium	0.099-0.117	0.178-0.358	4.01	79.0	70.3
Sulphate	0.215-0.290	0.300-0.379	8.29	52.7	55.3
Uranium	0.485	[a]	[a]	0	29.0
Calcium	0.100-0.134	0.171	6.17	92.4	75.6
Magnesium	0.065-0.089	0.227-0.428	5.49	94.4	66.9
Strontium	0.113-0.144	0.150-0.412	6.15 [b]	93.6	81.5
Zinc	0.060-0.090	0.220-0.430	5.47	67.9	55.7
Arsenic (V)	[a]	0.400	[a]	25.3	40.9
Selenium (VI)	0.042-0.305	0.384	[a]	33.1	47.6

[a] Data not available; [b] Calculated using $u = \lambda°equiv/zF$ where $\lambda°equiv = 59.4$ $cm^2/\Omega equiv$ and $z = 1$ (Robinson and Stokes (1970). Refs: 1. Collins (1995), Corti *et al*. (1980a), Kiriukhin and Collins (2002), Lide (2008), Marcus (1991), Pauling (1960), Samoilov (1953), Tansel *et al*. (2006), Volkov *et al*. (1997), Zhou *et al*. (2002); 2. Kiriukhin and Collins (2002), Marcus (1991), Nightingale (1959), Volkov *et al*. (1997); 3. Atkins (1990).

No correlation can be made between hydrated ionic radius, ionic mobility and the flux and removal of the inorganics from the groundwater (Figure 6.7). This demonstrates that flux of inorganic contaminants through ion-exchange membranes during ED of groundwater is dependent not only on the physicochemical properties of the inorganic contaminants (hydrated radius, concentration) but also on solute-solute interactions and membrane deposition.

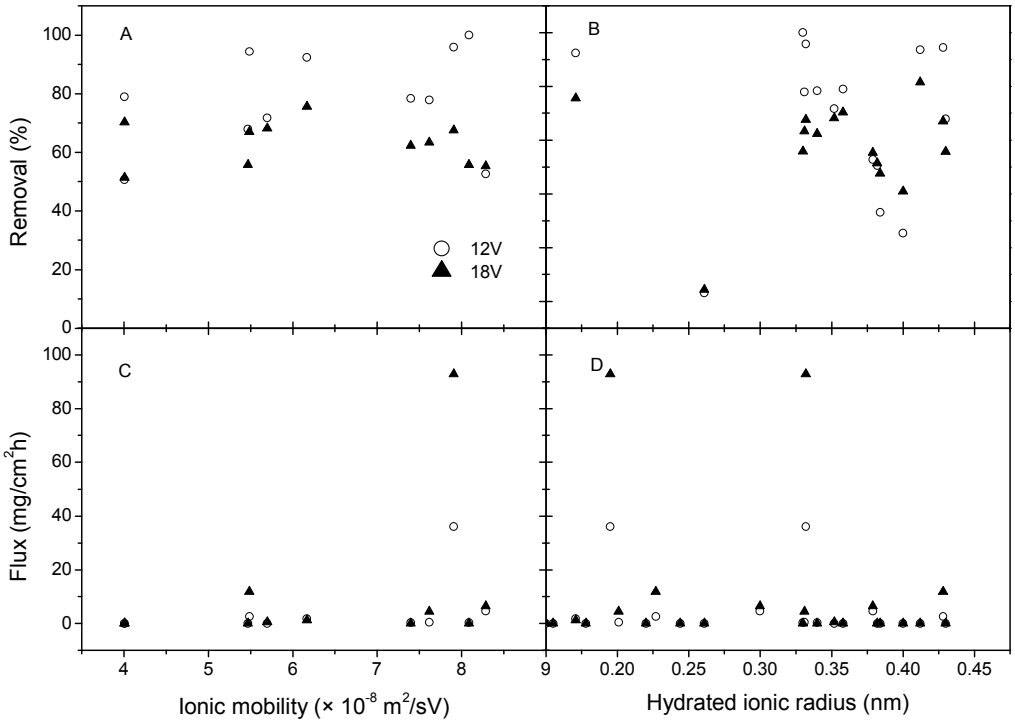

Figure 6.7. Correlation between ionic mobility (×10^{-8} m^2/sV), hydrated ionic radius (nm), inorganic contaminant removal (%) and initial flux (mg/cm^2h) (Hydrated radius date from Table 6.5).

6.4 Implications of Solution pH

6.4.1 Inorganic Contaminant Removal

Changes in solution chemistry have implications for the physicochemical characteristics (e.g. charge, speciation and solubility) of inorganic contaminants. Therefore, the influence of solution pH on inorganic contaminant removal from the groundwater was investigated. In Chapter 5, B removal from model solutions by ED was pH dependent. Similar results were seen in the removal of B from the brackish groundwater (Figure 6.8A). $B(OH)_3$ is undissociated between pH 3 and 9 and in consequence was not transported through the AEMs, as indicated by the negligible flux (Figure 6.9A). At pH 10, removal increased to 46.7 % due to $B(OH)_3$ dissociation. This removal was not solely due to $B(OH)_3$ dissociation and ionic transport through the AEMs as flux was minimal (pH 10: 0-0.009 mg/cm^{2}h, Figure 6.11K). Therefore, apparent B removal above pH 10 was due to membrane deposition. B was not reduced below the 0.5 mg/L DWG due to the high concentration of competitive ions within the diluate. B removal from the groundwater was greater than removal from the model solutions pH 10 (39 %) due to the higher applied voltage in the brackish groundwater experiments (12 V) compared to the model solution experiments (10 V).

The removal of Cl^-, Br^-, F^-, NO_3^- and Na^+ was pH independent (average removal: 99.9 ± 0.9 %, 99.4 ± 1.6 %, 95.8 ± 4.2 %, 97.6 ± 4.4 % and 92.1 ± 4.0 %, respectively; Figure 6.8A) due to their pH independent speciation (Figure 6.2). This is similar to the pH independent removal of F^- and NO_3^- from the model aqueous solutions in Chapter 5. The slight decrease in F^- removal corresponds to a decrease in speciation of the positively charged UO_2F^+ complex (pH 5: 36.0 %, pH 6: 31.8 %; Figure 6.2K). Therefore, transport of F^- through the AEMs decreased from 0.01 mg/cm^{2}h at pH 5 to no flux at pH 6 (Figure 6.9A). This demonstrates the implication of complexation and the formation of charged or uncharged species on ionic transport and the mechanisms of inorganic removal from the groundwater.

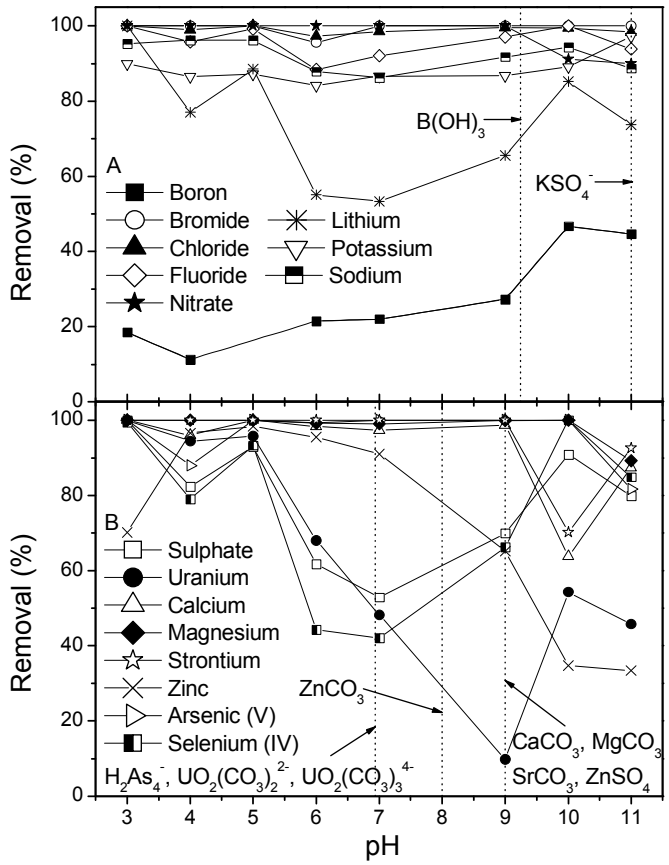

Figure 6.8. Inorganic contaminant removal of (A) monovalent and (B) multivalent ions as a function of solution pH (Experimental duration 110 min for each pH value; vertical lines indicate pK_a: $B(OH)_3$ 9.24; KSO_4^- 11; $H_2As_4^-$ 6.94; $UO_2(CO3)_2^{2-}$, $UO_2(CO_3)_3^{4-}$ 7; $ZnCO_3$ 8; $CaCO_3$, $MgCO_3$, $SrCO_3$, $ZnSO_4$ 9).

To accurately elucidate the mechanisms of inorganic removal it is imperative to look at removal (Figure 6.10) and flux (Figure 6.11) as a function of experimental time. Between pH 3 and 4, complete removal of Br^-, Cl^-, F^-, NO_3^- and Na^+ from the diluate occurred before experimental completion, thus accounting for the zero final flux shown in Figure 6.9A. This was also the case for Br^-, F^- and NO_3^- at pH 5 (Figure 6.11A, B, I). While apparent removal of Br^- and NO_3^- was observed above pH 7 (Figure 6.10B, E), flux was negligible (Figure 6.11A, I). This was also the case for F^- above pH 9 and Cl^- at pH 11 (Figure 6.11B, E). Between pH 3 and 11, Na^+ removal (Figure 6.10G) was accompanied by flux (Figure 6.11G). Therefore, the predominant removal mechanisms were postulated to be ionic flux coupled with membrane

deposition for F^- above pH 5, Br^- and NO_3^- above pH 7, Cl^- at pH 11 and Na^+ over the entire pH range. Inorganic membrane deposition is further discussed in Section 6.4.2. F^-, NO_3^- and Cl^- were reduced below their DWG between pH 3 and 11. Na^+ was reduced below the 200 mg/L DWG at pH 3-5, 9 and 11.

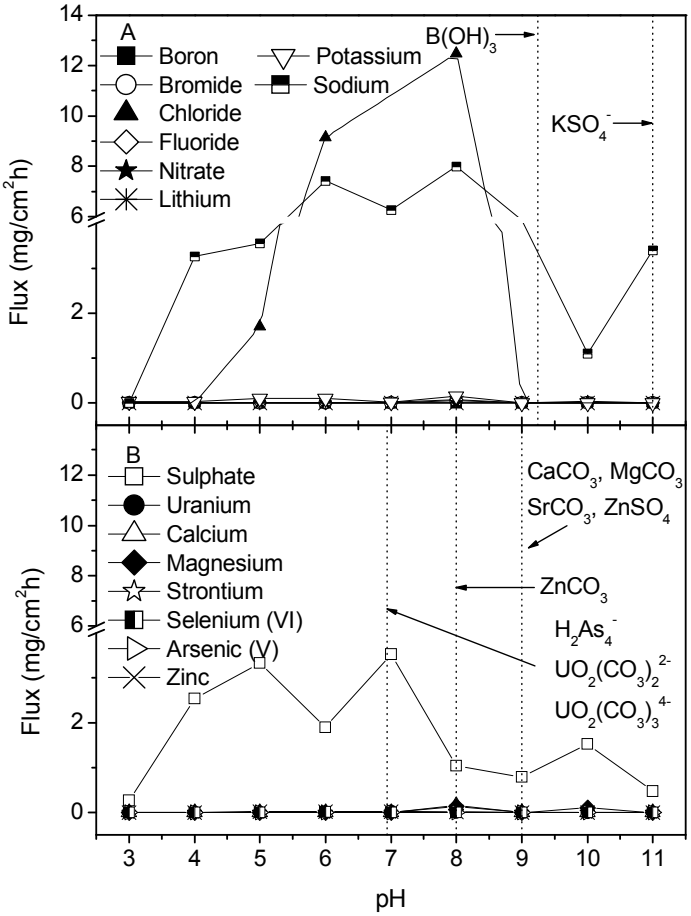

Figure 6.9. Inorganic contaminant flux (mg/cm^{2}h) of (A) monovalent and (B) multivalent ions as a function of solution pH (3-11) (Data corresponds to final experimental flux (110 min)).

The removal of K^+ was pH independent between pH 3 and 10 (88.4 ± 4.0 %) due to its pH independent speciation (Figure 6.2G). From pH 3 to 8, K^+ removal was due to flux through the membranes (final flux: 0.02 to 0.2 mg/cm^{2}h, Figure 6.11H). Although removal increased from 86.7 % at pH 9 to 97.2 % at pH 11, there was no flux. Therefore, apparent K^+ removal above pH 9 was postulated to be due to

membrane deposition. There is no DWG for K^+; however, diluate concentrations were significantly reduced ($K^+ < 6$ mg/L) from the initial concentration (35.4 mg/L).

The decrease in Li^+ removal between pH 3 (100 %) and pH 7 (53.3 %) was accompanied by a decrease in flux (2.95×10^{-4} to 1.25×10^{-5} mg/cm^{2}h, Figure 6.9B). Apparent Li^+ removal (Figure 6.10N) occurred without flux (Figure 6.11N). Therefore, the mechanisms of Li^+ removal were ionic flux coupled with membrane deposition. There is no DWG for Li^+; however, diluate concentrations were significantly reduced ($Li^+ < 0.03$ mg/L). Therefore,

The removal of the multivalent inorganic contaminants SO_4^{2-}, Ca^{2+}, Mg^{2+}, Sr^{2+}, Zn^{2+}, U, As(V) and Se(VI) was pH dependent (Figure 6.8B) due to their pH dependent speciation (Figure 6.2). Although the final SO_4^{2-} flux was shown to increase between pH 3 and 5 (0.3-3.3 mg/cm^{2}h, Figure 6.9), flux fluctuated with negligible flux observed during these experiments (Figure 6.11H). This accounts for the overall decrease in SO_4^{2-} removal from pH 4 (100 %) to pH 5 (52.9 %). The increase in removal from pH 9 (69.9 %) to pH 10 (90.9 %) was accompanied by an increase in the average flux during these experiments (1.3 and 1.9 mg/cm^{2}h, respectively). Therefore, the mechanisms of SO_4^{2-} removal between pH 3 and 11 were ionic flux and membrane deposition. The concentration of SO_4^{2-} in the groundwater was reduced below the aesthetic 500 mg/L DWG during each experiment.

Between pH 3 and 8 Ca^{2+}, Mg^{2+}, Sr^{2+} and Zn^{2+} removal was stable (70.2–100 %). At pH 3, 4 and 5 complete removal of Ca^{2+}, Mg^{2+} and $Sr^{2+}$from the diluate occurred before experimental completion, thus accounting for the negligible final flux (Figure 6.9A). Above pH 6 Ca^{2+}, Mg^{2+} and Sr^{2+} removal (Figure 6.10) occurred without flux (Figure 6.11). This was the case for Zn^{2+} above pH 10 (Figure 6.11J). Therefore, the apparent removal of Ca^{2+}, Mg^{2+}, Sr^{2+} and Zn^{2+} above pH 6 and pH 10, respectively, was postulated to be due to membrane deposition.

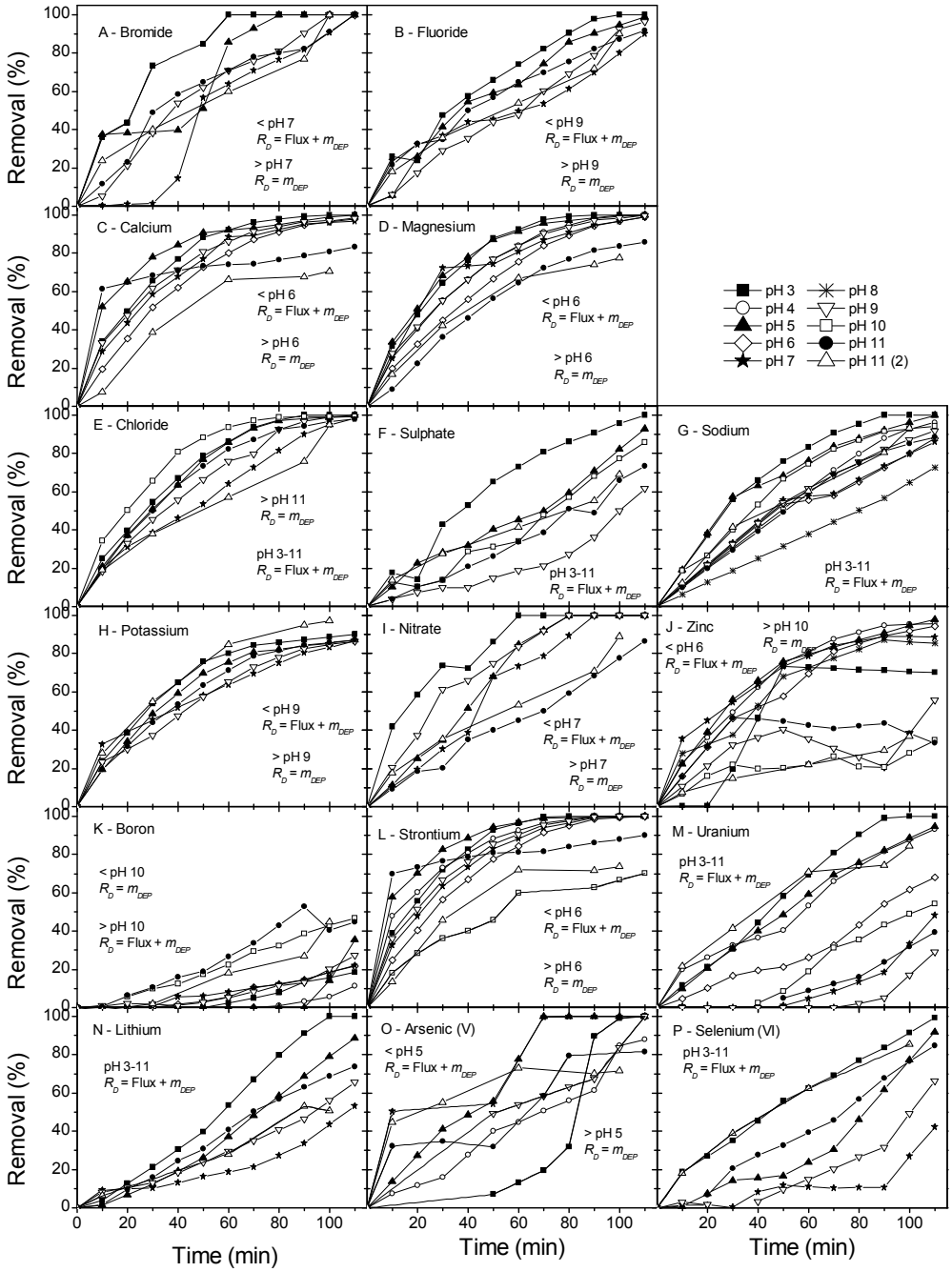

Figure 6.10. Inorganic contaminant removal (R_D, %) of (A) monovalent and (B) multivalent ions as a function of time (solution pH 3-11) (pH 11 (2) refers to repeated experiment at pH 11).

The significant drop in removal of U between pH 3 (100 %) and pH 7 (58.9 %) (Figure 6.8B) is attributed to a significant decrease in speciation of charged UO_2F^+ within the groundwater (pH 3: 56.7 %, pH 7: 1.7 %) and, therefore, a decrease in flux (average flux: 0.03 to 0.01 mg/cm^{2}h). However, removal of U (Figure 6.10M) occurred without flux (Figure 6.11M). The domination of charged $UO_2(CO_3)_3^{4-}$ between pH 9 and 10 (speciation: 45.1-99.4 %, Figure 6.2K, (Langmuir, 1978)) led to an increase in flux (0 to 0.02 mg/cm^{2}h) and thus removal (9.8 to 54.3 %). Therefore, the removal of U between pH 3 and 11 was due to ionic flux and membrane deposition. U was not reduced below the 0.02 mg/L DWG.

While Se(VI) speciation is pH independent (Figure 6.2R), removal decreased between pH 3 (99.5 %) and pH 7 (42.1 %) (Figure 6.8B). Although Se(VI) flux was minimal and sometimes zero (Figure 6.11P) removal was observed (Figure 6.10P); thus indicating that both flux and membrane deposition were the dominant removal mechanisms. Se(VI) was removed to below DWG levels during each pH experiment.

As(V) removal was pH independent (96.1 ± 7.2 %, Figure 6.8B) due to the dominance of charged $H_2AsO_4^-$ and $HAsO_4^{2-}$ in the groundwater over the entire pH range. Above pH 5, As(V) removal (Figure 6.10O) occurred without flux (Figure 6.11O), indicating membrane deposition. As(V) was reduced to below the 0.01 mg/L DWG during each pH experiment.

In summary, the removal of the inorganics Br^-, Cl^-, F^-, NO_3^- and As(V) were pH independent due to their pH independent speciation, whereas the removal of B, Li^+, K^+, SO_4^{2-}, U, Ca^{2+}, Mg^{2+}, Sr^{2+}, Zn^{2+} and Se(VI) was pH dependent due to their pH dependent speciation. Solution pH had implications for the charge of the inorganics whereby flux and, therefore, removal was enhanced when charged complexes were formed (e.g. $UO_2(CO_3)_3^{4-}$ above pH). Although removal of the inorganic contaminants from the diluate occurred from neutral to alkaline pH, the significant decrease in ionic flux indicated membrane deposition. The influence of solution pH on membrane deposition is discussed in Section 6.4.2.

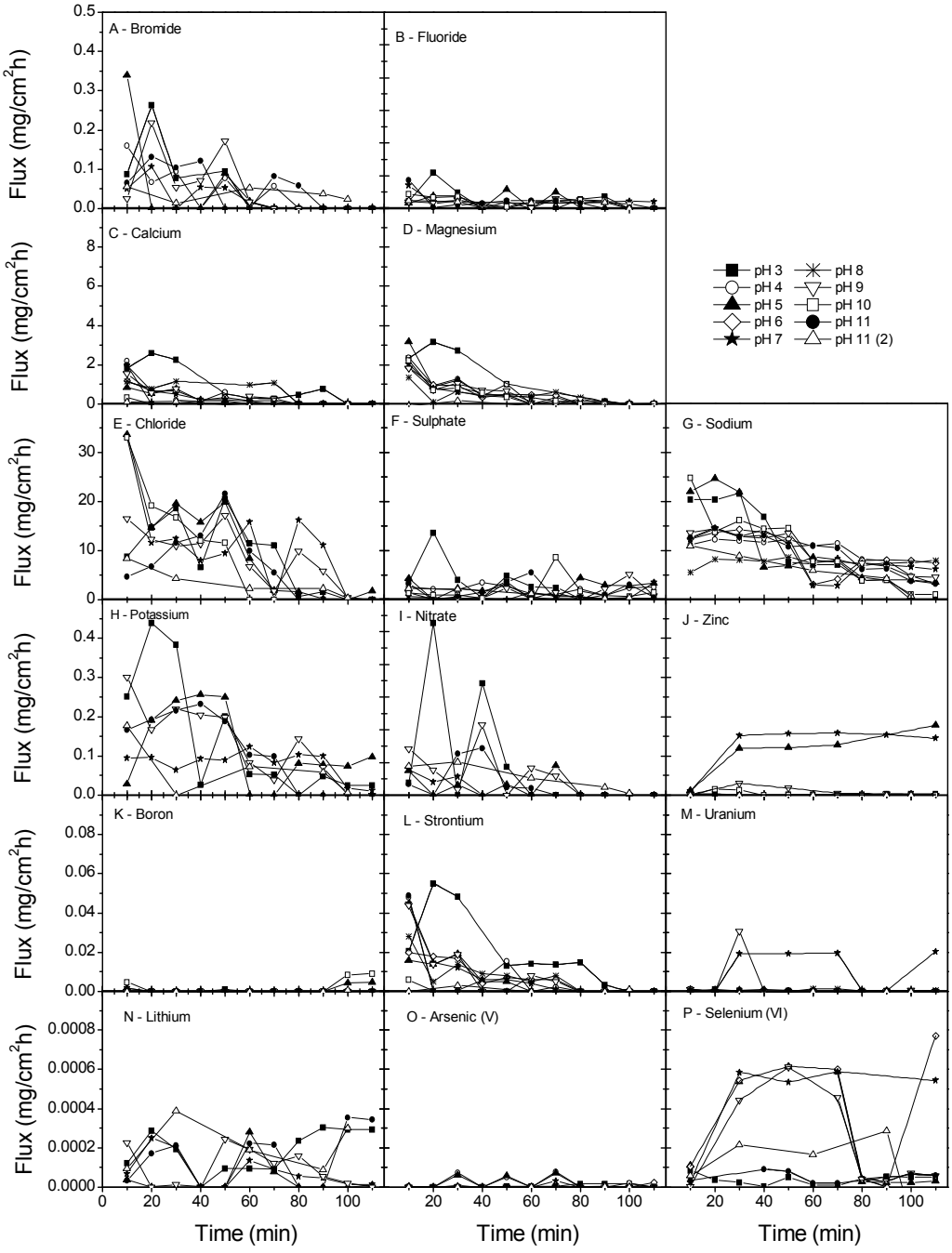

Figure 6.11. Inorganic contaminant flux (mg/cm^{2}h) of (A) monovalent and (B) multivalent ions (solution pH 3-11).

6.4.2 Inorganic Contaminant Membrane Deposition

Results in Section 6.4.1 showed that the apparent removal of inorganics occurred, especially at high pH, without ionic flux through the membranes; thus indicating membrane deposition in the form of scaling. Therefore, the mass of inorganic contaminants deposited on the membranes (m_{DEP}, mg/cm^3) was quantified through a mass balance which is shown in Figure 6.12.

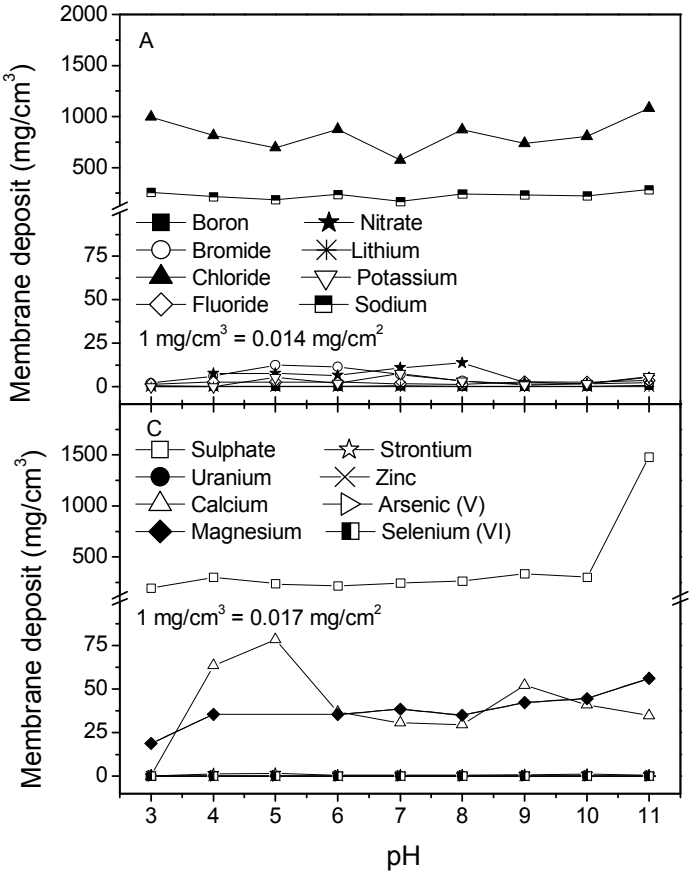

Figure 6.12. Inorganic contaminant membrane deposit (m_{DEP}, mg/cm^3) of (A, B) monovalent ions and (C, D) multivalent ions as a function of solution pH (3-11) (Vertical dotted lines indicate pK_a).

The condition for inorganic scale formation is exceedance of the solubility limit, i.e. the solubility product at thermodynamic equilibrium. A common method for determining the solubility limit and thus scaling potential of common inorganic scalants is the saturation index. This is a ratio between the ionic activity product

(*IAP*) and the solubility product (K_{sp}) as shown in eqn (6.1) (Schausberger *et al.*, 2009).

$$\Omega = \frac{IAP}{K_{sp}} \tag{6.1}$$

When the saturation index is ≤ 1 there is no potential for scaling, whereas a saturation index above 1 indicates scaling potential. The inorganic contaminants predicted to be above their saturation index during the solution pH experiments (e.g. Ca^{2+}, Mg^{2+} and Sr^{2+}) along with the complexes predicted to precipitate are shown in Table 6.6.

Table 6.6. Saturation index (Ω) for the inorganic contaminants predicted to precipitate at different solution pH.

Inorganic	pH	Saturation Index Ω	Mineral name	Stoichiometry and mineral components
Calcium	9	1.4-1.5	Aragonite, Calcite	Ca^{2+}, CO_3^{2-}
		3.2-3.8	Dolomite	Ca^{2+}, Mg^{2+}, CO_3^{2-}
	10	2.3	Aragonite	Ca^{2+}, CO_3^{2-}
		5.3-5.8	Dolomite	Ca^{2+}, CO_3^{2-}, H_2O
	11	2.3-2.4	Aragonite, Calcite	Ca^{2+}, CO_3^{2-}
		1.1	Calcium phosphate	3 Ca^{2+}, 2 PO_4^{3-}
		1.1	$CaCO_3H_2O$	Ca^{2+}, CO_3^{2-}, H_2O
		4.1-4.7	Dolomite	Ca^{2+}, Mg^{2+}, CO_3^{2-}
		10.4	Hydroxyapatite	4 Ca^{2+}, 3 PO_4^{3-}, 1 H_2O, -1 H^+
Magnesium	9	3.9	Huntite	3 Mg^{2+}, Ca^{2+}, 4 CO_3^{2-}
		1.1	Magnesite	Mg^{2+}, CO_3^{2-}
	10	1.4	Artinite	-2 H^+, 2 Mg^{2+}, CO_3^{2-}, 5 H_2O
		8.2	Huntite	3 Mg^{2+}, Ca^{2+}, 4 CO_3^{2-}
		4.0	Hydromagnesite	5 Mg^{2+}, 4 CO_3^{2-}, -2 H^+, 6 H_2O
		2.2	Magnesite	Mg^{2+}, CO_3^{2-}
	11	4.8	Huntite	3 Mg^{2+}, Ca^{2+}, 4 CO_3^{2-}
		1.1	Magnesite	Mg^{2+}, CO_3^{2-}
Strontium	11	1.6	Strontianite	Sr^{2+}, CO_3^{2-}

Ca^{2+}, Mg^{2+} and Sr^{2+} forms insoluble carbonate salts at high pH (Figure 6.2L, M, N, O), which was indicated by visible precipitation within the diluate and concentrate from pH 9 (Figure 6.13). These insoluble carbonate salts are known to form scaling layers on the CEMs during ED (Ayala-Bribiesca *et al.*, 2006b; Bazinet and Araya-Farias, 2005). Analysis of this precipitate using ICP-OES confirmed the presence of Ca^{2+}, Mg^{2+}, Sr^{2+} and Na^{+} (72, 173, 0.6 and 17 mg/g precipitate in 1 L, respectively). Membrane deposition of Ca^{2+}, Mg^{2+}, Sr^{2+} and Zn^{2+} as a scaling layer correspondingly increased from pH 3 (Mg^{2+}: 18.7 mg/cm^3; Ca^{2+}, Sr^{2+}, Zn^{2+}: no deposition) to pH 11 (Ca^{2+}: 34.5 mg/cm^3; Mg^{2+}: 56.2 mg/cm^3; Sr^{2+}: 0.7 mg/cm^3, Zn^{2+}: 0.7 mg/cm^3) (Figure 6.12B). In ED, the precipitation of insoluble carbonate or sulfate salts within the concentrate reduces ED performance by reducing ionic transport (Shaposhnik *et al.*, 2002). Therefore, the increase in precipitation and membrane deposition with solution pH explains the reduction in flux of inorganic contaminants from neutral to alkaline pH as described in Section 6.4.1.

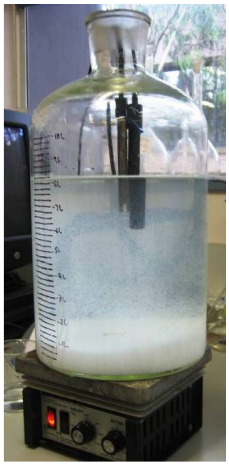

Figure 6.13. Visible precipitation within the Pine Hill groundwater at pH 11.

While only Ca^{2+}, Mg^{2+} and Sr^{2+} were predicted to be present above their saturation index at high pH, the remaining inorganic contaminants that were below their saturation index within the diluate and concentrate bulk solution may have been above their saturation index at the membrane surface as a result of concentration polarisation; thereby leading to precipitation and CEM deposition.

The mass of Zn^{2+} and U deposited on the membranes increased between pH 3 (Zn^{2+}: 0.01 mg/cm^3; U: 2.4 × 10^{-4} mg/cm^3) and pH 11 (Zn^{2+}: 0.05 mg/cm^3, U: 3.0 × 10^{-4} mg/cm^3) owing to the formation and membrane deposition of the insoluble $ZnCO_3$ and $CaUO_2(CO_3)_3$ species (pH 7-10). Electrostatic interactions between negatively charged $Zn(CO_3)_2^{2-}$ (pH 9-11), $(UO_2)_2CO_3(OH)_3^-$ (pH 6-8), $UO_2(CO_3)_3^{4-}$ (pH 11) and the ion-exchange membranes would contribute to this deposition .

The deposition of neutrally charged B on the membranes was stable between pH 3 (0.5 mg/cm^3) and pH 10 (0.3 mg/cm^3) (Figure 6.12A). Above pH 10, when ionic transport occurs (i.e. > pK_a 9.24), the mass of B deposited increased to 0.8 mg/cm^3 (42.7 % initial mass) due to electrostatic attraction between negatively charged $H_2BO_3^-$ and the positively charged AEMs.

The deposition of Br^-, Cl^-, F^-, NO_3^-, Li^+, K^+ and Na^+ was relatively stable over the studied pH range (pH 3: 2.1, 997, 1.6, 7.7, 13.0, 5.5 and 260.7 mg/cm^3; pH 11: 2.3, 1082, 3.5, 5.4, 11.7, 5.9 and 283.8 mg/cm^3) due to their general pH independent speciation and charge. The change in speciation of Li^+ and K^+ to $LiSO_4^{2-}$ and KSO_4^- did not significantly influence membrane deposition. The mass of Cl^- and Na^+ deposited was greater than the mass of the other monovalent inorganics due to the higher initial mass within the groundwater.

Between pH 3 and 10, the mass of SO_4^- deposited on the membranes was stable (average m_{DEP}: 263 ± 49 mg/cm^3, Figure 6.12B). The significant increase at pH 11 (1478 mg/cm^3) is attributed to the increase in negatively charged SO_4^{2-} species within the groundwater (pH 10 92.0 %, pH 11 99.3 %, Figure 6.2J) and, thus an increase in migration towards the AEMs. Similarly, the mass of Se(VI) deposited on the membranes, although small, increased from pH 3 (1.25 × 10^{-3} mg/cm^3) to pH 11 (1.04 × 10^{-4} mg/cm^3) as a result of the increase in charged SeO_4^{2-} species (pH 3: 96.2 %, pH 11: 99.9 %, Figure 6.2Q).

Like Se(VI), the mass of As(V) deposited on the membranes was relatively small but showed a strong pH dependent trend with an increase from 7.8 × 10^{-4} mg/cm^3 (pH 3)

to 2.1 × 10^{-3} mg/cm^3 (pH 11). As Se(VI) complexes with Ca^{2+} to form insoluble $CaSeO_4$, the increase in Ca^{2+} deposition on the CEMs with increasing solution pH, therefore, accounts for the increase in Se(VI) deposition.

In summary, the predominant mechanisms leading to apparent removal of the inorganic contaminants from the groundwater were ionic flux through the membranes at acidic pH (< pH 6) and ionic flux coupled with membrane deposition under neutral to alkaline conditions (> pH 6). Solution pH and, therefore, the charge of the inorganic had implications for ionic flux and removal. Inorganics present in solution below their pK_a (e.g. B) were neutrally charged and, therefore, were not transported through the ion-exchange membranes. Inorganics present in solution above their pK_a (e.g. U between pH 9 and 11) were transported through the ion-exchange membranes due to their increase in charge and subsequent electrostatic interactions with the membranes. Apparent inorganic removal from the diluate under acidic and alkaline conditions without ionic transport indicated membrane deposition. This was, however, more pronounced under alkaline conditions. The increase in solution pH leads to the precipitation of insoluble carbonate species, membrane scaling and a subsequent reduction in ionic flux.

6.4.3 Ionic Hydration and Mobility

The influence of hydrated radius on the removal of inorganic contaminants from aqueous model solutions by ED was shown in Chapter 5, whereby ions with a relatively smaller hydrated ionic radii and weaker hydration shell were removed more efficiently than ions with a larger hydrated ionic radius and stronger hydration shell. Although the removal of contaminants from groundwater is a more complex process and is influenced by other conditions (ED system operation parameters, physicochemical conditions); comparisons between the hydrated radii of the contaminants of interest were made. The trend of increasing removal with decreasing hydrated radius was not clear due to the wide range of hydrated ionic radii reported in literature. However, a positive correlation was seen between the contaminants Br^-, NO_3^-, F^- and SO_4^{2-} at pH 7 (0.330, 0.332, 0.340, 0.352 and 0.379 nm, respectively (Volkov *et al.*, 1997)); i.e. R_D, Br^-, NO_3^- 100 % > F^- 92.1 % > SO_4^{2-} 52.9 %. There

was no correlation between ionic mobility and inorganic removal and flux. As was discussed with the applied voltage experiments, these results demonstrate that removal of contaminants from real water is a more complex process compared to model solutions. Hydrated radius plays a less important role in the transport of the contaminants present due to the implication of solution pH on inorganic speciation, solute-solute interactions. The deposition of contaminants on the membranes reduces their subsequent ionic transport and removal efficiency.

6.5 Analysis of Membrane Scaling

After the ED experiments with the groundwater were completed the ED stack was dismantled, photographs and optical microscope images were taken of the membranes. Visible deposition of the precipitation formed within the groundwater at high pH, the resultant scaling and swelling of the CEMs in contact with the concentrate was observed (Figure 6.14A). The majority of the surface of the membrane was covered by deposits. This made it difficult for light to go through the membrane, as shown on the optical microscope image. However, the formation of crystals on the surface and parts of the woven structure of the membrane can be seen. Similar looking deposits have been reported by Bazinet and Araya-Farias (2005).

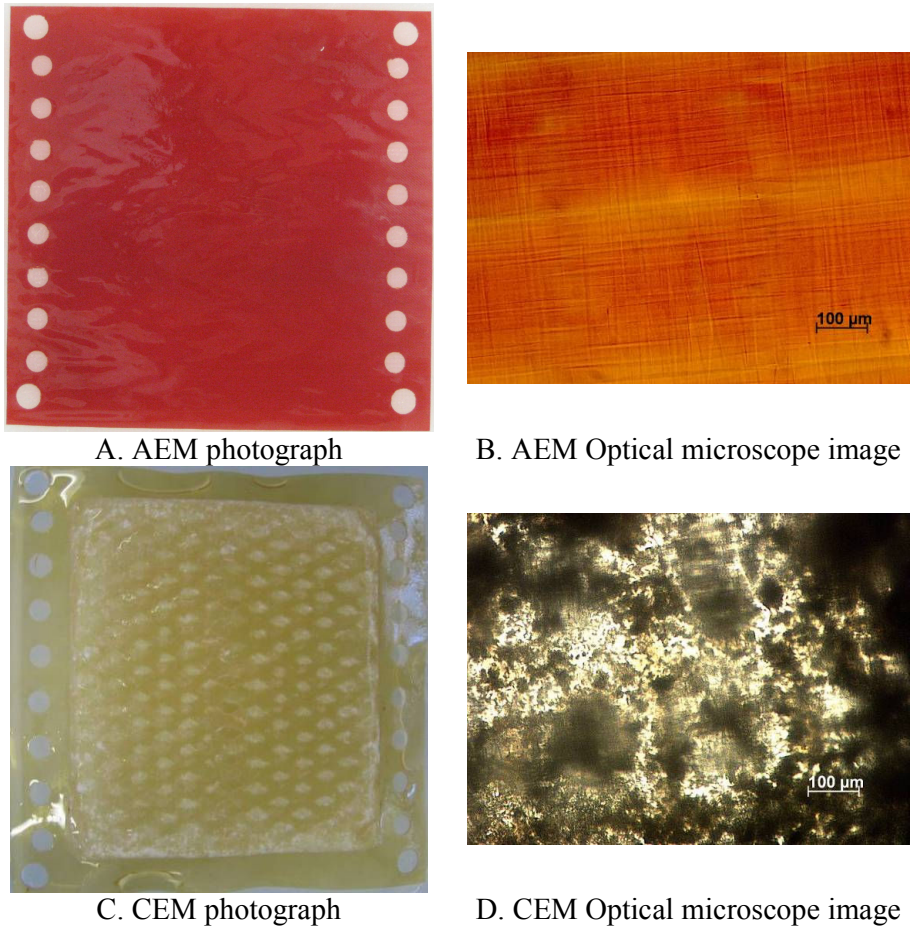

A. AEM photograph

B. AEM Optical microscope image

C. CEM photograph

D. CEM Optical microscope image

Figure 6.14. Top view of (A, B) AEM and (C, D) CEM exposed to Pine Hill groundwater. Photograph (A, C) (Canon IXUS 65), (B, D) Optical microscope image (Axioskop 2 MAT, Zeiss Optical, UK, Optical zoom 10×).

FIB-SEM analysis of the CEM exposed to the groundwater was performed to investigate the morphology of the scaling layer and confirm the elemental composition of the presumed deposit. Figure 6.15A reveals the presence of a scaling layer of approximately 60 µm on both surfaces of the CEM. No significant difference was noted between the spectrum of an unused AEM and an AEM exposed to the groundwater (Figure 6.15B). Figure 6.15C compares the elemental spectrum of an unused CEM and the scaled CEM, confirming the presence of O, Cl^-, Na^+, Ca^{2+}, Mg^{2+} and S. Although Cl^- and S are CEM components, the intensity of these peaks on the scaled CEM were greater than on the control CEM. The greater intensity of O within the scaled CEM is evidence for the scaling composition of carbonate salts.

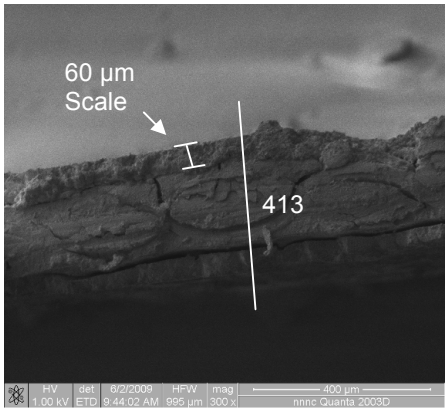

A. CEM cross-section

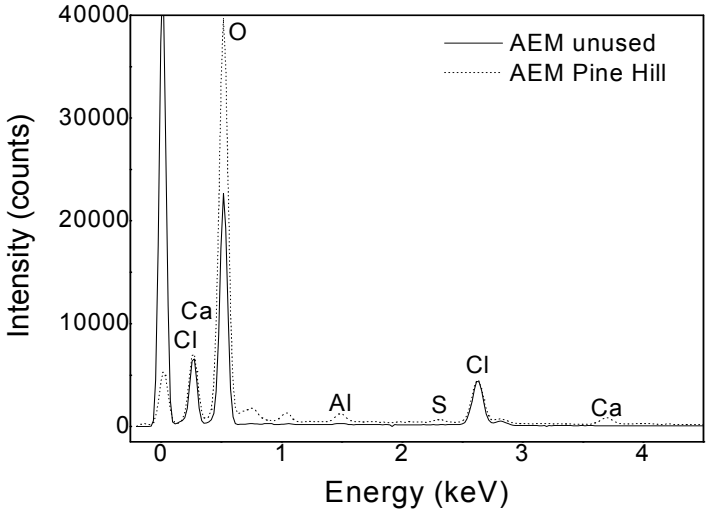

B. EDX cross-sectional sum spectrum of unused and used AEM

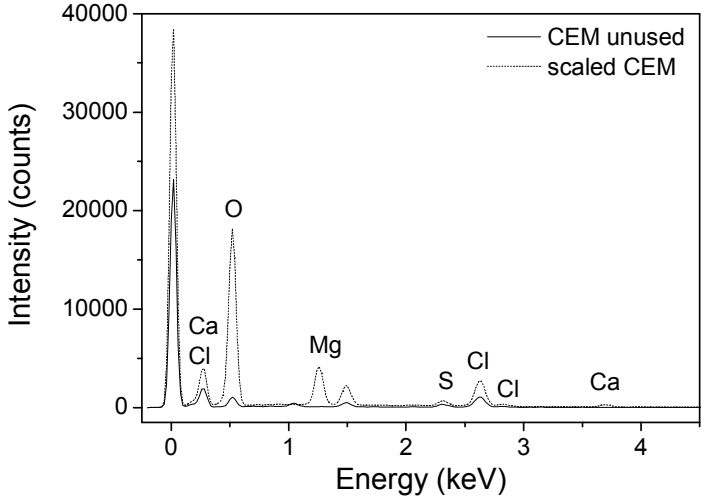

C. EDX cross-sectional sum spectrum of unused and used CEM

Figure 6.15. (A) Cross-section of scaled CEM (FEI Quanta 2003D, USA, 1 kV beam energy). EDX elemental sum spectrum of (B) unused CEM and scaled CEM and (C) unused AEM and AEM exposed to Pine Hill groundwater (Oxford Instruments INCAx-sight, UK, 15 kV beam energy).

Identification of the inorganic composition of the scaling layers is shown in Figure 6.16. Due to concentration polarisation, O, Mg^{2+} and Ca^{2+} in the scaling layer was enhanced on the CEM surface facing the concentrate, as indicated by higher intensity in counts. This high intensity of the Mg^{2+} and O peaks within the scaling layers is evidence for the significant increase in Mg^{2+} deposition under alkaline conditions (Figure 6.12B) in the form of $MgCO_3$. O, Cl^-, Na^+, Ca^{2+}, Mg^{2+} and S were found within the CEM cross-section indicating their penetration through the membrane resultant of ionic transport. However, peak intensity of Ca^{2+} was greater within the scaling layer. EDX scans at higher beam energy (20 kV) failed to identify any other elements located on or within the CEM. This is due to the lower concentration of the deposition inorganics (e.g. Sr^{2+}, Zn^{2+}, U) and the EDX detection limit.

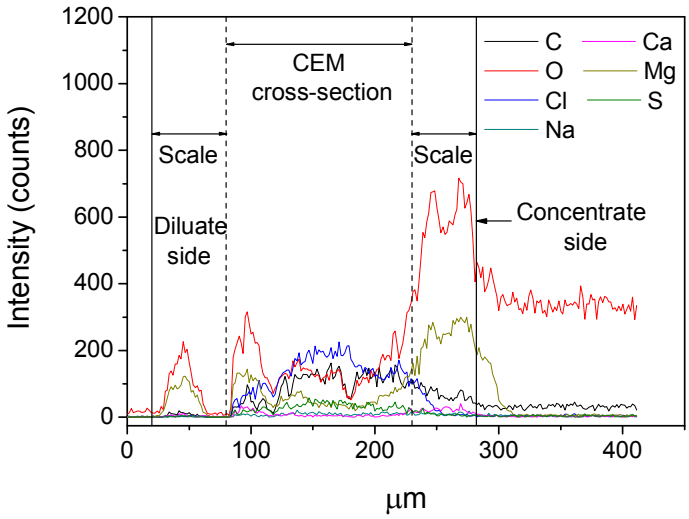

Figure 6.16. EDX spectrum of scaled CEM cross-section (15 kV beam energy).

Identification of elements on the CEM surfaces using EDX allowed further confirmation of the presence of inorganic deposition and led to identification of its morphological nature. Elemental mapping of the scaled CEM surface (Figure 6.17A) was undertaken. The inset image in Figure 6.17A shows the rough structure of the deposits. The deposition of O, Mg^{2+} and Na^+ on the CEM surface was amorphous i.e. distributed sparsely over the surface, whereas distinct patches of Cl^-, Ca^{2+} and S deposits were observed. The pattern of O and Mg^{2+} on the membrane surface is comparable and is further indication of $MgCO_3$ deposition.

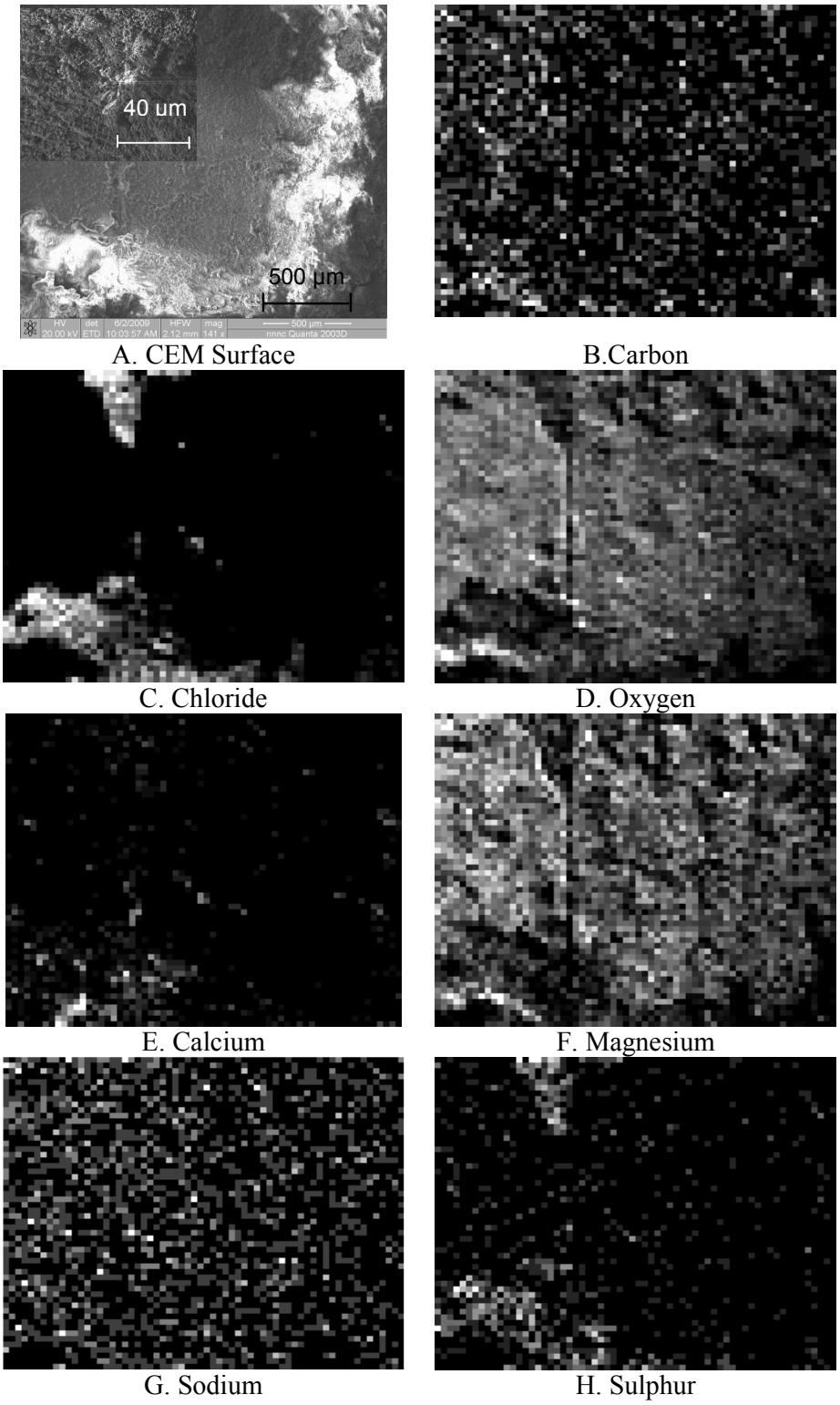

Figure 6.17. (A) FIB-SEM image of scaled CEM surface (20 kV beam energy). Inset (A) close-up of scaling (30 kV beam energy). (B-H) EDX elemental analysis of CEM surface (15 kV beam energy).

To summarise, membrane analysis using FIB-SEM/EDX showed the presence of scaling deposits on both surfaces of the CEM. These scaling deposits were composed of inorganic carbonate salts, particularly $MgCO_3$, as postulated in Section 6.4.2. The presence and, therefore, the penetration of inorganics such as Ca^{2+}, Mg^{2+}, Na^{+} and Cl^{-} through the CEM were observed. This would have implications for ionic transport, as demonstrated in Section 6.4.1. The presence of the CEM scaling layer demonstrates that a highly alkaline pH is a limiting factor when divalent ions such as Ca^{2+} and Mg^{2+} are abundant within the water to be treated.

6.6 Electrodialysis Parameters and Performance

6.6.1 Resistance and TDS Flux

The influence of the scaling layer on ED performance in regards to resistance and the overall flux of TDS were evaluated. The resistance across the ED stack as a function of applied voltage is shown in Figure 6.18A. The stack resistance was relatively stable in the beginning of the experiments followed by a significant increase towards the final stages of the experiment. This was especially noticeable at 18 V. The gradual increase occurs as a result of the depletion of ions within the diluate solution circulating through the ED stack and the resultant lowering of the current. The final resistance achieved during the 18 V experiment (40.9 Ω) is higher than the final resistance in the 12 V experiment (16.7 Ω) as a result of deeper demineralization of the diluate at 18 V (TDS R_D: 12 V 80.5 %, 18 V 94.9 %, Figure 6.18B) coupled with enhanced concentration polarisation as a result of operation above the LCD. The TDS DWG value of 0.5 g/L was reached in the 18V experiment as a direct result of this. The higher TDS removal at 18 V is comparable to the desalination results in Chapter 4, where NaCl removal increased with applied voltage. However, the significant increase in resistance at 18 V is also a resultant from the higher mass of inorganics deposited on the membranes and the resultant scaling (Section 6.3.2).

The mass of TDS deposited at 18 V (646 mg/cm^3) was significantly higher than the mass deposited at 12 V (536 mg/cm^3) (Figure 6.18C) as result of enhanced migration towards the membranes. This hampered the flux of inorganics and, thus, TDS through the membranes (Figure 6.4, Figure 6.18D). While initially TDS flux at 18 V

(36.7 mg/cm^{2}h) compared to 12 V (30.4 mg/cm^{2}h), the deposition of TDS with experimental time subsequently hampered TDS flux as indicated by the lower final flux at 18 V (0.9 mg/cm^{2}h) compared to 12 V (3.7 mg/cm^{2}h). Therefore, TDS deposition has serious implications for the ED performance.

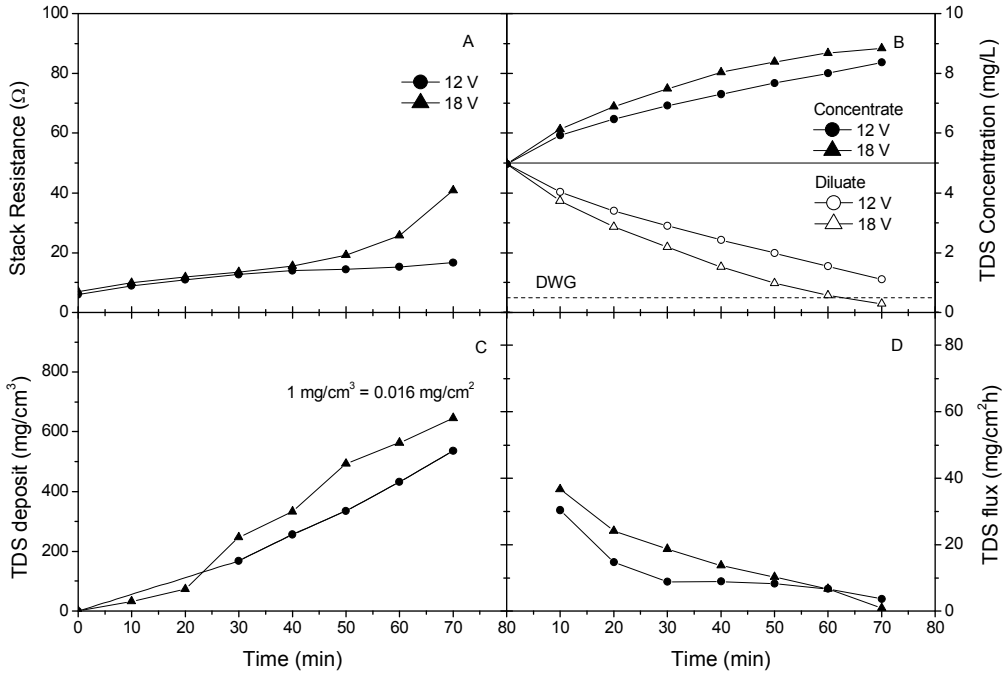

Figure 6.18. (A) ED stack resistance, (B) TDS concentration (mg/L), (C) TDS membrane deposit (mg/cm^3), and (D) TDS flux (mg/m^{2}h) as a function applied voltage (Horizontal dotted line in (B) indicates the 0.5 g/L TDS ADWG).

The precipitation of insoluble species within the diluate and concentrate at high pH and the consequent membrane scaling resulted in an increase in electrical resistance (Figure 6.19). In the groundwater experiments, an increase in resistance across the stack from 27.5 Ω (pH 3) to 50 Ω (pH 11) occurred. Similar increases in resistance due to membrane scaling have been reported (Bazinet and Araya-Farias, 2005; Casademont *et al.*, 2008a). Solution pH did not influence the desalination process in ED treatment of model aqueous solutions (Chapter 5). However, TDS removal decreased with increasing solution pH of the groundwater experiments (pH 3: 99.0 %, pH 11: 89.5 %, Figure 6.19).

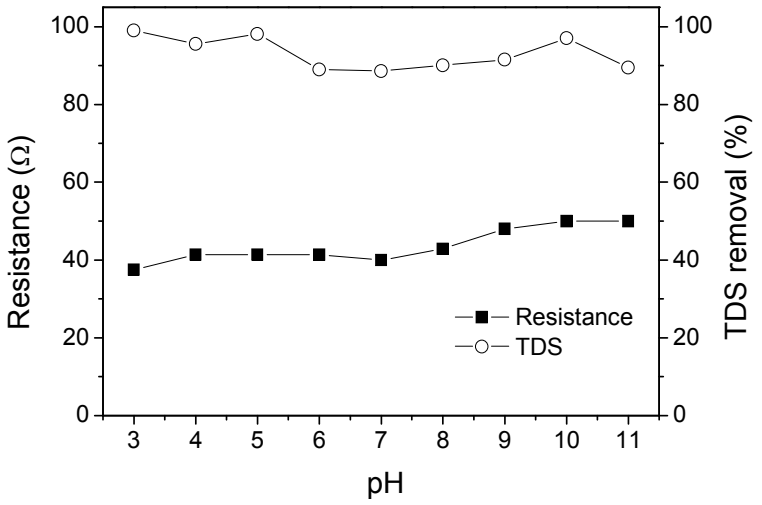

Figure 6.19. Electrical resistance (Ω) and TDS removal (R_D, %) as a function of solution pH (3-11) (12 V, experimental duration 110 min).

Figure 6.20A shows TDS (mg/L) concentration within the diluate and concentrate for each experiment. Approximately 90.0 % removal was needed to reach the DWG of 0.5 g/L. While this guideline was only reached in the pH 3-5 and pH 10 experiments, the average TDS removal achieved for all experiments was high (91.4 ± 7.5 %). TDS flux from the diluate to the concentrate significantly decreased with increasing pH as shown in Figure 6.20B. While the initial TDS flux was higher at pH 11, due to higher initial TDS concentration as a result of the pH change using NaOH, TDS flux dramatically decreased. This correlates with the increase in deposition of inorganics at high pH (Section 6.4.2) and demonstrates the implication of membrane scaling on ED performance.

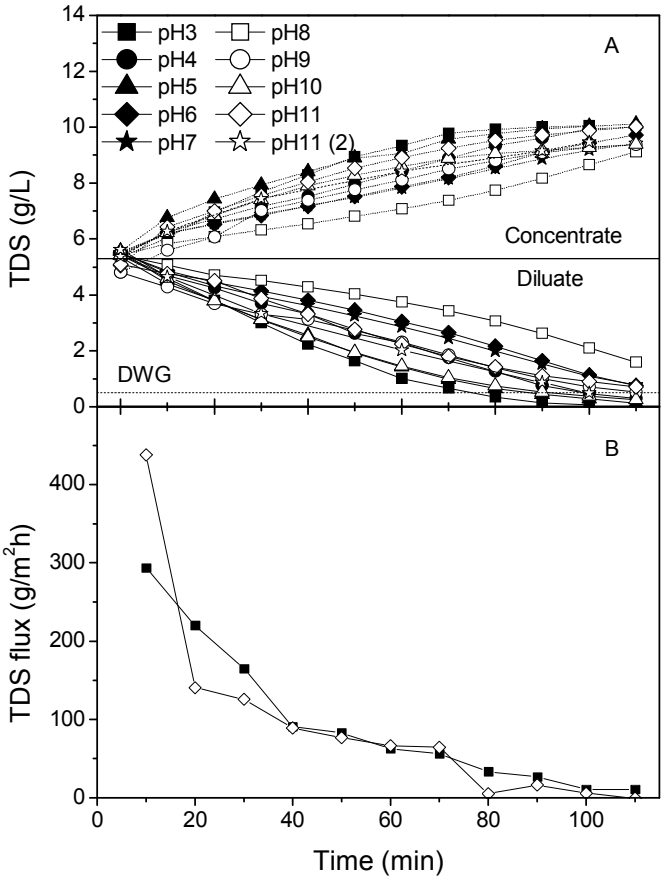

Figure 6.20. (A) TDS concentration (g/L) within the diluate and concentrate, (B) TDS flux (mg/cm^{2}h) at pH 3 and 11 (Horizontal dotted line indicates DWG (0.5 g/L TDS; TDS estimated as TDS = 0.64 × EC (McNeil and Cox, 2000)).

6.6.2 Power and Specific Energy Consumption

A comparison between the power consumed during the groundwater experiments and the desalination experiments (Chapter 4) is shown in Table 6.7. When the DWG was not reached (groundwater 12 V experiment) the power and energy consumed at experimental completion is given. Power consumption during the groundwater experiments increased with increasing applied voltage and was higher than the power consumed during the desalination experiments. This is understandable due to the high concentration of inorganic contaminants within the groundwater and, therefore, an increase in the power consumed to transport these contaminants through the ion-exchange membranes. Similarly, SEC at 18 V (7.8 ± 0.2 Wh/L) was higher than the

SEC at 12 V (5.9 ± 0.1 Wh/L) and both were above the SEC in the desalination experiments in Chapter 5.

Table 6.7. Comparison between the power consumption (Wh) and specific energy consumption (SEC, Wh/L) of the ED stack in the production of drinking water (DWG 0.5 g/L NaCl and TDS) during desalination and Pine Hill groundwater applied voltage experiments.

Experiment	Applied voltage (V)	Power consumption (Wh)	SEC (Wh/L)
Desalination (5 g/L NaCl)	12 V	16.8 ± 0.4	4.4 ± 0.1
	18 V	20.9 ± 0.5	5.7 ± 0.1
Without OM (Ch 5) (5 g/L NaCl)	10 V	20.5 ± 0.5	5.7 ± 0.1
Groundwater (5.3 g/L TDS)	12 V	17.9 ± 0.4	> 5.9 ± 0.1 [a]
	18 V	26.9 ± 0.6	7.8 ± 0.2

[a] SEC at completion of experiment presented since the TDS DWG was not reached in these experiments. Final TDS and experimental duration: 1.1 g/L at t = 70 min.

Power consumption and SEC during the groundwater experiments increased with solution pH (Table 6.8). The power consumed at pH 3 was 16.0 Wh compared to > 20.3 Wh at pH 11. SEC increased from pH 3 (5.3 Wh/L) to pH 11 (> 7.4 Wh/L). This increase in power consumption and SEC correlates with increasing resistance and inorganic membrane deposition. Due to the increase in inorganic membrane deposition with solution pH the energy needed to transport the contaminants through the membranes is greater. A comparison between SEC in this study and publish data on energy consumption in RO of brackish water was undertaken. However, it is difficult to make a comparison with published data as SEC varies greatly due to system size, feed water salinity and the membrane used. The SECs of brackish water-RO membrane systems range from 1.1-26 Wh/L for solar-powered systems (Joyce *et al.*, 2001; Schäfer *et al.*, 2007) and 0.8-1.7 Wh/L for non-solar powered systems (Pearce, 2008). SEC for the treatment of the Pine Hill groundwater, as well as the desalination experiments shown in Chapter 5, is greater than the published SEC values. While ED is usually more energy efficient in the treatment of brackish water compared to RO, small-scale membrane treatment systems have a tendency to

operate less efficiently and their SEC is usually higher than that of large-scale systems.

Table 6.8. Power consumption (Wh) and specific energy consumption (SEC, Wh/L) of the ED stack as a function of solution pH during Pine Hill groundwater experiments (TDS DWG 0.5 g/L).

Solution pH	Power consumption (Wh)	SEC (Wh/L)
3	16.0	5.3
4	17.1	5.3
5	17.1	5.3
6	> 17.0	> 5.2 [a, b]
7	> 17.3	> 5.8 [a, c]
8	> 17.2	> 6.2 [a, d]
9	> 17.6	> 5.9 [a, e]
10	16.6	6.6
11	> 20.3	> 7.4 [a, f]

[a] SEC at completion of experiment presented since the TDS DWG was not reached in these experiments. Final TDS concentration at 110 min: [b] 0.75 g/L, [c] 0.78 g/L, [d] 1.6 g/L, [e] 0.52 g/L, [f] 0.71 g/L.

6.7 Summary

This chapter aimed to elucidate the dominant mechanisms involved in the removal of inorganic contaminants from an Australian brackish groundwater and to investigate the influence of applied voltage and solution pH on these mechanisms. The predominant mechanisms leading to apparent removal of the inorganic contaminants from the groundwater were ionic flux through the membranes coupled with membrane deposition.

The apparent removal of the inorganics contaminants that were speciation dependent of solution pH (B, Li^+, SO_4^{2-}, U, As^{5+} and Se^{6+}) was enhanced at a higher applied voltage in comparison to the inorganic contaminants that were speciation independent of pH (Br^-, Cl^-, F^- and NO_3^-). At 12 V inorganic removal was attributed to ionic transport, electrostatic interactions between the inorganics and the membranes with minor contribution from membrane deposition. At a higher applied voltage, ionic transport was initially high due to enhanced migration towards the

membranes. However, this led to an increase in membrane deposition which subsequently hampered inorganic contaminant flux and a reduction in removal.

The removal of the inorganics B, Li^+, K^+, SO_4^{2-}, U, Ca^{2+}, Mg^{2+}, Sr^{2+}, Zn^{2+}, As(V) and Se(VI) was pH and thus speciation dependent, while the removal of other monovalent inorganics (Br^-, Cl^-, F^-, NO_3^-) was pH independent. Ionic transport was the predominant removal mechanism under acidic-neutral conditions (< pH 6) whereas membrane deposition with minor contribution from ionic transport dominated under neutral to alkaline conditions (pH 7-11). Solution pH had implications for the charge of the inorganic and, therefore, their flux and removal. Undissociated inorganics (< pK_a) were not transported through the membranes, whereas dissociated inorganics (> pK_a) were due to electrostatic interaction with the membranes. The precipitation of insoluble carbonate species at high pH led to membrane scaling and a subsequent reduction in inorganic flux.

This scaling led to an increase in stack resistance and a decrease in TDS removal. Unlike the results from Chapter 5, the hydrated radius and strength of hydration shells was found to play a less important role in the transport and removal of the inorganic contaminants during ED of the groundwater, in comparison to other parameters such as solution pH, solute-solute interactions and inorganic concentration. These results have significant importance in the treatment of such brackish groundwaters as solution pH varies greatly in groundwater and the inorganic contaminants studied are common in surface and groundwater. Consideration needs to be given to the long-term practical applicability of ED in groundwater treatment with regards to chemical and mechanical membrane stability and ED performance.

Chapter 7. Fate of Steroidal Hormones in Electrodialysis

Due to gaps in current knowledge, the mechanisms governing hormone sorption by ion-exchange membranes are not well understood. Therefore in this chapter, water-membrane partition coefficients (log $K_{AEM/CEM}$) for the steroidal hormones estradiol, estrone, progesterone and testosterone are studied in order to explicate the mechanisms governing membrane sorption. The sorption of the hormones to the ion-exchange membranes (PS-DVB polymer) will be compared to sorption reported for other polymer materials (polyamide and polyamide-urea).

Solution chemistry and the presence of OM have implications for the removal of trace contaminants in ED, as shown in Chapter 5. The behaviour of progesterone and estrone during batch and continuous ED experiments will be evaluated to identify differences in sorption between undissociated (progesterone, pH 7 and 11) and dissociated compounds (estrone pH 11). Comparisons between sorption during the isotherm and ED experiments will be made to assess the reliability of log $K_{AEM/CEM}$ values for predicting the fate of steroidal hormones during ED.

7.1 Hormone Sorption during Isotherm Experiments

7.1.1 Water-membrane Partitioning for Steroidal Hormones

The sorption of estradiol, estrone, progesterone and testosterone to the ion-exchange membranes was measured at neutral pH. The hormone-membrane isotherms are shown in Figure 7.1. The mass of hormone sorbed (log $C_{AEM/CEM}$, ng/cm^3) increased linearly (R > 0.99) as the freely dissolved hormone concentration (log C_w^t, ng/L) increased. The deviation of the isotherms from linearity at 2500 µg/L (0.1-100 µg/L: AEM n_i = 0.89-0.96 CEM n_i = 0.81-0.94; 1-2500 µg/L: AEM n_i = 0.81-0.93; CEM n_i = 0.81-0.85) indicates hormone concentration limited binding. However, the partition coefficients were derived for the 0.1-2500 µg/L concentration range. The linearity of the isotherms at low concentration (0.1-100 µg/L) suggests that the partitioning into the membranes was the dominant sorption mechanism and that adsorption sites

within the membranes were far from being saturated (Schwarzenbach *et al.*, 2003). Although both membranes are composed of the same polymer (PS-DVB), the affinity of the hormones for the AEM and CEM was different with estradiol and estrone showing significant differences in sorption between the AEM and CEM. This indicates that sorption to the ion-exchange membranes is dependent on the attached functional groups.

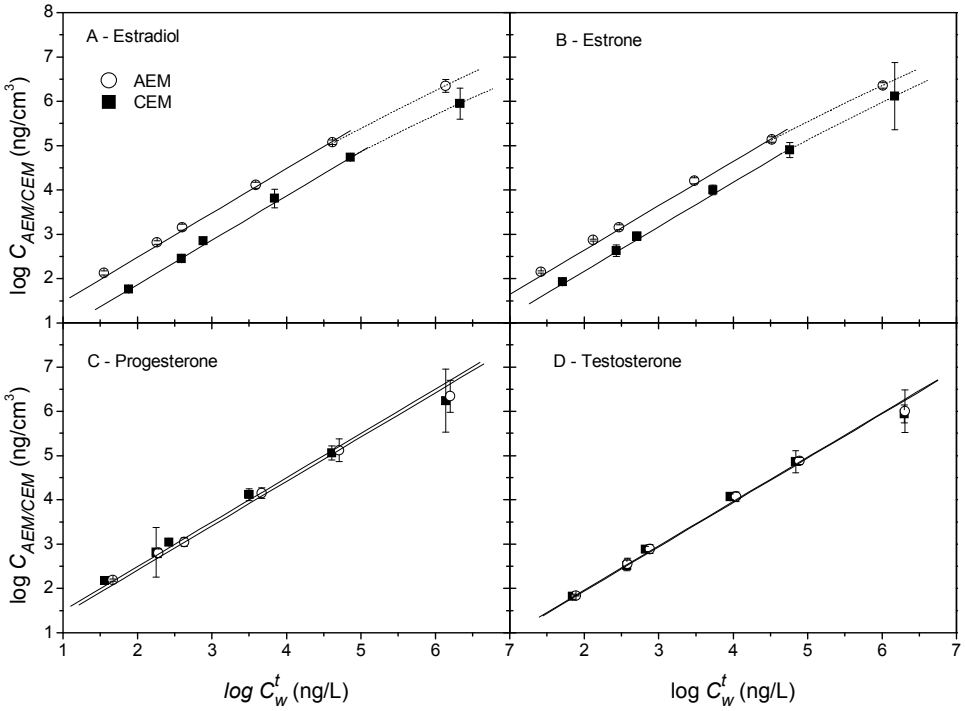

Figure 7.1. Hormone-membrane sorption isotherms for (A) estradiol, (B) estrone, (C) progesterone and (D) testosterone (1mM $NaHCO_3$, 85.5 mM NaCl, 0.1-2500 µg/L hormone, pH 7; time used for log $K_{AEM/CEM}$ determination: 170 h).

The determined membrane partition coefficients (log $K_{AEM/CEM}$) for the 0.1-2500 µg/L concentration range are presented in Table 7.1. The affinity of the hormones for the AEM increased in the following order: testosterone < progesterone < estradiol < estrone. The affinity of the hormones for the CEM increased in the following order: estradiol < testosterone < estrone < progesterone. There are various types of chemical, physical and electrostatic interactions that can explain the process of sorption. Chemical interactions include covalent and hydrogen bonds. Physical attractions or Van der Waals interactions (also known as London Dispersion Forces)

between a compound and material include dipole-dipole, dipole-induced dipole and instantaneous dipole-induced dipole interactions. Electrostatic interactions are involved in ion-ion and ion-dipole interactions (e.g. ion exchange). Pronk *et al.* (2006) postulated that sorption of the hormones to ion-exchange membranes was related to their hydrophobicity (log K_{ow}). Poor correlation between the log $K_{AEM/CEM}$ and log K_{ow} values Table 2.4 suggests that interaction mechanisms other than nonspecific hydrophobicity such as electrostatic interactions and hydrogen bonding are important in the sorption of hormones to ion-exchange membranes. However, electrostatic interactions between the hormones and ion-exchange membranes would not be possible due to the undissociated nature of the hormones at neutral pH (Table 2.4).

Table 7.1. Water-membrane partition coefficients (log $K_{AEM/CEM}$, L/cm^3) for the selected steroidal hormones (Initial hormone concentration 0.1-2500 µg/L).

Hormone	Log $K_{AEM/CEM}$ (L/cm^3)	
	AEM	CEM
Estradiol	0.50 ± 0.13	-0.12 ± 0.03
Estrone	0.67 ± 0.16	0.20 ± 0.04
Progesterone	0.43 ± 0.11	0.53 ± 0.19
Testosterone	- 0.05 ± 0.01	-0.02 ± 0.005

± indicates 95 % confidence interval (C.I.)

7.1.2 Steroidal Hormone Sorption Mechanisms

Previous studies have demonstrated that organic trace contaminants including hormones primarily interact with NF and RO polymeric membranes through hydrogen bonding (Nghiem and Schäfer, 2002; Nghiem *et al.*, 2004c; Schäfer *et al.*, 2003; Williams *et al.*, 1999). While NF and RO membranes are composed of different polymers (polyamide on polysulfone support) than the ion-exchange membranes used in this study (PS-DVB on PVC support), hydrogen bonding between the hormone and ion-exchange membrane functional groups is postulated as the sorption mechanism. Hormones can either be hydrogen-donors (contains phenolic hydroxyl groups, OH) or hydrogen-acceptors (contains carbonyl groups, C=O). Progesterone is monopolar (hydrogen-accepter) while estrone, testosterone and estradiol are bipolar (hydrogen-donor or acceptor) (Table 2.4). Anions of

alkylammonium salts, the functional group in the AEMs ($N(CH_3)_3$), are monopolar and thus take part in forming hydrogen bonds with molecules containing hydrogen-acceptor groups (Lipovski and Dem'yanova, 1971), while the functional group of the CEM (SO_3H) is bipolar (hydrogen-donor and acceptor). Therefore, differences in membrane sorption affinity, as observed in the determined log $K_{AEM/CEM}$ values, were evaluated in regards to differences in the hydrogen bonding capacity between the functional groups of the hormones and membranes.

Considering a single AEM functional group there are 9 hydrogen donor groups (methyl, CH_3). The CEM presents only one hydrogen donor group (hydroxyl, OH) and two hydrogen acceptor groups (S=O). Therefore, the AEM presents more opportunities for hydrogen bonding than the CEM, accounting for the higher log K_{AEM} values. Greater sorption to the AEM would be expected for a hormone containing more hydrogen accepting groups. The number of hydrogen bonding sites possible between the hormone functional groups and one AEM and CEM functional group is given in Table 7.2. Sorption between the hormone hydrogen acceptor and donor groups and the membranes is indicated by the letters A and D, respectively (i.e. the C-3 hydrogen-acceptor group in estradiol can bind with 9 hydrogen's in the AEM functional group). This table shows that although hormones may have similar possible hydrogen bonding capacities, sorption affinity may be markedly different. This is due to the fact that hydrogen bonding is influenced by the position of the hormone functional groups. The molecular structure of the hormones exhibiting strongest sorption to the AEM (estrone and estradiol) and CEM (progesterone and estrone) and possible hydrogen bonding formations with the AEM and CEM functional groups are illustrated in Figure 7.2 and Figure 7.3, respectively.

Table 7.2. Number of hydrogen bonding sites possible between the steroidal hormones functional groups (C-3 and C-17 position) and one ion-exchange membrane functional group (AEM Neosepta AMX-SB and CMX-SB).

Hormone [a]	AEM		CEM	
	C-3	C-17	C-3	C-17
Estradiol	9 A	9A	2 D, 1 A	2 D, 1 A
Estrone	9 A	9 A	2 D, 1 A	1 A
Progesterone	9 A	9 A [b]	1 A	1 A [b]
Testosterone	9A	9 A	1 A	2 D, 1 A

[a] A and D relate to hydrogen bonding facilitated through hormone hydrogen acceptor and donor groups, respectively; [b] C-20 position for progesterone.

While the structure of estrone and estradiol is similar (i.e. hydroxyl group in the C-3 position), estradiol has a hydroxyl group in the C-17 position instead of a carbonyl group. The C-3 hydroxyl group in estrone and estradiol contributes as both a hydrogen-bond donor and acceptor, although predominantly as a donor (Fang *et al.*, 2001). Progesterone and testosterone are structurally similar (i.e. carbonyl group in the C-3 position), however testosterone has a hydroxyl group in the C-17 position. Previous studies on the determination of steroids using molecularly imprinted polymers (MIP's) have found that the hydroxyl functional group in the C-17 position (C-20 position for progesterone) were more important for interactions with MIPs compared to the C-3 hydroxyl functional group (Rachkov *et al.*, 1998; Rachkov *et al.*, 2000). Hormone sorption to ion-exchange membranes would be influenced by hormone structure and the space available for interaction. Sorption of estrone and estradiol to the AEMs is facilitated predominantly through hydrogen bonding between the AEM CH_3 and the C-17 C=O and bipolar C-17 OH groups, respectively, coupled with minor contribution from the hydrogen-accepting C-3 OH group (Fang *et al.*, 2001). The higher log K_{AEM} for estrone (0.67 ± 0.16 L/cm^3) in comparison to estradiol (0.55 ± 0.13 L/cm^3) suggests that the C-17 bipolar hydroxyl group in estradiol is not as strong as the C-17 carbonyl group in estrone. The lower log K_{AEM} of progesterone can be attributed to the reduced space around the C-20 C=O group available for approaching the AEM compared to the C-3 C=O group (Le Questel *et al.*, 2000). The C-3 C=O group in testosterone induces a larger electrostatic potential and as result it is a poor hydrogen acceptor (Fang *et al.*, 2001; Schäfer *et al.*, 2003). Thus, testosterone exhibited the lowest sorption to the AEMs.

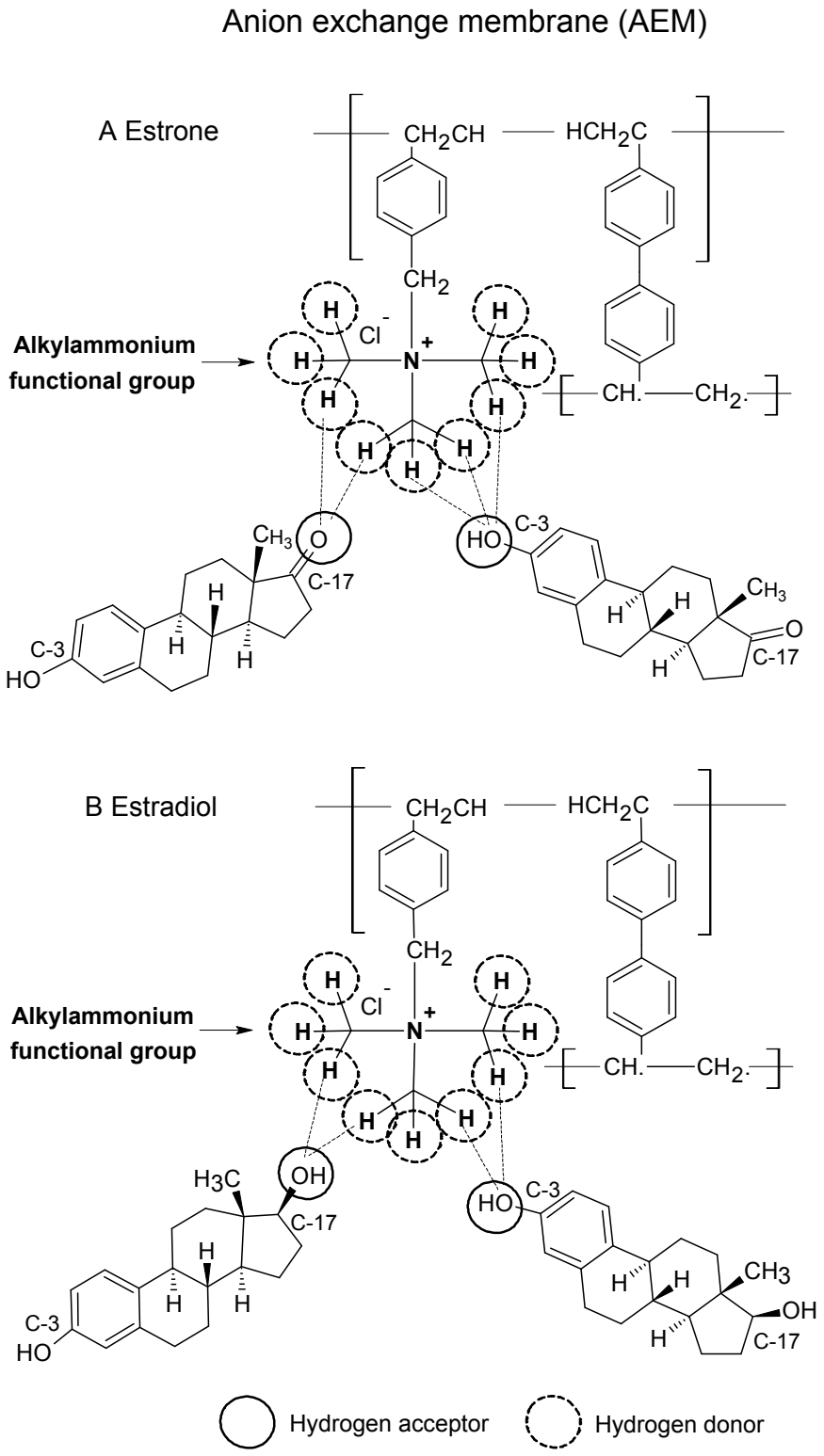

Figure 7.2. Schematic of possible hydrogen bonding between the hormone molecules (A) estrone and (B) estradiol and the AEM (Neosepta AMX-SB) functional groups at neutral pH.

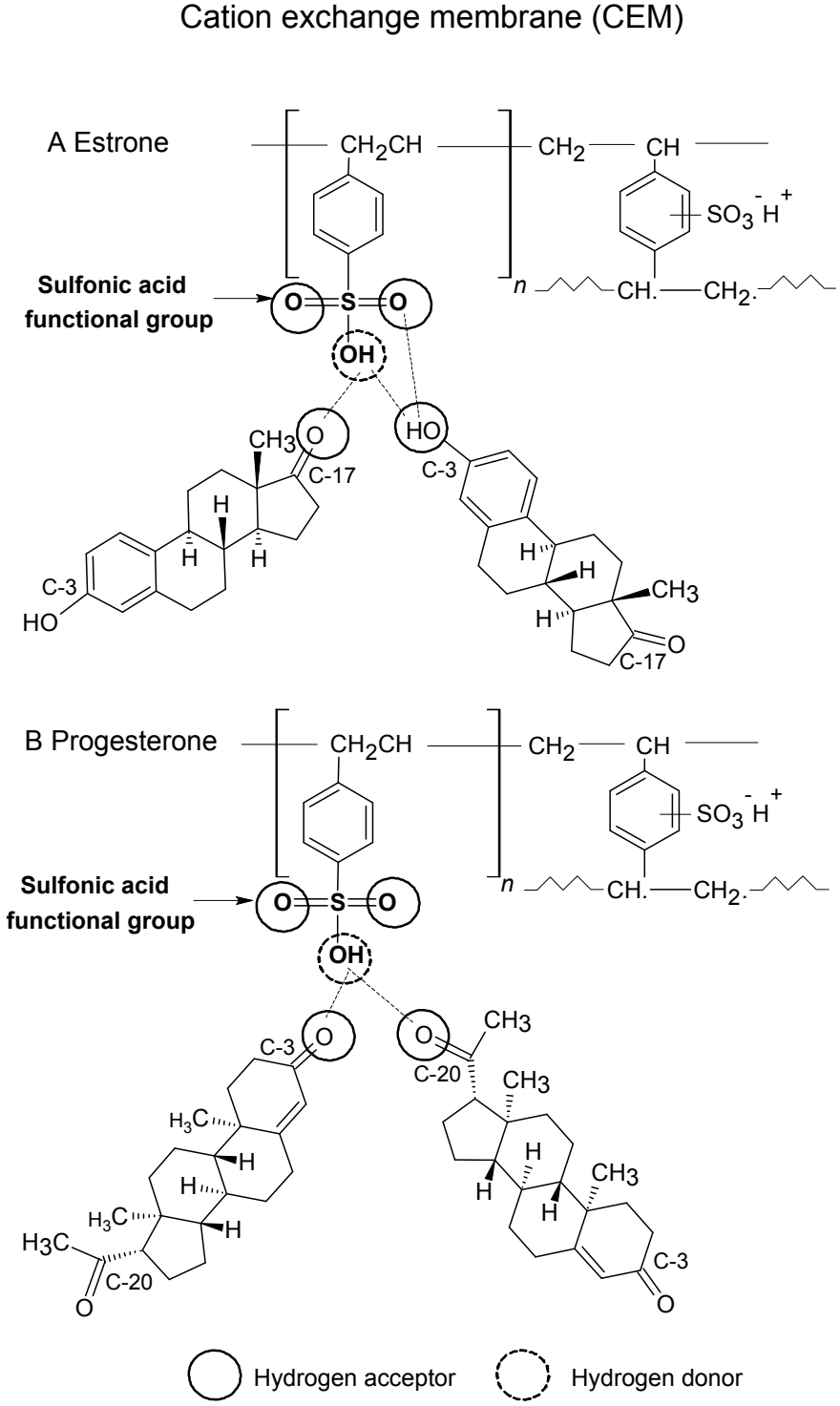

Figure 7.3. Schematic of possible hydrogen bonding between the hormone molecules (A) estrone and (B) progesterone and the CEM (Neosepta CMX-SB) functional groups at neutral pH.

Although progesterone and estrone both contain C-20 and C-17 carbonyl groups, studies have demonstrated that the C-20 carbonyl moiety in progesterone is a triple hydrogen acceptor (Hillisch *et al.*, 2003; Le Questel *et al.*, 2000); thus explaining the greater sorption of progesterone to the CEM (log K_{CEM} 0.53 ± 0.19 L/cm^3) than estrone (log K_{CEM} 0.20 ± 0.04 L/cm^3), testosterone (log K_{CEM} -0.02 ± 0.005 L/cm^3) and estradiol (log K_{CEM} -0.12 ± 0.03 L/cm^3). The higher log K_{CEM} values for progesterone and estrone suggest that the C-17 bipolar hydroxyl bipolar group of estradiol and testosterone are not as strong as the C-17 carbonyl hydrogen acceptor group in progesterone and estrone. This is substantiated by Gancia *et al*. (2001) who developed a method for the quantitative estimation of the hydrogen bonding strengths of hydroxyl and carbonyl functional groups in a range of chemical structures, which are summarised in Table 7.3, and found that hydrogen bonding of the C-17 carbonyl group (log K_β 1.52-1.61) was stronger than hydrogen bonding of the C-17 hydroxyl group (log K_α 0.91). This can explain the higher log K_{AEM} for estrone in comparison to estradiol.

Table 7.3. Strength of hydrogen bonding of steroidal hormone functional groups (Adapted from Gancia *et al.* (2001)).

Hormone	Hydrogen bonding strength			
	Hydrogen acceptor (log K_β)		Hydrogen donor (log K_α)	
	C-3	C-17	C-3	C-17
Estradiol	0.30	1.36	1.89	0.91
Estrone	0.30	1.61	1.89	-
Progesterone	1.70	1.52 [a]	-	-
Testosterone	1.70	1.36	-	0.91

[a] C-20 position for progesterone.

7.1.3 Hormone Degradation

Studies have shown the degradation of steroidal hormones from natural and experimental water samples with photodegradation and biotransformation highlighted as potentially significant removal mechanisms (Jurgens *et al.*, 2002; Lin and Reinhard, 2005). The hydroxyl groups within steroidal hormones makes them susceptible to microbial attack (Ying and Kookana, 2003). Jurgens *et al*. (2002)

studied the degradation of estradiol within river water by microorganisms and found a half-life between 0.2 and 9 days. Ying and Kookana (2003) reported 97.2 % degradation of estradiol from seawater within 56 days under aerobic conditions. While the experiments were conducted in a shaker out of direct light and in solutions with ultrapure water, hormone degradation was possible due to the length of the sorption isotherm experiments (~ 23 days). Therefore, control sorption experiments were undertaken with covered solutions and solutions with the addition of a biocide (0.5 % wt $Na_2S_2O_5$) to determine if photodegradation or biotransformation, respectively, had an influence on hormone sorption in the isotherm experiments. There was no significant difference between the control and experiments without degradation prevention (Figure 7.4), indicating that hormone photodegradation and biotransformation was not an issue in the sorption isotherm experiments.

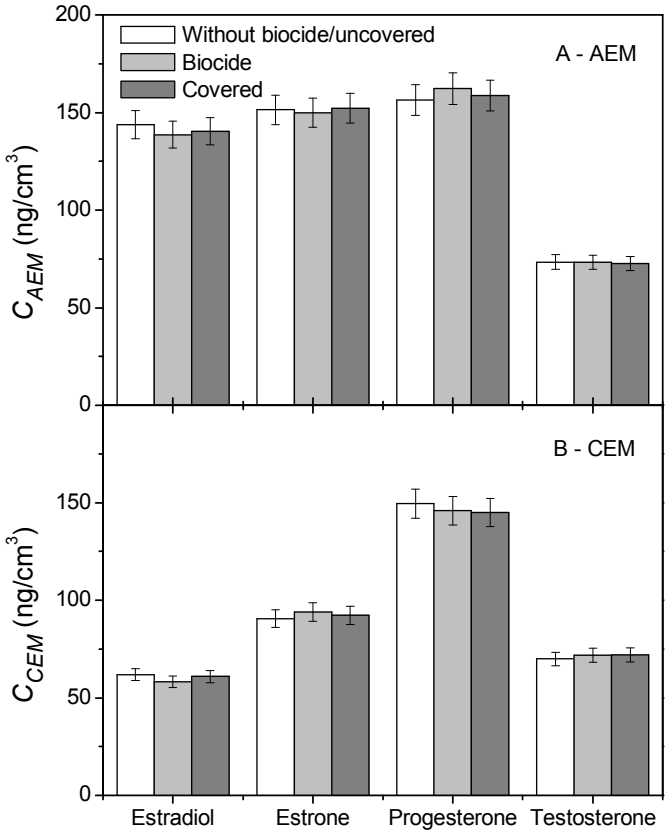

Figure 7.4. Comparison between hormone sorption (ng/cm^3) to the (A) AEM and (B) CEM with and without the addition of a biocide and in covered solutions (1 mM $NaHCO_3$, 85.5 mM NaCl, pH 7, 0.5 % wt $Na_2S_2O_5$, 0.1 µg/L hormone).

Sorption experiments were undertaken to measure hormone sorption to the glass sample bottles used during the sorption isotherm experiments. Sorption was minimal Figure 7.5) with the bulk sorbed within 48 hours. There was no significant difference in the average mass sorbed (% of initial hormone mass) between the hormones with an average of 3.7 ± 3.2 %, 2.7 ± 1.3 %, 2.5 ± 2.1 % and 3.0 ± 2.3 % for estradiol, estrone, progesterone and testosterone, respectively. The water-membrane partition coefficients (log $K_{AEM/CEM}$, L/cm^3) were adjusted accordingly to account for this sorption i.e. the mass of hormone sorbed in the sample bottles without a membrane was subtracted from the mass sorbed in the sample bottles with a membrane added for each sampling period.

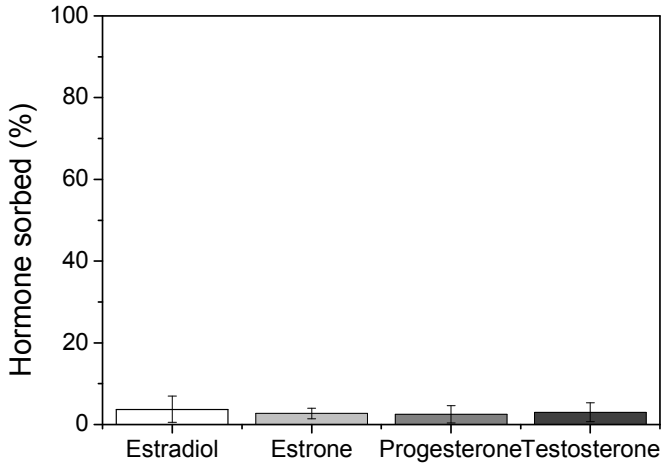

Figure 7.5. Average hormone sorption (% initial mass) during control sorption isotherm experiments (without membrane addition; 1mM $NaHCO_3$, 85.5 mM NaCl, pH 7; 0.1-2500 µg/L hormone).

7.1.4 Hormone Sorption and Desorption Kinetics during Isotherm Experiments

The hormone-membrane sorption kinetics for isotherm experiments is presented in Figure 7.6. Hormone sorption kinetics was the same for the AEM and CEM; however sorption was greatest for the AEM. Two separate sorption processes occur: (1) Initial surface sorption followed by (2) sorption into the depth of the membrane

which is gradual and diffusion limited. The sorption kinetics was the same for all steroidal hormone isotherm experiments, however, diffusion appears slower at the highest initial hormone concentration (2500 μg/L) compared the lowest initial hormone concentration (0.1 μg/L) as demonstrated with estradiol in Figure 7.7. This can be attributed to the larger initial mass per unit area of membrane exposed to the hormone in solution at 2500 μg/L. The initial mass of hormone per unit area during the 0.1, 0.5, 1, 10, 100 and 2500 μg/L sorption isotherm experiments were 0.001, 0.006, 0.01, 0.12, 1.2 and 30.8 μg/cm^2, respectively. As constant mass of hormone sorbed was not reached, 170 hours was arbitrarily chosen for the determination of the hormone-membrane partition coefficients and to allow comparison with the ES-membrane partition coefficients.

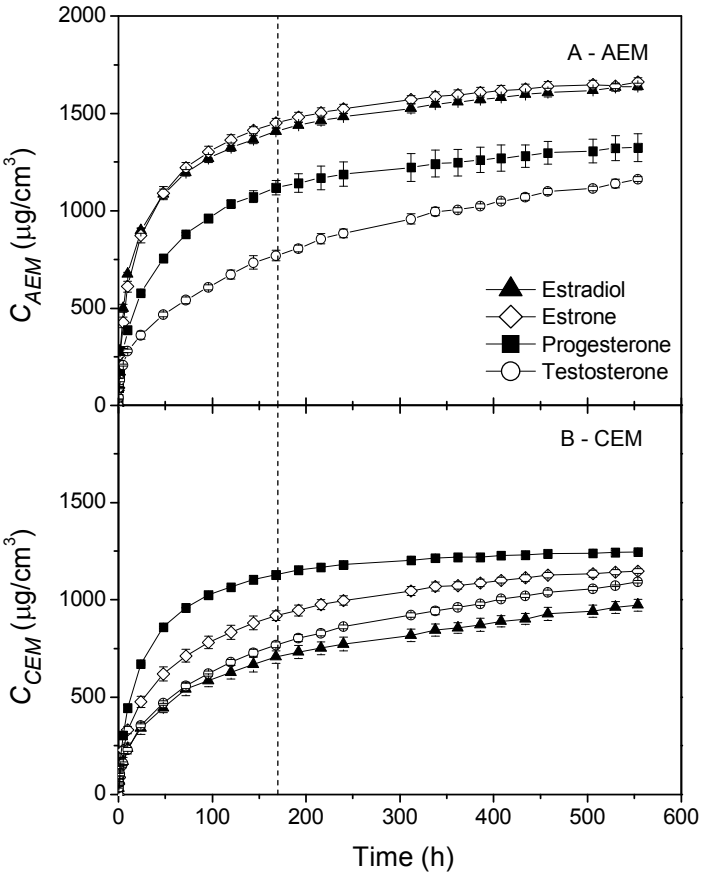

Figure 7.6. Hormone sorption kinetics for the (A) AEM and (B) CEM (1mM $NaHCO_3$, 85.5 mM NaCl, pH 7, 1 μg/L hormone; vertical dotted line indicates time chosen for log $K_{AEM/CEM}$ determination: 170 h).

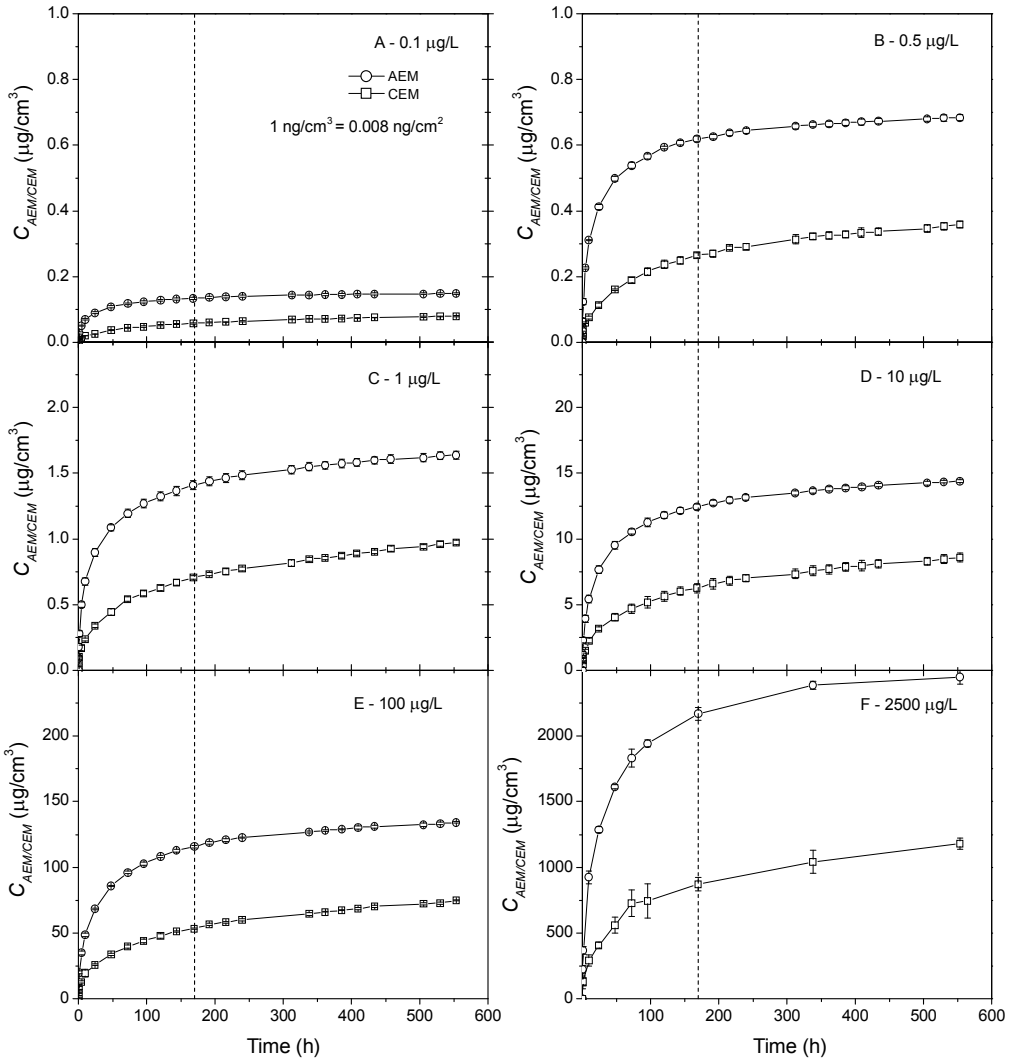

Figure 7.7. Estradiol sorption kinetics (A-B) 0.1-2500 µg/L (1mM $NaHCO_3$, 85.5 mM NaCl, pH 7; vertical dotted lines indicate time used for determination of log $K_{AEM/CEM}$: 170 h).

Results have shown that the steroidal hormones significantly sorb to the ion-exchange membranes. While this sorption was shown to be hormone and membrane dependent, changes in solution chemistry can influence this process and potentially release the sorbed hormones back into solution. This has serious membrane performance and environmental implications especially in the application of membranes for drinking water production. Chang *et al*. (2003) raised the issue of estrone desorption during backwashing and membrane cleaning of MF membranes.

Rapid desorption of estrone from membranes placed in a background buffer solution (1 mM $NaHCO_3$, 20 mM NaCl) was initially observed followed by an equilibrium state (180 min) when 14 % of the adsorbed estrone was released (initial sorbed concentration 105-209 ng/g of membrane). Hormone desorption could be enhanced at high solution pH, a common condition during membrane cleaning, due to charge repulsion between negatively charged hormones (estradiol and estrone) and negatively charged membrane surfaces (Schäfer *et al.*, 2004). Therefore, desorption of the hormones from the ion-exchanges membranes (from the 1 μg/L isotherm experiment) was investigated using different membrane cleaning solutions (0.002 M HCl, NaOH and UW).

Unlike the sorption kinetics, rapid desorption was observed initially for both the CEM and AEM under each solution condition and steady-state equilibrium was reached at 50 hours (Figure 7.8). Partial desorption (20-30 % initial mass sorbed) occurred indicating the irreversible nature of the hormone membrane sorption. As sorption was determined to be a result of hydrogen bonding, desorption was expected to be minimal since hydrogen bonding is strong compared to other van der Waals' forces. The percentage hormone desorbed (% of initial mass sorbed) varied between membrane and hormone type (Figure 7.9). Desorption from the CEMs, on average, was similar (HCl: 19.2 ± 5.1 %; NaOH: 18.8 ± 8.3 %; UW: 18.7 ± 0.8 %) while it varied for the AEMs (HCl: 13.3 ± 4.5 %; NaOH: 18.3 ± 12.6 %; UW: 11.8 ± 3.8 %). Membrane desorption was dependent on the initial mass sorbed, solvent pH, hormone physicochemical properties and subsequent hormone-membrane interactions. HCl and NaOH was less effective in desorption of progesterone from the CEMs (HCl: 12.0 ± 0.6 %; NaOH: 7.8 ± 0.4 %) in comparison to UW (18.6 ± 0.9 %). A similar trend was noted with estradiol (HCl: 12.8 ± 0.6 %; NaOH: 7.7 ± 0.4 %; UW: 9.5 ± 0.5 %) and estrone (HCl: 10.5 ± 0.5 %; NaOH: 7.2 ± 0.5 %; UW: 9.5 ± 0.5 %) desorption from the AEMs using NaOH. More estradiol (25.8 ± 1.3 %) and estrone (24.7 ± 1.2 %) was desorbed from the CEM with NaOH (pH ~ 10.8) in comparison to progesterone and testosterone, due to estradiol and estrone dissociation and subsequent electrostatic repulsion with the negatively charged CEM. Desorption of the neutral hormones progesterone and testosterone from the strongly

basic AEM with NaOH base was noted with 30.7 ± 1.5 % and 27.8 ± 1.4 % desorbed, respectively.

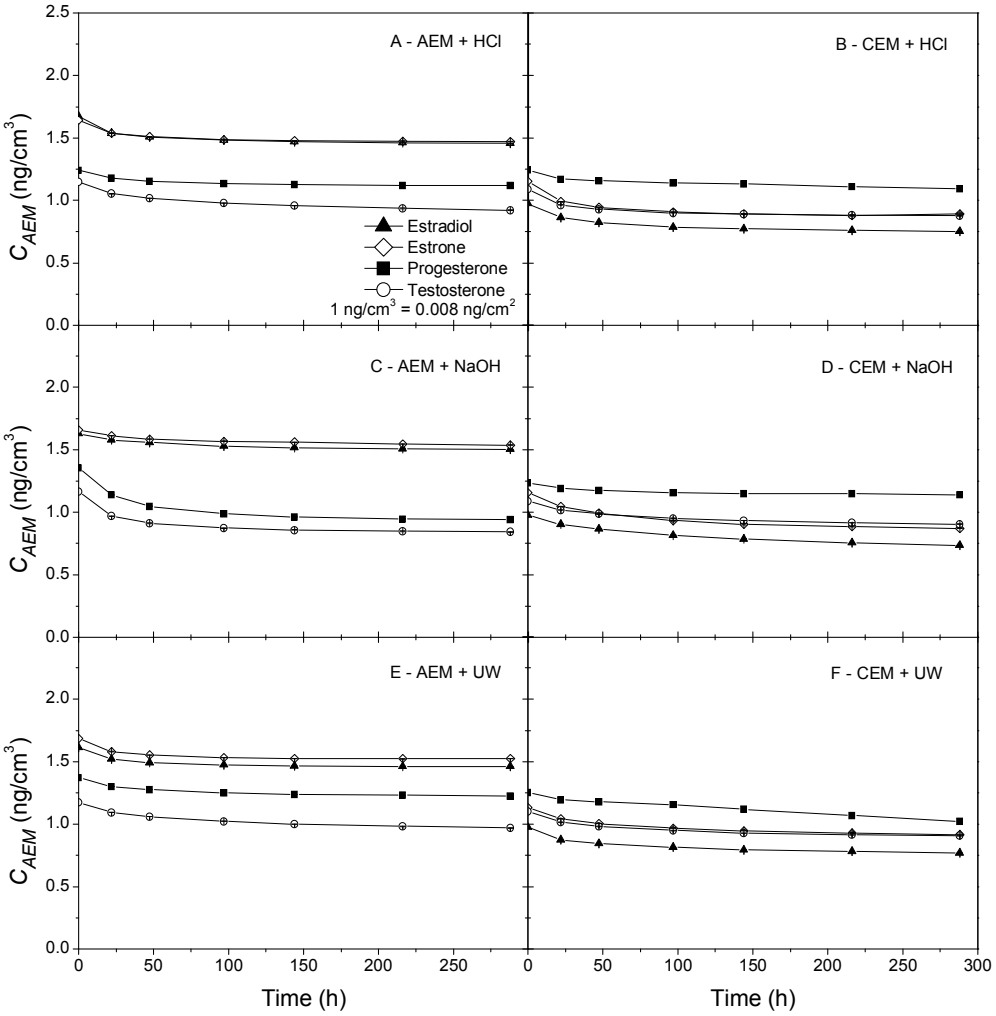

Figure 7.8. Hormone desorption kinetics with (A, B) 0.002 M HCl, (C, D) 0.002 M NaOH and (E, F) ultrapure water (initial hormone concentration 1 µg/L).

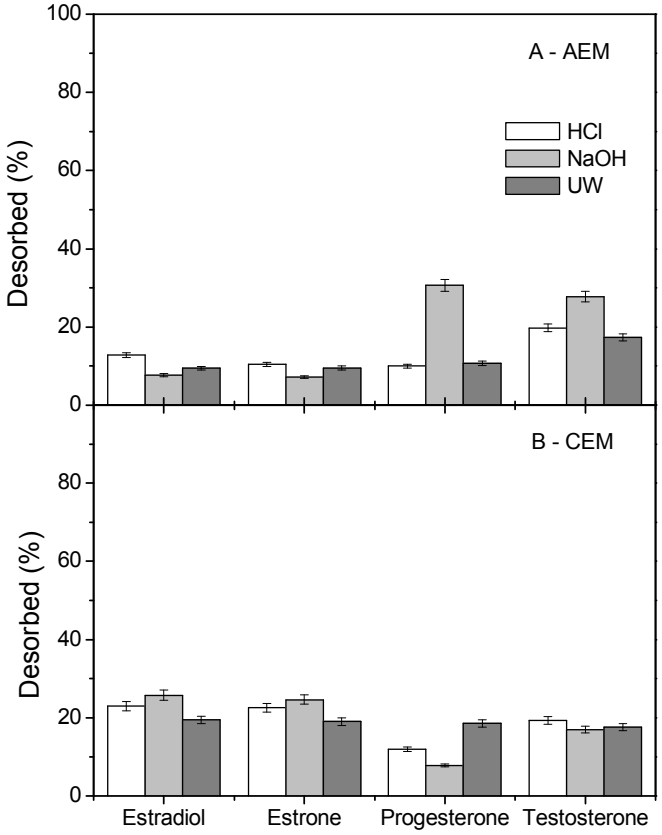

Figure 7.9. Hormone desorption (% of initial mass) from the (A) AEMs and (B) CEMs (0.002 M HCl and NaOH, UW); initial hormone concentration 1 µg/L).

7.2 Hormone Sorption during Electrodialysis

The removal of trace organic contaminants in other membrane processes is influenced by the operational parameters and hydrodynamic conditions (e.g. flow regime, membrane orientation) under which the membrane filtration process is carried out. Therefore, hormone sorption during ED is likely to be highly different to that noted during the sorption isotherm experiments. ED experiments were undertaken to elucidate the mechanisms involved in hormone sorption during ED and to identify differences in sorption during isotherm experiments and ED.

7.2.1 Influence of Solution pH

Solution pH can influence the charge of hormones and this, therefore, has implications for the interaction between the hormones and the ion-exchange membranes. As previously mentioned, the fate of progesterone and estrone during ED was examined to identify differences in sorption between undissociated and dissociated compounds. They were chosen due to the high sorption affinity noted during the isotherm experiments. The mass of progesterone and estrone sorbed per unit volume of membrane within the ED stack (C_{stack}, μg/cm^3) during the continuous ED experiments is shown in Figure 7.10.

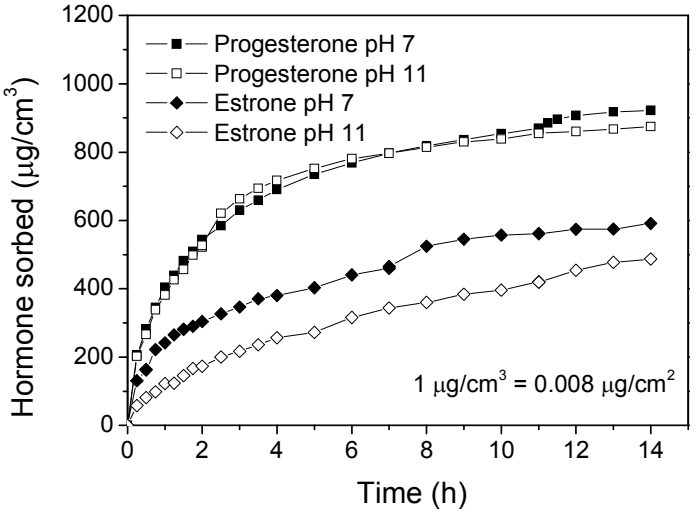

Figure 7.10. Mass of progesterone and estrone sorbed during ED per unit volume of membrane (C_{stack}, μg/cm^3) (1mM $NaHCO_3$, 85.5 mM NaCl, 10 V; initial concentration of progesterone: pH 7 1057 μg/cm^3, pH 11 1051 μg/cm^3; initial concentration of estrone: pH 7 880 μg/cm^3, pH 11 889 μg/cm^3).

Sorption of both progesterone and estrone increased rapidly within 4 hours. However, no steady state in the mass sorbed was reached within 14 hours. Although progesterone and estrone are both undissociated at pH 7, results show that progesterone had a greater capacity for sorption during ED than estrone. This can be explained by the greater partitioning of progesterone to the CEMs than estrone, due to the triple hydrogen acceptor ability of progesterone, and the larger volume of CEMs (6.9 cm^3) within the ED system in comparison to the volume of AEMs (4.9 cm^3).

The concentration of progesterone sorbed to the membranes at pH 7 (922 μg/cm^3) was similar to the concentration sorbed at pH 11 (874 μg/cm^3) due to progesterone being undissociated under both pH conditions. After the feed solution was separated, progesterone sorption continued within both the diluate and concentrate (Figure 7.11). Pronk *et al*. (2006) made the assumption that neutral compounds sorb to both CEM and AEMs, which is confirmed by these results.

The concentration of estrone sorbed at pH 11 (487 μg/cm^3) was less than the concentration sorbed at pH 7 (591 μg/cm^3) due to the dissociation of estrone at pH 11 (pK_a 10.4; Table 2.4). The fraction of neutral species ($f_{neutral}$, %) in dissociating hormones can be calculated using eqn (7.2).

$$f_{\text{neutral}} = \frac{1}{1+10^{\text{pH - p}K_a}} \tag{7.2}$$

At pH 7 there is almost 100 % neutral estrone species compared to 17.9 % at pH 11. At pH 7, sorption of estrone would occur on both the CEMs and AEMs facing the diluate and concentrate. This continues at pH 11 for the neutral fraction, while the dissociated estrone no longer sorbs. This is due to electrostatic repulsive forces between negatively charged estrone and the negatively charged CEM which decreases the proximity of estrone molecules to the membrane surface. At pH 11 the concentration of estrone within the diluate decreased faster than the concentration within the concentrate (Figure 7.11) which indicates preferential transport of negatively charged estrone towards the positively charged AEMs facing the diluate. Therefore, penetration of the AEMs by dissociated estrone is possible at pH 11. The sorption of trace organics on AEMs during ED has previously been reported. Although trace organics vary greatly in terms of their physicochemical characteristics (e.g. molecular weight, structure, pK_a etc), results from this study, in particular the behaviour of dissociated estrone, substantiate those from previous studies on the fouling of ion-exchange membranes by trace organics (Grebenyuk *et al.*, 1998; Lee *et al.*, 2009; Nagarale *et al.*, 2004; Takahashi *et al.*, 2003). These studies have, however, predominantly focused on electrostatic and hydrophobic

interactions and have not considered hydrogen bonding. Takahashi *et al*. (2003) studied the sorption of eight monocarboxylic acids (acetic, butyric, formic, heptanoic, hexanoic, lactic, propanoic and valeric acid) by an AEM (Selemion AMV) and found that membrane sorption increased with increasing pH (3-6.3) as a result of organic acid dissociation (pK_a 3.75-4.89) and interaction between the organic acid carboxylate groups and the membrane functional group. Lindstrand *et al*. (2000b) reported membrane fouling during the ED of octanoic acid (pK_a 4.89) at pH 9.

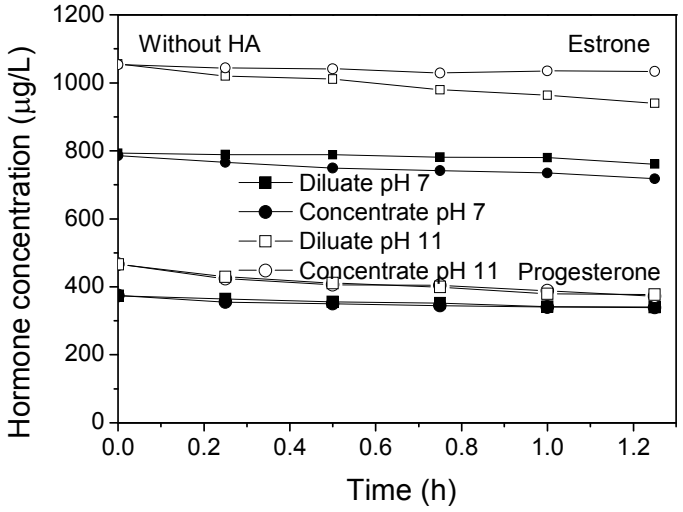

Figure 7.11. Concentration (µg/L) of estrone and progesterone in the diluate and concentrate at pH 7 and pH 11 in batch ED experiments (1 mM $NaHCO_3$, 85.5 mM NaCl, 10 V; diluate and concentrate feed solution sourced from continuous ED experiments; estrone initial concentration: pH 7 790 µg/L, pH 11 1055 µg/L; progesterone initial concentration: pH 7 374 µg/L, pH 11 466 µg/L).

7.2.2 Estrone Breakthrough Observations

While estrone flux is very low (30-100 ng/cm^{2}h), breakthrough of estrone into the concentrate was noted after 10 hours of extended batch ED experiments (Figure 7.12), confirming AEM diffusion. The low flux indicates that after the estrone molecules penetrate the AEM they find more binding sites to interact with. A further 1.7 ug/cm^3 of estrone was sorbed to the AEMs up to 14 hours. The permeation mechanism of estrone is, therefore, dependent on the mass sorbed on and within the ion-exchange membranes. These results are in accordance with literature (Pronk *et*

al., 2006) where permeation of dissociated trace organic contaminants increased with membrane sorption. As a dissociated trace organic partitions into an AEM, it finds more binding sites to interact with. As the number of available binding sites decreases with increasing sorption, permeation of the trace organic through the membrane and into the concentrate decreases. Therefore, estrone permeation is dependent on sorption, AEM diffusion, desorption and diffusion from the membrane boundary layer.

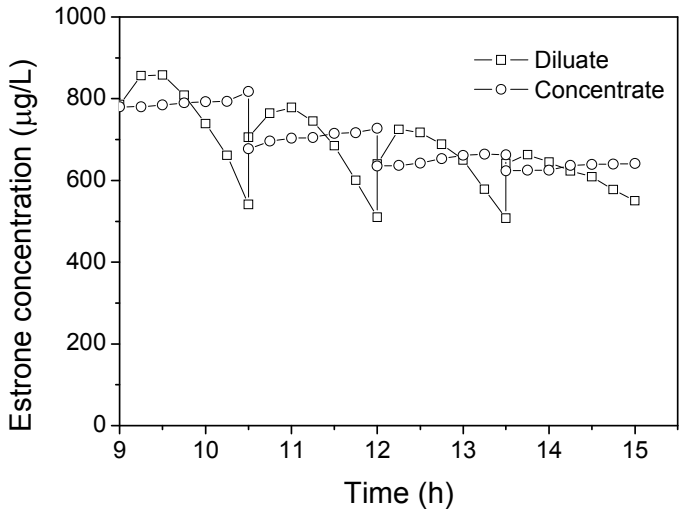

Figure 7.12. Concentration of estrone (µg/L) within the diluate and concentrate during continued ED experiments (1 mM $NaHCO_3$, 85.5 mM NaCl, pH 11, 10 V; 2500 µg/L estrone; step function indicates repetition of batch ED experiments).

7.2.3 Influence of Organic Matter

Solute-solute interactions, such as the complexation of steroidal hormones and OM, have implications on the removal of hormones during wastewater treatment using other membrane processes (McCallum *et al.*, 2008; Nghiem *et al.*, 2004a; Yoon *et al.*, 2004). Therefore, the influence of HA on the sorption of the hormones progesterone and estrone to the ion-exchanges membranes was evaluated in continuous ED. The influence of HA on the concentration of progesterone and estrone sorbed per unit volume of membrane within the ED stack (C_{stack}, µg/cm^3) during continuous ED experiments is shown in Figure 7.13. Greater progesterone

sorption in comparison to estrone was observed in the presence of HA. A comparison between sorption in the absence and presence of HA is shown in Figure 7.14. The mass of progesterone sorbed to the membranes decreased in the presence of HA. A decrease of 758 μg/cm^3 was noted at pH 7 and a decrease of 739 μg/cm^3 was noted at pH 11 (Figure 7.14). The same trend of lower sorption in the presence of HA was observed with estrone at pH 7 (535 μg/cm^3). The mass of estrone sorbed at pH 11 was slightly higher in the presence of HA (508 μg/cm^3). After the feed solution was separated, progesterone sorption continued within both the diluate and concentrate (Figure 7.15), which similarly occurred without HA. At pH 11 the concentration of estrone within the diluate again decreased faster than the concentration within the concentrate as a result of electrostatic interaction between negatively charged estrone and the positively charged AEMs.

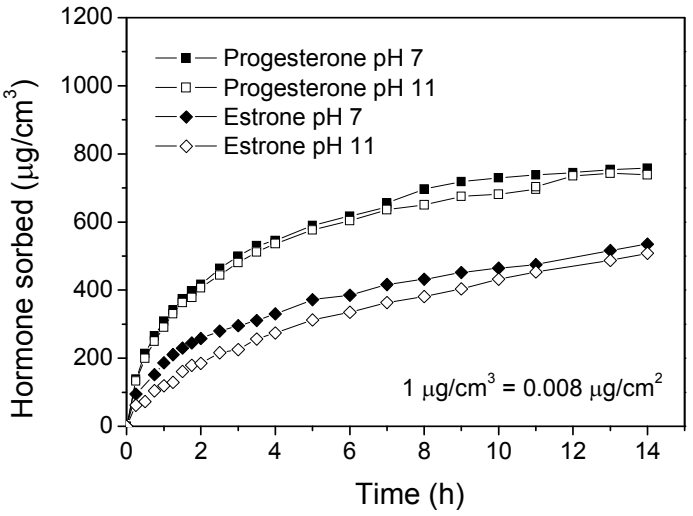

Figure 7.13. Concentration (C_{stack}, μg/cm^3) of progesterone and estrone sorbed during ED in the presence of HA (1mM $NaHCO_3$, 85.5 mM NaCl, 12.5 mgC/L HA, 10 V; initial concentration of progesterone: pH 7 897 μg/cm^3 and pH 11 901 μg/cm^3; initial concentration of estrone: pH 7 847 μg/cm^3, pH 11 887 μg/cm^3).

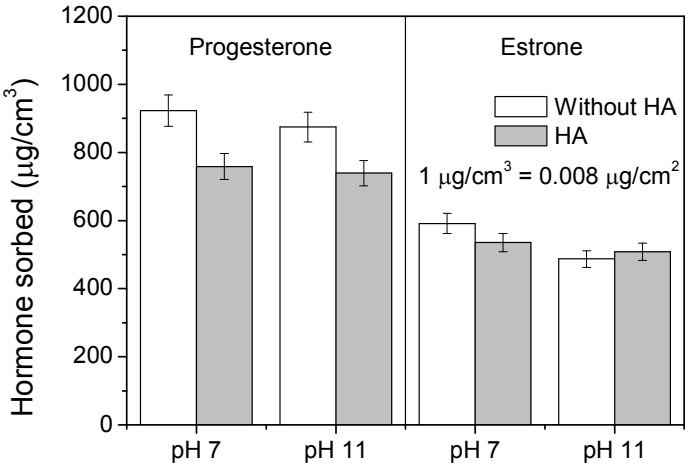

Figure 7.14. Comparison between the mass of progesterone and estrone sorbed to the membranes (C_{stack}, μg/cm^3) during ED experiments in the presence and absence of HA (1 mM $NaHCO_3$, 85.5 mM NaCl, pH 7-11, 10 V).

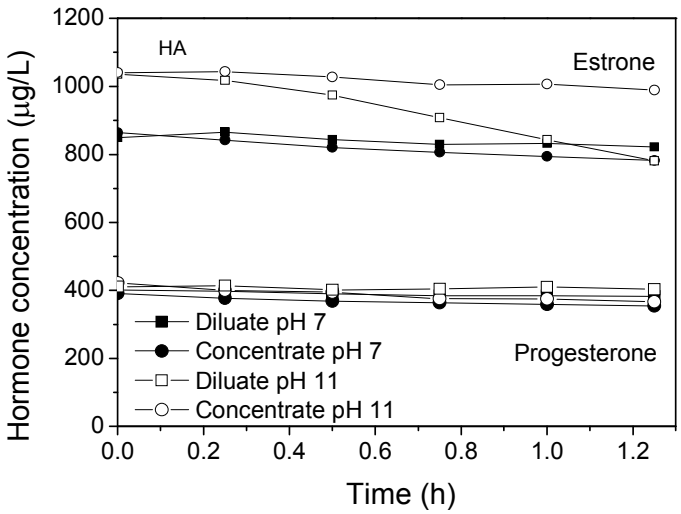

Figure 7.15. Concentration (μg/L) of estrone and progesterone in the diluate and concentrate in batch ED experiments (1 mM $NaHCO_3$, 85.5 mM NaCl, 12.5 mg C/L HA, 10 V; estrone initial concentration: pH 7 857 μg/L, pH 11 1039 μg/L; progesterone initial concentration: pH 7 396 μg/L, pH 11 417 μg/L).

The strength of solute-solute interactions between trace organics and OM are related to characteristics of the hormones and the OM including functional group content and charge as well as solution pH and ionic strength. Neale *et al*. (2009) studied the pH dependence (pH 4-12) of hormone partitioning to HA. The organic matter-water partition coefficients (log K_{OM}, L/kg) determined for progesterone and estrone using solid-phase microextraction (SPME) are summarised in Table 7.4.

Table 7.4. Organic matter-water partition coefficients (log K_{OM}, L/kg) for progesterone and estrone with Aldrich HA (Adapted from (Neale *et al.*, 2009)).

Hormone	Organic matter-water partition coefficients (log K_{OM}, L/kg) [a]				
	pH 4	pH 7	pH 9	pH 10	pH 12
Progesterone	4.73 ± 0.26	4.59 ± 0.25	4.58 ± 0.25	4.48 ± 0.24	4.54 ± 0.25
Estrone	5.27 ± 0.28	4.82 ± 0.26	4.75 ± 0.26	4.52 ± 0.24	-

± indicates measurement uncertainty associated with the log K_{OM} values due to experimental error (SPME fibre length, analytical instrument error); [a] 1 mM $NaHCO_3$, 20 mM NaCl, 0.1-100 μg/L hormone, 12.5 mgC/L HA).

The sorption of estrone and progesterone to HA between pH 4 and 7 was attributed to interactions between the C-17 and C-20 carbonyl hydrogen acceptor groups of estrone and progesterone, respectively, and the phenolic hydrogen donor groups of HA. Estrone was found to have a higher log K_{OM} for HA than progesterone between pH 4 and 10, which would be due to the greater strength of the C-17 hydrogen acceptor group of estrone (Table 7.3, Gancia *et al*. (2001)). The decrease in partitioning in alkaline solutions was attributed to HA speciation and conformational changes. Zeta potential measurements of HA have shown an increase in the negative charge of HA between pH 4 and 7 (-27 to -38 mV) as a result of dissociation of the carboxylic functional groups (Yan and Bai, 2005). As previously mentioned, HA changes from a rigid spherocolloids structure at low pH to a flexible linear polyelectrolyte at neutral and alkaline pH due to charge repulsion (Ghosh and Schnitzer, 1980), which is thought to reduce HA hydrophobicity (Ra *et al.*, 2008). Therefore, the increase in HA charge and hydrophobicity may account for the decreases in hormone partitioning with increasing solution pH. Log K_{OM} for estrone above pH 10 could not be determined due to SPME limitations in extracting dissociated compounds (Escher *et al.*, 2002). The mass of estrone sorbed to HA at

alkaline pH would be negligible due to charge repulsion. Therefore, the mass of estrone partitioned to HA during the ED experiments at pH 11 could not be accurately predicted.

The mass of progesterone and estrone predicted to partition to HA within the ED feed solutions at pH 7 and 11 ($m_{ADS\text{-}HA}$), calculated using the log K_{OM} values in Table 7.4 and eqn (4.18) is shown in Table 7.5. The initial mass of hormone in the feed (m_{FD}^{0}) was calculated using eqn (4.15) and the fraction of progesterone and estrone freely dissolved in the feed (f_w, %) was 69.0 % and 43.0 %, respectively (Neale, 2009). For further details on these calculations refer to Chapter 4. The mass of neutrally charged estrone in the ED feed solution at pH 7 and 11 was calculated using eqn (7.3), which is a combination of eqn (4.15) and eqn (7.4).

$$m_{FD}^{e} = (m_{FD}^{0} \cdot f_{neutral}\%) \cdot f_{w}\% \qquad (7.3)$$

Table 7.5. Predicted mass of progesterone and estrone sorbed to Aldrich HA (µg and % of the initial mass of freely dissolved hormone) in the ED feed solution at pH 7 and 11.

Hormone	Mass hormone freely dissolved in feed (m_{FD}^{e}, µg)		Mass of hormone sorbed to HA ($m_{ADS\text{-}HA}$,)			
			µg		% of mass freely dissolved in feed	
	pH 7	pH 11	pH 7	pH 11 [a]	pH 7	pH 11 [a]
Progesterone	7285	7323	3780	3103	48.6	37.7
Estrone	5683 [b] -5685	1069 [b]-5954	4765	-	82.6	-

[a] Calculated using log K_{OM} of progesterone at pH 10 (4.48 ± 0.24 L/kg); [b] Mass of neutrally charged estrone within the feed solution (µg) calculated using eqn (7.3).

The mass of hormone partitioned to HA is significant compared to the initial mass of hormone within the ED feed solution, particularly for estrone at pH 7 where 82.6 % of the initial mass freely dissolved in the feed was predicted to be partitioned to HA. The mass of estrone partitioned to HA at pH 7 (4765 µg) is greater than the mass of progesterone sorbed to HA (3780 µg). The mass of progesterone sorbed to HA decreases with increasing solution pH. Therefore, it would be expected that the

presence of HA would have a greater influence on sorption of estrone than progesterone during ED.

The prediction of sorption to the ion-exchange membranes during ED as a result of hormone-HA partitioning (PR_{FD}, %) in comparison to experimental hormone sorption (R_{FD}, %) is given in Table 7.6. The influence of hormone-HA partitioning on sorption during ED was evaluated using eqn (4.19). Possible limitations of these predictions include differences in solution chemistry (ionic strength, hormone concentration) and experimental errors associated with the ED experiments (LSC counting 2 %, UV-Vis Spectrophotometer 2 %) and the SPME experiments (5.4 %) and sorption isotherm experiments (2 %). As hormone partitioning to HA decreased with increasing solution pH, the mass of progesterone predicted to sorb at pH 11 is an overestimation due to the higher log K_{OM} at pH 10. The log K_{OM} values were determined at a lower ionic strength (20 mM NaCl) than the ionic strength of the ED experiments (85.5 mM). As ionic strength has implications for the charge and conformation of OM, as well as charge and solubility of trace contaminants (Ghosh and Schnitzer, 1980; Schwarzenbach *et al.*, 2003), partitioning of progesterone and estrone to HA within the ED feed solutions would be expected to be reduced at a higher ionic strength due to charge negative charge shielding (Ghosh and Schnitzer, 1980). However, studies on the influence of ionic strength on the partitioning of trace organics to OM present conflicting results with some reporting no significant difference with increasing ionic strength (Bowman *et al.*, 2002; Yamamoto and Liljestrand, 2003) and others reporting a slight decrease in partitioning (Neale, 2009; Schlautman and Morgan, 1993).

While these limitations do need to be considered, experimental results correlate well with the predictions. The experimental hormone sorption R_{FD} was greater than PR_{FD}, indicating that the contribution of solute-solute interactions to hormone sorption was negligible. This reiterates that membrane sorption was the dominant mechanism during ED. However, if HA removal during ED, which was relatively low (15.2-19.7 %), had been higher, solute-solute interactions would have contributed more to hormone sorption.

The sorption of progesterone and estrone during ED was, however, influenced by the presence of HA. The decrease in progesterone sorption during ED in the presence of HA at pH 7 and pH 11 and estrone at pH 7 (Figure 7.14) is a result of the high partitioning to HA (Table 7.5) and the low contribution of hormone-HA complexation on sorption. A reduction in the influence of HA on progesterone sorption from pH 7 to pH 11 correlates with a decrease in the predicted progesterone sorption from pH 7 (7.1 %) to pH 11 (4.4 %). The deposition of negatively charged HA on the positively charged AEMs as a result of electrostatic attraction, though minimal, would reduce the area available for progesterone sorption. At pH 11, charge repulsion between dissociated estrone and HA coupled with electrostatic attraction between estrone and the AEMs resulted in the slight increase in membrane sorption in the presence of HA compared to experiments without HA.

Table 7.6. Comparison between experimental hormone sorption (R_{FD}, %) with predicted hormone sorption (PR_{FD}, %) calculated using log K_{OM} values (L/kg) determined by (Neale *et al.*, 2009).

Hormone	Experimental HA removal (R_{FD}, %)		Predicted hormone sorption (PR_{FD}, %)		Experimental hormone sorption (R_{FD}, %)	
	pH 7	pH 11	pH 7	pH 11 [a]	pH 7	pH 11
Progesterone	19.7 ± 0.6	15.2 ± 0.5	7.1	4.4	84.6 ± 0.3	82.0 ± 0.4
Estrone	17.8 ± 0.5	16.0 ± 0.5	8.4	-	63.2 ± 0.7	57.3 ± 0.8

[a] Based on log K_{OM} of progesterone at pH 10 (4.48 ± 0.24 L/kg); ± S.D. calculated using eqn (4.5).

7.2.4 Hormone Desorption during Electrodialysis

While minimal desorption of hormones from the membranes used during the sorption isotherm experiments were noted (Section 7.1.4), desorption of estrone from the ion-exchange membranes used during the continuous and batch desalination experiments with estrone at pH 7 was investigated to determine if hormone desorption was facilitated by applied voltage. After 2 hours, 18.7 μg/cm^3 (3.8 % of initial mass of 489 μg/cm^3 sorbed) of estrone was desorbed (Figure 7.16). A greater mass was desorbed from the membrane surfaces adjacent to the diluate (13.7 μg/cm^3) in

comparison to the surfaces adjacent to the concentrate (4.9 μg/cm^3). These results indicate that desorption of estrone from ion-exchange membranes during desalination (at pH 7) is limited and not an appropriate method for membrane regeneration. However, desorption using EDR or at a higher solution pH may enhance this process. Irreversible fouling of the membranes as a result of hormone sorption has implications on the long-term performance of ED in regards to membrane performance and membrane replacement costs.

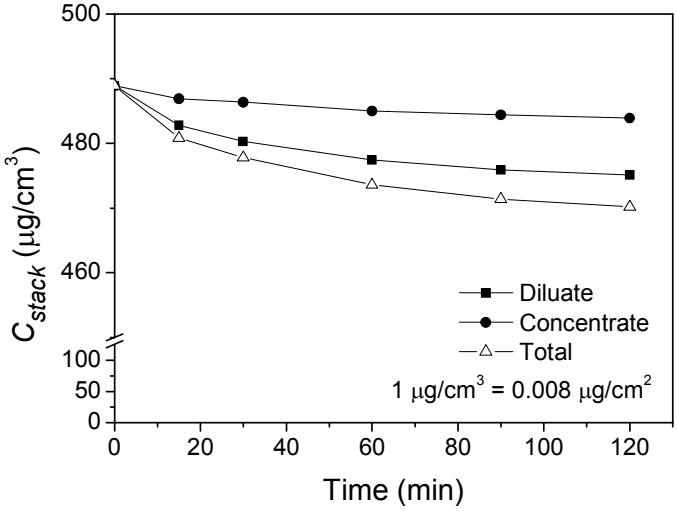

Figure 7.16. Estrone desorption kinetics during ED (1 mM $NaHCO_3$, 85.5. mM NaCl, pH 7; estrone concentration sorbed to membranes was 489 μg/cm^3).

7.3 Comparison between Sorption in Isotherm and Electrodialysis Experiments

A comparison between the mass of progesterone and estrone sorbed to the membranes during the sorption isotherm and ED experiments at pH 7 was undertaken to elucidate differences in sorption and to assess the reliability of the log $K_{AEM/CEM}$ values for determining membrane sorption during ED. The mass of progesterone and estrone sorbed during the isotherm and ED experiments (μg/cm^3) is given in Table 7.7, along with the mass predicted to sorb to during ED. The mass of progesterone and estrone predicted to sorb to the membrane during ED was calculated using the determined log $K_{AEM/CEM}$ values (Table 7.1), eqn (4.13), eqn

(4.14) and eqn (4.15). For more details refer to Chapter 4. The mass of progesterone and estrone sorbed was greater in the isotherm experiments (Progesterone: AEM 2194 μg/cm^3, CEM 1719 μg/cm^3; Estrone: AEM 2630 μg/cm^3, CEM 1545 μg/cm^3) in comparison to the ED experiments. Therefore, the predicted mass of progesterone and estrone sorbed during ED was greater than the experimental mass.

Table 7.7. Comparison between progesterone and estrone sorption in batch sorption isotherm and ED experiments at pH 7 in the absence of HA.

Hormone	Membrane volume (cm^3)	Sorption time (h)	Hormone sorbed to ion-exchange membranes (μg/cm^3)
Sorption isotherm experiments [a, b]			
Progesterone - AEM	0.056	170	2194
Progesterone - CEM	0.068	170	1719
Estrone - AEM	0.056	170	2630
Estrone - CEM	0.068	170	1545
Predicted mass sorbed during ED experiments [c, d, e]			
Progesterone - AEM [f]	11.8	-	2953 ± 851
Progesterone - CEM [f]	11.8	-	3717 ± 2040
Estrone - AEM [f]	11.8	-	7591 ± 3381
Estrone - CEM [f]	11.8	-	2572 ± 248
ED experiments [b]			
Progesterone	11.8	14	922
Estrone	11.8	14	591

[a] pH 7; [b] 1mM $NaHCO_3$, 85.5 mM NaCl, 2500 μg/L progesterone and estrone; [c] Minimum (CEM) and maximum (AEM) calculated using eqn (4.13), eqn (4.14) and eqn (4.15); [d] Calculated using log $K_{AEM/CEM}$ values for 0.1-2500 μg/L concentration range; [e] ± 95 % C.I.; [f] Based on presence of only AEMs or CEMs within the ED stack.

There are two possible explanations for the difference in sorption between the batch sorption isotherm experiments and the ED experiments: (1) Difference in experimental times and the (2) difference in sorbent/water ratio. Figure 7.17 compares the sorption kinetics during the 2500 μg/L hormone sorption isotherms and ED experiments at pH 7 over the same experimental period. The experimental duration of the sorption isotherm experiments was 170 hours compared to 14 hours in the ED experiments. However, from this figure it can be seen that it is unlikely that the mass of hormone sorbed during ED would reach the same mass sorbed

during the batch sorption isotherm experiments if the ED experiments had continued for a longer duration.

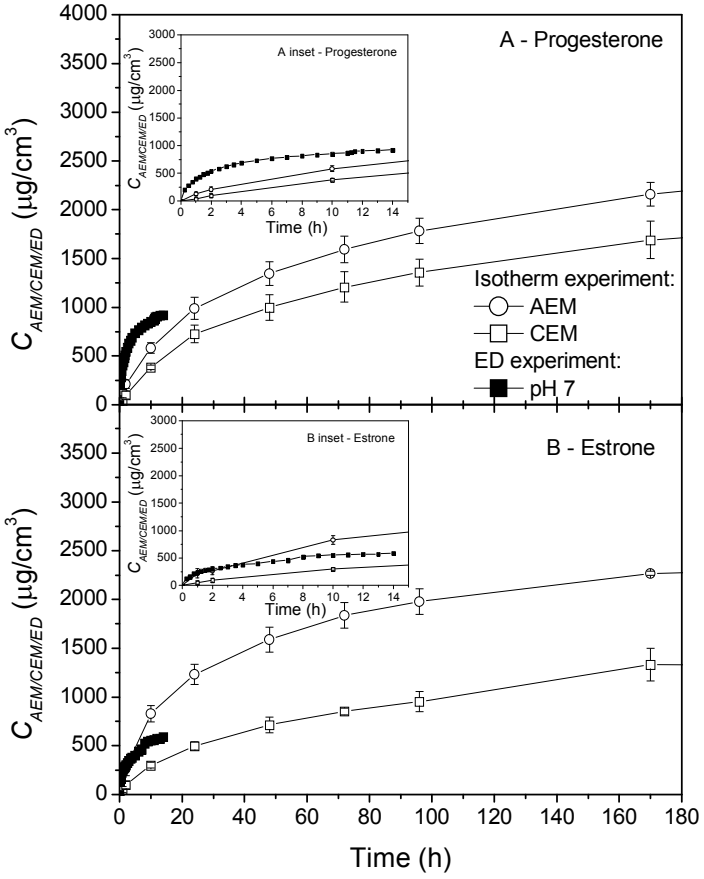

Figure 7.17. Comparison between (A) progesterone and (B) estrone sorption during sorption isotherm and continuous ED experiments. Inset (A) and (B) close-up of sorption up to 14 hours (1mM $NaHCO_3$, 85.5 mM NaCl, pH 7, 2500 mg/L hormone).

Another important factor affecting sorption in solid-liquid systems is the sorbent/water ratio i.e. in this study this refers to the membrane/trace organic ratio. However, the effects of variations in the sorbent/water ratio are unclear. In most batch sorption studies, a higher sorbent/water ratio is employed (Chang and Wang, 2002). Therefore, the partition coefficients derived are larger than the real values that exist in the environment or in this study in ED. Numerous studies have shown a decrease in sorption with an increase in sorbent/water ratio (Chang *et al.*, 2002;

Voice and Weber Jr, 1985; You *et al.*, 1999). This phenomenon has been postulated to occur because the higher sorbent concentration dilutes the sorbate in the solid phase at higher sorbent/water ratios. The initial mass of hormone per unit area of membrane exposed to the hormone solution is significantly greater in the sorption isotherm experiments (AEM: 30.7 μg/cm^2, CEM: 30.8 μg/cm^2) compared to the ED experiments (7.2 μg/cm^2). Therefore, in the case of the ED experiments the sorbent/water ratio is higher; thus a possible explanation for the lower sorption observed in ED. The effect of experimental artifacts on the evaluation of trace organic fate in ED and the environment is, therefore, obvious.

7.4 Estrone Sorption to other Membrane Polymers

The sorption of estrone to the ion-exchange membranes was compared to other membrane polymers. The purpose of this is to emphasise the importance of polymer type on trace organic sorption. Estrone sorption isotherms (ng/cm^2) for three different types of membrane polymers, PS-DVB (AEM AMX-SB and CEM CMX-SB), polyamide (TFC-SR2 NF, Koch Membrane Systems) and polyamide-urea (X-20, RO, Trisep Corporation) are shown in Figure 7.18. The ion-exchange membranes exhibited the greatest sorption of estrone. Although the estrone sorption isotherms for TFC-SR2 and X-20 were determined at pH 8 and 20 mM NaCl in comparison to pH 7 and 85.5 mM for the AEM and CEM, estrone is undissociated under both solution conditions. Water-membrane partition coefficients for estrone (K_M, L/cm^2) and each membrane polymer were determined using eqn (7.4).

$$K_M = \frac{C_s}{C_w} \tag{7.4}$$

where C_s is the concentration of estrone sorbed to the membrane per unit area (ng/cm^2) and C_w is the concentration of estrone freely dissolved in solution (ng/L).

The estrone partition coefficients for the PS-DVB AEM (3.16×10^{-2} L/cm^2) and CEM (1.28×10^{-2} L/cm^2) were 19 and 47 times greater than the estrone partition coefficients for the TFC-SR2 membrane (6.72×10^{-4} L/cm^2) and 37 and 91 times greater than the polyamide X-20 membrane (3.49×10^{-4} L/cm^2), respectively.

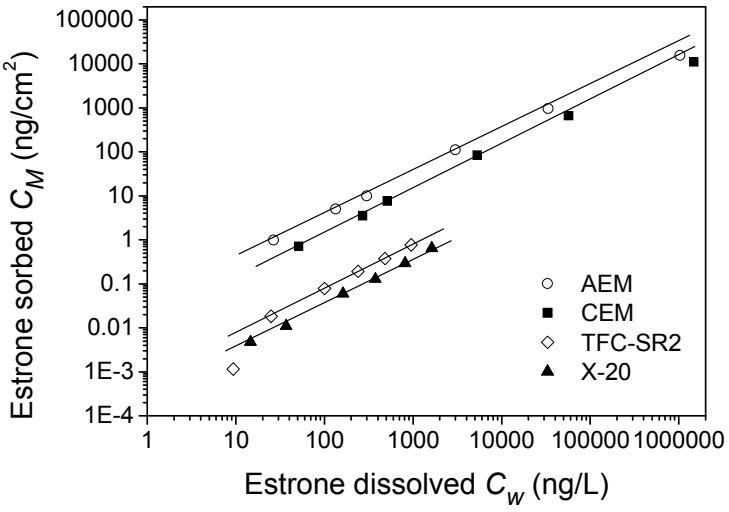

Figure 7.18. Estrone sorption isotherms (ng/cm^2) for PS-DVB (AEM, CEM) (1 mM $NaHCO_3$, 85.5 mM NaCl, pH 7), polyamide NF (TFC-SR2) (Nghiem, 2005) and polyamide-urea RO (X-20) membranes (Nghiem, 2005) (1 mM $NaHCO_3$, 20 mM NaCl, pH 8).

Differences in sorption between the membrane polymers can be evaluated in relation to hydrogen bonding capacity and membrane hydrophobicity. Hydrogen bonding between estrone and polyamide is shown in Figure 7.19. Nghiem (2005) reported that estrone can hydrogen bond with polyamide through carbonyl and amine ($–NH_2$) functional groups. The lower sorption of estrone to the X-20 membrane was attributed to its smaller pore size in comparison to the estrone molecule and that adsorption can only occur at the surface of the active layer. By comparing the schematics for hydrogen bonding with the different polymers (PS-DVB Figure 7.2 and Figure 7.3, polyamide Figure 7.19) and the number of possible hydrogen bonding sites (Table 7.8) it can be seen that the PS-DVB AEM presents more opportunities for hydrogen bonding with estrone than polyamide. Sorption may be influenced by the number of functional groups attached to the polymers. Although one functional group of the CEM presents the same number of hydrogen bonding sites between the hormone C-17 position as the active layer of the polyamide membranes, sorption to the CEM was greater. Therefore, the PS-DVB ion-exchange membranes may have more functional groups attached in comparison the polyamide membranes.

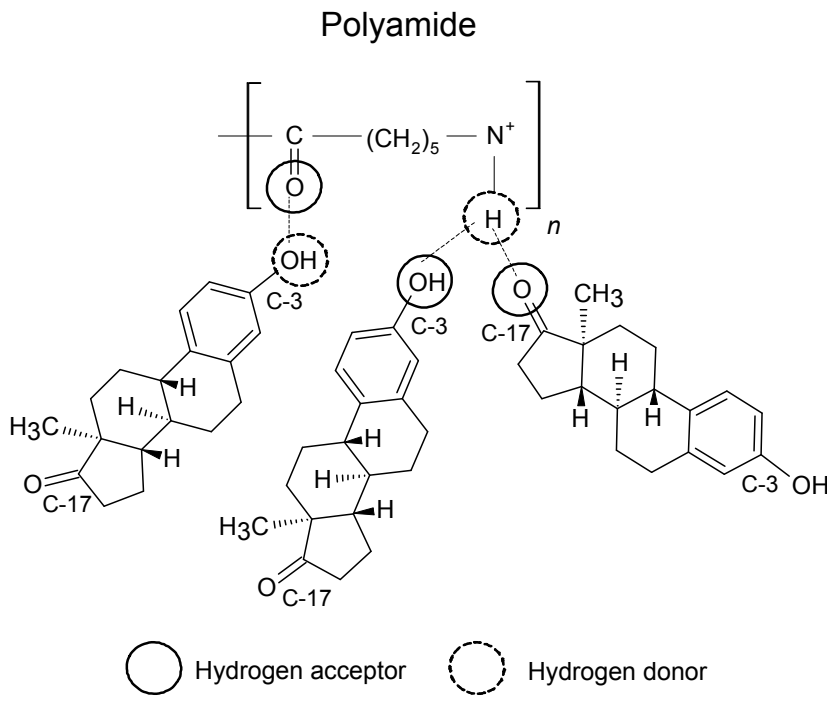

Figure 7.19. Schematic of possible hydrogen bonding between estrone of polyamide membrane polymer (TFC-SR2, X-20) (Adapted from Schäfer *et al.* (2003)).

Table 7.8. Number of hydrogen bonding sites between estrone functional groups (C-3 and C-17 position) and the ion-exchange (AMX-SB AEM, CMX-SB CEM) functional groups, polyamide (TFC-SR2) and polyamide-urea (X-20) membranes.

Membrane	Polymer	C-3	C-17
AMX-SB	PS-DVB	9 A	9 A
CMX-SB	PS-DVB	2 D, 1 A	2 D, 1 A
TFC-SR2	Polyamide	1 D, 1 A	1 A
X-20	Polyamide-urea	1 D, 1 A	1 A

[a] A and D relates to hydrogen bonding facilitated through hormone hydrogen acceptor and donor groups, respectively.

Membrane hydrophobicity (determined by membrane contact angle) can influence the sorption of organic contaminants with a higher contact angle representing higher hydrophobicity (Lee *et al.*, 2002a) and thus greater sorption affinity. Despite the similar hydrophilic nature of the membrane active layers of TFC-SR2 and X-20

(Nghiem, 2005) and the hydrophilic CEM functional group, the support layer of TFC-SR2 (polysulphone) and the AEMs and CEMs are hydrophobic. The contact angle of the AEM (69.9 ± 3.4°) and CEM (61.8 ± 5.1°) is significantly greater than TFC-SR2 (11°) and X-20 33° (Nghiem, 2005). Therefore, there is a positive correlation between estrone sorption and membrane hydrophobicity.

7.5 Estrone Sorption during Electrodialysis and Nanofiltration

As the removal of hormones during wastewater treatment by conventional methods is vastly different, so is the sorption of hormone during water treatment using different membrane processes (Koyuncu *et al.*, 2008; Nghiem *et al.*, 2004a). Therefore, a comparison between estrone sorption to the ion-exchange membranes during ED and the TFC-SR2 membranes during NF filtration within stirred cells (Nghiem, 2005) was undertaken. At a feed concentration of 100 ng/L, approximately 0.4 ng/cm^2 estrone was sorbed to the TFC-SR2 membranes. As the feed estrone concentration during the ED experiments (2500 µg/L) was significantly greater than the feed concentration in the NF filtration experiments, the estimated mass of estrone sorbed to the TFC-SR2 membrane during filtration (m_m, ng/cm^2) with an initial estrone concentration of 2500 µg/L was calculated using eqn (7.3).

$$m_m = m_w^e \cdot \frac{K_M}{V_w} \cdot A_M \tag{7.3}$$

This calculation was based on the following assumptions and used data from (Nghiem, 2005): m_w^e: 356125 ng, calculated using eqn (4.15) and f_w of 23.0 % (determined from sorption isotherm data for estrone and TFC-SR2); K_m 6.72 ×10^{-4} L/cm^2; V_w: 0.185 L; TFC-SR2 membrane area A_m: 21.2 cm^2.

The mass of estrone sorbed to the ion-exchange membranes during ED and the mass predicted to sorb to the TFC-SR2 membrane during NF filtration is given in Table 7.9. Based on the different membrane physiochemical properties (e.g. functional groups, charge, hydrophobicity) it was expected that estrone sorption to the membranes would differ greatly. The sorption of estrone during the ED experiments was greater than levels reported for other membrane processes. This indicates the

influence of membrane physiochemical properties on the sorption of organic compounds. As described in Section 7.4, there are more opportunities of hydrogen bonding between estrone and the ion-exchange membranes than the TFC-SR2 membrane. The NF membranes are less hydrophobic than the ion-exchange membranes thus resulting in less estrone sorption. Differences in hydrodynamic conditions (e.g. flow channel geometry, flow rate, Reynolds number and flow regime) within the ED stack and the NF filtration stirred cells would influence membrane sorption.

Table 7.9. Comparison between the mass of estrone sorbed to ion-exchange membranes (AMX-SB, CMX-SB) and predicted mass sorbed to the TFC-SR2 NF membrane (based on data from Nghiem *et al.* (2005)).

Membrane process	Membrane	Membrane area (A_m, cm^2)	Estrone sorbed at pH 7 (m_m, ng/cm^2)
ED [a]	AMX-SB CMS-SB	1392	4999
NF [b]	TFC-SR2	21.2	386 [c]

[a] 1 mM $NaHCO_3$, 85.5 mM NaCl, 2500 µg/L estrone; [b] 1 mM $NaHCO_3$, 20 mM NaCl, pH 8 100 ng/L estrone; [c] Prediction calculated using eqn (7.2).

7.6 Summary

The measurement of water-membrane partition coefficients (log $K_{AEM/CEM}$) for the steroidal hormones estradiol, estrone, progesterone and testosterone indicated the high sorption affinity of to ion-exchange membranes. It can be concluded that this sorption is due to both hydrogen bonding mechanisms between the hormone functional groups and the AEM and CEM functional groups. The strength of this bonding is highly dependent on hormone type, the strength of hydrogen bonding of the carbonyl and hydroxyl groups within the hormone molecules and the hydrogen bonding capacity of the membrane. The AEM was found to present more opportunities for hydrogen bonding than the CEM due to the presence of 9 hydrogen donor groups per AEM functional group; thus accounting for greater AEM sorption affinity. The investigation of potential methodology problems such as hormone

degradation during the sorption isotherm experiments has enhanced confidence in the determined log $K_{AEM/CEM}$ values.

The sorption of progesterone and estrone during ED was governed by both hydrogen bonding and electrostatic interactions, which was influenced by changes in solution chemistry. Electrostatic repulsion between dissociated estrone (which behaves similar to a charged organic acid) at alkaline pH and negatively charged CEMs reduces membrane sorption. Adsorption/partitioning and diffusion mechanisms play an important role in trace organic sorption with breakthrough of dissociated estrone observed. The permeation of trace organics is a possible environmental and health risk where removal is essential.

While solute-solute interactions between steroidal hormones and HA did not significantly contribute to hormone sorption during ED, the decrease in progesterone sorption in the presence of HA (pH 7 and 11) and estrone at pH 7 was resultant from high partitioning to HA coupled with the low contribution of hormone-HA complexation on sorption. The deposition of HA on the AEMs, although minimal, would reduce the area available for sorption; thus indicated by lower progesterone sorption in the presence of HA. Electrostatic repulsion between estrone and HA at high pH led to a slight increase in sorption. A comparison between estrone sorption to the ion-exchange membranes, NF and RO membranes highlighted that hydrogen bonding influenced membrane sorption. However, greater sorption of estrone was observed for the ion-exchange membranes due to their greater capacity for bonding and higher membrane hydrophobicity.

Partial hormone desorption during ED with solutions frequently used during membrane cleaning indicated the irreversible nature of membrane sorption. This highlights the implication of trace organic sorption on ED performance and long-term membrane stability. Although hormone desorption was minimal, wastewater obtained during membrane cleaning may contain harmful trace organics and thus appropriate disposal must be taken into account.

Chapter 8. Fate of Pesticides in Electrodialysis

The mechanisms governing the behaviour of endosulfan (ES) in ED and its interaction with ion-exchange membranes have not been identified. Preliminary results from batch ED experiments are presented in this chapter to highlight the significant difficulties encountered with ES mass balance. This includes investigations of losses to equipment, ES volatilisation and degradation.

Water-membrane partition coefficients (log $K_{AEM/CEM}$) for ES are studied to identify the mechanism governing ES membrane sorption in the presence and absence of OM. The sorption of ES to the ion-exchange membranes is compared to other polymeric materials (low density polyethylene (LDPE) and ethylene vinyl acetate (EVA)).

The influence of solution pH on ES behaviour during batch and continuous ED experiments will be evaluated to identify differences in sorption between undissociated (pH 7) and degraded ES (pH 11). Comparisons between sorption during the isotherm and ED experiments are made to measure the applicability of the log $K_{AEM/CEM}$ values for predicting the fate of ES during ED.

The partitioning of ES will be compared to that observed for the steroidal hormones. Correspondingly, a comparison between the behaviour of ES, progesterone and estrone during continuous ED experiments is undertaken.

8.1 Problem Development

In the early stages of this research, significant difficulties were encountered with the ES mass balance. Preliminary batch ED experiments showed a decrease in the concentration of the ES isomer α-ES and the degradation product ES sulfate within the diluate and concentrate (Figure 8.1 A and B). The concentration of α-ES within the diluate and concentrate decreased more than the concentration of ES sulfate. As previously mentioned in Chapter 2, ES sulfate is generally more stable than the ES

isomers, which was thought to account for the greater decrease in α-ES within the diluate and concentrate (74.7 and 86.9 µg/L, respectively) in comparison to ES sulfate (Diluate: 67.7 µg/L, Concentrate: 59.3 µg/L). ED experiments were repeated at pH 3 with the same removal trends noted (Figure 8.1 C and D). This led to thorough investigations of (a) losses to equipment, (b) volatilisation and (c) degradation.

Peterson and Batley (1993) found that polystyrene sample containers absorb both ES isomers strongly, compared with glass. Therefore, all solution stream lines were converted from plastic to stainless steel where possible. ED experiments with α-ES and ES sulfate were repeated with results showing a similar trend as shown in Figure 8.1.

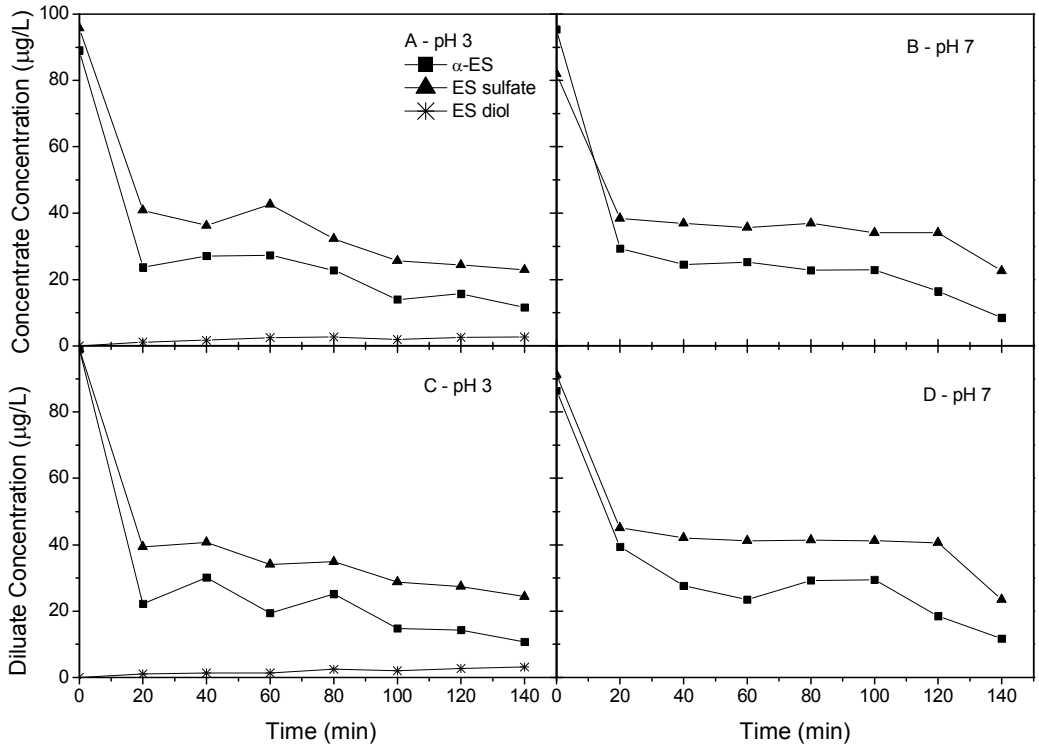

Figure 8.1. Concentration of α-endosulfan, endosulfan sulfate and endosulfan diol within the diluate and concentrate at pH 3 and pH 7 (5 g/L NaCl, Average initial concentration of α-ES and ES sulfate were 92.4 and 92.0 µg/L, respectively).

Another source of ES loss from aqueous environments is volatilisation. Volatilisation of ES from aqueous surfaces in the environment and in laboratory experiments has been attributed to its concentration in the liquid-air interface (surface microlayer) (Cotham and Bidleman, 1989; Guerin, 1993). The range of values reported for the apparent half-lives of α- and β-ES via volatilisation from simple aqueous media in the absence of suspended material are between 5.5-88 and 4.2-40 days, respectively (Guerin, 2001; Singh *et al.*, 1991). Guerin (1993) studied the dissipation of α-ES and β-ES from sterile aqueous media in glass incubation vessels sealed with Teflon (PTFE) and found apparent half-lives of 46 and 24 days at 30°C, respectively. ES sulfate was much more persistent than either α-ES or β-ES under the same incubation conditions with a half-life of 770 days. Such physical losses are expected to occur due to the low water solubility and high volatility. High volatilisation of α-ES and ES sulfate is due to their low water solubility (0.51 mg/L and 0.48 mg/L, respectively, Table 2.6), relatively high vapour pressure (0.006 and 0.0001 Pa at 25°C, respectively) (Hinckley *et al.*, 1990) and high Henry's law constant (HLC, H_c) (1.1×10^{-5} and 2.61×10^{-5} atm.m^3/mol at 25°C in distilled water, respectively) (Cotham and Bidleman, 1989; EPA, 1982).

Calculations were undertaken to estimate the concentration of α-ES and ES sulfate in air within the diluate and concentrate containers in comparison to the concentration within solution. Firstly H_c for α-ES and ES sulfate needed to be converted to the dimensionless form by converting gas concentrations from atmospheres (atm) to mol/m^3. To do this the ideal gas law was used (eqn 8.1).

$$\frac{n}{V} = \frac{P}{RT} \tag{8.1}$$

where, n is the number of moles, V is the volume of the gas (L), p is the absolute pressure of the gas, R is the universal gas constant (0.082 L·atm/mol/K) and T is the temperature (K). Thus, it can be seen that:

$$H_c = \frac{H}{RT} \tag{8.2}$$

Therefore, dimensionless H for α-ES and ES sulfate is 2.74×10^{-4} and 6.38×10^{-4}.

The concentration of α-ES and ES sulfate in air at equilibrium was calculated using eqn (8.3).

$$H = \frac{\text{mol/L (air)}}{\text{mol/L (water)}} \tag{8.3}$$

Considering a closed container that contains both solution and air (4 L diluate/concentrate solution, 7 L air) and an initial α-ES and ES sulfate concentration of 100 μg/L (2.46×10^{-7} and 2.36×10^{-7} mol/L, respectively), the concentration of α-ES and ES sulfate in air at equilibrium is 6.74×10^{-11} and 1.51×10^{-10} mol/L. This correlates to only 0.02 and 0.06 % of the initial concentration of α-ES and ES sulfate in water, respectively. However, HLC's measured in saline water vary from those determined in distilled water. Rice *et al*. (1997) measured the *H* values for the ES isomers as a function of ionic strength and temperature and found that *H* for α-ES increased with ionic strength (saline conditions 5.29×10^{-3} at 20 °C) suggesting that 'salting out' caused more α-ES to be driven out of the aqueous phase. This value was used to calculate the concentration of α-ES in air at equilibrium under saline conditions (1×10^{-9} mol/L). This corresponds to only 0.5 % of the initial ES concentration. The initial concentration of α-ES and ES sulfate within the diluate and concentrate (100 μg/L) was well below the solubility of these compounds (0.51 and 0.48 mg/L, Table 2.6) to minimise volatilisation that may occur above these levels. Therefore, volatilisation of ES from the diluate and concentrate would be expected to be minimal.

It was postulated that the decrease in α-ES and ES sulfate within both the diluate and concentrate was a result of degradation. It has been reported that ES isomers can be readily degraded from aqueous systems at neutral pH in the absence of biological material or chemical catalysts, in the presence or absence of oxygen, according to the degradation pathway shown in Figure 8.2. Isomerisation between α- and β-ES can occur with isomerisation from β-ES to α-ES favoured approximately 3:1 over α-ES to β-ES in estuarine mesocosms (Walse *et al.*, 2003).

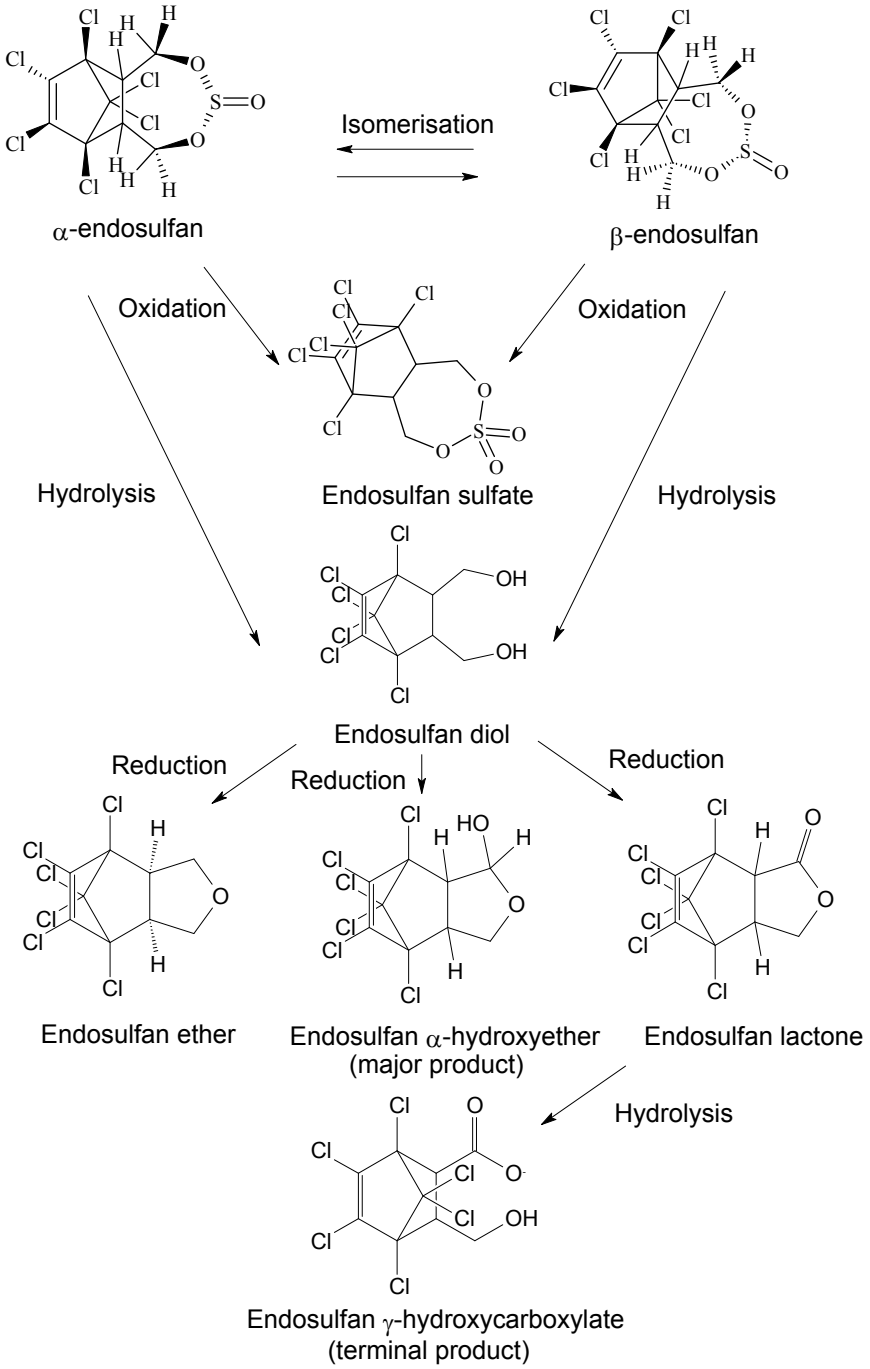

Figure 8.2. Endosulfan transformation pathway (Adapted from Walse *et al.* (2003)).

Studies on the fate of ES in both sterile and non-sterile aqueous systems have shown that hydrolysis is the dominant mechanism of degradation with β-ES selectively hydrolysed over α-ES under alkaline conditions. El Beit *et al*. (1983) has shown that

leachates from soil containing low levels of both ES isomers demonstrated higher losses of ES at high pH values, compared to acidic conditions. In leachates of pH 12.7, the pesticides degraded rapidly, whereas in the pH range 0.8 and 5.8 pesticides were relatively stable. Reported hydrolytic half-lives for α- and β-ES vary in literature in relation to difference physicochemical conditions such as solution pH and water source. Under anaerobic conditions at pH 7 Greve and Wit (1971) reported half-lives of 35 and 37 days for α- and β-ES, respectively. Under aerobic conditions the half-lives decreased to 23 and 25 days, respectively. Kaur *et al*. (1998) reported α-ES half-lives of 11.3 and 5.3 days in distilled water at 20°C at pH 5.5 and 8, respectively. Losses of ES, at an initial concentration of 0.5 mg/L, from natural lake water and tap water were 89 and 69 %, respectively, with the natural water more alkaline than the tap water (Ferrando *et al.*, 1992). The half-life of ES in tap water was approximately 68 hours. Guerin and Kennedy (1992) and Coleman and Dolinger (1982) reported half-lives of months at pH 7, days at pH 8, hours at pH 9 and minutes at pH 10-11.

Incubation of ES with river water at pH 8.3 resulted in the disappearance of ES and the formation of ES diol due to the alkaline pH (Shivaramaiah *et al.*, 2005). This has been attributed to low steric hindrance of the S=O bond within the ES structure leading to susceptibility for nucleophilic (OH^-) attack of the S atom, as shown in Figure 8.3. ES diol is more polar than ES and can be readily reduced to endosulfan ether (ES ether), endosulfan α-hydroxyether (ES HE), endosulfan lactone (ES lactone) and the terminal end product endosulfan γ-hydroxycarboxylate (ES γ-hydroxycarboxylate) under both abiotic (Walse *et al.*, 2002) and biotic conditions (Miles and Moy, 1979).

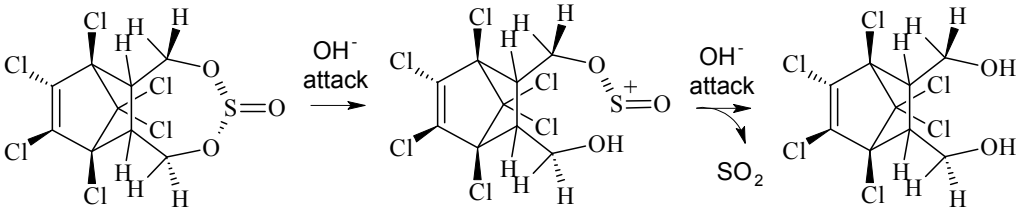

Figure 8.3. Hydrolysis of endosulfan to form endosulfan diol.

Numerous studies have shown the electrochemical degradation of organic compounds on membranes and electrodes. Tanaka *et al*. (1999) examined the electrochemical decomposition of bisphenol A and nonylphenol (NP) using a platinum coated titanium (Pt/Ti) electrode by monitoring the amount of TOC present. Complete elimination of 1.0 mM bisphenol A and NP was achieved after 120 and 240 minutes, respectively, with the formation of a range of aromatic intermediate compounds such as hydroquinone, catechol and benzoquinone derivates. Zanoni *et al*. (2003) reported 70 % TOC reduction of Remazol Brilliant Orange 3R (RBO), a reactive organic dye, by photoelectrocatalytic degradation on titanium dioxide thin-film electrodes (TiO_2). It was suggested that charges generated on the electrode surface gave rise to Cl^- and OH^- that cause the dye to degrade. Similarly, Szpyrkowicz *et al*. (2001) undertook trials on the electrochemical oxidation of reactive acidic organic dyes at Pt/Ti electrodes. After 40 minutes 79 % elimination of the chemical oxidation demand (COD) had occurred.

While α-ES and ES sulfate do not come into contact with the electrodes within the ED stack degradation as a result of pH changes within the membrane boundary layer may occur. Another hypothesis was that the α-ES and ES sulphate degrade to ES diol when they come into contact with the charged and highly basic AEMs. Given the polarity of the sulfite group in α-ES, it is expected to be reducible on a charged surface. While degradation of α-ES and ES sulfate was not expected to occur at pH 3 during the ED experiments, the diluate and concentrate were analysed for the presence of the degradation product ES diol. ES diol was not detected in the initial diluate and concentrate samples at pH 3 but showed a slight increase to 10.1 and 9.5 µg, respectively (Figure 8.1C and D). This only corresponds to 2.5 and 2.6 % of the initial mass of α-ES present within the diluate and concentrate. The presence of ES diol, however, does not account for the decrease in the mass of ES sulfate. The octanol-water partition coefficients (log K_{ow}) of α-ES and ES sulfate α-ES (3.68 and 3.66, respectively, Table 2.6) are relatively high suggesting that they would be readily adsorbed onto hydrophobic materials (e.g. macromolecules) in water and

membrane polymers. For this reason, sorption isotherm experiments were undertaken to determine sorption of the ES compounds to the ion-exchange membranes.

8.2 Endosulfan Sorption during Isotherm Experiments

8.2.1 Water-membrane Partitioning for Endosulfan

The sorption of ES to the ion-exchange membranes was measured at neutral pH to allow comparisons with water-membrane partitioning of estradiol, estrone, progesterone and testosterone. The ES-membrane isotherms are shown in Figure 8.4. The concentration of ES decreased significantly in the isotherm experiments indicating membrane sorption. The amount of ES sorbed (log $C_{AEM/CEM,}$ ng/cm^3) increased as solution phase concentration (log C_w^t, ng/L) increased (R > 0.99). At 1-100 μg/L ES, the linearity of the sorption isotherms demonstrate that the partitioning of ES into the ion-exchange membranes was the dominant sorption mechanism and that saturation of the adsorption sites within the membranes had not occurred. Deviation from linearity at high ES concentration (2500 μg/L) was similar to that noted for the steroidal hormones (Chapter 7, Section 7.1); however, this deviation was only noted for ES and the CEM. The deviation of the CEM isotherms from linearity at 2500 μg/L (1-100 μg/L n_i 0.95; 1-2500 μg/L n_i 0.88) indicates ES concentration limited binding. However, the partition coefficients for ES were derived for the 1-2500 μg/L concentration range.

The determined membrane partition coefficients (log $K_{AEM/CEM}$) for the 1-2500 μg/L concentration range in the absence and presence of HA are given in Table 8.1. Although the sorption affinity of ES for the AEM (log K_{AEM} 0.60 ± 0.13 L/cm^3) was greater than the sorption affinity for the CEM (log K_{CEM} 0.24 ± 0.08 L/cm^3), both membranes are composed of a PS-DVB polystyrene matrix; thus indicating the functional group dependent sorption of ES. This is similar the partitioning of the steroidal hormones to the ion-exchange membranes, as presented in Chapter 7.

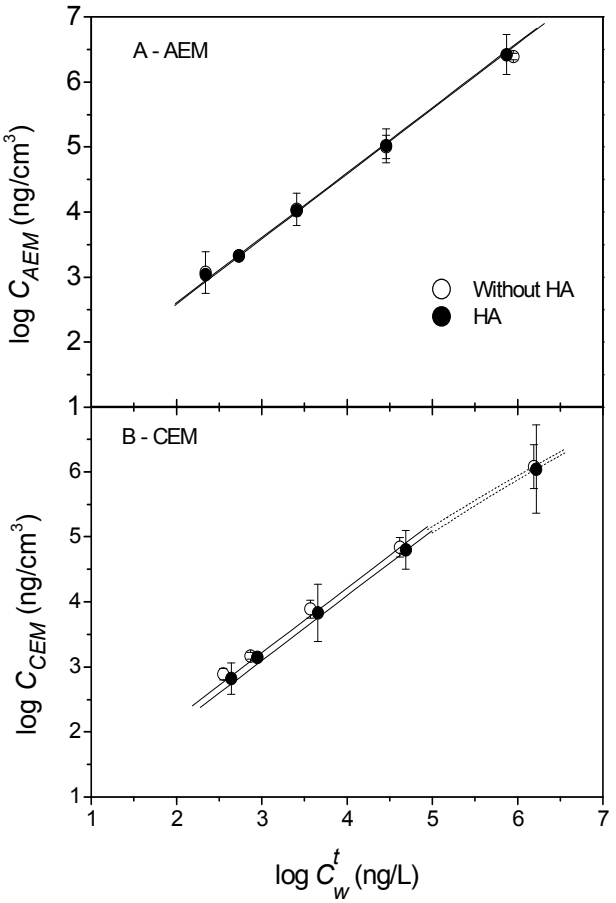

Figure 8.4. Endosulfan-membrane isotherms for the (A) AEM and (B) CEM in the presence and absence of HA (1mM $NaHCO_3$, 85.5 mM NaCl, 1-2500 µg/L ES, pH 7; time used to determine log $K_{AEM/CEM}$: 170 h).

Table 8.1. Water-membrane partition coefficients (log $K_{AEM/CEM}$, L/cm^3) for endosulfan in the absence and presence of HA (Initial ES concentration 1-2500 µg/L, 12.5 mgC/L HA).

	Log $K_{AEM/CEM}$ (L/cm^3)	
	AEM	**CEM**
ES	0.60 ± 0.13	0.24 ± 0.08
ES + HA	0.61 ± 0.07	0.11 ± 0.03

± indicates 95 % confidence interval (C.I.).

8.2.2 Endosulfan Sorption Mechanisms

Studies have shown that ES, its isomers and degradation products are strongly sorbed to OM. Reported organic carbon-water partition coefficients (K_{OC}) for α-ES, β-ES,

ES sulfate and ES diol are 7969-21347, 8612-13906, 5667-11445 and 724-1216 cm^3/g (German Federal Environment Agency, 2004). Kumar and Philip (2006) investigated the sorption and sorption kinetics of ES to four Indian soils, namely clayey soil (lean clay with sand), red soil (silty gravel with sand), sandy soil (silty sand with gravel) and composted soil (peat). Maximum sorption (q_{max}) took place in clay soil (α-ES: 0.448 mg/g, β-ES: 0.2722 mg/g) followed by composted soil (α-ES: 0.3876 mg/g, β-ES: 0.2018 mg/g) and red soil (α-ES: 0.2186 mg/g, β-ES: 0.1966 mg/g) with sorption equilibrium reached at 4 hours. The presence of OM playing a significant role in the sorption process with a positive correlation between OM % within the soil and the rate of sorption observed. The lower OM content of red soil (5.28 ± 0.1 %) as compared to composted soil (9.51 ± 0.05 %) reduced the sorption rate of α-ES from 1.12 to 0.960 $mg/gh^{0.5}$ and β-ES from 0.933 to 0.618 $mg/gh^{0.5}$. The greater decrease in sorption rate for β-ES (33 %) compared to α-ES (15 %) was postulated to be due to difference in interaction of ES isomers with the OM. The importance of OM in soil on the sorption of pesticides has been highlighted by other studies with sorption attributed to chemical adsorption, physical adsorption due to van der Waals forces and hydrogen bonding (El Beit *et al.*, 1981; Gao *et al.*, 1998; Martins and Mermoud, 1998).

Hydrogen bonding to HS is suggested to play a vital role in the adsorption of several non-ionic pesticides (Senesi *et al.*, 1987; Senesi, 1992). Senesi and Testini (1980) studied the interaction between atrazine and *s*-triazines with HS by infrared spectroscopy (IR), differential thermal analysis (DTA) and ^{1}H-NMR and suggested that hydrogen bonding occurred between HA carbonyl groups and secondary amine groups of the *s*-triazines. The interaction of ES with HA has been reported. Prosen *et al*. (2002) studied interaction of three organochlorine insecticides lindane, heptachlor and dieldrin (4.2 μg/L) onto with Aldrich HA in water suspensions as a function of pH (pH 2-3 and pH 9-10), ionic strength (tap water and solutions of 40 g/L NaCl) and HA concentration (0.1-1.0 μg/L), under both acidic (pH 2-3) and alkaline (pH 9-10) conditions, using GC-ECD and SPME. The use of α-ES as an internal standard to improve method repeatability was abandoned as it was bound to HA. Therefore, no sorption data for ES was presented. Between 85 and 90 % of lindane, heptachlor and

dieldrin were bound to HA within 35 days with equilibrium between the fraction of pesticides bound to HA and the fraction freely dissolved attained between 10 and 15 days. No significant difference in binding to HA within the water suspensions were observed with the change in solution pH, ionic strength and HA concentration. Binding was attributed to hydrophobic interaction.

In regards to sorption equilibrium between OM and ES the times reported are less than 24 hours. Gupta and Ali (2008) investigated the sorption of ES on a carbon slurry (fuel-oil-based generated waste material, 92 % organic carbon (OC)) and observed equilibrium from 120 minutes. The time of equilibration adsorption was unaffected by initial concentration, but the amount adsorbed increased with increasing ES concentration. Parkpian *et al*. (1998) observed sorption equilibrium in two Thailand tropical soils (clay and clay loam, 3 % OC) within 2 hours. Thus, ES was assumed to be in equilibrium (24 hours before membrane addition) with HA in the sorption isotherm experiments with HA present. Although the log K_{AEM} values were similar in the presence of HA, greater sorption to the AEM would be expected due to attraction between negatively charged ES-HA complexes and the positively charged AEM. Therefore, results suggest that sorption of ES and ES-HA complexes to the ion-exchange membranes during the sorption isotherm experiments would be influence by other interaction mechanisms such as hydrogen bonding. Electrostatic interactions between freely dissolved ES (i.e. not complexed with HA) would not be possible due to the undissociated nature of ES at neutral pH.

Previous studies (Nghiem *et al.*, 2002; Williams *et al.*, 1999) and Chapter 7 showed that trace organics interact with the ion-exchange membranes by hydrogen bonding. Pesticides can be hydrogen-donors or acceptors. As seen in Chapter 7, the AEM is capable of taking part in forming hydrogen bonds with organic contaminants containing hydrogen-donor groups and presents more opportunities for hydrogen bonding than the CEM. The number of hydrogen bonding sites possible between ES and ES diol functional groups and one AEM and CEM functional group is given in Table 8.2. This shows that the AEM presents more opportunities for bonding with ES

and ES diol; thus accounting for the higher log K_{AEM} values in the presence and absence of HA.

Table 8.2. Number of hydrogen bonding sites possible between endosulfan functional groups (S-1, C-7 and C-10 position) and one ion-exchange membrane functional group (AEM Neosepta AMX-SB, CEM Neosepta CMX-SB).

ES compound [a]	AEM			CEM		
	S-1	C-7	C-10	S-1	C-7	C-10
ES (α-ES + β-ES)	9 A	9 A	9 A	1 A	1 A	1 A
ES diol	-	9 A	9 A	-	2 D, 1 A	2 D, 1 A

[a] A and D relate to hydrogen bonding facilitated through ES hydrogen acceptor and donor groups, respectively.

ES is monopolar given it can only accept hydrogen atoms with 1 sulphur monoxide group (S=O) in the S-1 position and 2 C-O in the C-7 and C-10 position. ES diol contributes as both a hydrogen-bond donor and acceptor in the C-7 and C-10 position (Table 2.6). The molecular structure of ES and ES diol and the possible hydrogen bond formations with the AEM and CEM functional groups are illustrated in Figure 8.5. Sorption of ES to the AEMs is facilitated through hydrogen bonding between the S-1 S=O, C-7 C-O, C-10 C-O hydrogen acceptor groups and the methyl CH_3 hydrogen-donor groups. While the formation of ES diol was not quantified during the sorption isotherm experiments, it is postulated that ES may be hydrolysed to the more polar ES diol on contact with the strongly basic AEMs membranes. Detection of ES diol (but not individual identification) in the form of ES was possible because of the utilisation of radiolabeled ES and the position of the ^{14}C label (Table 2.6). Hydrogen bonding between the bipolar ES diol to the functional group in the AEM would be facilitated through the C-7 and C-10 hydrogen-acceptors in ES diol with the CH_3 group. Hydrogen bonding of ES and ES diol to the SO_3H functional group in the CEM is facilitated only through hydrogen-acceptors in ES (S-1, C-7, and C-10) and ES diol (C-7, C-10). The strength of the hydrogen bonding of the functional groups in ES and ES diol are summarised in Table 8.3. The S-1 hydrogen acceptor group in ES (log K_β 3.06) is much stronger than the strength of the hydrogen acceptor and donor groups in ES diol (log $K_{\alpha, b}$ 1.21).

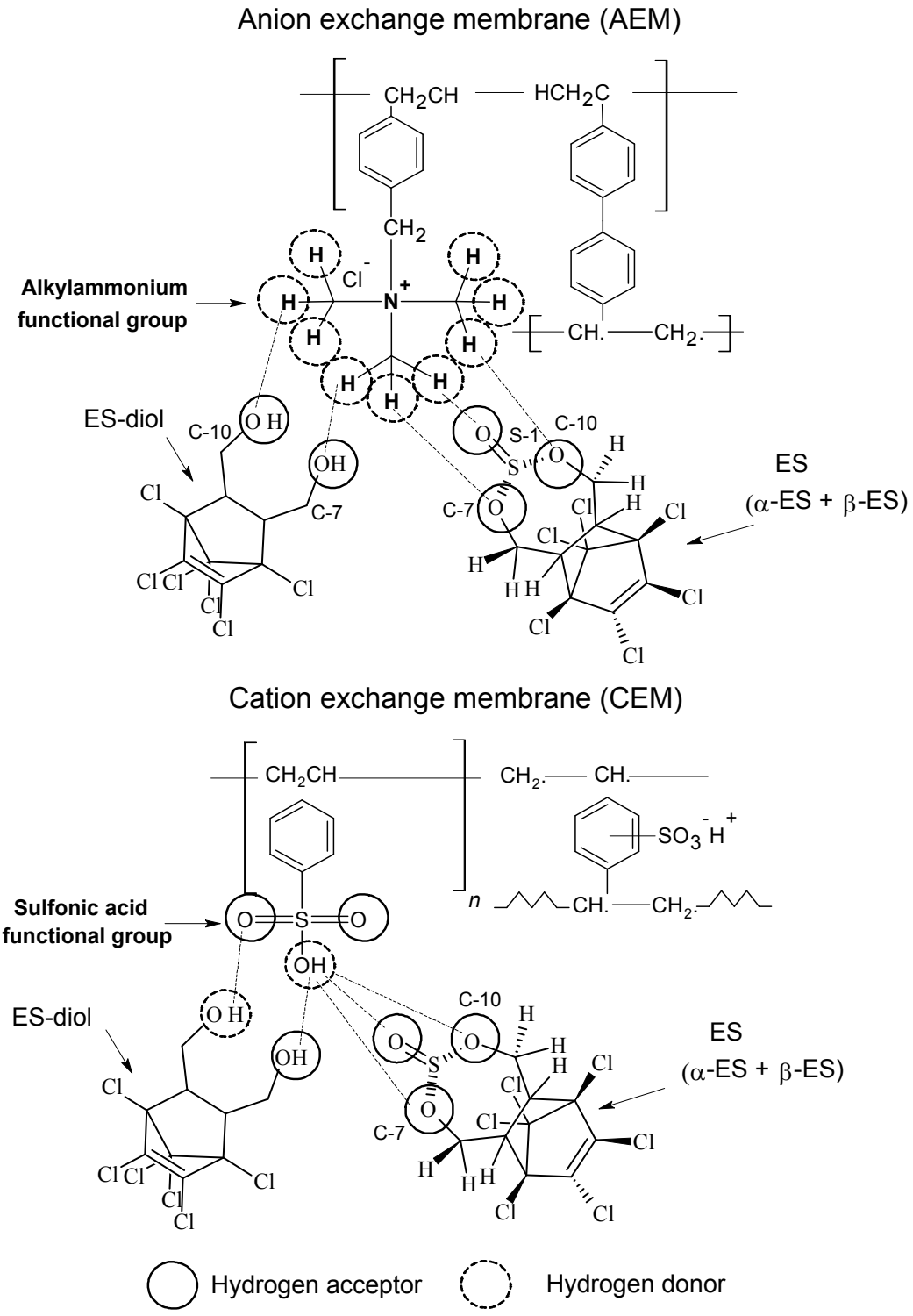

Figure 8.5. Schematic of possible hydrogen bonding between endosulfan and endosulfan diol molecules and the AEM and CEM functional groups (Neosepta AMX-SB and CMX-SB, respectively) at neutral pH.

Table 8.3. Strength of hydrogen bonding of endosulfan and steroidal hormone functional groups (Adapted from Gancia *et al.* (2001)).

Endosulfan compound	Hydrogen bonding strength					
	Hydrogen acceptor (log K_β)			Hydrogen donor (log K_α)		
	S-1	C-7	C-10	S-1	C-7	C-10
ES	3.06	[a]	[a]	-	-	-
ES diol	-	1.21	1.21	-	1.21	1.21

[a] No data available.

The presence of HA influences hydrogen bonding. Neale *et al*. (2008) showed that the partitioning of undissociated estrone with HA was greatest at pH 7 due to hydrogen bonding due to hydrogen bonding between the carbonyl group in estrone and HA. At pH 7, when HA is > 99 % dissociated, hydrogen bonding between the S=O and C-O groups in ES and hydroxyl groups in HA would occur. Therefore, the lower log K_{CEM} value (0.11 ± 0.03 L/cm^3) and thus sorption affinity of ES to the CEM in the presence of HA in comparison to ES sorption in the absence of HA (0.24 ± 0.08 L/cm^3) can be attributed to electrostatic repulsion between negatively charged ES-HA complexes and the negatively charged CEM. Greater HA sorption to the AEMs (0.19 mg C, 15.2%) in comparison to the CEMs (0.01 mg C, 0.6%) was noted.

8.2.3 Endosulfan Degradation

Studies have shown the degradation of ES compounds from both natural and environmental water samples with volatilisation, hydrolysis and biodegradation the predominant contributing mechanisms. The degradation of ES via photolysis has been highlighted (El Beit *et al.*, 1983; Singh *et al.*, 1991). The degradation of ES by volatilisation and hydrolysis were discussed in Section 8.1. Therefore, only biodegradation and photodegradation of ES will be discussed in this section.

Both α- and β-ES are oxidised by soil microorganisms in sediments and on crops, with ES diol, sulfate, ether, hydroxyether and lactone reported as the major metabolites formed during the microbial metabolism of ES isomers (Awasthi *et al.*,

1997; Kullman and Matsumura, 1996; Martens, 1976; Singh *et al.*, 1991; Sutherland *et al.*, 2000). Sutherland *et al*. (2000) studied the enzymatic bioremediation of ES and found that degradation of ES occurred with bacterial growth. ES was both oxidized and hydrolysed with oxidation favouring α-ES and ES sulfate production. Studies conducted with raw river water with microbial activity present showed that α-ES and β-ES were dissipated completely after 4 weeks incubation, forming traces of ES diol (Eichelberger and Lichtenberg, 1971).

Degradation of ES as a result of UV exposure has been reported in the literature. Singh (1991) reported half-lives of 48 and 33 hours of α- and β-ES, respectively, when aqueous α- and β-ES solutions were exposed to sunlight. El Beit *et al*. (1983) studied the photolysis of ES from a soil leachate. After 168 hours of exposure (representing 14 days of 12-hour sunlight per day) to ultraviolet irradiation of 2537°A wavelength), 9.9 % of the initial ES concentration (1020 mg/L) was lost by photodecomposition. Four degradation products of ES were detected in the irradiated leachate, including ES diol and ES ether.

While the ES sorption isotherm experiments were conducted in a shaker out of direct light and in solutions of ultrapure water, ES degradation was possible due to the duration of the experiments (~ 7 days, 170 hours to sorption equilibrium). Therefore, control sorption isotherm experiments were undertaken with 100 mL covered solutions and solutions with the addition of a biocide (0.5 % wt $Na_2S_2O_5$) to determine if photodegradation or biotransformation, respectively, had an influence on ES sorption during the sorption isotherm experiments. There was no significant difference between the control and experiments without degradation prevention (Figure 8.6), indicating that ES photodegradation and biotransformation was not an issue.

Sorption isotherm experiments were undertaken to quantify ES sorption to the glassware used. While minimal loss (~ 6 %) was noted in the first 140 minutes (experimental duration in Figure 8.1), a loss of up to 20 % was noted at 170 hours. Hengpraprom *et al*. (2006) reported sorption of less than 7 % sorption of α-ES to

glassware (50 mL glass centrifuge tubes) for a contact time of 30 minutes. Log $K_{AEM/CEM}$ values (L/cm^3) determined in the sorption experiments (Section 8.2.1) were adjusted accordingly to account for this dissipation from and/or sorption to the glass bottles i.e. the mass of ES sorbed in the sample bottles without a membrane was subtracted from the mass orbed in the samples with a membrane added for each sampling period.

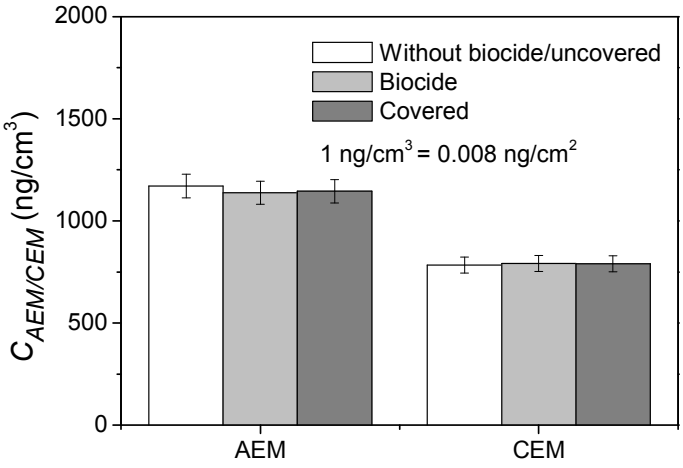

Figure 8.6. Comparison between endosulfan sorption ($C_{AEM/CEM}$, ng/cm^3) to the (A) AEM and (B) CEM with and without the addition of a biocide and in covered solutions (1 mM $NaHCO_3$, 85.5 mM NaCl, pH 7, 0.5 % wt $Na_2S_2O_5$, 1 µg/L ES).

8.2.4 Endosulfan Sorption and Desorption Kinetics during Isotherm Experiments

The ES-membrane sorption kinetics for isotherm experiments is presented in Figure 8.7. ES sorption kinetics was the same for the AEM and CEM with rapid sorption occurring within 10 hours. Like the sorption of the steroidal hormones, two sorption processes appear to occur: (1) Initial surface sorption and (2) sorption into the depth of the membrane which is slow and diffusion limited. At high ES concentration (e.g. 2500 µg/L), the process of diffusion is slower, as indicated by the increase in slope between 10 and 170 hours at 2500 µg/L. This diffusion is slower due to the large initial mass of ES per unit area of membrane. The initial mass of ES per unit area during the 1, 2, 10, 100 and 2500 µg/L sorption isotherm experiments were 0.01,

0.02, 0.12, 1.2 and 30.8 μg/cm^2, respectively. As constant mass sorbed was not reached, 170 hours was arbitrarily chosen for the determination of the ES-membrane partition coefficients.

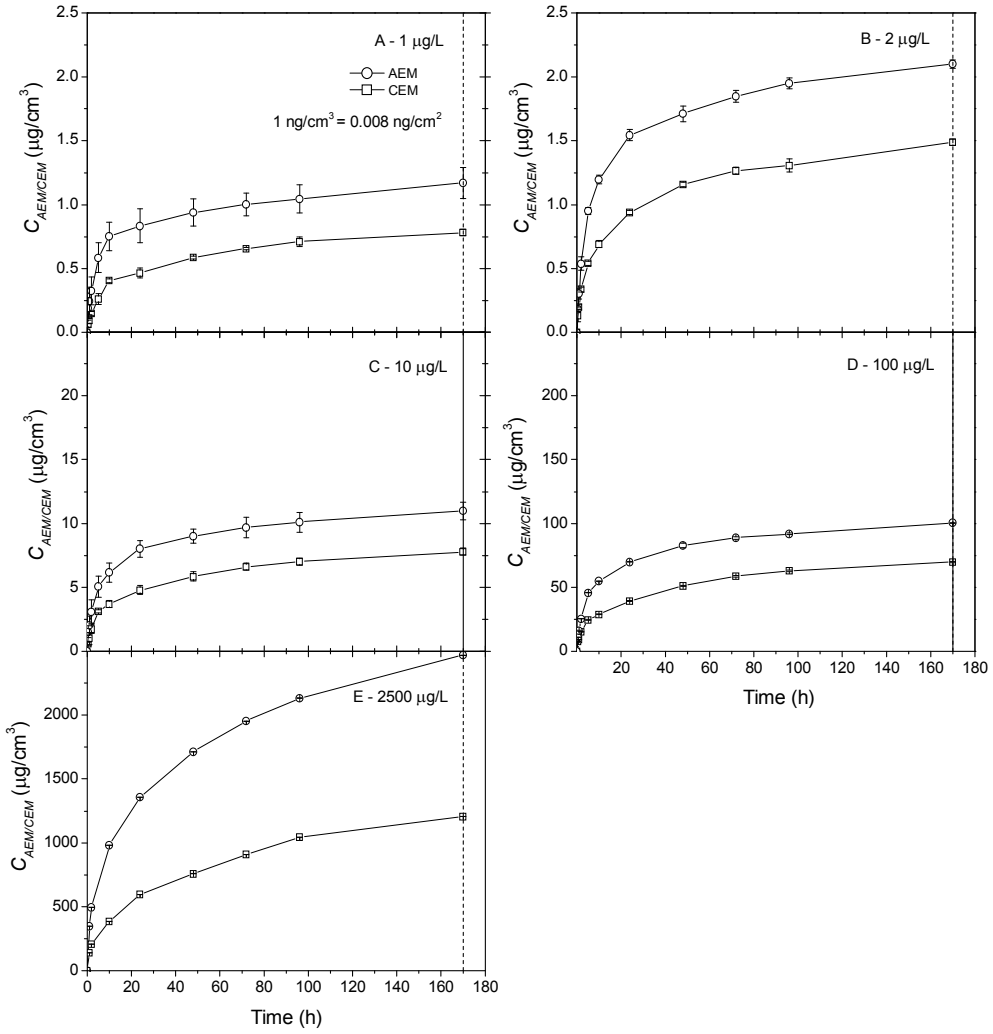

Figure 8.7. Endosulfan sorption kinetics (A-B) 1-2500 μg/L (1mM NaHCO3, 85.5 mM NaCl, pH 7; vertical dotted line indicates time used for determination of log $K_{AEM/CEM}$: 170 h).

Analyses were carried out in order to determine whether ES could be desorbed from the ion-exchanges membranes used in the sorption isotherm experiments in order to regenerate the membranes and identify the possible risk of ES release back into solution. Desorption of ES from the ion-exchange membranes used in the 1 μg/L

isotherm experiment was investigated using the same membrane cleaning solutions used in the steroidal hormone desorption experiments (0.002 M HCl, NaOH and UW). Partial desorption in the presence of HCl, NaOH and UW was noted with rapid desorption occurring within 24 hours followed by a steady-state up to 170 hours (Figure 8.8B). This indicates the irreversible nature of ES sorption. Desorption from the CEMs at 24 hours (HCl: 24.3 % initial mass sorbed; NaOH: 27.9 %; UW: 15.1 %) was greater than desorption from the AEMs (HCl: 12.4 %; NaOH: 3.1 %; UW: 8.3 %) (Figure 8.9). The lower desorption of ES from the AEMs corresponds to the greater mass of ES sorbed to the AEMs. More ES was desorbed from the CEMs with NaOH (pH ~ 11) due to ES degradation and the subsequent repulsion with the CEM. Membrane desorption of ES is thus not only dependent on the initial mass sorbed but on solvent pH, ES physicochemical properties and ES-membrane interactions. A similar trend was noted with desorption of hormones from the ion-exchange membranes in Chapter 7.

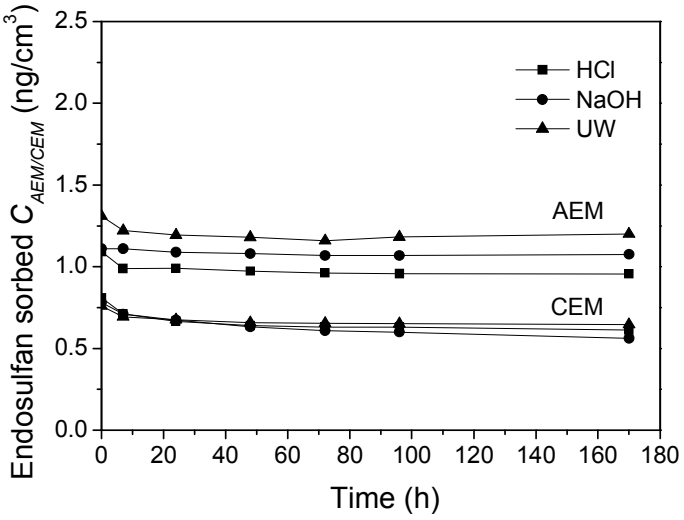

Figure 8.8. Endosulfan desorption kinetics (0.002 M HCl, 0.002 M NaOH and ultrapure water (UW)).

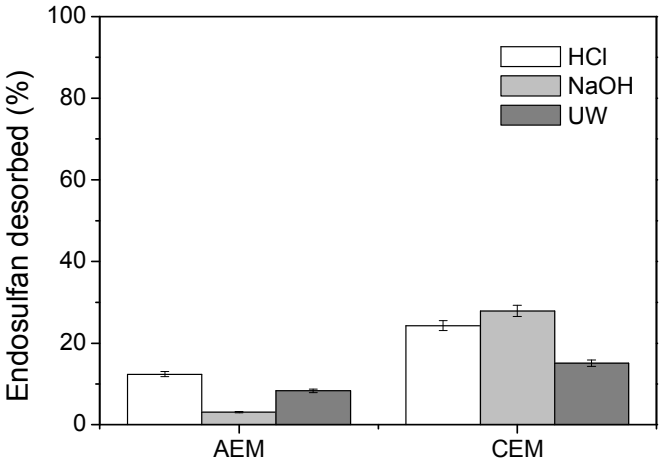

Figure 8.9. Endosulfan desorption (% of initial mass) from the AEMs and CEMs (0.002 M HCl and NaOH, ultrapure water (UW); initial endosulfan concentration 1 µg/L, data relates to desorption at 24 hours).

8.3 Endosulfan Sorption during Electrodialysis

8.3.1 Influence of Solution pH

ED experiments were undertaken to elucidate the mechanisms involved in ES sorption during ES to identify differences in sorption during isotherms and ED. In aqueous media, the solution pH has a marked influence on the stability of ES. Therefore, the implication of solution pH on the sorption of ES during ED was investigated. The mass of ES sorbed per unit volume of membrane within the ED stack (C_{stack}, µg/cm^3) during the continuous ED experiments in the absence of HA is shown in Figure 8.10A. The sorption kinetics exhibited rapid sorption within 15 minutes followed by a steady increase to 550 µg/cm^3 at 4 hours. Constant ES mass sorbed was not reached at pH 7 and 11 and the slope of the kinetics indicates diffusion into the membranes. When the feed solution was separated, ES sorption continued within both the diluate and concentrate at pH 7 (Figure 8.11). This is similar to the sorption of progesterone during ED (Figure 7.13). Therefore at pH 7, sorption of ES occurs on both the AEMs and CEMs facing the diluate and concentrate.

The mass of ES sorbed to the membranes at pH 11 at 4 hours (306 µg/cm^3) was significantly less than the mass sorbed at pH 7 due to the alkaline hydrolysis of the

cyclic sulfite diester group (Figure 8.3) leading to the formation of the inorganic sulfite group and ES diol. This process is accelerated by the addition of NaOH used to change and maintain the feed solution pH. While electrostatic repulsive forces between the sulfite group and the positively charged AEM may decrease the proximity of the ES molecules to the AEM surface and thus reduce membrane sorption at pH 11, the concentration of ES within both the diluate and concentrate decreased slightly (Figure 8.11A). Therefore, the lower sorption of ES at pH 11 is predominantly due to the lower hydrogen bonding capability between ES diol and the ion-exchange membranes.

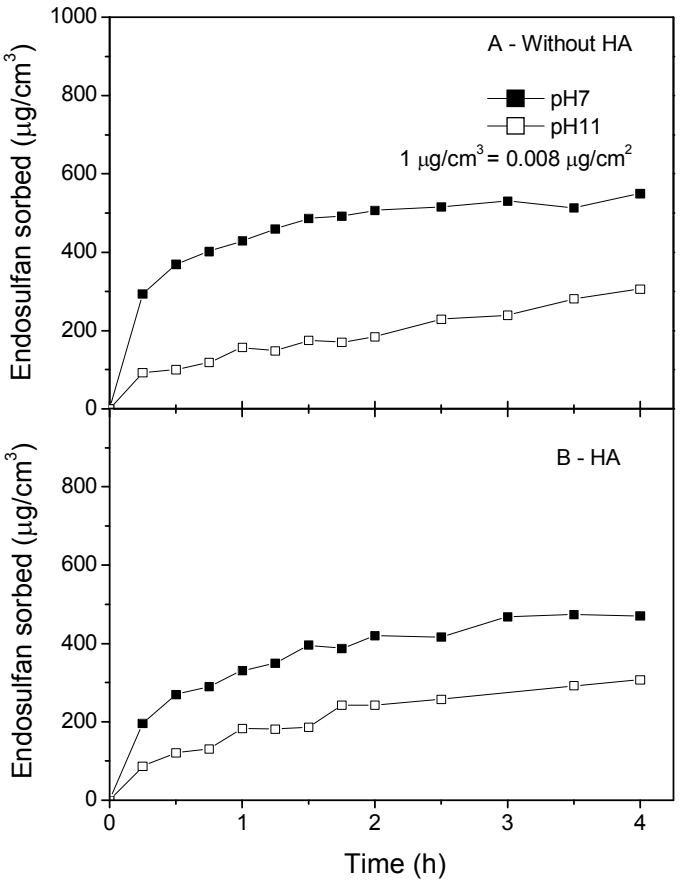

Figure 8.10. Mass of endosulfan sorbed (C_{stack}, µg/cm^3) during ED per unit volume of membrane (µg/cm^3) (1 mM $NaHCO_3$, 85.5 mM NaCl, 10 V; average initial mass of endosulfan: without HA 938 ± 39 µg/cm^3, with HA 960 ± 14 µg/cm^3).

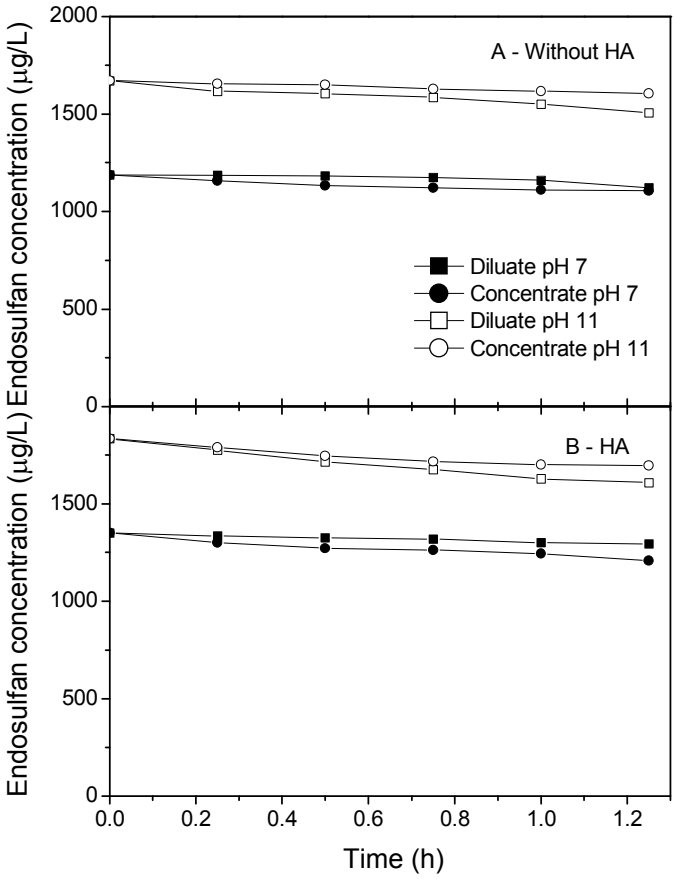

Figure 8.11. Concentration (µg/L) of endosulfan in the diluate and concentrate at pH 7 and pH 11 in batch ED experiments (1 mM $NaHCO_3$, 85.5 mM NaCl, 10 V; diluate and concentrate feed solution sourced from continuous ED experiments; endosulfan initial concentration: without HA pH 7-1188 µg/L, pH 11-1670 µg/L, with HA pH 7-1350 µg/L, pH 11-1834 µg/L).

8.3.2 Influence of Organic Matter

The influence of HA on ES sorption to the ion-exchange membranes was evaluated in continuous ED experiments. The influence of HA on the mass of ES sorbed per unit volume of membrane within the ED stack (C_{stack}, µg/cm^3) is shown in Figure 8.10B. Greater ES sorption at pH 7 in comparison to pH 11 was observed in the presence of HA. A comparison between the mass sorbed in the absence and presence of HA is given in Figure 8.12. The mass of ES sorbed to the membranes at pH 7 decreased by 79 µg/cm^3 in the presence of HA (471 µg/cm^3). The mass of ES sorbed to the membranes at pH 11 in the presence of HA (307 µg/cm^3) was not significantly different from the mass sorbed in the absence of HA. After the feed solution was

separated, ES sorption continued within both the diluate and concentrate at pH in the presence of HA (Figure 8.11B). Like without HA, at both pH 7 and pH 11 the concentration of ES within the diluate and concentration decreased slightly.

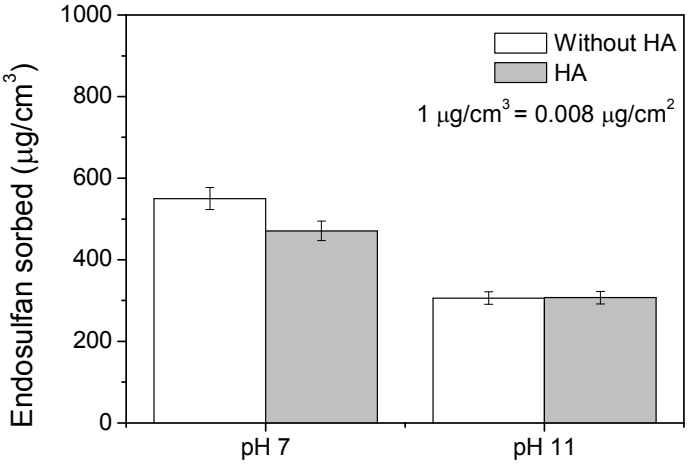

Figure 8.12. Comparison between the mass of endosulfan sorbed to the membranes during ED experiments (C_{stack}, µg/cm^3) in the presence and absence of HA (1 mM $NaHCO_3$, 85.5 mM NaCl, pH 7-11, 10 V; experimental duration 4 hours).

While K_{OC} values have been reported, there are no studies specifically on the partitioning of ES to Aldrich HA and thus the fraction of ES freely dissolved in the feed (f_w, %) at ES-HA equilibrium is unknown. Therefore, the mass of ES sorbed to HA within the ED feed solutions at pH 7 and 11 ($m_{ADS\text{-}HA}$) could not be predicted. However, sorption of ES to HA is expected to be high due to the high partitioning of ES to HA, as represented by the K_{OC} values for ES and its isomers and degradation products (724-21347 cm^3/g). The sorption of HA at pH 7 was low (1.1 mgC, 2.6 % initial mass of HA). Therefore, the decrease in ES sorption during ED in the presence of HA at pH 7 is due to high partitioning of ES to HA and electrostatic repulsion between negatively charged ES-HA complexes and the negatively charged CEMs. This is different to studies on the effect of OM on atrazine rejection using NF (Devitt *et al.*, 1998) and dialysis (Devitt and Wiesner, 1998) which suggested that the formation of pesticide-OM complexes resulted in subsequent enhancement of rejection through OM membrane sorption.

The complexation of ES diol and HA at pH 11 would not be as strong as ES-HA complexation at pH 7 as ES diol contains only 2 hydrogen acceptors compared to 3 hydrogen acceptors of ES (Table 2.6). Hengpraprom *et al*. (2006) found that the sorption of ES diol to HA-mineral complexes (kaolinite and montmorillonite) was less than α-ES due to its higher water solubility (300 mg/L, Table 2.6). Therefore, the minimal difference in sorption at pH 11 in the absence and presence of HA is due to the reduction in ES diol-HA complexation coupled with the low mass of HA sorbed to the membranes at pH 11 (0.52 mgC, 1.0 % initial mass of HA).

8.4 Comparison between Sorption in Isotherm and Electrodialysis Experiments

A comparison between the mass of ES sorbed to the membranes during the sorption isotherm and continuous ED experiments at pH 7 was undertaken to explicate the differences in sorption and to consider the accuracy of the log $K_{AEM/CEM}$ values for estimating membrane sorption during ED. The mass of ES sorbed per unit volume of membrane during the isotherm and ED experiments (μg/cm^3) is given in Table 8.4, along with the mass predicted to sorb during ED. The mass of ES predicted to sorb to the membranes during ED was calculated using the log $K_{AEM/CEM}$ values (Table 8.1), eqn (4.13), eqn (4.14) and eqn (4.15). For further details on these calculations refer to Chapter 4. The mass of ES sorbed was greater in the AEM isotherm experiments (Without HA: 2469 μg/cm^3, HA: 2659 μg/cm^3) in comparison to the ED experiments (Without HA: 550 μg/cm^3, HA: 471 μg/cm^3). Therefore, the predicted mass of ES sorbed during ED (Without HA: based on AEM 4124 ± 1439 μg/cm^3, CEM 2570 ± 592 μg/cm^3; HA: AEM 4316 ± 723 μg/cm^3, CEM 2044 ± 303 μg/cm^3) was greater than the experiment mass.

Figure 8.13 compares the sorption kinetics during the 2500 μg/L ES sorption isotherm and ED experiments at pH 7. It is unlikely that the mass of ES sorbed during ED would reach the same mass sorbed during the batch sorption isotherm experiments if the ED experiments had continued for a longer duration. Like with the steroidal hormones, the initial mass of ES per unit area of membrane was greater in the sorption isotherm experiments (AEM: 30.7 μg/cm^2, CEM: 30.8 μg/cm^2)

compared to the ED experiments (7.2 μg/cm^2). The higher sorbent/water ratio in the isotherm experiments explains the larger partition coefficients derived and, thus, the significantly higher predicted mass of ES sorbed but lower experimental mass sorbed during ED. Therefore, the sorption isotherm experiments and determined partition coefficients cannot represent the sorption regime during ED.

Table 8.4. Comparison between endosulfan sorption in batch sorption isotherm and ED experiments at pH 7.

	Membrane volume (cm^3)	Sorption time (h)	ES sorbed to ion-exchange membranes (μg/cm^3)	
			Without HA	HA
Sorption isotherm experiments [a]				
AEM	0.056	170	2469	2659
CEM	0.068	170	1206	1107
Predicted mass sorbed during ED experiments [b, c, d]				
AEM [e]	11.8	-	4124 ± 1439	4316 ± 723
CEM [e]	11.8	-	2570 ± 592	2044 ± 303
ED experiments [a]				
Experimental	11.8	4	550	471

[a] 1mM $NaHCO_3$, 85.5 mM NaCl, 2500 μg/L ES, 12.5 mg C/L HA, pH 7 [b] Minimum (CEM) and maximum (AEM) calculated using eqn (4.13), eqn (4.14) and eqn (4.15); [c] Calculated using log $K_{AEM/CEM}$ values for 1-2500 μg/L; [d] ± 95 % C.I.; [e] Based on presence of only AEMs or CEMs within the ED stack.

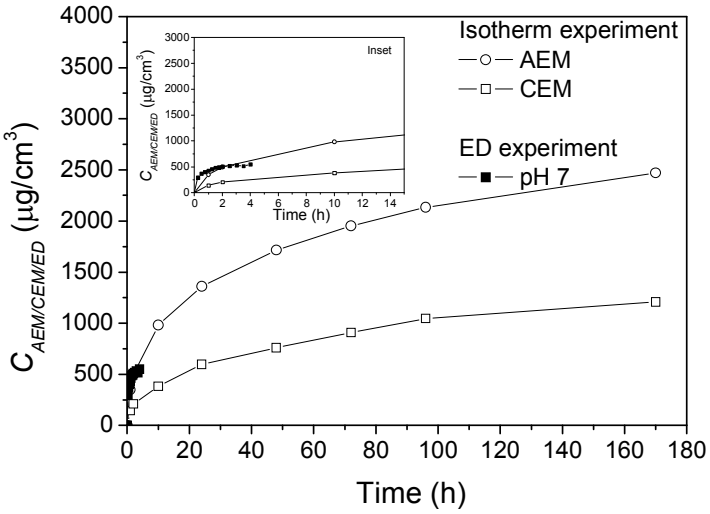

Figure 8.13. Comparison between endosulfan sorption during sorption isotherm and continuous ED experiments. Inset is close-up of sorption up to 14 hours (1mM $NaHCO_3$, 85.5 mM NaCl, pH 7, 2500 mg/L ES).

8.5 Endosulfan Sorption to other Polymer Materials

The sorption of pesticides to plastics and polymeric materials will vary depending on the physicochemical properties of the pesticide as well as the type of plastic or polymer, as was shown in Chapter 7 with differences in estrone sorption to different polymer materials. Literature on the sorption of ES to other polymeric materials is limited; however there are a few reported studies on the sorption of pesticides to plastic materials particular for agricultural usage (Nerin *et al.*, 1996; Topp and Smith, 1992; Vuik *et al.*, 1990). Nerin *et al*. (1996) studied the absorption of pesticides, including ES, on four different types of LDPE (black, normal, thermic and extra low density) and EVA films used as agricultural soil covers. Experimental protocols were similar to those employed in the ES sorption isotherm experiments in this current study, except the pieces of LDPE and EVA films were placed in only deionised water and not a buffer solution (i.e. not pH adjusted or 1mM $NaHCO_3$, 85.5 mM NaCl). Complete sorption was observed after 15 days of contact time and no degradation was observed once the pesticides were sorbed. Although the initial ES concentration used in the study by Nerin *et al*. (1996) (1000 μg/L; α-ES and β-ES unmixed) was a factor of 2.5 less than the highest ES concentration used in the sorption isotherm experiments (2500 μg/L) in this current study, a comparison between the mass sorbed per unit area (ng/cm^2) showed that the polystyrene based ion-exchange membranes have a significantly greater sorption affinity than LDPE and EVA (Table 8.5).

While the mechanisms involved in the sorption of ES to the LDPE and EVA were not reported, hydrogen bonding between ES and LDPE and EVA is possible (Figure 8.14). The polymerisation of ethylene results in a high molecular weight hydrocarbon straight chain polymer with polyethylene characterised by its degree of chain formation. LDPE is extensively branched and compact in structure. EVA copolymers are long chains of ethylene hydrocarbons with acetate groups randomly attached throughout the chains. The molecular structure of EVA shows that there are more opportunities for hydrogen bonding than LDPE, thus accounting for the greater sorption (α-ES: LDPE normal 0.3 ng/cm^2, EVA 0.7 ng/cm^2).

Table 8.5. Comparison between the mass of endosulfan sorbed to ion-exchange membranes (AMX-SB, CMX-SB) and the mass sorbed to low density polyethylene (LDPE) and ethylene/vinyl acetate copolymer (EVA) (Nerin *et al.*, 1996).

Polymer	Membrane area (cm^2)	Sorbed at 7 days (ng/cm^2)
PS-DVB (AMX-SB) [a]	8.136	17048
PS-DVB (CMX-SB) [a]	8.112	10081
LDPE (black) [b]	192	0.3 α-ES, 1.2 β-ES
LDPE (normal) [b]	192	0.3 α-ES, 0.9 β-ES
LDPE (thermic) [b]	192	0.6 α-ES, β-ES
LDPE (extra low density) [b]	192	0.2 α-ES, 0.7 β-ES
Ethylene/vinyl acetate (EVA) [b]	192	0.7 α-ES, 0.8 β-ES

[a] 1 mM $NaHCO_3$, 85.5 mM NaCl, 2500 µg/L ES; [b] Deionised water, 1000 µg/L; α-ES and β-ES unmixed).

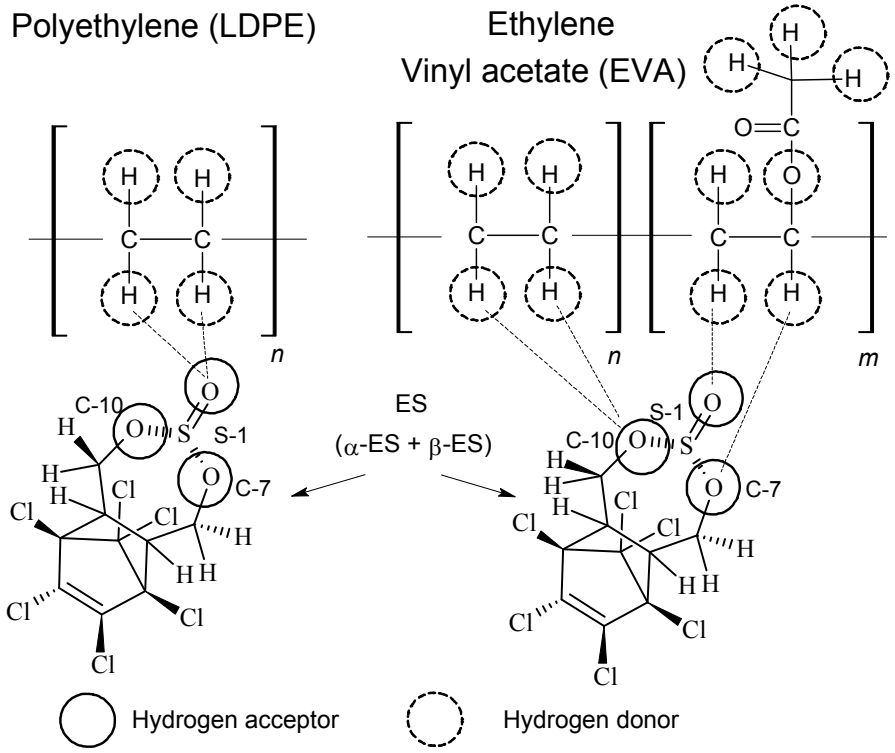

Figure 8.14. Schematic of possible hydrogen bonding between endosulfan and polyethelene membrane polymer.

By comparing the schematics for hydrogen bonding with the different polymers (PS-DVB Figure 8.5, LDPE and EVA Figure 8.14) and the number of possible hydrogen

bonding sites (Table 8.6) it can be seen that the PS-DVB AEM presents more opportunities for hydrogen bonding than LDPE. While the hydrogen bonding capacity of EVA may be greater than PS-DVB due to the acetate group (EVA (ethylene + acetate) and EVA (ethylene) combined, Table 8.6), the sorption affinity for ES to PS-DVB (AEM 17048 ng/cm^2) is greater than the sorption affinity to EVA (α-ES: 0.7 ng/cm^2, β-ES 0.8 ng/cm^2). This may because the acetate groups are only randomly attached to the EVA ethylene chain. These results demonstrate the influence of polymer type on ES sorption affinity.

Table 8.6. Number of hydrogen bonding sites between ES functional groups (S-1, C-3 and C-10 position) and the ion-exchange (AMX-SB AEM, CMX-SB CEM) functional groups, low density polyethylene (LDPE) and ethylene/vinyl acetate copolymer (EVA).

Polymer	S-1 [a]	C-7 [a]	C-10 [a]
PS-DVB (AMX-SB)	9 A	9 A	9 A
PS-DVB (CMX-SB)	1 A	1 A	1 A
LDPE	4 A	4 A	4 A
EVA (ethylene) [b]	4 A	4 A	4 A
EVA (ethylene + acetate) [c]	7 A	7 A	7 A

[a] A and D relates to hydrogen bonding facilitated through hormone hydrogen acceptor and donor groups, respectively; [b] Bonding with ethylene group; [c] Bonding with ethylene/acetate group.

8.6 Comparison between Steroidal Hormone and Endosulfan Sorption

8.6.1 Water-membrane Partition Coefficient Comparison

A comparison between the log $K_{AEM/CEM}$ values for ES and the hormones (estradiol, estrone, progesterone and testosterone) is shown in Figure 8.15. As ES sorption to the AEM was postulated to be due to ES diol formation and hydrogen bonding interaction with the membrane, the log K_{AEM} for ES (0.60 ± 0.13 L/cm^3) is similar to that of estradiol (0.50 ± 0.13 L/cm^3), which is structurally similar in that it contains two hydrogen-acceptor and donor groups (Table 2.4 and Table 2.6). Therefore, the number of hydrogen bonding sites possible between ES, estradiol and the AEM is the same (Table 8.7). However, the sorption affinity of estrone to the AEM (0.67 ± 0.16 L/cm^3) was greater than that of ES diol but the number of possible hydrogen bonding

sites is less. Therefore, this sorption is influenced by the strength of hydrogen bonding. The strength of hydrogen bonding of the C-7 and C-10 acceptor and donor functional groups of ES diol (log K_β and log K_α both 1.21, Table 8.3) is correspondingly less than the strength of hydrogen bonding of the C-17 functional group of estrone (log K_β 1.61) (Table 7.3). ES and progesterone both contain 3 hydrogen acceptor groups, however the log K_{CEM} for ES (0.24 ± 0.08 L/cm^3) is significantly lower than that of progesterone (0.53 ± 0.19 L/cm^3). While the strength of hydrogen bonding of the S-1 functional group of ES (log K_β 3.06) is greater than the C-3 (log K_β 1.70) and C-17 (log K_β 1.52) functional groups of progesterone, the fact that the C-3 group in progesterone acts as a triple hydrogen acceptor may account for the higher sorption.

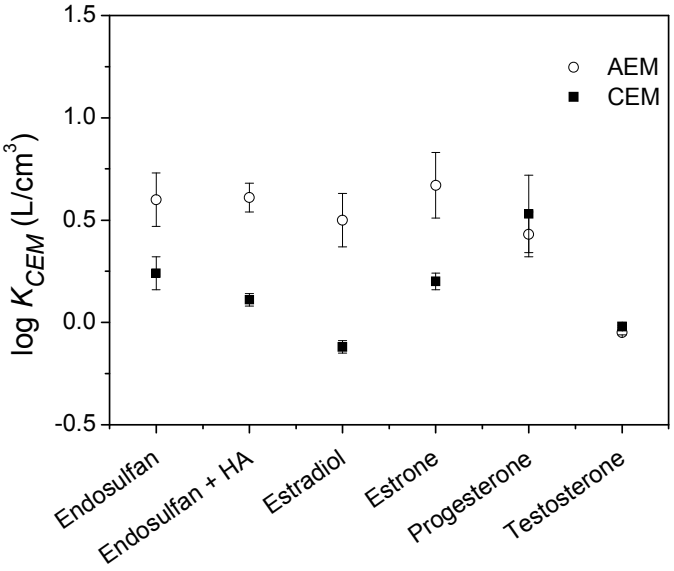

Figure 8.15. Comparison between endosulfan and steroidal hormone partition coefficients (log $K_{AEM/CEM}$, L/cm^3) (1mM $NaHCO_3$, 85.5 mM NaCl, 1-100 µg/L endosulfan and hormone, pH 7).

Table 8.7. Number of hydrogen bonding sites possible between endosulfan and steroidal hormone functional groups and one ion-exchange membrane functional group (AEM Neosepta AMX-SB, CEM Neosepta CMX-SB).

ES compound [a]	AEM	CEM
ES (α-ES + β-ES)	27 A	3 A
ES diol	18 A	4 D, 2 A
Estradiol	18 A	4 D, 2 A
Estrone	18 A	2 D, 2 A
Progesterone	18 A	2 A
Testosterone	18 A	2 D, 2 A

[a] A and D relate to hydrogen bonding facilitated through ES hydrogen acceptor and donor groups, respectively

8.6.2 Electrodialysis Sorption Comparison

A comparison between the sorption of ES, progesterone and estrone during ED is shown in Figure 8.16. At pH 7 ES exhibited similar sorption behaviour to progesterone. While the mass of ES sorbed to the membranes up to 1.5 hours was greater than that of progesterone, the mass of ES sorbed at 4 hours (550 μg/cm^3) was less the mass of progesterone sorbed (690 μg/cm^3). ES and progesterone are both undissociated at pH 7. The greater sorption affinity of progesterone for both the AEM and CEM accounts for the higher sorption. The higher mass of progesterone sorbed during ED compared to that of estrone was postulated to be a result of greater partitioning of progesterone to the CEM (log K_{CEM} 0.53 ± 0.19 L/cm^3) in comparison to estrone (log K_{CEM} 0.20 ± 0.04 L/cm^3) and the larger volume of CEMs (6.9 cm^3) within the ED system in comparison to the volume of AEMs (4.9 cm^3). The log K_{CEM} for ES (0.24 ± 0.08 L/cm^3) was greater than the log K_{CEM} of estrone and presented greater sorption at pH 7. At pH 7 the hydrogen bonding capacity of ES is greater than that of estrone (Figure 8.14); thus accounting for the higher sorption of ES.

At pH 11 the sorption behaviour of ES resembled that of estrone. However, the decrease in estrone sorption at pH 11 is due to electrostatic repulsion between negatively charged estrone and the negatively charged CEM while the decrease in sorption of ES is due to the lower hydrogen bonding capacity between ES diol and

the ion-exchange membranes. The same affinity for sorption was noted in the absence and presence of HA i.e. progesterone > ES > estrone.

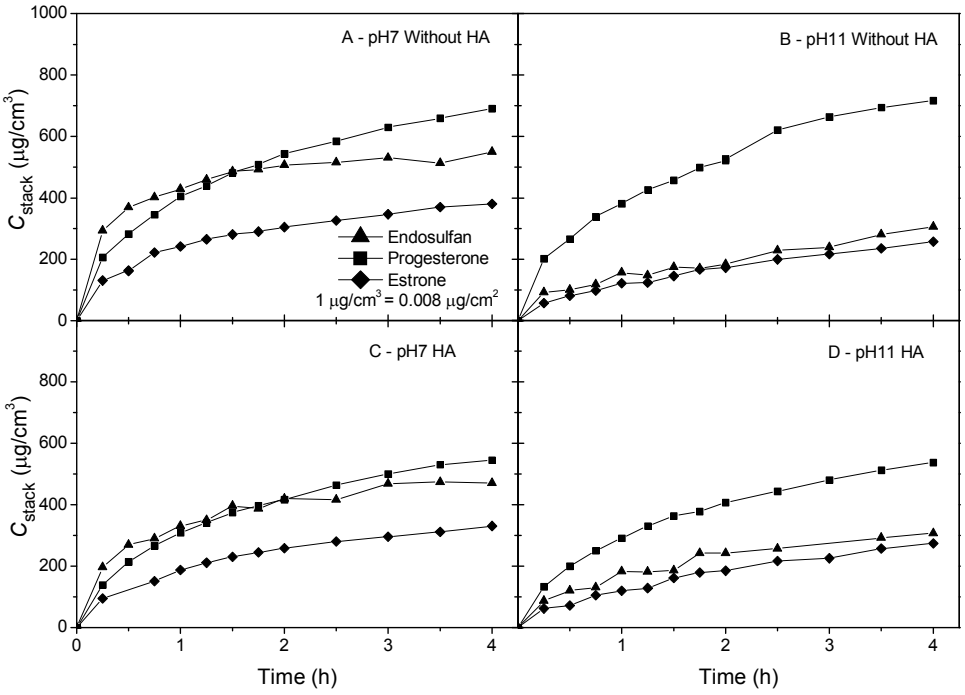

Figure 8.16. Mass of endosulfan, progesterone and estrone sorbed per unit volume of membrane (C_{stack}, μg/cm^3) (1 mM $NaHCO_3$, 85.5 mM NaCl, 2500μg/L hormone and ES).

8.6.3 Dual Compound Endosulfan and Estrone Electrodialysis Experiments

As ES and estrone demonstrated similar behaviour at pH 11, a dual compound ED experiment with both ES and estrone was undertaken at pH 7 and 11 to determine the if competition for sorption occurred. Preferential sorption of ES at both pH 7 and 11 was noted (Figure 8.17). It can be seen that sorption of both ES and estrone was reduced at pH 11 as a result of competitive sorption. A comparison between the mass of ES and estrone sorbed during the single and dual compound experiments is shown in Figure 8.18. Comparisons between the single and dual compound ED experiments were made at 4 hours. It is interesting to note that ES sorption was greater in the dual compound experiment (pH 7: 596 μg/cm^3; 67.8 % initial mass; pH 11: 414 μg/cm^3, 46.1 %,) than in the single compound experiment (pH 7: 550 μg/cm^3, 57.0 %; pH 11:

306 μg/cm^3, 33.6 %). A similar trend was noted for estrone at pH 11 (Single: 257 μg/cm^3, 28.9 %; Dual: 278 μg/cm^3, 31.6 %). The mass of estrone sorbed in the single compound experiment at pH 7 (380 μg/cm^3, 43.2 %) was similar to the mass sorbed in the dual compound experiment (381 μg/cm^3, 40.9 %). These results indicate that saturation of the membranes was not reached and that the sorption capacity of the ion-exchange membranes during ED is considerable.

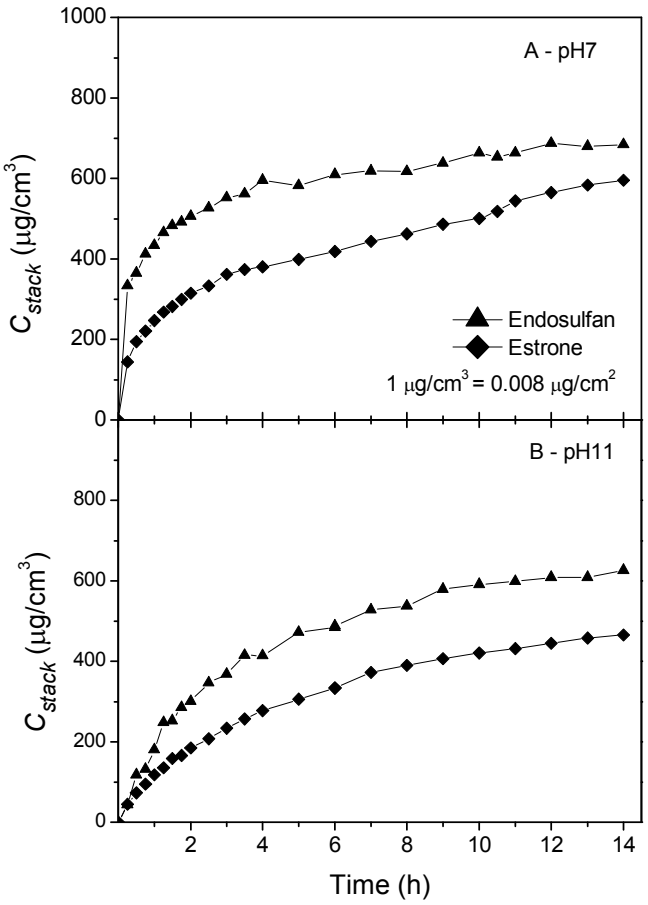

Figure 8.17. Mass of endosulfan and estrone sorbed per unit volume of membrane (C_{stack}, μg/cm^3) during dual compound ED experiments ((1 mM $NaHCO_3$, 85.5 mM NaCl; initial concentration endosulfan: pH 7 880 μg/cm^3, pH 11 898 μg/cm^3; initial concentration estrone: pH 7 930μg/cm^3, pH 11 878 μg/cm^3).

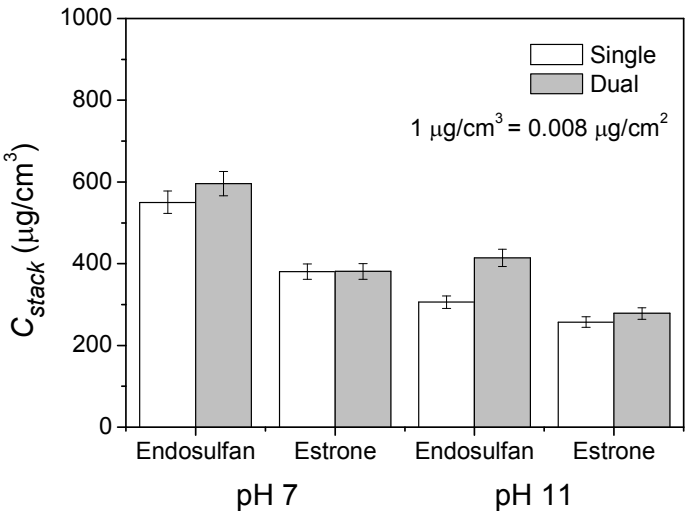

Figure 8.18. Comparison between the mass of endosulfan and estrone sorbed per unit volume of membrane (C_{stack}, μg/cm^3) during single and dual compound ED experiments.

8.7 Summary

While preliminary ED experiments demonstrated the significant problems in distinguishing the fate of ES during ED, a thorough investigation of the possible losses of ED due to non-biological (losses to equipment, volatilisation, photolysis and electrochemical degradation) and biological processes indicated that sorption was the dominant mechanism. The formation of the ES degradation product ES diol was noted but at low concentrations. It was, therefore, critical to investigate the possible modes of degradation in order to ascertain true values for the sorption of ES to the ion-exchange membranes.

The quantification of ES-membrane partition coefficients (log $K_{AEM/CEM}$) indicated strong sorption of ES to the ion-exchange membranes due to specific hydrogen bonding interactions between the ES functional groups (S-1 S=O, C-7 C-O, C-10 C-O) and the AEM (methyl CH_3) and CEM (SO_3H) functional groups. It was postulated the AEM sorption was enhanced as a result of membrane catalysed ES degradation and hydrogen bonding between the hydrogen acceptor groups (C-7 and C-10) in ES diol and the AEM functional group (CH_3). Hydrogen bonding to HA played a role in the sorption of ES to the CEM. Hydrogen bonding between the S=O and C-O groups in ES and hydroxyl groups in HA occurs and results in electrostatic

repulsion between negatively charged ES-HA complexes and the negatively charged CEM, as indicated by the reduced sorption affinity of ES in the presence of HA. The AEM presented more opportunities for bonding with ES and ES diol, thus accounting for the higher sorption affinity in the absence and presence of HA. Overall, results demonstrated that sorption was highly dependent on the hydrogen bonding capacity of the membrane and the strength of hydrogen bonding of the S=O, C-O and OH groups within ES and ES diol as well as the presence of OM.

It can be concluded that the removal of ES by ED is governed by sorption/partitioning due to hydrogen bonding between ES compounds and the ion-exchange membranes. Solution pH had important implications for this process. Alkaline hydrolysis of ES to ES diol was found to influence sorption whereby reduced hydrogen bonding between ES diol and the ion-exchange membranes reduced membrane sorption at pH 11. The influence of solute-solute interactions between ES and HA on the sorption of ES to the ion-exchange membranes during ED were generally minimal. The sorption behaviour of ES during ED was found to be similar to that of the steroidal hormones progesterone (undissociated at pH 7) and estrone (dissociated at pH 11) with sorption increasing in the following order: progesterone > ES > estrone. This was correlated with the strength of hydrogen bonding and the thus the sorption affinity of the organic contaminants for the ion-exchange membranes. Considering the sorption of ES to the membranes in the small-scale ED system used in this study, the mass of ES sorption in an industrial sized ED system would be significant. For a commercially available Ed stack with a membrane area of 370 m^2, approximately 17 kg of ES could potentially sorb. This could have serious implications for the performance of the ED process with regards to brackish water desalination, membrane life and subsequent maintenance costs.

The sorption of ES to the PS-DVB ion-exchange membranes, LDPE and EVA films were compared. While hydrogen bonding facilitate sorption of ES with each polymer is possible, the PS-DVB exhibited the greatest sorption of ES. This is related to the molecular structure of the PS-DVB polymer and attached functional groups.

While minimal desorption of ES from the ion-exchange membranes indicated the irreversible nature of trace organic membrane sorption, the re-release of this toxic pesticide back into solution has implications not only for the environment but for animal and human health. This reiterates the importance of appropriate disposal methods of membrane cleaning solutions.

Chapter 9. Conclusions

An increase in the awareness over the last few decades of the presence of inorganic and trace organic contaminants in ground, surface, drinking and wastewaters worldwide has led to intensive scientific research on potential water treatment processes. A review of the concentrations of inorganic and trace organic contaminants identified enabled targeted research on those contaminants of particular concern and highlighted the need for more advanced treatment technologies. Consequently, the focus of this thesis was contaminant removal by the electromembrane process ED. Despite the importance, there are a number of uncertainties regarding the mechanisms of contaminant removal in ED and the conditions that influence them. Therefore, the main objectives of this thesis were to:

1. Elucidate the mechanisms of inorganic contaminant removal from model solutions and compare these results with those from a real system
2. Undertaken membrane-contaminant interaction studies to evaluate the partitioning of organic trace contaminants in ED membranes
3. Identify the implications of solution chemistry (pH, presence of OM) and ED operational parameters (applied voltage) on these mechanisms.

This study successfully elucidated the mechanisms of contaminant removal by ED, which are summarised schematically in Figure 9.1. The predominant removal mechanism of pH independent inorganics (F^-, NO_3^-) and those in dissociated form ($B(OH)_4^-$) in the absence of OM were electrostatic interactions with minimal contribution from membrane deposition. The pH independent removal of F^- (R_D 68.3 ± 4.5 %) and NO_3^- (R_D 94.1 ± 1.3 %) was due to their pH independent speciation. NO_3^- with a relatively smaller hydrated radius was transported more effectively through the membranes than F^- with a relatively larger hydrated radius, thus enhancing removal. Above pH 9, where $B(OH)_3$ dissociates removal increased from 13.7 % to 61.2 %. In the presence of OM the dominant removal mechanism for F^- and $B(OH)_4^-$ was territorial binding and OM complexation, respectively, electrostatic repulsion between negatively charged inorganic-OM complexes and negatively

charged CEMs and the subsequent membrane deposition on the positively charged AEMs. Results demonstrated the mutual dependence of inorganic and OM in ED.

The complexity of the brackish groundwater investigated made the explication of the removal mechanisms difficult. At a higher voltage (18V), transport was initially high due to enhanced ionic migration. However, this increased membrane deposition which subsequently hampered inorganic flux and removal. The removal of B, Li^+, K^+, SO_4^{2-}, U, Ca^{2+}, Mg^{2+}, Sr^{2+}, Zn^{2+}, As(V) and Se(VI) was pH and thus speciation dependent, while Br^-, Cl^-, F^-, NO_3^- removal was pH independent. Undissociated inorganics (< pK_a) were not transported through the membranes, whereas dissociated inorganics (> pK_a) were due to electrostatic attraction. At acidic-neutral conditions (< pH 6) ionic transport was the predominant removal mechanism coupled with minor contribution from membrane deposition. At neutral to alkaline conditions (pH 7-11) membrane deposition dominated due the precipitation and deposition of insoluble carbonate species (e.g. $MgCO_3$, $CaCO_3$) as a scaling layer. This scaling increased ED stack resistance (pH 3: 27.5 Ω, pH 11: 50 Ω), SEC (pH 3: 5.3 Wh/L, pH 11 > 7.4 Wh/L) and decreased TDS flux and removal (pH 3: 99 %, pH 11: 89.5 %).

While the aim of this study was not to remove trace organics, their presence in water treatment plant effluents negates an understanding of their fate during ED; a potential treatment option. Membrane-water partition coefficients (log $K_{AEM/CEM}$) for estradiol estrone, progesterone and testosterone indicated significant sorption, which was attributed to hydrogen bonding. Sorption to the AEMs was greater than sorption to the CEMs as a result of the enhanced hydrogen bonding capacity of the AEM functional group ($N(CH_3)_3$: 9 hydrogen acceptors) compared to the CEM functional group (SO_3H: 1 hydrogen donor and 2 hydrogen acceptors). Sorption was dependent on hormone type and the strength of hydrogen bonding of the hormone carbonyl (C=O) and hydroxyl (OH) groups. The higher log K_{AEM} for estrone (0.67 ± 0.16 L/cm^3) compared to estradiol (log K_{AEM} 0.50 ± 0.13 L/cm^3) was due to the stronger C-17 carbonyl group in estrone. The contribution of the C-3 carbonyl moiety in progesterone as a triple hydrogen acceptor accounted for the greater sorption to the CEM (log K_{CEM} 0.53 ± 0.19 L/cm^3) than the other hormones.

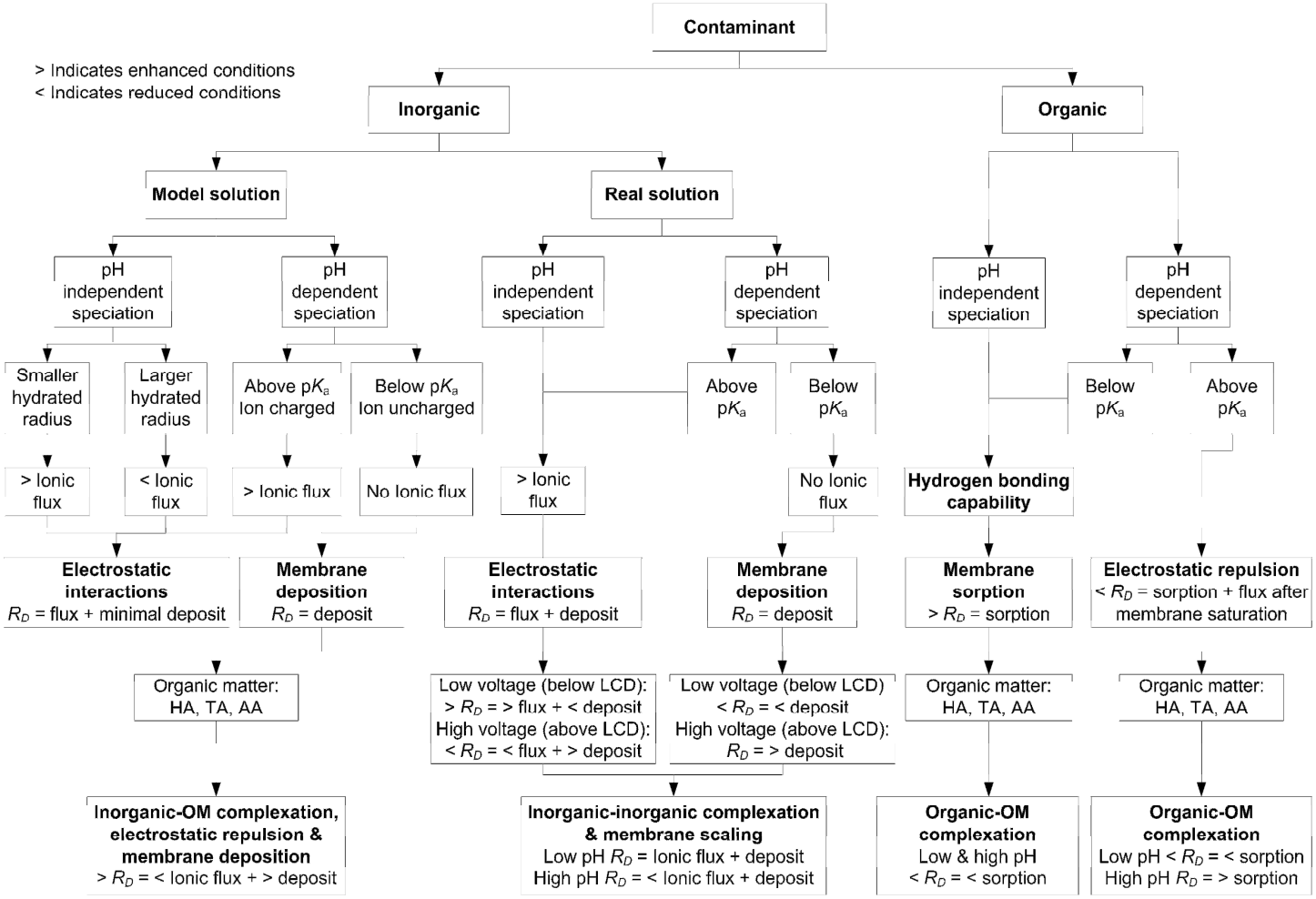

Figure 9.1. Mechanisms of contaminant removal by Electrodialysis during this study.

Hormone sorption during ED was influenced by solution pH and the presence of HA. At pH 7 when progesterone and estrone were both uncharged the dominant removal mechanism was sorption as governed by hydrogen bonding. Greater sorption of progesterone at pH 7 (922 μg/cm^3) compared to 591 μg/cm^3 of estrone was due to the triple hydrogen acceptor of progesterone. At pH 11, sorption of dissociated estrone was reduced (487 μg/cm^3) as a result of electrostatic CEM repulsion. Diffusion of estrone through the AEMs was observed. For undissociated progesterone in the presence of HA the dominant removal mechanism was sorption due to hydrogen bonding with minimal contribution from hormone-HA interactions. At pH 11, charge repulsion between dissociated estrone and HA coupled with electrostatic attraction with the AEMs resulted in a slight increase in membrane sorption.

The sorption of endosulfan and its degradation product endosulfan diol to the membranes was a result of specific hydrogen bonding between the S=O (S-1), C-O and OH (C-7, C-10) functional groups. However, unlike estrone the reduction in sorption during ED at pH 11 (306 μg/cm^3) compared to pH 7 (550 μg/cm^3) was attributed to alkaline hydrolysis of endosulfan to endosulfan diol and a reduction in hydrogen bonding between ES diol and the membranes. The influence of ES-HA complexation on ES sorption during ED was minimal; indicating that sorption due to hydrogen bonding was the dominant removal mechanism for ES.

Looking back at the main objectives of this thesis, the mechanisms governing inorganic and trace organic contaminant removal in the absence and presence of OM have been elucidated; namely electrostatic interactions, solute-solute interactions and membrane deposition/sorption. While this thesis is of a fundamental nature, the knowledge gained has direct applications to current problems and uncertainties in water and wastewater treatment with regards to the fate and transport of contaminants. Results have demonstrated that the application of ED for the treatment of RO concentrates is a real option that needs further consideration. Greater knowledge of the effect of key controlling parameters of ED will ensure further growth beyond desalination and salt production and foster ED applications in other sectors including chemical, pharmaceutical and municipal effluent treatment.

Chapter 10. Recommendations for Future Research

While this thesis has improved understanding of the mechanisms of trace contaminant removal in ED, it has revealed avenues for further fundamental and applied research. This chapter proposes future research needs identified during this study.

The potentialities of ED have not been fully exploited due to a number of process issues including high membrane costs and short lifetime. Further research is necessary in order to apply this treatment process to other contaminants and improve its feasibility in the treatment of natural waters. To overcome problems, long-term lab and pilot-scale ED experiments are required to assess ion-exchange membrane process performance, reliability and applicability in regards to extensive OM fouling and its influence on inorganic and organic trace contaminant removal. Although it is convenient to undertake experiments with small-scale ED stacks, a scale-up to pilot or industrial scale is possible with respect to the limiting current density and the specific cell pair resistances if the membranes used are identical and the spacers used are similar. Results from this study have shown that solution chemistry (solution pH, presence of OM) and ED operational parameters (applied voltage) influence the removal mechanisms of inorganics and trace organics. Therefore, it would be necessary for these parameters to be taken into consideration when translating the fundamental findings from this study to a real life situation. This study has elucidated the mechanisms of trace contaminant removal by ED as well as the factors influencing them. These results combined with a larger scale study of the removal mechanisms of clean and extensively fouled ion-exchange membranes would be beneficial for the development of a quantitative and qualitative model. Attempts to minimise inorganic membrane deposition and OM fouling would enhance ion mobility through ion-exchange membranes. Extending membrane life would minimise the overall surface area of ion-exchange membranes to be installed and thus reduce future investment and process maintenance costs.

This work highlighted the strong sorption of organic trace contaminants on polymeric materials. The measured partition coefficients and the quantification of trace contaminant sorption on membrane polymers would be useful for the development of a dynamic transport model that will facilitate improved quantitative and qualitative prediction for other organic compounds which have similar physical and chemical properties to the compounds investigated in this thesis. Measurement of the hydrogen bonding energies between the trace organics and the ion-exchange membranes would be beneficial. Although ED does not successfully remove neutrally charged steroidal hormones and pesticides from aqueous solutions, the high sorption affinity of ion-exchange membranes for these organic compounds may be utilised. The development and use of engineered membranes to exploit this process would be advantageous. The use of nanotechnology to develop new ion-exchange membranes for ED technology may lead to advanced highly efficient and possibly cost-effective technologies in both the treatment of organic contaminants, desalination and the treatment of RO concentrates.

Application of ED to a real RO concentrate would prove beneficial and requires extensive characterisation and the systematic study of the removal of inorganic and trace organic contaminants. While it was not possible to undertake this during the current study, the salt concentration used (5 g/L NaCl) is within the range of salinity of RO concentrates (Al-Rifai, 2008) and, therefore, results are applicable to concentrate treatment.

An important question that is generally not answered on an international scale is ‘what to do with the ED concentrates?’ The generation of a waste stream is a common element in all desalination processes. This stream contains the salts removed from the feed to produce the ‘clean water’ diluate product, as well as the chemicals that may have been added during the treatment process (e.g. acids, anti-scalants). It may also contain corrosion by-products. While the concentrate varies in volume depending on the treatment process, it will usually be a considerable quantity of water. Given the concentration of inorganic and organic contaminants in natural water, the concentration within the ED concentrates may be significantly greater (not

including those sorbed to the membranes). Similarly, the disposal of membrane cleaning solutions is an issue that needs to be investigated. Therefore, the disposal of these concentrates and membrane cleaning solutions in an environmentally appropriate manner is an important part of the feasibility and operation of any desalination treatment plant with regards to water efficiency (recovery). If an unsuitable disposal method is applied, significant environmental and possibly human and animal health implications arise. Therefore, further research is required on the treatment and disposal of such concentrates and membrane cleaning solutions and ultimately the successful process integration of ED.

Appendix 1. Instrument Calibration

Appendix 1 presents detailed descriptions of the instrument calibration methods and their limitations. The analytical instruments included: membrane contact angle and zeta potential measurement instruments, pH/conductivity meter, ISE's, nutrient analyser, UV-visible spectrophotometer, TOC analyser, liquid scintillation counter and a gas chromatograph. Experimental protocols (e.g. liquid-liquid extraction (LLE)) are also presented in greater detail.

A1.1 Membrane Contact Angle

The most widely used method for measuring contact angles (θ) is the sessile drop technique, which is a direct measurement of the contact angle of a liquid drop deposited on a surface. The angle is determined by creating a tangent to the profile at the point of contact of the drop with the membrane surface (Krüss, 2009). The instrument used for the measurement of the AEM and CEM contact angle is shown in Figure A1.1.

Figure A1.1. Krüss FM40 EasyDrop Contact Angle instrument (photograph courtesy of Annalisa de Munari).

The membranes were rinsed thoroughly and soaked in ultrapure water 24 hours prior to measurement. The membrane was left to dry for at least 8 hours at room temperature to ensure that the results were not affected by the degree of dryness of the membranes (Zhang *et al.*, 1989). The membranes were then glued to a glass slide

to obtain a perfect plane surface. A pure water drop was placed onto the membrane surface, which was photographed within 15 seconds and then every minute for at least 6 minutes after which the contact angles were automatically calculated.

A1.2 Membrane Zeta Potential

The zeta potential is related to the charge and electric double layer of surfaces in aqueous solutions. The surface charge characteristics of membranes are highly dependent on the membrane chemical properties and solution chemistry. Therefore, zeta potential measurements were undertaken on the ion-exchange membranes used in this study. The instrument used for the zeta potential measurements (electrokinetic analyser EKA, Anton Paar KG, Gratz, Austria) is shown in Figure A 1.2.

Figure A 1.2. Anton Paar KG Electrokinetic analyser (photograph courtesy of Annalisa de Munari).

Each membrane was rinsed thoroughly and soaked in ultrapure water 24 hour prior to measurement. The membrane was cut in two pieces (7.5 cm × 2.5 cm) and soaked in an electrolyte solute (1mM $NaHCO_3$, 20 mM NaCl) for 30 minutes. The membrane pieces were assembled in the measuring cell and the system was flushed with ultra-pure water for 3 minutes. The system was flushed for 30 minutes with the electrolyte solution, taking care to remove all air bubbles from the cell. The pH of the electrolyte solution was adjusted automatically by an autotritator with 1M HCl and 1M KOH. Six measurements were taken for each pH value; three in each direction, the average value was taken. All measurements were performed at room temperature, (approximately 21°C). At the end of the measurement the cell was dismantled and the system was flushed for 30 minutes with ultrapure water till the pH was stable.

A1.3 Electrical Conductivity and NaCl Concentration

EC (mS/cm) of the diluate and concentrate samples (Chapter 5) taken using a pH/Conductivity meter (Multiline P4, WTW Germany) was converted to NaCl concentration (mg/L). Calibration standards of 0.2, 0.4, 0.6, 0.8, 1, 2, 4 and 5 g/L were prepared from a 5 g/L NaCl stock solution. NaCl concentration (mg/L) in the experimental samples was ascertained from a linear regression performed on the calibration standards (Figure A1.3).

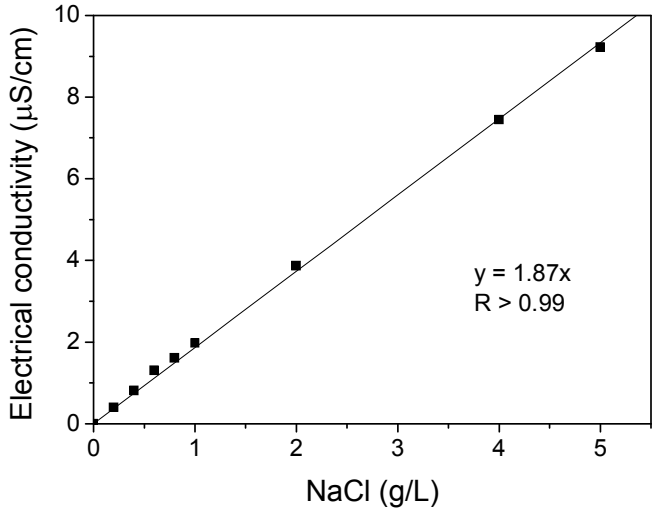

Figure A1.3. NaCl concentration (mg/L) vs. Electrical conductivity (mS/cm) (1mM $NaHCO_3$; pH 7).

A1.4 Ion-selective Electrode Calibration

ISE's are widely used for the determination of inorganic ions in aqueous solutions. ISE's permit the passage of only those ions to be measured through the membrane in the selective electrode. When an ISE is immersed in a sample containing say fluoride ions they diffuse through the membrane until equilibrium is reached between the external and internal fluoride ion concentrations. There is a build up of charge on the inside of the membrane which is proportional to the number of fluoride ions in the sample. In this case, there is little current flow and a potential difference can only be measured relative to a standard single-junction reference electrode which is also in

contact with the sample (but not affected by it) (Freiser, 1980). This potential difference is measured externally via a pH meter with a millivolt (mV) scale.

Although ISE are quick and easy to use, they are not without their limitations. The three main problems with the use of ISE are the effect of interference from other ions, the effect of the ionic strength of the solution reducing the measured activity relative to the real concentration at high ion concentration, and potential drift during sets of measurements. Total ionic strength buffers (TISAB) of 1 M NaCl and 0.1 M ammonium sulphate ($(NH_4)_2SO_4$) were used for fluoride and nitrate measurements, respectively. TISAB adjusts ionic strength, buffers pH to 5-5.5, and contains a chelating agent to break up possible metal-ion complexes. For fluoride and nitrate analysis, standards and samples were mixed 1:1 and 50:1 with the TISAB, respectively. The inner electrolyte for the reference electrode was 3 M potassium chloride (KCl).

The presence of OM can interfere with the selectivity of ISE's. Therefore, calibration standards of fluoride and nitrate were analysed using ISE in the absence and presence of the studied organics (HA, TA and AA). Calibration standards of 0.1, 1, 5, 10, 25 and 50 mg/L fluoride were prepared from a 50 mg/L stock solution. Calibration standards of 0.1, 1, 5, 10, 25, 50, 100 and 150 mg N/L as nitrate were prepared from a 200 mg/L nitrate stock solution. Fluoride and nitrate calibration standards containing 12.5 mgC/L HA, TA or AA were analysed and the change in ISE response (mV) was recorded. Figure A1.4 shows the influence of OM on the fluoride and nitrate ISE response. The presence of OM reduced the ISE response, particularly with HA at low fluoride and nitrate concentrations. Subsequently, fluoride and nitrate concentration in the absence and presence of OM (12.5 mgC/L HA, TA or AA) was ascertained using different regressions performed on the calibration standards (Table A1.1).

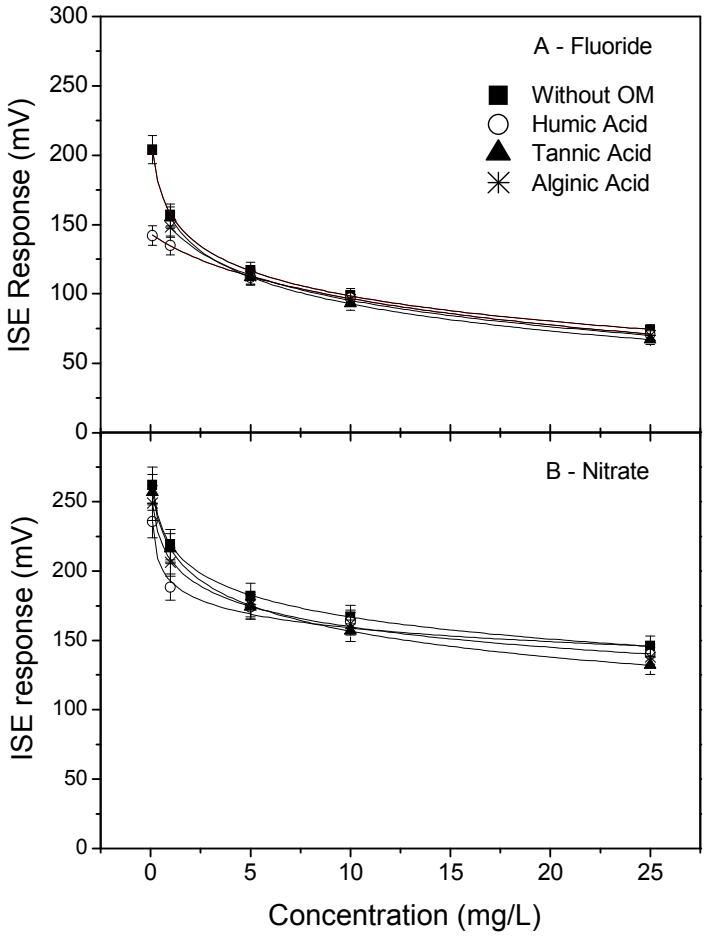

Figure A1.4. Ion-selective electrode (ISE) response (mV) calibration for (A) fluoride and (B) nitrate in the absence and presence of organic matter (1mM $NaHCO_3$; 85.5 mM NaCl; 12.5 mgC/L HA, TA or AA; pH 7).

Table A1.1. Regression equations used to quantify fluoride and nitrate concentration in experimental samples and correlation coefficients (R).

Inorganic	Fluoride	Nitrate
Without OM	y = -23.497 ln(x) + 152.89 R > 0.99	y = -21.085 ln(x) + 215.56 R > 0.99
Humic Acid	y = -12.317 ln(x) + 123.29 R > 0.85	y = -16.194 ln(x) + 196.05 R > 0.97
Tannic Acid	y = -27.281 ln(x) + 155.38 R > 0.99	y = -22.665 ln(x) + 209.14 R > 0.99
Alginic Acid	y = -24.001 ln(x) + 149.54 R > 0.99	y = -19.689 ln(x) + 205.25 R > 0.99

A1.5 Nutrient Analyser

The instrument (Quickchem 8500 FIA Nutrient Analyser, Lachat Instruments, Colorado, USA) used for the determination of nitrate in experimental samples is shown in Figure A1.5. Samples are buffered to pH 8.5 with an ammonium chloride (NH_4Cl) buffer solution before nitrate is quantitatively reduced to nitrite by passage of the samples through a copperised cadmium column. Possible interferences can arise from other metals present in the samples, therefore, disodium ethylenediamine tetraacetic acid dehydrate (EDTA) is added to the NH_4Cl buffer solution. The nitrate (reduced nitrate plus nitrite) is then determined by diazotising (to convert an amine into a diazo compound (R-N:N- where R is an aromatic hydrocarbon)) with a sulphanilamide colour reagent followed by coupling with N-(1-napthyl)ethylenediamine dihydrochloride (NED). This converts the sample to a water soluble dye (magenta in colour) which is read at a wavelength of 520 nm and the resultant peak area is reported in mV/s.

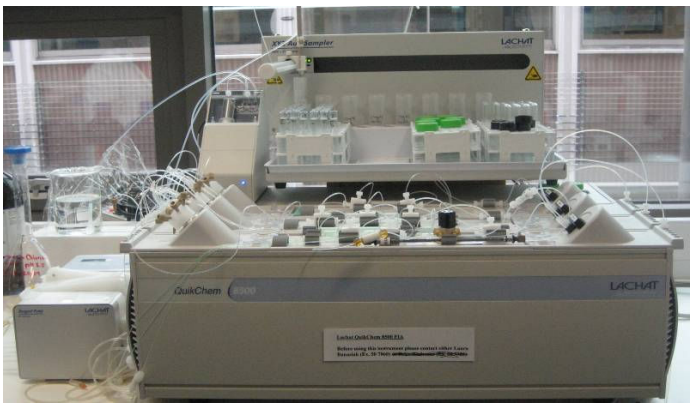

Figure A1.5. Quickchem 8500 FIA Nutrient Analyser.

Calibration standards of 0.2, 0.4, 1, 4, 8 and 20 mg N/L as nitrate were prepared from a 200 mg N/L stock solution. Nitrate concentration in the experimental samples was ascertained from a linear regression performed on the calibration standards (Figure A1.6). The detection limit for the determination of nitrate was 0.01 mg N/L. The standards and samples were both measured in 4 replicates.

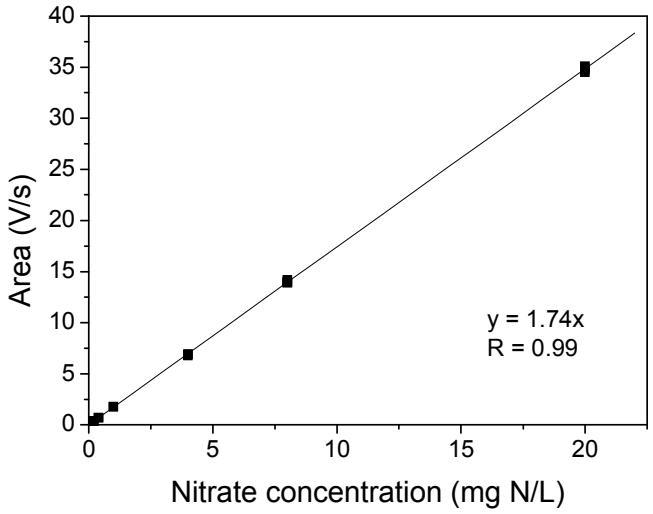

Figure A1.6. Nitrate (mg N/L) calibration (mgC/L) calibration (1mM $NaHCO_3$; 85.5 mM NaCl; 0.2, 0.4, 1, 4, 8 and 20 mg N/L as NO_3; pH 7).

A1.6 UV-Visible Spectroscopy

The UV spectrophotometer shown in Figure A1.7 (Varian Cary 100 Scan, Palo Alto, USA) measures light absorbed by an aqueous sample at a specific wavelength (λ). When light passes through a sample containing different organic compounds the light will be absorbed by the organics causing a reduction in the strength of the light. UV-Vis spectra are good surrogates to monitor the concentration of aqueous OM in environmental and experimental samples. In general, OM in water absorbs light in UV (200-400 nm) and visible (Vis: 400-700 nm) regions (Wang and Hsieh, 2001). UV absorbance at 254 nm is the most commonly used method. An absorbance of zero at a particular wavelength means that no light is absorbed, while an absorbance of 1 means that 90 % of light at that wavelength is absorbed. An absorbance greater than 1 means that more than 90 % of light at that wavelength is absorbed.

Figure A1.7. Varian Cary 100 Scan UV-Visible Spectrophotometer.

Calibration standards and experimental samples (3.5 mL) were analysed in a 1 cm path length quartz cuvette (Sigma Aldrich, Gillingham, UK). Ultrapure water was used as a reference and samples were measured at room temperature. Standards and samples were analysed prior to refrigeration to avoid possible coagulation changes, which can be enhanced at low temperature. UV-Vis spectroscopy in scanning mode (200-500 nm) was performed on standards (12.5 mgC/L) of HA, TA and AA in order to determine the suitable wavelengths for OM concentration estimation in experimental samples. The absorbance of HA, TA and AA (1/cm) as a function of wavelength and solution pH are shown in Figure A1.8. The UV-VIS spectra for HA showed no distinct absorbance peaks and was not affected by solution pH. No absorbance was detected for AA due to its lack of aromatic functional groups. The spectra of TA varied with solution pH, with peaks appearing at 225 nm above pH 9. The limits of the absorption scan at low (< 200 nm) and high wavelengths (500 nm) can be attributed to interferences from inorganic compounds within the OM and low absorbance, respectively (Schäfer, 2001).

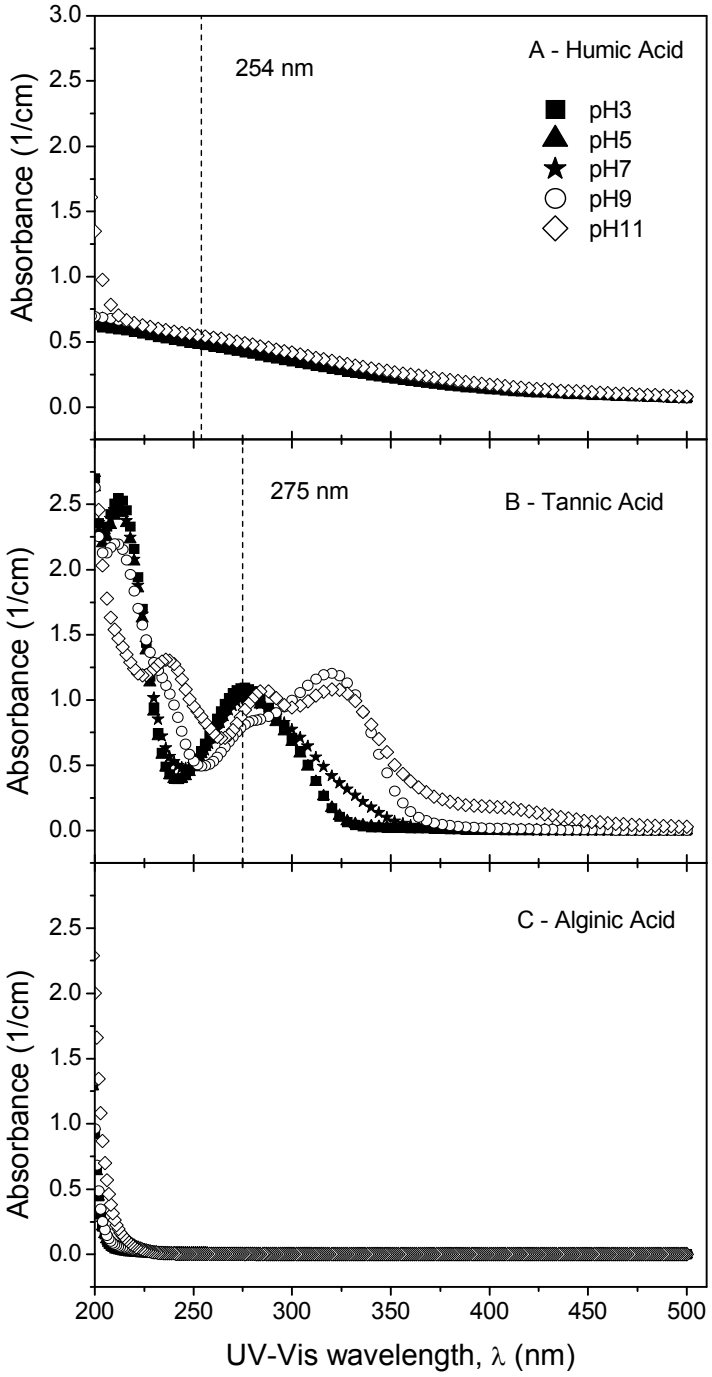

Figure A1.8. UV spectra of HA, TA and AA (1mM $NaHCO_3$, 85.5 mM NaCl, 12.5 mgC/L; pH 3-11).

Absorbance is also dependent on OM concentration; thus an absorbance scan of HA was undertaken at various concentrations (0.1, 0.5, 1, 5, 7, 10, 12.5, 20, 50, 70, 80 and 100 mgC/L). UV spectra of HA as a function of HA concentration is shown in

Figure A1.9. The absorbance measured at wavelengths less than 250 nm was higher than those measured at longer wavelengths and sharp increases in slope were noted at shorter wavelengths. This phenomenon was more pronounced at higher HA concentration, particularly at a HA concentration of 12.5 mgC/L. The absorbance at longer wavelengths (> 350 nm) was relatively low compared with those observed between 190 and 350 nm. Therefore, for the quantification of HA, higher resolution and accuracy in measurement of OM concentration would be achieved at a shorter wavelength. These results are comparable to those reported by Wang and Hsieh (2001).

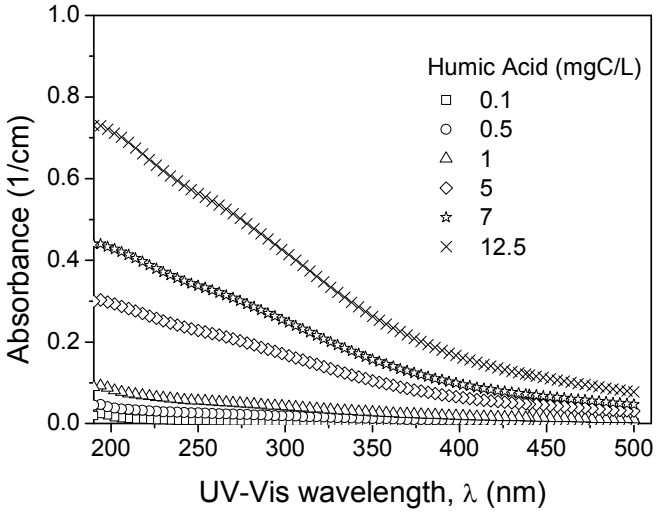

Figure A1.9. UV-Vis spectra of HA in water at different concentrations (1mM $NaHCO_3$, 85.5 mM NaCl, 0.1, 0.5,1 5, 7 and 12.5 mgC/L HA).

HA and TA were measured at wavelengths of 254 and 275 nm, respectively, which is in accordance with literature (Shutava and Prouty, 2005; Wang and Hsieh, 2001). Since no absorbance was observed for AA, concentration analysis could not be undertaken using UV-Vis spectroscopy. TOC analysis was undertaken to determine the concentration of AA within experimental samples in Chapter 5. Calibration standards of 0.1, 0.5, 1, 5, 7, 10 and 12.5 mgC/L were prepared from 100 mgC/L stock solutions of each OM. An estimation of the concentration of HA and TA within samples in Chapter 5, 7 and 8 was ascertained from a linear regression performed on the calibration standards (Figure A1.10A).

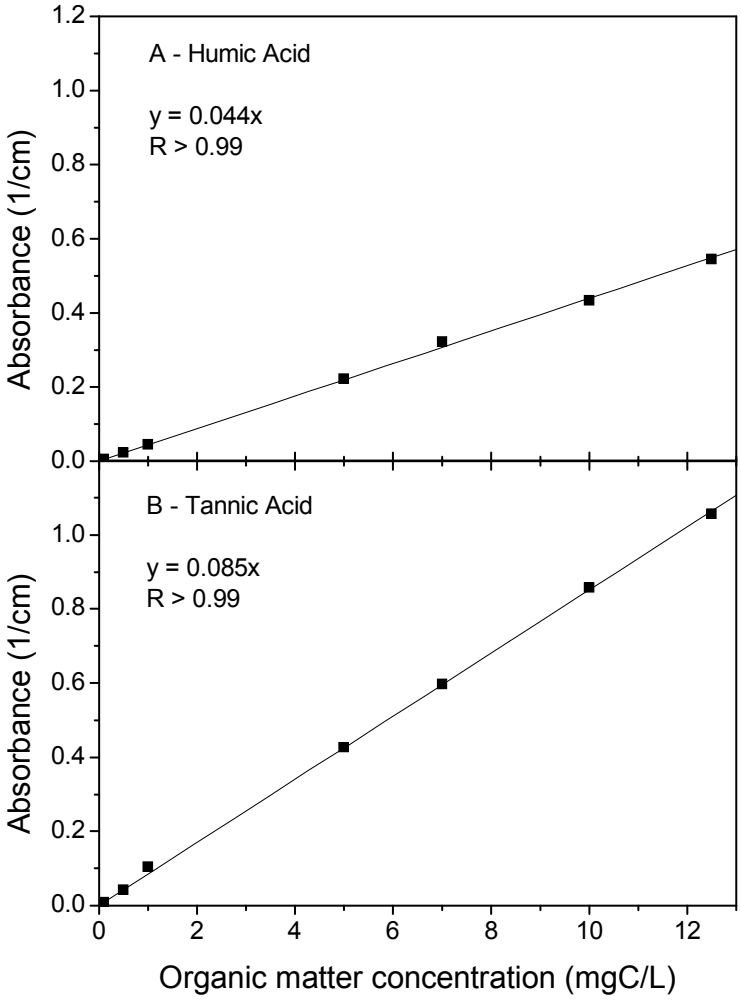

Figure A1.10. Organic matter concentration (mgC/L) calibration for HA and TA using UV-Vis (1mM $NaHCO_3$, 85.5 mM NaCl, pH 7).

A1.7 Total Organic Carbon Analysis

The instrument used for TOC analysis of HA, TA and AA (TOC-VCPH, Shimadzu, Milton Keyes, UK) is shown in Figure A1.11. Non-purgeable organic carbon (NPOC) mode is recommended for samples with more inorganic carbon (IC) than TOC i.e. samples that do not contain significant levels of purgeable organic carbon (volatile organics which could be sparged from the sample during the sparging process). Samples and standards are pre-acidified to pH 2-3 with HCl (1.5 % of 2 M) in order to convert the IC component to CO_2. Sparge gas (nitrogen) is introduced into the sample vials to eliminate the IC component. The sample is then subjected to total

carbon (TC) analysis where the remaining TC is introduced into a combustion tube, filled with a TOC standard oxidation catalyst, and heated to 680°C. The sample is burned in the combustion tube and as a result the TC components are converted to CO_2. Immediately following this, the sample is measured as TOC using the NPOC method.

Figure A1.11. Shimadzu TOC-VCPH total organic carbon analyser.

The oxidation efficiency of an OM is generally not 100 % during TOC analysis due to the stability of the OM and solution chemistry within the TOC analyser (Spyres *et al.*, 2000). In order to assess the oxidation efficiency of each OM, calibration standards of HA, TA and AA (0.5, 1, 2, 5 and 10 mgC/L from a 100 mgC/L stock solution) were measured against potassium hydrogen phthalate (PHP) standards (an IC reference standard with high oxidation efficiency). Calibration standards of 0.5, 1, 2, 5 and 10 mg C/L were prepared from a 1000 mgC/L PHP stock solution. The PHP was dried at 105-120°C for 1 hour and cooled in a dessicator prior to use. Figure A1.12 represents the calibration of the HA, TA and AA standards. If the oxidation efficiency was 100 % the slope is 1. The oxidation efficiencies of TA and AA were significantly higher than that of HA, as shown in Table A1.2. These results are dependent on the reliability of information regarding the carbon content of HA, TA and AA along with small error during calibration standard preparation.

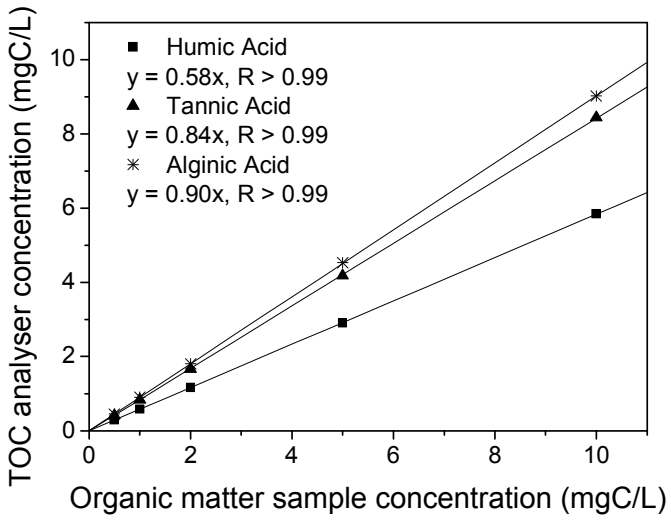

Figure A1.12. Calibration of TOC analyser from 0.5 to 10 mgC/L organic matter (1mM NaHCO3, 85.5 mM NaCl, pH 7).

Table A1.2. Oxidation efficiencies of humic, tannic and alginic acid with the Shimadzu TOC-VCPH total organic carbon analyser.

	Humic Acid	Tannic Acid	Alginic Acid
Oxidation efficiency (%)	58.3	84.2	90.3

To avoid sample carryover within the TOC analyser, it was never operated at an OM concentration greater than 12.5 mgC/L. Therefore, any samples that were suspected of being above this concentration were diluted (using the auto dilution mode on the TOC analyser) prior to analysis. The operating parameters of the system are outlined in Table A1.3. If the maximum standard deviation and coefficient of variation were met no additional sample injections are required. If both were exceeded, the samples were re-injected up to a maximum number of times specified (i.e. 5 injections as given in Table A1.3).

Table A1.3. Operational parameters of Shimadzu TOC-VCPH.

Parameter	Value
Sample volume (mL)	10
2M HCl acid addition volume (%)	1.5
Sparge time (min)	2
Number of needle washes with sample	2
Number of flow line washes	2
Calibration and sample replicates	3 of 5
Maximum standard deviation (S.D.)	0.1
Maximum coefficient of variation (C.V.) (%)	2

Organic matter concentration of HA, TA and AA (mgC/L) in experiments in Chapter 5 was subsequently ascertained from a linear regression performed on the PHP calibration standards (Figure A1.13). Due to the high organic content of samples in Chapter 7 and 8, from methanol in stock hormone and ES solutions, an estimation of HA concentration of these samples was undertaken using UV-Vis spectroscopy.

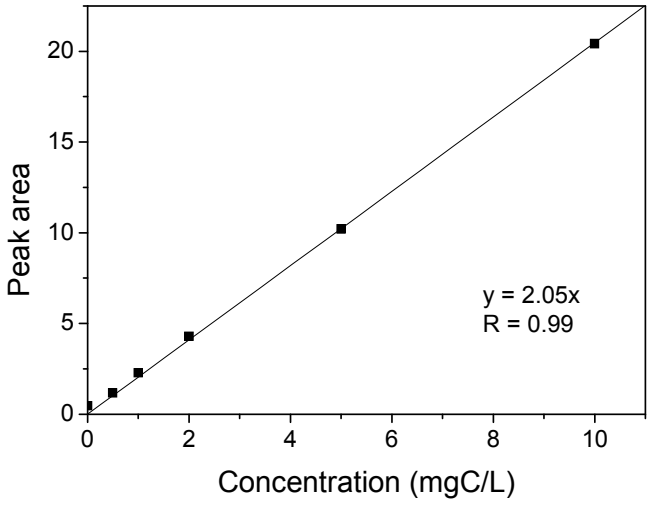

Figure A1.13. TOC concentration (mgC/L) vs. peak area (1mM NaHCO3, 85.5 mM NaCl, pH 7).

Check standards of PHP and HA, TA and AA were regularly analysed. A TOC system can accumulate organic substances in the instrument flow lines that can produce peaks. This affects the accuracy of TOC analysis; thus blank checks using

ultrapure water were run pre-, during and after sample analysis to flush the flow lines and check for sample carry-over.

A1.8 Liquid Scintillation Counting

A Beckman LS6500 liquid scintillation counter (Fullerton, USA), shown in Figure A1.14, was used to measure the concentration of radiolabeled hormones and ES within experimental samples in Chapter 7 and 8, respectively. Liquid scintillation counting involves the incorporation of a radiolabeled compound within a liquid medium (liquid scintillation cocktail) capable of converting the radioactive energy emitted by the compound during radioactive decay into light energy. This light energy is subsequently detected by the counter as counts per minute (CPM, number of light flashes/min). CPM is converted to disintegrations per minute (DPM), which are the units of activity, using an auto DPM calibration stored within the counter system.

Figure A1.14. Beckman Coulter LS 6500 scintillation counter.

The steroidal hormones were labelled with tritium (^{3}H) and ES was labelled with carbon (^{14}C), which are both beta emitters. Aqueous samples were mixed with a low level tritium counting liquid scintillation cocktail (Ultima Gold® LLT), which was also effective for ^{14}C counting. For the analysis of the radiolabeled hormones, a 0.5 mL sample was added to 3.5 mL liquid scintillation cocktail. The sample was shaken to allow for thorough mixing. Each sample was analysed in triplicate and counted for 10 minutes each. Counting precision was set at 2 % on the counter, indicating that in

95 out of 100 cases, the CPM will be within 2 % of the mean value. The percent error associated with ^{3}H DPM measurements was 2 %. Chemiluminescence (Lum-Ex, %), which indicates the percentage of the total CPM that is due to non-radioactive events (Beckman Coulter, 1999), was negligible in the analysis of radiolabeled hormones.

Although the counting efficiency of ^{14}C (≥95 %) counting is greater than that of ^{3}H (≥60 %), when using the same analysis method (10 minutes counting time, 3 replicates), the error associated with CPM values for ^{14}C-labelled ES was 10 %. This is attributed to the low activity of ES, which is radiolabeled in only 1 position compared to 4 positions for the hormones. Therefore, CPM and DPM values measured for a ^{14}C-labelled ES standard was significantly less than that measured for a ^{3}H-labelled hormone standard of the same concentration. This high error meant that calibration of ^{14}C-labelled ES using the same counting method as ^{3}H-labelled hormones was not possible. Another issue with ^{14}C counting was the chemiluminescence of the ES standards and samples. Although, Lum-EX values were less than 5-10 % (it needs to be less than this value) it was still higher (0.22 %) than that detected for the steroidal hormones. Therefore, adjustments to the ^{14}C method, as outlined in the following paragraph, needed to be made to reduce both the % error and % Lum-EX in-line with that of ^{3}H.

Initially the number of replicates was increased to 5, which reduced the error to approximately 6 %. The sample volume was increased from 0.5 mL to 1 mL in 7 mL liquid scintillation cocktail (to double the DPM values) and the counting time was then increased from 10 to 20 minutes per replicate. Like the ^{3}H-labelled hormone analysis, counting precision for ^{14}C-labelled ES was set at 2 %. The percent error associated with ^{14}C DPM measurements was reduced to 3 %. Lum-EX was also reduced to 0.01-0.02 %.

The presence of colour within the samples can reduce counting efficiency as it can absorb light emitted by the liquid scintillation cocktail (Beckman Coulter, 1999). Therefore, calibration of the steroidal hormones and ES were undertaken in the presence of 12.5 mgC/L HA (the OM concentration used during hormone and ES

sorption isotherm and ED experiments). For the hormones, calibration standards of 0.01, 0.1, 1, 10, 100 and 1000 ng/L were prepared from radiolabeled hormone stock solutions (100 μg/L). For ES, calibration standards of 0.01, 0.1, 1, 10, 100, 1000, 2000 and 5000 ng/L were prepared from radiolabeled ES stock solutions (100 μg/L). From these results, the liquid scintillation counting efficiency was determined by dividing the DPM values reported with HA by those without (Table A1.4). The influence of error in calibration standard preparation was minimal.

Table A1.4. Liquid scintillation counting efficiency (%), linear regression equations and correlation coefficients (R) in the absence and presence of humic acid.

Compound	Counting efficiency (%)		Linear equations and correlation coefficient (R)	
	Without OM	Humic Acid	Without OM	Humic Acid
Estradiol	100	99	y = 461.1x R > 0.99	y = 456.5x R > 0.99
Estrone	100	99	y = 286.8x R > 0.99	y = 283.9x R > 0.99
Progesterone	100	99	y = 391.5x R > 0.99	y = 387.6x R > 0.99
Testosterone	100	99	y = 371.7x R > 0.99	y = 367.9 R > 0.99
Endosulfan	100	99	y = 0.1054x R > 0.99	y = 0.1043x R > 0.99

Figure A1.15 shows the calibration curve for the hormones and ES without HA. The detection limits for estradiol, estrone, progesterone and testosterone were 1.02, 1.11, 1.03 and 1.07 ng/L, respectively. The detection limit for ES was 100 ng/L. As significant sorption of ES was expected to the ion-exchange membranes, 2000 ng/L was selected as the minimum radiolabeled ES concentration to be used in the sorption isotherm batch and ED experiments so as to reduce the error in samples with low ES concentrations.

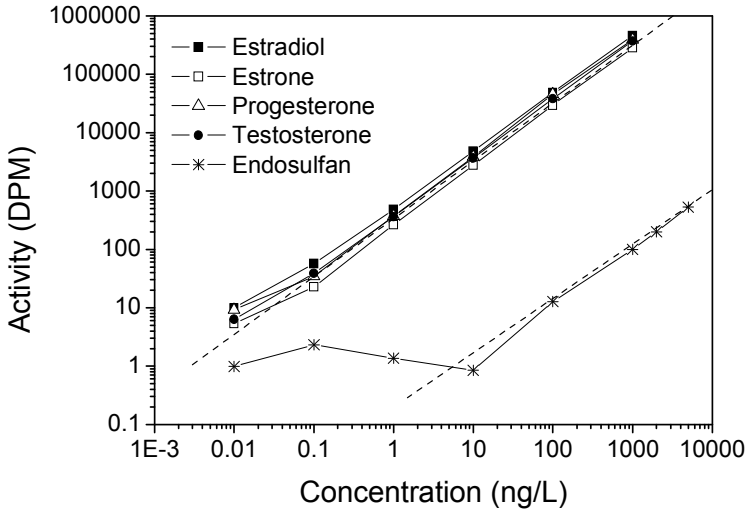

Figure A1.15. Calibration curves for radiolabeled steroid hormones and endosulfan (1mM $NaHCO_3$, 85.5 mM NaCl, pH 7).

A1.9 Liquid-Liquid Extraction

The analysis of the non-labelled ES compounds required pre-treatment and extraction as organochlorine pesticides need to be in a solvent phase before gas chromatographic analysis. Liquid-liquid extraction (LLE), which is also known as solvent-extraction, involves the separation of compounds depending on their relative solubilities within water and solvent. There are many methods used for extracting pesticides from aqueous solutions using the principle of liquid-liquid partitioning, with those involving the use of separation funnels or flasks the most common.

The equipment used for LLE is shown in Figure A1.16 and the extraction procedure was undertaken in a fumehood. Samples (100 mL) collected during ED experiments carried out at KU Leuven were added to separation flasks and firstly extracted with a 30 mL aliquot of analytical grade dichloromethane (CH_2Cl_2) (solvent phase). Trifluralin (5 µL of concentration 75 mg/L; 99.1 % purity; Reidel-de-Haën, Germany), an internal standard to calculate the recovery of organic compounds during the extraction and analysis procedure, was injected into the water phase. The separation flask was manually shaken and any gas that formed during this was

released. The flask was then mechanically shaken for 30 minutes (mark 160) on a KS501 Labortechnik digital shaker table (IKA, Germany). After allowing the water and solvent phase's time to separate, the solvent layer was filtered through anhydrous Na_2SO_4 (Acros Organics, Belgium) to remove all traces of water prior to GC analysis. A second 20 mL aliquot of dichloromethane was added and the same shaking and filtering method was repeated. The extracted sample (~ 50 mL) was heated to 65°C using a water bath (Haake W19, Thermo Fisher Scientific) to reduce the extracted volume to 1mL. This extract was transferred to a vial for analysis using gas chromatography with electron capture detection (GC-ECD), as described in the next section.

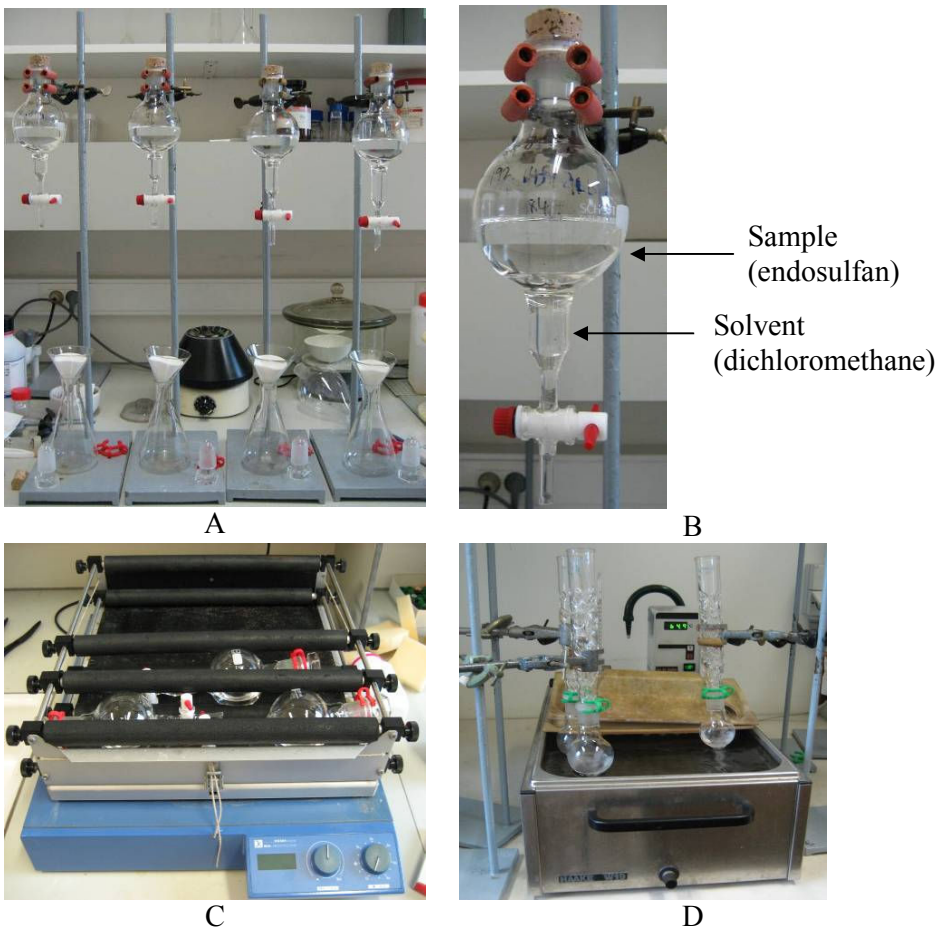

Figure A1.16. Liquid-liquid extraction equipment (LLE) (A) Separation, drying and solvent collection (B) Close up of separation flask showing sample water and solvent phases (C) mechanical shaker and (D) water bath.

A1.10 Gas Chromatography-Electron Capture Detection

GC-ECD has been the most widely used analytical technique for determining low μg/L to ng/L levels of organochlorine pesticides including α- and β-ES and ES sulfate in air, water, wastewater, sediment, soil, fish, and various foods (Guerin, 2001). GC-ECD involves the vaporisation and injection of a liquid sample onto the head of the chromatographic column. The sample is then transported through the column by the flow of inert, gaseous mobile phase (e.g. N_2, He, H, CO_2). The column itself contains a liquid stationary phase which is adsorbed onto the surface of an inert solid. There are many detectors, with different levels of selectivity, which can be used in GC. The ECD contains electrodes and a beta emitting radiation source. Plasma is produced by the collision of electrons with the carrier gas. If a compound containing electronegative atoms is present, those electrons are 'captured', negative ions are formed, and the rate of electron collection decreases (Wentworth and Chen, 1981). The response of the detector is measured in mV and peaks areas of the detected compounds are reported as volts per second (V/s).

An Autosystem XL gas chromatograph equipped with an electron-capture detector (ECD) (Perkin Elmer, Waltham, USA) was used for the determination of ES compounds in the extracted samples. Table A1.5 outlines important characteristics of the gas chromatograph column used. The longer the column is the better the separation usually is. The carrier gas used was helium (He) and nitrogen (N_2) was used as the make-up gas in the detector. Sample volumes of 1 μL were injected. Identification of α-ES, β-ES, ES sulfate, ES diol and trifluralin was by retention times and observations of peak shape (Table A1.6). Quantitation of the ES compounds was made from the injection of standard solutions (10-2500 μg/L). All of the compounds analysed were measured at concentrations within their linear range on the ECD gas chromatograph.

Table A1.5. Gas chromatograph (GC) column details.

Parameter	Value
Column type	WCOT Fused Silica
Stationary phase	CP-Sil-8 CB
Column length (m)	50
Inside diameter (mm)	0.32
Outside diameter (m)	0.45
Film thickness (m)	1.20

Table A1.6. Retention times (min) of compounds analysed by Gas chromatography - Electron Capture Detection (GC-ECD).

Compound	Retention time (min)
Trifluralin	16.6
ES diol	24.4
α-ES	27.7
B-ES	32.2
ES sulfate	36.4

ES in the experimental samples was determined through a series of calculations relating to the extraction procedure and gas chromatographic analysis. The volume (ml) of sample extracted is given by eqn (A.1).

$$\begin{aligned}\text{Weight of sample (g)} &= \text{Sample and bottle weight (g) - Bottle weight (g)} \\ &= \text{Sample volume (mL)}\end{aligned} \quad \text{(A.1.)}$$

The above calculation assumes that at ambient temperature and pressure the sample has a density of 1 g/mL.

This sample volume is used in the calculation of the extraction 'concentration factor' (*CF*) (eqn (A.2)).

$$CF = \frac{\text{Sample volume (mL)}}{\text{Extract volume (mL)}} \quad \text{(A.2)}$$

The concentration factor was used to calculate the ES concentration within the sample (eqn (A.3)).

$$\text{Sample concentration } (\mu g / L) = \frac{\text{Extract concentration } (\mu g / L)}{CF} \quad \text{(A.3)}$$

The analytical results for each individual ES compound must be corrected for the extraction efficiency of the LLE procedure. The extraction efficiency of trifluralin was determined to be 85.7 ± 4.1 %.

The recovery correction factor (*RCF*) was calculated according to eqn (A.4).

$$RCF = \frac{\text{Concentration spiked } (\mu g/L)}{\text{Concentration analysed } (\mu g/L)} \quad \text{(A.4)}$$

The *RCF* of trifluralin was converted to recovery using eqn (A.5).

$$\text{Recovery } (\%) = \frac{1}{RCF} \times 100 \quad \text{(A.5)}$$

The concentration of the ES compounds analysed were multiplied by the *RCF* to give the original concentration present in the sample (eqn (A.6)).

$$\text{Sample concentration } (\mu g/L) = \text{Concentration analysed } (\mu g/L) \times RCF \quad \text{(A.6)}$$

Interferences arise from any substance capable of producing a response on the ECD at a retention time indistinguishable from the pesticide compounds to be analysed. Therefore, to avoid contamination of the ECD and the occurrence of errant peaks, all glassware was routinely cleaned. The glassware was rinsed with the last solvent used (dichloromethane). This was followed by detergent washing in a dishwasher. The glassware was then dried in an oven for 1 hour, cooled and rinsed with dichloromethane again prior to use. The limitations of the method are also governed by the linear range of the detector used and can be overcome by dilution or by adjustment of the initial sample volume. This was not an issue due to the low initial ES concentration (100 µg/L).

List of Abbreviations

AA	Alginic acid
ADWG	Australian drinking water guideline
AEM	Anion-exchange membrane
CEM	Cation-exchange membrane
CF	Concentration factor
C.I.	Confidence interval
COD	Chemical oxygen demand
CPM	Counts per minute
CPMAS	Cross-polarisation magic-angle spinning
C.V.	Coefficient of variation
DBPs	Disinfection-by-products
DOC	Dissolved organic carbon
DPM	Disintegrations per minute
DTA	Differential thermal analysis
DW	Drinking water
DWG	Drinking water guideline
E1	Estrone
E2	Estradiol
ED	Electrodialysis
EDCs	Endocrine disrupting chemicals
EDI	Electrodeionisation
EDR	Electrodialysis reversal
EDTA	Disodium ethylenediamine tetraacetic acid dehydrate
EDX	Energy dispersive x-ray spectroscopy
EEC	European Union Directive on the Quality of Water Intended for Human Consumption
ES	Endosulfan
EU	European Union
EVA	Ethylene vinyl acetate
FA	Fulvic acid
FIB-SEM	Focussed ion beam -Scanning electron microscopy
GAC	Granular activated carbon
GC-ECD	Gas chromatography-Electron capture detection
GW	Groundwater
HA	Humic acid
HLC	Henry's law constant
HS	Humic substances
IC	Ion chromatography
IC	Inorganic carbon
ICP-MS	Inductively coupled plasma-Mass spectroscopy
ICP-OES	Inductively coupled plasma-Optical emission spectroscopy
IEP	Isoelectric point
IR	Infrared spectroscopy
ISEs	Ion-selective electrodes

K.U. Leuven	Katholieke Universiteit Leuven
LCD	Limiting current density
LDPE	Low density polyethylene
LLE	Liquid-liquid extraction
LSC	Liquid scintillation counting
Lum-EX	Chemiluminescence
MAC	Maximum admissible concentration
MF	Microfiltration
MIPs	Molecularly imprinted polymers
MW	Molecular weight
NED	N-(1-napthyl)ethylenediamine dihydrochloride
NF	Nanofiltration
NMR	Nuclear magnetic resonance
NP	Nonylphenol
NPOC	Non-purgeable organic carbon
OC	Organic carbon
OM	Organic matter
P	Progesterone
PAC	Powdered activated carbon
PHP	Potassium hydrogen phthalate
PS-DVB	Polystyrene-divinylbenzene
PTFE	Teflon
PVC	Polyvinyl chloride
RBO	Remazol Brilliant Orange 3R
RCF	Recovery correction factor
RPM	Revolutions per minute
RO	Reverse osmosis
SEC	Specific energy consumption
S.D.	Standard deviation
SDBS	Sodium dodecylbenzene sulfonate
SPME	Solid-phase microextraction
STP	Sewage treatment plant
SUVA	Specific UV absorbance
SW	Surface water
T	Testosterone
TA	Tannic acid
TC	Total carbon
TDS	Total dissolved solids
THMs	Trihalomethanes
TISAB	Total ionic strength adjustment buffer
TOC	Total organic carbon
UF	Ultrafiltration
UV Abs	UV absorbance
UV-Vis	UV visible spectrophotometry
UW	Ultrapure water
VTG	Plasma vitellogenin
WHO	World Health Organization

List of Symbols

Chapter 1

K_M	Membrane-water partition coefficient (L/cm^3)

Chapter 2

B	Jones-Dole viscosity coefficient at 25°C (L/mol)
ΔG_{HB}	Relative number hydrogen bonds with water in ionic and pure solution (-)
$\Delta_{hyd}G^0$	Molar Gibbs free energy of hydration (kJ/mol)
K_{ow}	Octanol-water partition coefficient (-)
n	Number of water molecules within ion hydration shell (-)
pK_a	Acid dissociation constant (-)
Δr	Hydrated ionic radius (nm)
r	Crystal ionic radius (nm)
u	Ionic mobility ($\times 10^{-8}$ m^2/sV)

Greek Symbols

λ°equiv	Ion equivalent conductivity (cm^2/Ωequiv)
μ	Dipole moment (Debye units, D)

Chapter 3

A_{eff}	Effective membrane area (cm^2)
C_i	Concentration of component i in the solution phase (mol/m^3)
C_i^{c}	Product concentration of component i in the concentrate (mol/L)
C_i^{c}	Product concentration of component i in the concentrate (mol/L)
C_i^{d}	Product concentration of component i in the diluate (mol/L)
C_i^{fc}	Feed concentration of component i in the concentrate (mol/L)
C_i^{fd}	Feed concentration of component i in the diluate (mol/L)
C_i^m	Concentration of component i in the membrane phase (mol/m^3)
${}^bC_i^{\mathrm{c}}$	Concentration of component i in the concentrate bulk solution (mol/L)
${}^bC_i^{\mathrm{d}}$	Concentration of component i in the diluate bulk solution (mol/L)
${}^bC_{\mathrm{c}}^{\mathrm{d}}$	Concentration of cation c in the diluate bulk solution (mol/L)
${}^bC_s^{\mathrm{d}}$	Concentration of salt s in the diluate bulk solution (mol/L)
${}^mC_i^{\mathrm{c}}$	Concentration of component i in the concentrate membrane boundary layer (mol/L)
${}^mC_{\mathrm{c}}^{\mathrm{d}}$	Concentration of cation c in the diluate membrane boundary layer (mol/L)

${}^{m}C_i^{\mathrm{d}}$	Concentration of component *i* in the diluate membrane boundary layer (mol/L)
C_{oc}	Concentration of the solute in octanol (mol/L)
C_w	Concentration of the solute in water (mol/L)
D_i	Diffusion coefficient of component *i* in the solution phase (m^2/s)
D_i^m	Diffusion coefficient of component *i* in the membrane phase (m^2/s)
E_{stack}	Energy requirement for an electrodialysis stack (Wh/L)
F	Faraday constant (96500 C/mol)
G	Gibbs free energy
$\Delta_{hyd}G^0$	Molar Gibbs free energy of hydration (kJ/mol)
J_i	Flux of component *i* in the solution phase and membrane boundary layer (mol/m^2s)
J_i^m	Flux of component *i* in the membrane phase (mol/m^2s)
J_i^{con}	Flux of component *i* in the solution phase by convection (mol/m^2s)
J_{a}^m	Flux of anion *a* in the membrane phase (mol/m^2s)
J_{c}^m	Flux of cation *c* in the membrane phase (mol/m^2s)
h	Membrane spacer distance (m)
i	Current density (A/cm^2)
i_{lim}	Limiting current density (A/cm^2)
I	Current (A)
κ	Specific conductivity (S/m)
k_s^s	Mass transfer coefficient (m/s)
K_M	Membrane-water partition coefficient (L/cm^2, L/cm^3)
K_{OM}	Organic matter-water partition coefficient (L/kg)
K_{ow}	Octanol-water partition coefficient (-)
ΔL	Spacer mesh width (m)
m_i	Mobility coefficient of component *i* in solution phase (mol m/Js)
m_i^m	Mobility coefficient of component *i* in membrane phase (mol m/Js)
n	Number of cell pairs in electrodialysis stack (-)
$\mathrm{p}K_{\mathrm{a}}$	Acid dissociation constant (-)
P	Power consumption (Wh)
Q^{c}	Flow rate of concentrate parallel to the membrane surface (m^3/s)
Q^{d}	Flow rate of diluate parallel to the membrane surface (m^3/s)
Δr	Hydrated ionic radius (nm)
r	Crystal ionic radius (nm)
R	Gas constant (8.314 J/molK)
R^-	Cation-exchange membrane fixed charge (- charge)
r_{AEM}	Anion-exchange membrane specific resistance ($\Omega\ cm^2$)
r_{CEM}	Cation-exchange membrane specific resistance ($\Omega\ cm^2$)
R_{AEM}	Resistance of the anion-exchange membrane (Ω)
R_{cell}	Electrical resistance of a membrane cell pair (Ω)
R_{CEM}	Resistance of the cation-exchange membrane (Ω)
R_C	Concentrate electrical resistance (Ω)
R_D	Diluate electrical resistance (Ω)

R_{stack}	Electrical resistance of ED stack (Ω)
Re	Reynolds number (-)
Sc	Schmidt number (-)
Sh	Sherwood number (-)
t	Time (h)
T	Absolute temperature (K)
T_c	Transport number of cation c in the membrane boundary layer
T_i	Transport number of counter-ion component i in the membrane boundary layer
T_c^m	Transport number of a cation c in the membrane
T_i^m	Transport number of counter-ion component i in the membrane
u	Ionic mobility ($\times 10^{-8}$ m^2/sV)
U	Electrical potential/applied voltage (V)
v	Linear flow velocity (m/s)
V_D	Volume of the diluate (L)
x, y, z	Direction coordinate
Δz	Membrane boundary layer thickness (m)
z_c	Valence of cation (C/mol)
z_i	Valence of component i (equiv/mol)

Greek Symbols

φ	Electrochemical potential in the solution phase (V)
φ_{Don}	Donnan potential (V)
φ^m	Electrochemical potential in the membrane phase (V)
η_m	Membrane manifold efficiency (-)
η_p	Pump efficiency (-)
η_s	Membrane selectivity (-)
η_w	Water transport efficiency (-)
ξ	Current utilisation (-)
δ	Membrane boundary layer thickness (m)
δ^+	Hydrogen donor
δ^-	Hydrogen acceptor
μ	Dipole moment (Debye units, D)
μ_i	Electrochemical potential of component i in the solution phase (J/mol)
μ_i^m	Electrochemical potential of component i in the membrane phase m (J/mol)
μ_i°	Electrochemical potential of a pure component i under standard temperature and pressure conditions in the solution phase (J/mol)
$\mu_i^{m\circ}$	Electrochemical potential of a pure component i under standard temperature and pressure conditions in the membrane phase m (J/mol)
ν	Kinematic viscosity (m^2/s)
ν_c	Stoichiometric coefficient for a cation c (-)
γ_i	Activity coefficient of component i in the solution phase (-)
γ_i^m	Activity coefficient of component i in the membrane phase m (-)

Chapter 4

A_{eff}	Effective membrane area (cm^2)
A_{trans}	Membrane area used in the transport of the respective component (m^2)
$C_{AEM/CEM}$	Concentration of solute sorbed per unit volume of AEM or CEM (ng/cm^3, $\mu g/cm^3$)
C_D^0	Initial diluate concentration or value (mg/L, mS/cm, g/L)
$C_{D/C}^0$	Initial diluate or concentrate OM concentration or value (mgC/L)
$C_{FD/D/C}^0$	Initial concentration of hormone or ES in the feed, diluate or concentrate (µg/L)
$C_{FD/D/C}^t$	Concentration of hormone or ES in the feed, diluate or concentrate (µg/L) at time t (h)
$C_{D/C}^t$	Diluate or concentrate concentration (mgC/L) in time t (h)
C_D^t	Diluate concentration or value (mg/L, mS/cm, g/L) in time t (h)
C_{FD}	Feed concentration (mg/L)
C_{stack}	Mass of solute sorbed per unit volume of membrane within ED stack ($\mu g/cm^3$)
C_w^0	Initial solute concentration in solution phase w (µg/L, ng/L)
C_w^t	Solute concentration in solution phase w at time t (ug/L, ng/L)
D_s	Diffusion coefficient of salt s in the solution phase (m^2/s)
f_w	Fraction of solute freely dissolved at equilibrium (%)
F	Faraday constant (96500 C/mol)
h	Membrane spacer distance (m)
i	Current density (mA/cm^2)
i_{lim}	Limiting current density (mA/cm^2)
I	Current (A)
J	Flux (mg/cm^2h, g/m^2h, $mS/cm/cm^2h$)
k	Total dissolved solids conversion factor
$K_{AEM/CEM}$	Water-membrane partition coefficient for the AEM or CEM (L/cm^3)
K_{OM}	Organic matter-water partition coefficient (L/kg)
ΔL	Spacer mesh width (cm)
$m_{ADS\text{-}HA}$	Mass of hormone sorbed to HA (µg)
$m_{AEM/CEM}$	Mass of solute sorbed on the AEM or CEM (µg, ng)
m_C	Mass of solute within the concentrate (mg, g, mS/cm)
$m_{FD/D/C}^0$	Initial mass of hormone or ES in the feed, diluate or concentrate (µg)
m_{FD}^e	Mass of hormone freely dissolved in the feed at hormone-HA equilibrium (µg)
$m_{FD/D/C}^t$	Mass of hormone or ES in the feed, diluate or concentrate (µg) at time t (h)
m_{DEP}	Mass of solute deposited on the membranes per unit volume(mg/cm^3)
m_{HA}	Mass of HA (kg)
m_w^0	Initial mass of solute in the solution phase w (µg, ng)
m_{FD}^0	Initial mass of solute in the feed (µg)
m_{FD}^t	Mass of hormone in the feed (µg) at time t (h)

m_{stack}	Mass of solute sorbed to membranes within ED stack (µg)
m_w^t	Mass of solute in the solution phase *w* at time *t* (h)
n	Number of samples taken
n_i	Sorption isotherm linearity (-)
P	Power consumption (Wh)
PR_{FD}	Predicted membrane sorption of hormone due to hormone-HA interactions (%)
Q	Flow rate (L/min)
R_C	Removal from the concentrate (%)
R_D	Removal from the diluate (%)
R_{FD}	Removal from the feed (%)
R_{stack}	Electrical resistance of ED stack (Ω)
s	Standard deviation
Sc	Schmidt number (-)
Sh	Sherwood number (-)
t	Time (s, h)
t	Degrees of freedom (95 %)
U	Electrical potential/applied voltage (V)
v	Linear flow velocity (m/s)
$V_{AEM/CEM}$	Volume of AEM or CEM (cm^3)
V_C^t	Concentrate volume (L) at time *t* (h)
V_D^t	Diluate volume (L) at time *t* (h)
V_{FD}	Feed volume (L)
$V_{FD/D/C}^0$	Initial feed, diluate or concentrate volume (L)
$V_{FD/D/C}^t$	Feed, diluate or concentrate volume (L) at time *t* (h)
V_{stack}	Total membrane volume in the ED stack (cm^3)
V_{trans}	Membrane volume used in solute transport (cm^3)
V_w^0	Initial solution volume (L)
V_w^t	Solution volume in time *t* (h)
x_i	Sample value
$\bar{x}$	Sample mean
z	Valence (equiv/mol)

Greek Symbols

θ	Contact angle (º)
ν	Kinematic viscosity (m^2/s)

Chapter 5

A	Electrostatic constant (-)
c	Concentration (mol)
B	Jones-Dole viscosity coefficient at 25°C (L/mol)
ΔG	Change in Gibbs free energy
ΔG_{HB}	Relative number hydrogen bonds with water in ionic and pure solution (-)
$\Delta_{hyd}G_{calc}^0$	Calculated Gibbs free energy (kJ/mol)

$\Delta_{tr}G^*$	Gibbs free energy of transfer of ions from heavy to light water
ΔH	Change in Enthalpy (Joule)
I	Current (A)
η	Viscosity of salt solution (mPa.s)
η_0	Viscosity of water (mPa.s)
pK_a	Acid dissociation constant (-)
R	Correlation coefficient (-)
R	Electrical resistance (Ω)
R_D	Removal from the diluate (%)
ΔS	Change in entropy (Joule/K)
t	Time (min)
t_{DWG}	Time to drinking water guideline (min)
ΔT	Change in temperature (K)
U	Electrical potential/applied voltage (V)

Greek Symbols

δ	Membrane boundary layer thickness (m)
δ^+	Hydrogen donor
δ^-	Hydrogen acceptor

Chapter 6

aq	Dissolved uncharged species
Eh	Redox value
F	Faraday constant (96500 C/mol)
$i_{\lim}$	Limiting current density (mA/cm^2)
IAP	Ionic activity product
K_{sp}	Solubility product
m_{DEP}	Mass of inorganic deposited (mg/cm^3)
pK_a	Acid dissociation constant (-)
Δr	Hydrated ionic radius (nm)
r	Crystal ionic radius (nm)
R_D	Removal from the diluate (%)
s	Solid species
t	Time (min)
u	Ionic mobility ($\times 10^{-8}$ m^2/sV)
z	Valence

Greek Symbols

Ω	Saturation index/Scaling potential
λ°equiv	Ion equivalent conductivity (cm^2/Ωequiv)

Chapter 7

A	Hydrogen bonding facilitated through hormone hydrogen acceptor groups
A_m	Membrane area (cm^2)

$C_{AEM/CEM}$	Concentration of hormone sorbed per unit volume of AEM or CEM (ng/cm^3, µg/cm^3)
C_s	Concentration of estrone sorbed to the membrane per unit area (ng/cm^2)
C_{stack}	Mass of hormone sorbed per unit volume of membrane within ED stack (µg/cm^3)
C_w	Concentration of estrone freely dissolved in solution (ng/L)
C_w^t	Hormone concentration (ng/L) in solution phase w at time t = 170 hours
D	Hydrogen bonding facilitated through hormone hydrogen donor groups
f_{neutral}	Fraction of neutral species (%)
f_w	Fraction of hormone freely dissolved in the feed (%)
K_{OM}	Organic matter-water partition coefficient (L/kg)
K_{ow}	Octanol-water partition coefficient (-)
$K_{AEM/CEM}$	Water-membrane partition coefficient for the AEM or CEM (L/cm^3)
K_M	Membrane-water partition coefficient (L/cm^2)
log K_α	Hydrogen bonding strength of hydrogen acceptor (-)
log K_β	Hydrogen bonding strength of hydrogen donor (-)
$m_{ADS\text{-}HA}$	Mass of hormone sorbed to HA (µg)
m_{FD}^0	Initial mass of hormone in the feed (µg)
m_{FD}^e	Mass of hormone freely dissolved in the feed at hormone-HA equilibrium (µg)
m_m	Mass of estrone sorbed to membranes (ng/cm^2)
n_i	Sorption isotherm linearity (-)
pK_a	Acid dissociation constant (-)
PR_{FD}	Predicted membrane sorption of hormone due to hormone-HA interactions (%)
R_{FD}	Removal of hormone from the feed (%)
R	Correlation coefficient (-)
V_w	Solution volume (L)

Chapter 8

A	Hydrogen bonding facilitated through hormone hydrogen acceptor groups
$C_{AEM/CEM}$	Concentration of endosulfan sorbed per unit volume of AEM or CEM (ng/cm^3, µg/cm^3)
C_{stack}	Mass of endosulfan sorbed per unit volume of membrane within ED stack (µg/cm^3)
C_w^t	Endosulfan concentration (ng/L) in solution phase w at time t = 170 hours
D	Hydrogen bonding facilitated through hormone hydrogen donor groups
f_w	Fraction of solute freely dissolved at equilibrium (%)
H	Dimensionless Henry's law constant (-)
H_c	Henry's law constant (atm.m^3/mol)

$K_{AEM/CEM}$	Water-membrane partition coefficient for the AEM or CEM (L/cm^3)
K_{OC}	Organic carbon-water partition coefficient (cm^3/g)
K_{ow}	Octanol-water partition coefficient (-)
log K_{α}	Hydrogen bonding strength of hydrogen acceptor (-)
log K_{β}	Hydrogen bonding strength of hydrogen donor (-)
$m_{ADS\text{-}HA}$	Mass of solute sorbed to HA (μg)
n	Number of moles (-)
n_i	Sorption isotherm linearity (-)
V	Volume of gas (L)
p	Absolute pressure of gas (-)
q_{max}	Maximum sorption of endosulfan (mg/g)
R	Gas constant (0.082 L·atm/mol/K)
R	Correlation coefficient (-)
T	Temperature (K)

Chapter 9

R_D	Removal from the diluate (%)
pK_a	Acid dissociation constant (-)
$K_{AEM/CEM}$	Water-membrane partition coefficient for the AEM or CEM (L/cm^3)

Appendix 1

CF	Concentration factor (-)
RCF	Recovery correction factor (-)
R	Correlation coefficient (-)

Greek Symbols

θ	Contact angle (º)
λ	Wavelength (nm)

References

ABS, (2002). *Housing and Infrastructure in Aboriginal and Torres Strait Islander Communities Australia 2001*, Australian Bureau of Statistics, Canberra.

Abu, R. and Alsokhny, K., (2004). Geochemical assessment of groundwater contamination with special emphasis on fluoride concentration, North Jordan. *Chemie der Erde - Geochemistry*, **64** (2): 171-181.

ACD, (2007). *Chemsketch*, 10.0; Advanced Chemistry Development.

Agbedoko, K. M.; Legube, B. and Dard, S., (1996). Atrazine and simazine removal mechanisms by nanofiltration: Influence of natural organic matter concentration. *Water Research*, **30** (11): 2535-2542.

Ali, S. M.; Bowes, G. W. and Cohen, D. B., (1984). *Endosulfan Special Projects Report No. 84-7SP, Toxic Substances Control Program*, California State Water Resources Control Board, Sacramento, US.

Allison, R. P., (1995). Electrodialysis reversal in water reuse applications. *Desalination*, **103** (1-2): 11-18.

Al-Rifai, J. H., (2008). *Performance of water recycling technologies*. Doctor of Philosophy, The University of Wollongong, Wollongong, Australia.

Amor, Z.; Bariou, B.; Mameri, N.; Taky, M.; Nicolas, S. and Elmidaoui, A., (2001). Fluoride removal from brackish water by electrodialysis. *Desalination*, **133** (3): 215-223.

An, J. H. and Dultz, S., (2007). Adsorption of tannic acid on chitosan-montmorillonite as a function of pH and surface charge properties. *Applied Clay Science*, **36** (4): 256-264.

Antonius, G. F.; Byers, M. E. and Snyder, J. C., (1998). Residues and Fate of Endosulfan on Field-Grown Pepper and Tomato. *Pesticide Science*, **54** (1): 61-67.

Apperley, D., (2009). Personal communication, Solid-state ^{13}C NMR detection limits.

Araya-Farias, M. and Bazinet, L., (2006). Effect of calcium and carbonate concentrations on anionic membrane fouling during electrodialysis. *Journal of Colloid and Interface Science*, **296** (1): 242-247.

Asahi Glass Co Ltd, http://www.agc.co.jp.

Asahi Kasei Chemicals Co, http://www.asahi-kasei.co.jp/.

Astom Corporation, http://www.astom-corp.jp/en.

Astom Corporation, (2009). Neosepta product information. http://www.astom-corp.jp/en/en-main2-neosepta.html.

Atkins, P. W., (1990). *Physical chemistry*. 4 ed.; Oxford University Press, Oxford.

ATSDR, (2000a). *Toxicological profile for fluoride*, Agency for Toxic Substances and Disease Registry, Atlanta, USA.

ATSDR, (2000b). *Toxicological profile for boron*, Agency for Toxic Substances and Disease Registry, Atlanta, USA.

ATSDR, (2000c). *Toxicological profile for endosulfan*, Agency for Toxic Substances and Disease Registry, Atlanta, USA.

ATSDR, (2000d). *Toxicological Profile for Uranium*, Agency for Toxic Substances and Disease Registry, Atlanta, USA.

Audinos, R., (1989). Fouling of ion-selective membranes during electrodialysis of grape must. *Journal of Membrane Science*, **41**, 115-126.

Avaltroni, F.; Seijo, M.; Ulrich, S.; Stoll, S. and Wilkinson, K. J., (2007). Conformational Changes and Aggregation of Alginic Acid as Determined By Fluorescence Correlation Spectroscopy. *Biomacromolecules*, **8** (1): 106-112.

Avena, M. J.; Vermeer, A. W. P. and Koopal, L. K., (1999). Volume and structure of humic acids studied by viscometry: pH and electrolyte concentration effects. *Colloids and Surfaces A: Physicochemical and Engineering Aspects*, **151** (1-2): 213-224.

Awasthi, N.; Manickam, N. and Kumar, A., (1997). Biodegradation of endosulfan by a bacterial coculture. *Bulletin of Environmental Contamination and Toxicology*, **59** (6): 928-934.

Ayala-Bribiesca, E.; Araya-Farias, M.; Pourcelly, G. and Bazinet, L., (2006a). Effect of concentrate solution pH and mineral composition of whey protein diluate solution on membrane fouling formation during conventional electrodialysis *Journal of Membrane Science*, **280** (1-2): 790-801.

Ayala-Bribiesca, E.; Pourcelly, G. and Bazinet, L., (2006b). Nature identification and morphology characterization of cation-exchange membrane fouling during conventional electrodialysis. *Journal of Colloid and Interface Science*, **300** (2): 663-672.

Badruzzaman, M.; Oppenheimer, J.; Adham, S. and Kumar, M., (2009). Innovative beneficial reuse of reverse osmosis concentrate using bipolar membrane electrodialysis and electrochlorination processes *Journal of Membrane Science*, **326** (2): 392-399.

Barceló, D., (1993). Environmental Protection Agency and other methods for the determination of priority pesticides and their transformation products in water. *Journal of Chromatography A*, **643** (1-2): 117-143.

Baronti, C.; Curini, R. D.; Ascenzo, G.; Di Corcia, A.; Gentili, A. and Samperi, R., (2000). Monitoring natural and synthetic estrogens in activated sludge sewage treatment plants and in receiving river water. *Environmental Science and Technology*, **34** (24): 5059-5066.

Bassett, R. L.; Buszka, P. M.; Davidson, G. R. and Chong-Diaz, D., (1995). Identification of groundwater solute sources using boron isotopic composition. *Environmental Science and Technology*, **29** (12): 2915-2922.

Bazinet, L. and Araya-Farias, M., (2005). Effect of calcium and carbonate concentrations on cationic membrane fouling during electrodialysis. *Journal of Colloid and Interface Science*, **281** (1): 188-196.

Beckman Coulter, (1999). *LS 6500 Scintillation System Operating Manual*, Fullerton, USA.

Belfroid, A. C.; Van der Horst, A.; Vethaak, A. D.; Schafer, A. J.; Rijs, G. B. J.; Wegener, J. and Cofino, W. P., (1999). Analysis and occurrence of estrogenic hormones and their glucuronides in surface water and waste water in The Netherlands. *Science of the Total Environment*, **225** (1-2): 101-108.

Berg, P.; Hagmeyer, G. and Gimbel, R., (1997). Removal of pesticides and other micropollutants by nanofiltration. *Desalination*, **113** (2-3): 205-208.

Berg, P., (2002). *Rückhaltung von in der Trinkwasseraufbereitung relevanten*

organischen Spurenstoffen durch Nanofiltrationsmembranen. PhD, Duisburg-Essen University, Germany.

Bertolino, F. A.; Torriero, A. A. J.; Salinas, E.; Olsina, R.; Martinez, L. D. and Raba, J., (2006). Speciation analysis of selenium in natural water using square-wave voltammetry after preconcentration on activated carbon. *Analytica Chimica Acta*, **572** (1): 32-38.

Boulay, F. and Perdiz, D., (2005). 17β-Estradiol modulates UVB-induced cellular responses in estrogen receptors positive human breast cancer cells. *Journal of Photochemistry and Photobiology B: Biology*, **81** (3): 143-153.

Bowman, J. C.; Zhou, J. L. and Readman, J. W., (2002). Sediment-water interactions of natural oestrogens under estuarine conditions. *Marine Chemistry*, **77** (4): 263-276.

Braungardt, C. B.; Achterberg, E. P.; Elbaz-Poulichet, F. and Morley, N. H., (2003). Metal geochemistry in a mine-polluted estuarine system in Spain *Applied Geochemistry*, **18** (11): 1757-1771

Browne, D.; Whelton, H. and O'Mullane, D., (2005). Fluoride metabolism and fluorosis. *J. Dentistry*, **33** (3): 177-186.

Budavari, S., (1996). *The Merck Index. An encyclopedia of Chemicals, Drugs, and Biologicals*. 11th ed.; Merck & Co., Inc., Rahway, NJ, USA.

Burke, K., (2009). Pesticide blamed for fish mutations. *Sydney Morning Herald*, http://www.smh.com.au/news/national/pesticide-blamed-for-fish-mutations/2009/01/13/1231608708295.html.

Capkin, E.; Altinok, I. and Karahan, S., (2006). Water quality and fish size affect toxicity of endosulfan, an organochlorine pesticide, to rainbow trout. *Chemosphere*, **64** (10): 1793-1800.

Carey, C. and Bryant, C. J., (1995). Possible interrelations among environmental toxicants, amphibian development, and decline of amphibian populations possible interrelations among environmental toxicants, amphibian development, and decline of amphibian populations. *Environmental Health Perspectives*, **103** (Supp. 4): 13-18.

Carson, R., (1962). *Silent Spring*. Houghton Mifflin, Boston, USA.

Casademont, C.; Araya-Farias, M.; Pourcelly, G. and Bazinet, L., (2008a). Impact of electrodialytic parameters on cation migration kinetics and fouling nature of ion-exchange membranes during treatment of solutions with different magnesium/calcium ratios. *Journal of Membrane Science*, **325** (2): 570-579.

Casademont, C.; Pourcelly, G. and Bazinet, L., (2008b). Effect of magnesium/calcium ratios in solutions treated by electrodialysis: Morphological characterization and identification of anion-exchange membrane fouling. *Journal of Colloid and Interface Science*, **322** (1): 215-223.

Cerrillo, I.; Granada, A.; Lopez-Espinosa, M. J.; Olmos, B.; Jimenez, M.; Cano, A.; Olea, N. and Fatima Olea-Serrano, M., (2005). Endosulfan and its metabolites in fertile women, placenta, cord blood, and human milk. *Environmental Research*, **98** (2): 233-239.

Chang, T. W. and Wang, M. K., (2002). Assessment of sorbent/water ratio effect on adsorption using dimensional analysis and batch experiments. *Chemosphere*, **48** (4): 419-426.

Chang, T. W.; Wang, M. K. and Lin, C., (2002). Adsorption of copper in the different sorbent/water ratios of soil systems. *Water, Air and Soil Pollution*,

138 (1-4): 199-209.
Chang, S.; Waite, T. D.; Schäfer, A. I. and Fane, A. G., (2003). Adsorption of the endocrine-active compound estrone on microfiltration hollow fiber Membranes. *Environmental Science and Technology*, **37** (14): 3158-3163.
Chang, M. Y. and Juang, R. S., (2004). Adsorption of tannic acid, humic acid, and dyes from water using the composite of chitosan and activated clay. *J. Colloid Interface Science*, **278** (1): 18-25.
Chauveheid, E. and Denis, M., (2004). The boron–organic carbon correlation in water. *Water Research*, **38** (7): 1663–1668.
Chefetz, B.; Ilani, T.; Schultz, E. and Chorover, J., (2006). Wastewater dissolved organic matter: Characteristics and sorptive capabilities. *Water Science and Technology*, **53** (7): 51-57.
Chen, Y. and Schnitzer, M., (1976). Viscosity measurements on soil humic substances. *Soil Science Society of America Journal*, **40**, 866-872.
Chian, E. S. K.; Bruce, W. N. and Fang, H. H. P., (1975). Removal of pesticides by reverse osmosis. *Environmental Science and Technology*, **9** (1): 52-59.
Chin, Y. P.; Aiken, G. and O'Loughlin, E., (1994). Molecular Weight, Polydispersity, and Spectroscopic Properties of Aquatic Humic Substances. *Environmental Science and Technology*, **28** (11): 1853-1858.
Clarkson, J. J. and McLoughlin, J., (2000). Role of fluoride in oral health promotion. *International Dental Journal*, **50** (3): 119-128.
Clotfelter, E. D.; Bell, A. M. and Levering, K. R., (2001). The role of animal behaviour in the study of endocrine-disrupting chemicals. *Animal Behaviour*, **68** (4): 665-676.
Cockell, K. A., (2003). Calcium. Properties and Determination. *Encyclopedia of Food Sciences and Nutrition*, 765-771.
Coleman, P. F. and Dolinger, P. M., (1982). *Endosulfan monograph number four: Environmental health evaluations of California restricted pesticides*, State of California Department of Food and Agriculture, Sacramento, USA.
Collins, M. R.; Amy, G. and Steelink, C., (1986). Molecular weight distribution, carboxylic acidity, and humic substances content of aquatic organic matter: implications for removal during water treatment. *Environmental Science and Technology*, **20** (10): 1028-1032.
Collins, K. D., (1995). Sticky ions in biological systems. *Proceedings of the National Academy of Sciences US*, **92** (12): 5553-5557.
Collins, K. D., (1997). Charge density-dependent strength of hydration and biological structure. *Biophysical Journal*, **72** (1): 65-76.
Comerton, A. M.; Andrews, R. C. and Bagley, D. M., (2009). The influence of natural organic matter and cations on the rejection of endocrine disrupting and pharmaceutically active compounds by nanofiltration. *Water Research*, **43** (3): 613-622.
Conway, B. E., (1981). *Ionic Hydration in Chemistry and Biophysics*. Elsevier, New York, USA.
Coradin, T. and Livage, J., (2003). Synthesis and characterization of alginate/silica biocomposites. *Journal of Sol-Gel Science and Technology*, **26** (1-3): 1165-1168.
Corti, H.; Crovetto, R. and Fernandez-Prini, R., (1980a). Mobilities and ion-pairing in $LiB(OH)_4$ and $NaB(OH)_4$ aqueous solutions. A conductivity study. *Journal*

of Solution Chemistry, **9** (8): 617-625.
Cotham, W. E. and Bidleman, T. F., (1989). Degradation of malathion, endosulfan, and fenvalerate in seawater and seawater/sediment microcosms. *Journal of Agricultural and Food Chemistry*, **37** (3): 824-828.
Cowan, D. A. and Brown, J. H., (1959). Effect of turbulence on limiting current in electrodialysis cells. *Industrial and Engineering Chemistry Research*, **51** (12): 1445-1448.
Croué, J. P.; Violleau, D.; Bodaire, C. and Legube, B., (1999). Removal of hydrophobic and hydrophilic constituents by anion exchange resin. *Water Science and Technology*, **40** (9): 207-214.
Cruz, B. H.; Díaz-Cruz, J. M.; Ariño, C. and Esteban, M., (2000). Heavy metal binding by tannic acid: A voltammetric study. *Electroanalysis*, **12** (14): 1130-1137.
Cui, C. W.; Ji, S. L. and Ren, H. Y., (2006). Determination of steroid estrogens in wastewater treatment plant of a contraceptives producing factory *Environmental Monitoring and Assessment*, **121** (1-3): 409-419.
D'Ascenzo, G.; Di Corcia, A.; Gentili, A.; Mancini, R.; Mastropasqua, R.; Nazzari, M. and Samperi, R., (2003). Fate of natural estrogen conjugates in municipal sewage transport and treatment facilities. *Science of the Total Environment*, **302** (1-3): 199-209.
Daughton, C. G., (2000). Pharmaceuticals in the environment: Overarching issues and concerns. *Abstracts of Papers American Chemical Society*, **219** (1-2): ENVR 29.
Davis, T. A.; Volesky, B. and Mucci, A., (2003). A review of the biochemistry of heavy metal biosorption by brown algae. *Water Research*, **37** (18): 4311-4330.
De Stefano, C.; Gianguzza, A.; Piazzese, D.; Porcino, N. and Sammartano, S., (2006). Sequestration of biogenic amines by alginic and fulvic acids. *Biophysical Chemistry*, **122** (3): 221-231.
Dean, J. A., (1999). *Lange's handbook of chemistry*. 15 ed.; McGraw-Hill, New York.
DEFRA, (2002). *The government's strategic review of diffuse water pollution from agriculture in England and Wales*, Department for Environment, Food and Rural Affairs, London, UK.
Demircioglu, M.; Kabay, N.; Kurucaovali, I. and Ersoz, E., (2003). Demineralization by electrodialysis (ED) - separation performance and cost comparison for monovalent salts. *Desalination*, **153** (1-3): 329-333.
Desbrow, C.; Routledge, E. J.; Brighty, G. C.; Sumpter, J. P. and Waldock, M., (1998). Identification of estrogenic chemicals in STW effluent: 1. Chemical fractionation and in vitro biological screening. *Environmental Science and Technology*, **32** (11): 1549-1558.
Devitt, E. C.; Ducellier, F.; Cote, P. and Wiesner, M. R., (1998). Effects of natural organic matter and the raw water matrix on the rejection of atrazine by pressure-driven membranes. *Water Research*, **32** (9): 2563-2568.
Devitt, E. C. and Wiesner, M. R., (1998). Dialysis investigations of atrazine-organic matter interactions and the role of a divalent metal. *Environmental Science and Technology*, **32** (s): 232-237.
Dray, J.; Dray, F.; Tiller, F.; Ulman, A. and –857., A. I. P., (1972). Hydrolysis of urine metabolites of different steroid hormones by (-glucuronidase from

Escherichia coli. *Annales de l''Institut Pasteur*, **123** (6): 853-857.
Dydo, P.; Turek, M.; Ciba, J.; Trojanowska, J. and Kluczka, J., (2005). Boron removal from landfill leachate by means of nanofiltration and reverse osmosis. *Desalination*, **185** (1-3): 131-137.
Earl, S. R. and Blinn, D. W., (2003). Effects of wildfire ash on water chemistry and biota in South-Western USA streams. *Freshwater Biology*, **48** (6): 1015-1030.
Eddleston, M.; Karalliedde, L.; Buckley, N.; Fernando, R.; Hutchinson, G.; Isbister, G.; Konradsen, F.; Murray, D.; Piola, J. C.; Senanyake, N.; Sheriff, R.; Singh, S.; Siwach, S. B. and Smit, L., (2002). Pesticide poisoning in the developing world - a minimum pesticides list. *The Lancet*, **360** (9340): 1163-1167.
Edge, V. E.; Ahmed, N. and Rohas, P., (1999). Aerial transport of endosulfan: vapour and dust movement, In: Schofield, N. J. and Edge, V. E., (Eds), *Minimising the impact of pesticides on the riverine environment: Key findings from research with the cotton industry-1998 Conference*, LWRRDC Occasional Paper 23/98, Land and Water Resources Research and Development Corporation, Canberra, Australia.
EEA, (2009). Present concentration of nitrate in groundwater bodies in European countries, European Environment Agency. http://dataservice.eea.europa.eu/atlas/viewdata/viewpub.asp?id=3423.
Einav, R.; Harussi, K. and Perry, D., (2002). The footprint of the desalination processes on the environment. *Desalination*, **152** (1-3): 141-154.
El Beit, I. O. D.; Wheelock, V. and Cotton, D. E., (1981). Factors affecting soil residues of dieldrin, endosulfan, γ-HCH, dimethoate, and pyrolan. *Ecotoxicology and Environmental Safety*, **5** (2): 135-160.
El Beit, I. O. D.; Cotton, D. E. and Wheelock, V., (1983). Persistence of pesticides in soil leachates: Effect of pH, ultraviolet irradiation and temperature. *International Journal of Environmental Studies*, **21** (3/4): 251-259.
Elleuch, M.; Sistat, P.; Pourcelly, G. and Amor, M. B., (2006b). Brackish water desalination by electrodialysis: opposing scaling. *Desalination*, **200** (1-3): 752-753.
Elmidaoui, A.; Elhannouni, F.; Menkouchi Sahli, M. A.; Chay, L.; Elabbassi, H.; Hafsi, M. and Largeteau, D., (2001). Pollution of nitrate in Moroccan ground water: removal by electrodialysis. *Desalination*, **136** (1-3): 325-332.
Elmidaoui, A.; Elhannouni, F.; Taky, M.; Chay, L.; Menkouchi Sahli, M. A.; Echihabi, L. and Hafsi, M., (2002). Optimization of nitrate removal operation from ground water by electrodialysis. *Separation and Purification Technology*, **29** (3): 235.
Environment Agency, (2006). *Pesticides Report 2006: Pesticides in rivers, groundwater and pollution incidents*, Rotherham, UK.
EPA, (1982). *Aquatic fate process data for organic priority pollutants Final report EPA-440/4-81-014*, U.S. Environmental Protection Agency, Washington DC, USA.
Ernst, W. R.; Jonah, P.; Doe, K.; Julien, G. and Hennigar, P., (1991). Toxicity to aquatic organisms of off-target deposition of endosulfan applied by aircraft. *Environmental Toxicology and Chemistry*, **10** (1): 103-114.
Escher, B. I.; Berg, M.; Mühlemann, J.; Schwarz, M. A. A.; Hermens, J. L. M.; Vaes, W. H. J. and Schwarzenbach, R. P., (2002). Determination of liposome/water partition coefficients of organic acids and bases by solid-phase

microextraction. *Analyst*, **127** (1): 42-48.
Escher, B. I.; Pronk, W.; Suter, M. J. and Maurer, M., (2006). Monitoring the removal efficiency of pharmaceuticals and hormones in different treatment processes of source-separated urine with bioassays. *Environmental Science and Technology*, **40** (16): 5095-5101.
EU, (1998). Council Directive 98/83/EC of 3 November 1998 on the quality of water intended for human consumption. *Official Journal L 330*, European Union.
Fan, L.; Harris, J. L.; Roddick, F. A. and Booker, N. A., (2001). Influence of the characteristics of natural organic matter on the fouling of microfiltration membranes. *Water Research*, **35** (18): 4455–4463.
Fang, H.; Tong, W.; Shi, L. M.; Blair, R.; Perkins, R.; Branham, W.; Hass, B. S.; Xie, Q.; Dial, S. L.; Moland, C. L. and Sheehan, D. M., (2001). Structure-activity relationships for a large diverse set of natural, synthetic, and environmental estrogens. *Chemical Research in Toxicology*, **14** (3): 280-294.
Favre-Réguillon, A.; Lebuzit, G.; Murat, D.; Foos, J.; Mansour, C. and Draye, M., (2008). Selective removal of dissolved uranium in drinking water by nanofiltration. *Water Research*, **42** (4-5): 1160-1166.
Fawell, J.; Bailey, K.; Chilton, J.; Dahi, E.; Fewtrell, L. and Magara, Y., (2006). *Fluoride in drinking water*. IWA Publishing, London, UK.
Ferrando, M. D.; Alarcon, V.; Fernández-Casalderrey, A.; Gamón, M. and Andreu-Moliner, E., (1992). Persistence of some pesticides in the aquatic environment. *Bulletin of Environmental Contamination and Toxicology*, **48** (5): 747-755.
Fielding, M.; Barcelo, D.; Helweg, A.; Galassi, S.; Torstensson, L.; Van Zoonen, P.; Wolter, R. and Angeletti, G., (1992). *Pesticides in ground water and drinking water,* In: *Water Pollution Research, Rep. 27*, Commission of the European Communities, Brussels, Belgium.
Firdaous, L.; Maleriat, J. P.; Schlumpf, J. P. and Quemeneur, F., (2007). Transfer of monovalent and divalent cations in salt solutions by electrodialysis *Separation Science and Technology*, **42** (5): 931-948.
Flores-Céspedes, F.; Fernández-Pérez, M.; Villafranca-Sánchez, M. and González-Pradas, E., (2006). Cosorption study of organic pollutants and dissolved organic matter in a soil. *Environmental Pollution*, **142** (3): 449-456.
Forman, S. E.; Durbetaki, A. J.; Cohen, M. V. and Olofson, R. A., (1965). Conformational Equilibria in Cyclic Sulfites and Sulfates. The Configurations and Conformations of the Two Isomeric Thiodans. *Journal of Organic Chemistry*, **30** (1): 169-175.
Fox, P.; Davis, J. A. and Zachara, J. M., (2006). The effect of calcium on aqueous speciation and adsorption to ferrihydrite and quartz. *Geochimica et Cosmochimica Acta*, **70** (6): 1379-1387.
Freiser, H., (1980). *Ion-selective electrodes in analytical chemistry*. Plenum Press, New York, USA.
Frimmel, F. H., (1998). Characterization of natural organic matter as major constituents in aquatic systems. *Journal of Contaminant Hydrology*, **35**, 201-216.
Gancia, E.; Montana, J. G. and Manallack, D. T., (2001). Theoretical hydrogen bonding parameters for drug design. *Journal of Molecular Graphics and Modelling*, **19** (3-4): 349-362.
Gao, J. P.; Maguhn, J.; Spitzauer, P. and Kettrup, A., (1998). Sorption of pesticides

in the sediment of the Teufelesweiher pond (southern Germany). I: equilibrium assessments, effect of organic carbon content and pH. *Water Research*, **32** (5): 1662-1672.

Ge, F.; Shu, H. and Dai, Y., (2007). Removal of bromide by aluminium chloride coagulant in the presence of humic acid. *Journal of Hazardous Materials*, **147** (1-2): 457-462.

Ge Water, http://www.gewater.com.

Geoscience Australia, (2005). Map of Australia: Basic outline with state borders and capital city locations, Commonwealth of Australia, Canberra, Australia.

German Federal Environment Agency, (2004). *Endosulfan Preliminary Dossier*, Umweltbundesamt, Berlin, Germany.

Gevao, B.; Semple, K. T. and Jones, K. C., (2000). Bound pesticide residues in soils: a review. *Environmental Pollution*, **108** (1): 3-14.

Ghosh, K. and Schnitzer, M., (1980). Macromolecular structures of humic substances. *Soil Science*, **129** (5): 266-276.

Goebel, H.; Gorbach, S. G.; Knauf, W.; Rimpau, R. H. and Huttenbach, H., (1982). Properties, effects, residues and analytics of the insecticide endosulfan. *Residue Reviews*, **83** 1-122.

Gonçalves, C. M.; Esteves da Silva, J. C. G. and Alpendurada, M. F., (2007). Evaluation of the pesticide contamination of groundwater sampled over two years from a vulnerable zone in Portugal. *Journal of Agricultural and Food Chemistry*, **55** (15): 6227-6235.

Gower, D. B., (1975). Catabolism and excretion of steroids, In: Makin, H. L. J., (Ed), *Biochemistry of steroid hormones*, Blackwell, Oxford.

Grebenyuk, V. D.; Chebotareva, R. D.; Peters, S. and Linkov, V., (1998). Surface modification of anion-exchange electrodialysis membranes to enhance anti-fouling characteristics. *Desalination*, **115** (3): 313-329.

Greve, P. A. and Wit, S. L., (1971). Endosulfan in the Rhine River. *Journal of the Water Pollution Control Federation*, **43** (12): 2338-2348.

Grossman, G. and Sonin, A. A., (1973). Membrane fouling in electrodialysis: a model and experiments. *Desalination*, **12** (1): 107-125.

Guerin, T. F. and Kennedy, I. R., (1992). Distribution and Dissipation of Endosulfan and Related Cyclodienes in Sterile Aqueous Systems: Implications for Studies on Biodegradation. *Journal of Agricultural and Food Chemistry*, **40** (11): 2315-2323.

Guerin, T. F., (1993). *The relative significance of biodegradation and physico-chemical dissipation of endosulfan from water and soil*. Doctor of Philosophy, University of Sydney, Sydney, Australia.

Guerin, T. F., (2001). Abiological loss of endosulfan and related chlorinated organic compounds from aqueous systems in the presence and absence of oxygen. *Environmental Pollution*, **115** (2): 219-230.

Gupta, V. K. and Ali, I., (2008). Removal of endosulfan and methoxychlor from water on carbon slurry. *Environmental Science and Technology*, **42** (3): 766-770.

Haagen, K. and Helfferich, F., (1959). Ionenaustauschermembranen. German Patent 971 729.

Hábová, V.; Melzoch, K.; Rychtera, M. and Sekavova, B., (2004). Electrodialysis as a useful technique for lactic acid separation from a model solution and a

fermentation broth. *Desalination*, **162** (1-3): 361-372.
Halling-Sørensen, B.; Nors Nielsen, S.; Lanzky, P. F.; Ingerslev, F.; H.C., H. L. and Jørgensen, S. E., (1998). Occurrence, fate and effects of pharmaceutical substances in the environment - A review *Chemosphere*, **36** (2): 357-393.
Hansch, C.; Leo, A. and Hoekman, D., (1995). *Exploring QSAR: Hydrophobic, Electronic, and Steric Constants*. American Chemical Society, Washington, DC.
Hayes, D., (1989). Extraction of humic substances from soil, In: Aiken, G. R.; McKnight, D. M.; Wershaw, R. L. and MacCarthy, P., (Eds), *Humic substances in soil, sediment, and water: Geochemistry, isolation, and characterization*, Wiley, New York, USA.
Hayes, D.; Carter, J. and Manning, T. J., (1995). Fluoride binding to humic acid. *Journal of Radioanalytical and Nuclear Chemistry Letters*, **201** (2): 135-141.
Hengpraprom, S.; Lee, C. M. and Coates, J. T., (2006). Sorption of humic acids and α-endosulfan by clay minerals. *Environmental Toxicology and Chemistry*, **25** (1): 11-17.
Hess, R. A.; Bunick, D.; Lee, K. H.; Bahr, J.; Taylor, J. A.; Korach, K. S. and Lubahn, D. B., (1997). A role for oestrogens in the male reproductive system. *Nature*, **390** (6659): 509-512.
Hester, R. E. and Harrison, R. M., (1999). *Endocrine disrupting chemicals*. Royal Society of Chemistry, Cambridge, UK.
Hetrick, J.; Parker, R.; Pisigan, R. and Thurman, N., (2000). *Progress report on estimating pesticide concentrations in drinking water and assessing water treatment effects on pesticide removal and transformation: a consultation*, US EPA, Office of Pesticide Programs, Washington, D.C, USA.
Hillisch, A.; von Langen, J.; Menzenbach, B.; Droescher, P.; Kaufmann, G.; Schneider, B. and Elger, W., (2003). The significance of the 20-carbonyl group of progesterone in steroid receptor binding: a molecular dynamics and structure-based ligand design study. *Steroids*, **68** (10-13): 869-878.
Hinckley, D. A.; Bidleman, T. F. and Foreman, W. T., (1990). Determination of vapor pressure for nonpolar and semipolar organic compounds from gas chromatographic retention data. *Journal of Chemical & Engineering Data*, **35** (3): 232-237.
Hofman, J. A. M. H.; Beerendonk, E. F.; Folmer, H. C. and Kruithof, J. C., (1997). Removal of pesticides and other micropollutants with cellulose-acetate, polyamide and ultra-low pressure reverse osmosis membranes. *Desalination*, **113** (2-3): 209-214.
Hong, S. and Elimelech, M., (1997). Chemical and physical aspects of natural organic matter (NOM) fouling of nanofiltration membranes. *Journal of Membrane Science*, **132** (2): 159-181.
Hose, G. C.; Lim, R. P.; Hyne, R. V. and Pablo, F., (2003). Short-term exposure to aqueous endosulfan affects macroinvertebrate assemblages. *Ecotoxicology and Environmental Safety*, **56** (2): 282-294.
Ikemoto, T.; Tu, N. P. C.; Okuda, N.; Iwata, A.; Omori, K.; Tanabe, S.; Tuyen, B. C. and Takeuchi, I., (2008). Biomagnification of trace elements in the aquatic food web in the Mekong Delta, South Vietnam using stable carbon and nitrogen isotope analysis. *Archives of environmental contamination and toxicology*, **54** (3): 504-515.

International Desalination Association, (2008-2009). *IDA Desalination Yearbook*. Global Water Intelligence, Oxford, UK.

Jansen, J.; Treiner, C. and Vaution, C., (1996). Coadsorption of steroids and nonionic surfactants on polystyrene latex particles from aqueous solutions. *Journal of Colloid and Interface Science*, **179** (2): 578-586.

Jenkins, H. D. B. and Marcus, Y., (1995). Viscosity B-Coefficients of ions in solution. *Chemical Reviews*, **95** (8): 2695-2724.

Jeon, C.; Park, J. Y. and Yoo, Y. J., (2002). Characteristics of metal removal using carboxylated alginic acid. *Water Research*, **36** (7): 1814-1824.

Jobling, S.; Nolan, M.; Tyler, C. R.; Brighty, G. and Sumpter, J. P., (1998). Widespread sexual disruption in wild fish. *Environmental Science and Technology*, **32** (17): 2498-2506.

Joffe, M., (2000). Are problems with male reproductive health caused by endocrine disruption? *Occupational and Environmental Medicine*, **58** (4): 281-287.

Johnson, A. C. and Sumpter, J. P., (2001). Removal of endocrine-disrupting chemicals in activated sludge treatment works. *Environmental Science and Technology*, **35** (24): 4697-4703.

Joyce, A.; Loureiro, D.; Rodrigues, C. and Castro, S., (2001). Small reverse osmosis units using PV systems for water purifications in rural places. *Desalination*, **137** (1-3): 39-44.

Jurgens, M. D.; Holthaus, K. I. E.; Johnson, A. C.; Smith, J. J. L.; Hetheridge, M. and Williams, R. J., (2002). The potential for estradiol and ethinylestradiol degradation in English Rivers. *Environmental Toxicology and Chemistry*, **21** (3): 480-488.

Kabay, N.; Arda, M.; Kurucaovali, I.; Ersoz, E.; Kahveci, H.; Can, M.; Dal, S.; Kopuzlu, S.; Haner, M.; Demircioglu, M. and Yuksel, M., (2003). Effect of feed characteristics on the separation performances of monovalent and divalent salts by electrodialysis. *Desalination*, **158** (1-3): 95-100.

Kabay, N.; Yuksel, N.; Samatya, S.; Arar, O. and Yuksel, U., (2006). Effect of process parameters on separation performance of nitrate by electrodialysis *Separation Science and Technology*, **41** (14): 3201-3211.

Kabay, N.; Arar, O.; Samatya, S.; Yuksel, U. and Yuksel, M., (2008). Separation of fluoride from aqueous solution by electrodialysis: Effect of process parameters and other ionic species. *Journal of Hazardous Materials*, **153** (1-2): 107-113.

Kariduraganavar, M. Y.; Nagarale, R. K.; Kittur, A. A. and Kulkarni, S. S., (2006). Ion-exchange membranes: preparative methods for electrodialysis and fuel cell applications. *Desalination*, **197** (1-3): 225-246.

Katsoyiannis, A. and Samara, C., (2007). Ecotoxicological evaluation of the wastewater treatment process of the sewage treatment plant of Thessaloniki, Greece. *Journal of Hazardous Materials*, **141** (3): 614-621.

Kaur, I.; Mathur, R. P.; Tandon, S. N. and Dureja, P., (1998). Persistence of endosulfan (technical) in water and soil. *Environmental Technology*, **19** (1): 115-119.

Kesore, K.; Janowski, F. and Shaposhnik, V. A., (1997). Highly effective electrodialysis for selective elimination of nitrates from drinking water. *Journal of Membrane Science*, **127** (1): 17-24.

Kesting, R. E., (1985). *Synthetic polymeric membranes: A structural perspective*. John Wiley & Sons, New York, USA.

Khan, S. J.; Wintgens, T.; Sherman, P.; Zaricky, J. and Schäfer, A. I., (2004). Removal of hormones and pharmaceuticals in the Advanced Water Recycling Demonstration Plant in Queensland, Australia. *Water Science and Technology*, **50** (5): 15-22.

Khan, S. J.; Wintgens, T.; Sherman, P.; Zaricky, J. and Schäfer, A. I., (2005). A performance comparison of individual and combined treatment modules for water recycling. *Environmental Progess*, **24** (4): 383-391.

Kim, J. I.; Buckau, G.; Li, G. H.; Duschner, H. and Psarros, N., (1990). Characterization of humic and fulvic acids from Gorleben groundwater *Fresenius' Journal of Analytical Chemistry*, **338** (3): 245-252.

Kim, D. H.; Moon, S. H. and Cho, J., (2002). Investigation of the adsorption and transport of natural organic matter (NOM) in ion-exchange membranes. *Desalination*, **151** (1): 11-20.

Kinniburgh, D. G.; van Riemsdijk, W. H.; Koopal, L. K.; Borkovec, M.; Benedetti, M. F. and Avena, M. J., (1999). Ion binding to natural organic matter: competition, heterogeneity, stoichiometry and thermodynamic consistency. *Colloids and Surfaces A: Physicochemical and Engineering Aspects*, **151** (1-2): 147-166.

Kiriukhin, M. Y. and Collins, K. D., (2002). Dynamic hydration numbers for biological important ions. *Biophysical Chemistry*, **99** (2): 155-168.

Kiso, Y.; Nishimura, Y.; Kitao, T. and Nishimura, K., (2000). Rejection properties of non-phenylic pesticides with nanofiltration membranes. *Journal of Membrane Science*, **171** (2): 229-237.

Kiso, Y.; Sugiura, Y.; Kitao, T. and Nishimura, K., (2001). Effects of hydrophobicity and molecular size on rejection of aromatic pesticides with nanofiltration membranes. *Journal of Membrane Science*, **192** (1-2): 1-10.

Kolpin, D. W.; Furlong, E. T.; Meyer, M. T.; Thurman, E. M.; Zaugg, S. D.; Barber, L. B. and Buxton, H. T., (2002). Pharmaceuticals, hormones, and other organic wastewater contaminants in US streams 1999-2000: a national reconnaissance. *Environmental Science and Technology*, **36** (6): 1202-1211.

Koparal, A. and Ogutveren, U., (2002). Removal of nitrate from water by electroreduction and electrocoagulation. *Journal of Hazardous Materials*, **89** (1): 83-94.

Koprivnjak, J. F.; Perdue, E. M. and Pfromm, P. H., (2006). Coupling reverse osmosis with electrodialysis to isolate natural organic matter from fresh waters. *Water Research*, **40** (18): 3385-3392.

Korngold, E.; De Korosy, F.; Rahav, R. and Taboch, M. F., (1970). Fouling of anionselective membranes in electrodialysis. *Desalination*, **8** (2): 195-220.

Korngold, E., (1975). *Principles of Electrodialysis*, Research and Development Authority Ben-Gurion University of the Negev, Beer-Sheva, Israel.

Koyuncu, I.; Arikan, O. A.; Wiesner, M. R. and Rice, C. R., (2008). Removal of hormones and antibiotics by nanofiltration membranes. *Journal of Membrane Science*, **309** (1-2): 94-101.

Kraal, P.; Jansen, B.; Nierop, K. G. J. and Verstraten, J. M., (2006). Copper complexation by tannic acid in aqueous solution. *Chemosphere*, **65** (11): 2193-2198.

Krol, J. J., (1997). *Monopolar and bipolar ion exchange membranes: Mass Transport Limitations*. Doctor of Philosophy, University of Twente, Enschede,

Netherlands.
Krüss, (2009). Measuring the contact angle. http://www.kruss.de/en/theory/measurements/contact-angle/measurement-contact-angle.html.
Kuch, H. M. and Ballschmiter, (2001). Determinations of endocrine disrupting phenolic compounds and estrogens in suface and drinking water by HRGC-(NCI)-MS in the pictogram per liter range. *Environmental Science and Technology*, **35** (15): 3201-3206.
Kullman, S. W. and Matsumura, F., (1996). Metabolic pathways utilized by Phanerochaete chrysosporium for degradation of the cyclodiene pesticide endosulfan. *Applied and Environment Microbiology*, **62** (2): 593-600.
Kumar, M. and Philip, L., (2006). Adsorption and desorption characteristics of hydrophobic pesticide endosulfan in four Indian soils. *Chemosphere*, **62** (7): 1064-1077.
Kwon, J. H.; Liljestrand, H. M. and Katz, L. E., (2006). Partitioning of moderately hydrophobic endocrine disrupters between water and synthetic membrane vesicles. *Environmental Toxicology and Chemistry* **25** (8): 1984-1992.
Lai, K. M.; Johnson, K. L.; Scrimshaw, M. D. and Lester, J. N., (2000). Binding of Waterborne Steroid Estrogens to Solid Phases in River and Estuarine Systems. *Environmental Science and Technology*, **34** (18): 3890–3894.
Lambert, J.; Avila-Rodriguez, M.; Durand, G. and Rakib, M., (2006). Separation of sodium ions from trivalent chromium by electrodialysis using monovalent cation selective membranes. *Journal of Membrane Science*, **280** (1-2): 219-225.
Lange, R.; Hutchinson, T. H.; Croudace, C. P.; Siegmund, F.; Schweinfurth, H.; Hampe, P.; Panter, G. H. and Sumpter, J. P., (2001). Effects of the synthetic estrogen 17α-ethinyl estradiol on the life-cycle of the fathead minnow (*Pimephales promelas*). *Environmental Toxicology and Chemistry*, **20** (6): 1216-1227.
Langmuir, D., (1978). Uranium solution-mineral equilibria at low temperatures with applications to sedimentary ore deposits. *Geochimica et Cosmochimica Acta*, **42** (6): 547-569.
Langmuir, D., (1997). *Aqueous environmental geochemistry*. Prentice Hall, New Jersey, USA.
Law, R. J.; Allchin, C. R.; de Boer, J.; Covaci, A.; Herzke, D.; Lepom, P.; Morris, S.; Tronczynski, J. and de Wit, C. A., (2006). Levels and trends of brominated flame retardants in the European environment. *Chemosphere*, **64** (2): 187-208.
Le Questel, J. Y.; Boquet, G.; Berthelot, M. and Laurence, C., (2000). Hydrogen Bonding of Progesterone: a Combined Theoretical, Spectroscopic, Thermodynamic, and Crystallographic Database Study. *Journal of Physical Chemistry B*, **104** (49): 11816-11823.
Lee, S. and Lee, C. H., (2000). Effect of operating conditions on $CaSO_4$ scale formation mechanism in nanofiltration for water softening *Water Research*, **34** (15): 3854-3866.
Lee, H. J.; Choi, J. H.; Cho, J. and Moon, S. H., (2002a). Characterization of anion exchange membranes fouled with humate during electrodialysis. *Journal of Membrane Science*, **203** (1-2): 115-126.
Lee, H. J.; Kim, D. H.; Cho, J. and Moon, S. H., (2002b). Characterization of anion

exchange membranes with natural organic matter (NOM) during electrodialysis. *Desalination*, **151** (1): 43-52.

Lee, H. J.; Moon, S. H. and Tsai, S. P., (2002c). Effects of pulsed electric fields on membrane fouling in electrodialysis of NaCl solution containing humate. *Separation and Purification Technology*, **27** (2): 89-95.

Lee, H. J.; Sarfert, F.; Strathmann, H. and Moon, S. H., (2002d). Designing of an electrodialysis desalination plant. *Desalination*, **142** (3): 267-286.

Lee, H. J.; Strathmann, H. and Moon, S. H., (2006). Determination of the limiting current density in electrodialysis desalination as an empirical function of linear velocity. *Desalination*, **190** (1-3): 43-50.

Lee, H. J.; Hong, M. K.; Han, S. D.; Cho, S. H. and Moon, S. H., (2009). Fouling of an anion exchange membrane in the electrodialysis desalination process in the presence of organic foulants. *Desalination*, **238** (1-3): 60-69.

Lemarchand, E.; Schott, J. and Gaillardet, J., (2005). Boron isotopic fractionation related to boron sorption on humic acid and the structure of surface complexes formed. *Geochimica et Cosmochimica Acta*, **69** (14): 3519-3533.

Li, Y. and Xu, T., (2008). Permselectivities of monovalent anions through pyridine-modified anion-exchange membranes *Separation and Purification Technology*, **61** (3): 430-435.

Lide, D. R., (2008). *CRC Handbook of Chemistry and Physics*. CRC Press/Taylor and Francis, Boca Raton, USA.

Lin, A. Y. C. and Reinhard, M., (2005). Photodegradation of common environmental pharmaceuticals and estrogens in river water. *Environmental Toxicology and Chemistry*, **24** (6): 1303-1309.

Lindstrand, V.; Jonsson, A. S. and Sundstrom, G., (2000a). Organic fouling of electrodialysis membranes with and without applied voltage. *Desalination*, **130** (1): 73-84.

Lindstrand, V.; Sundstrom, G. and Jonsson, A. S., (2000b). Fouling of electrodialysis membranes by organic substances. *Desalination*, **128** (1): 91-102.

Lipovski, A. A. and Dem'yanova, T. A., (1971). Investigation of hydrogen bonding involving anions of alkylammonium salts. *Journal of Applied Spectroscopy*, **15** (3): 550–552.

Luek Wong, S.; Wainwright, J. F. and Nakamoto, L., (1995). Monitoring toxicity in four wastewaters in the Bay of Quinte, Lake Ontario. *Journal of Great Lakes Research*, **21** (3): 340-352.

Magara, Y.; Aizawa, T.; Matumoto, N. and Souna, F., (1994). Degradation of pesticides by chlorination during water purification. Groundwater Contamination, Environmental Restoration, and diffuse Source Pollution. *Water Science and Technology*, **30** (7): 119-128.

Malaxos, P. J. and Morin, O. J., (1990). Surface water discharge of reverse osmosis concentrates. *Desalination*, **78** (1): 27-40.

Marcus, Y. and Ben-Naim, A., (1985). A study of the structure of water and its dependence on solutes, based on the isotope effects on solvation thermodynamics in water. *Journal of Chemical Physics*, **83** (9): 4744-4759.

Marcus, Y., (1991). Thermodynamics of solvation of ions Part 5.- Gibbs free energy of hydration at 298.15 K. *Journal of the Chemical Society, Faraday Transactions*, **87** (18): 2995-2999.

Marcus, Y., (1994). Viscosity B-coefficients, structural entropies and heat capacities,

and the effects of ions on the structure of water. *Journal of Solution Chemistry*, **23** (7): 831-848.

Marcussen, H.; Dalsgaard, A. and Holm, P. E., (2008). Content, distribution and fate of 33 elements in sediments of rivers receiving wastewater in Hanoi, Vietnam. *Environmental Pollution*, **155** (1): 41-51.

Marder, L.; Bernardes, A. M. and Zoppas Ferreira, J., (2004). Cadmium electroplating wastewater treatment using a laboratory-scale electrodialysis system. *Separation and Purification Technology*, **37** (3): 247-255.

Mariñas, B. J. and Selleck, R. E., (1992). Reverse osmosis treatment of multicomponent electrolyte solutions *Journal of Membrane Science*, **72** (3): 211-229.

Martens, R., (1976). Degradation of (8,9 C^{14}) endosulfan by soil microorganisms. *Applied and Environmental Microbiology*, **31** (6): 853-858.

Martins, J. M. and Mermoud, A., (1998). Sorption and degradation of four nitroaromatic herbicides in mono and multi-solute saturated/unsaturated soil batch systems. *Journal of Contaminant Hydrology*, **33** (1-2): 187-210.

Mathur, V.; Bhatnagar, P.; Sharma, R. G.; Acharya, V. and Sexana, R., (2002). Breast cancer incidence and exposure to pesticides among women originating from Jaipur. *Environment International*, **28** (5): 331-336.

Matthiessen, P.; Arnold, D.; Johnson, A. C.; Pepper, T. J.; Pottinger, T. G. and Pulman, K. G. T., (2006). Contamination of headwater streams in the United Kingdom by oestrogenic hormones from livestock farms *Science of the Total Environment*, **367** (2-3): 616-630.

McCallum, E. A.; Hyung, H.; Anh Do, T.; Huang, C. H. and Kim, J. H., (2008). Adsorption, desorption, and steady-state removal of 17β-estradiol by nanofiltration membranes. *Journal of Membrane Science*, **319** (1-2): 38-43.

McNeil, V. H. and Cox, M. E., (2000). Relationship between conductivity and analysed composition in a large set of natural surface-water samples, Queensland, Australia. *Environmental Geology*, **39** (12): 1325-1333.

Mega, a. s., http://www.mega.cz/en/.

Melnik, L.; Vysotskaja, O. and Kornilovich, B., (1999). Boron behavior during desalination of sea and underground water by electrodialysis. *Desalination*, **124** (1-3): 125-130.

Melnyk, L.; Goncharuk, V.; Butnyk, I. and Tsapiuk, E., (2005). Boron removal from natural and wastewaters using combined sorption/membrane process. *Desalination*, **185** (1-3): 147-157.

Menkouchi Sahli, M. A.; Annouar, S.; Tahaikt, M.; Mountadar, M.; Soufiane, A. and Elmidaoui, A., (2007). Fluoride removal for underground brackish water by adsorption on the natural chitosan and by electrodialysis. *Desalination*, **212** (1-3): 37-45.

Menkouchi Sahli, M. A.; Annouar, S.; Mountadar, M.; Soufiane, A. and Elmidaoui, A., (2008). Nitrate removal of brackish underground water by chemical adsorption and by electrodialysis. *Desalination*, **227** (1-3): 327-333.

Merdy, P.; Huclier, S. and Koopal, L. K., (2006). Modeling metal-particle interactions with an emphasis on natural organic matter *Environmental Science and Technology*, **40** (24): 7459-7466.

Metcalfe and Eddy; Tchobanoglous, G.; Burton, F. and Stensel, H. D., (2003). *Wastewater engineering: Treatment and reuse*. McGraw-Hill, New York,

USA.
Michaelis, L. and Fujita, A., (1925). The electric phenomenon and ion permeability of membranes II. Permeability of apple peel. *Biochemische Zeitschrift*, **158**, 28-37.
Miles, J. R. and Moy, P., (1979). Degradation of endosulfan and its metabolites by a mixed culture of soil microorganisms. *Bulletin of Environmental Contamination and Toxicology*, **23** (1): 13-19.
Miller, J. N. and Miller, J. C., (2000). *Statistics and Chemometrics for Analytical Chemistry*. Prentice Hall, Harlow, UK.
Mondor, M.; Ippersiel, D.; Lamarche, F. and Masse, L., (2009). Fouling characterization of electrodialysis membranes used for the recovery and concentration of ammonia from swine manure. *Bioresource Technology*, **100** (2): 566-571.
Montgomery, J. M., (1985). *Water treatment principles and design*. John Wiley & Sons, New York, USA.
Montgomery, M. A. and Elimelech, M., (2007). Water and sanitation in developing countries: Including health in the equation. *Environmental Science and Technology*, **41** (1): 17-24.
Moorman, T. B.; Jayachandran, K. and Reungsang, A., (2001). Adsorption and desorption of atrazine in soils and subsurface sediments. *Soil Science*, **166** (12): 921-929.
Morel, F. M. M. and Hering, J. G., (1993). *Principles and applications of aquatic chemistry*. Wiley-Interscience, New York, USA.
Morse, H. W. and Pierce, G. W., (1903). Diffusion und Übersättigung in Gelantine. *Zeitschrift fur Physikalische Chemie*, **45**, 589-607.
Mukhopadhyay, A. and Law, B. M., (2001). Dipole orientational order at the critical interface. *Physical review. E, Statistical physics, plasmas, fluids, and related interdisciplinary topics*, **63** (1): 011507.
Mulder, M., (1996). *Basic principles of membrane technology*. 2nd ed.; Kluwer Academic Publishers, Dordrecht, Netherlands.
Nagarale, R. K.; Gohil, G. S.; Shahi, V. K.; Trivedi, G. S.; Thampy, S. K. and Rangarajan, R., (2004). Studies on transport properties of short chain aliphatic carboxylic acids in electrodialytic separation. *Desalination*, **171** (2): 195-204
Nagarale, R. K.; Gohil, G. S. and Shahi, V. K., (2006). Recent developments on ion-exchange membranes and electro-membrane processes. *Advances in Colloid and Interface Science*, **119** (2-3): 97-130.
Naqvi, S. M. and Vaishnavi, C., (1993). Bioaccumulative potential and toxicity of endosulfan insecticide to non-target animals. *Comparative Biochemistry and Physiology Part C: Pharmacology, Toxicology and Endocrinology*, **105** (3): 347-361.
Neal, C.; Jarvie, H. P.; Neal, M.; Hill, L. and Wickham, H., (2006). Nitrate concentrations in river waters of the upper Thames and its tributaries. *Science of the Total Environment*, **365** (1-3): 15-32.
Neale, P. A.; Escher, B. I. and Schäfer, A. I., (2008). pH dependence of steroid hormone-organic matter interactions at environmental concentrations. *Science of the Total Environment*, **407** (3): 1164-1173.
Neale, P. A., (2009). *The influence of solute-solute interactions in membrane filtration*. Doctor of Philosophy, The University of Edinburgh, Edinburgh, UK.

Neale, P. A.; Escher, B. I. and Schäfer, A. I., (2009). pH dependence of steroid hormone-organic matter interactions at environmental concentrations. *Science of the Total Environment*, **407** (3): 1164-1173.

Nerin, C.; Tornés, A. R.; Demoño, C. and Cacho, J., (1996). Absorption of pesticides on plastic films used as agricultural soil covers. *Journal of Agricultural and Food Chemistry*, **44** (12): 4009-4014.

Ng, H. Y. and Elimelech, M., (2004). Influence of colloidal fouling on rejection of trace organic contaminants by reverse osmosis. *Journal of Membrane Science*, **244** (1-2): 215-226.

Nghiem, L. D. and Schäfer, A. I., (2002). Adsorption and transport of trace contaminant estrone in NF/RO membranes. *Environmental Engineering Science* **19** (6): 441-451.

Nghiem, L. D.; Schäfer, A. I. and Waite, T. D., (2002). Adsorptive interactions between membranes and trace contaminants. *Desalination*, **147** (1-3): 269-274.

Nghiem, L. D.; Manis, A.; Soldenhoff, K. and Schäfer, A. I., (2004a). Estrogenic hormone removal from wastewater using NF/RO membranes. *Journal of Membrane Science*, **242** (1-2): 37-45.

Nghiem, L. D.; Schäfer, A. I. and Elimelech, M., (2004c). Removal of natural hormones by nanofiltration membranes: measurement, modeling, and mechanisms. *Environmental Science and Technology*, **38** (6): 1888-1896.

Nghiem, L. D., (2005). *Emerging trace organic contaminant removal using nanofiltration and reverse osmosis membranes*. Doctor of Philosophy, The University of Wollongong, Wollongong, Australia.

NHMRC, (2004). *Australian Drinking Water Guidelines*, National Health and Medical Research Council, Canberra, Australia.

Nightingale, E. R., (1959). Phenomological theory of ion solvation-effective radii of hydrated ions. *Journal of Physical Chemistry*, **63** (9): 1381-1387.

Nriagu, J. O. and Hem, J. D., (1978). Chemistry of pollutant sulfur in natural waters, In: Nriagu, J. O., (Ed), *Sulfur in the environment*, Wiley-Interscience, New York, pp. 211-270.

Nriagu, J. O. and Pacyna, J. M., (1988). Quantitative assessment of worldwide contamination of air, water and soils by trace metals. *Nature*, **333** (6169): 134-139.

Nyström, M.; Ruohomäki, K. and Kaipia, L., (1996). Humic acid as a fouling agent in filtration. *Desalination*, **106** (1-3): 79-87.

Ohlenbusch, G.; Kumke, M. U. and Frimmel, F. H., (2000). Sorption of phenols to dissolved organic matter investigated by solid phase microextraction *Science of the Total Environment*, **253** (1-3): 63-74.

Oldani, M.; Killer, E.; Miquel, A. and Shock, G., (1992). On the nitrate and monovalent cation selectivity of ion exchange membranes used in drinking water purification. *Journal of Membrane Science*, **75** (3): 265-275.

Ormad, M. P.; Miguel, N.; Claver, A.; Matesanz, J. M. and Ovelleiro, J. L., (2008). Pesticides removal in the process of drinking water production. *Chemosphere*, **71** (1): 97-106.

Ortiz, J. M.; Sotoca, J. A.; Exposito, E.; Gallud, F.; Garcia-Garcia, V.; Montiel, V. and Aldaz, A., (2005). Brackish water desalination by electrodialysis: batch recirculation operation modeling. *Journal of Membrane Science*, **252** (1-2): 65-75.

Ottinger, M. A.; Abdelnabi, M.; Quinn, M.; Golden, N.; Wu, J. and Thompson, N., (2002). Reproductive consequences of EDCs in birds: What do laboratory effects mean in field species? *Neurotoxicology and Teratology*, **24** (1): 17-28.

Owen, B. B. and King, E. J., (1943). The effect of sodium chloride upon the ionization of boric acid at various temperatures. *Journal of the American Chemical Society*, **65** (8): 1612-1620.

Park, J. S.; Lee, H. J.; Choi, S. J.; Geckeler, K. E.; Cho, J. and Moon, S. H., (2003a). Fouling mitigation of anion exchange membrane by zeta potential control. *Journal of Colloid and Interface Science*, **259** (12): 293-300.

Park, J. S.; Choi, J. H.; Yeon, K. H. and Moon, S. H., (2006). An approach to fouling characterization of an ion-exchange membrane using current-voltage relation and electrical impedance spectroscopy. *Journal of Colloid and Interface Science*, **294** (1): 129-138.

Parkpian, P.; Anurakpongsatorn, P.; Pakkong, P. and Patrick, W. H. J., (1998). Adsorption, desorption and degradation of α-endosulfan in tropical soils of Thailand. *Journal of Environmental Science and Health, Part B Pesticides, Food Contaminants, and Agricultural Wastes*, **33** (3): 211-233.

Pauling, L., (1960). *The nature of the chemical bond and the structure of molecules and crystals: An introduction to modern structural chemistry*. Cornell University Press, New York, USA.

Pearce, G. K., (2008). UF/MF pre-treatment to RO in seawater and wastewater reuse applications: a comparison of energy costs. *Desalination*, **222** (1-3): 66-73.

Peterson, S. M. and Batley, G. E., (1993). The fate of endosulfan in aquatic ecosystems. *Environmental Pollution*, **82** (2): 143-152.

Pitts, L.; Fisher, A.; Worsfold, P. and Hill, S. J., (1995). Selenium speciation using high performance liquid chromatography-hydride generation atomic fluorescence with on-line microwave reduction. *Journal of Analytical Atomic Spectrometry*, **10** (8): 519-520.

Prausnitz, P. H. and Reiststotter, J., (1931). *Elektrophorese, Elektroosmose, Elektrodialyse in Flüssigkeiten*. Steinkopff, T., Dresden, Germany.

Pronk, W.; Biebow, M. and Boller, M., (2006). Electrodialysis for recovering salts from a urine solution containing micropollutants. *Environmental Science and Technology*, **40** (7): 2414-2420.

Prosen, H.; Troha, A. and Zupančič-Kralj, L., (2002). Studies on interaction between some organochlorine insecticides and humic acid using solid-phase microextraction and gas chromatography. *Acta Chimica Slovenica*, **49** (3): 561-573.

Purdom, C. E.; Hardiman, P. A.; Bye, V. J.; Eno, N. C.; Tyler, C. R. and Sumpter, J. P., (1994). Estrogenic effects of effluents from sewage treatment works. *Journal of Chemical Ecology*, **8** 275-285.

Ra, J. S.; Oh, S. Y.; Lee, B. C. and Kim, S. D., (2008). The effect of suspended particles coated by humic acid on the toxicity of pharmaceuticals, estrogens and phenolic compounds. *Environment International*, **34** (2): 184-192.

Rachkov, A.; McNiven, S.; Cheong, S. H.; El'skaya, A.; Yano, K. and Karube, I., (1998). Molecularly imprinted polymers selective for β-estradiol. *Supramolecular Chemistry*, **9** (4): 317-323.

Rachkov, A.; McNiven, S.; El'skaya, A.; Yano, K. and Karube, I., (2000). Fluorescence detection of β-estradiol using a molecularly imprinted polymer.

Analytica Chimica Acta, **405** (1-2): 23-29.
Rautenbach, R. and Albrecht, R., (1989). *Membrane Processes*. John Wiley & Sons, Chichester, UK.
Rebhun, M.; Weir, S. and Laor, Y., (1998). Using dissolved humic acid to remove hydrophobic contaminants from water by complexation-flocculation process. *Environmental Science and Technology*, **32** (7): 981-986.
Rice, C. P.; Chernyak, S. M.; Hapeman, C. J. and Bilboulian, S., (1997). Air-water distribution of the endosulfan isomers. *Journal of Environmental Quality*, **26** (4): 1101-1107.
Richards, L. A.; Richards, B. S.; Rossiter, H. M. A. and Schäfer, A. I., (2009). Impact of speciation on fluoride, arsenic and magnesium retention by nanofiltration/reverse osmosis in remote Australian communities. *Desalination*, 10.1016/j.desal.2008.05.054.
Ritchie, J. D. and Perdue, E. M., (2003). Proton-binding study of standard and reference fulvic acids, humic acids, and natural organic matter *Geochimica et Cosmochimica Acta*, **67** (1): 85-96.
Ritter, L.; Solomon, K.; Sibley, P.; Hall, K.; Keen, P.; Mattu, G.; Linton, B., (2002). Sources, pathways, and relative risks of contaminants in surface water and groundwater: a perspective prepared for the Walkerton Inquiry. *Journal of Toxicology and Environmental Health Part A*, **65**, 1-142.
Robinson, R. A. and Stokes, R. H., (1970). *Electrolyte solutions*. Butterworths, London, UK.
Rodgers-Gray, T. P.; Jobling, S.; Kelly, C.; Morris, S.; Brighty, G.; Waldock, M. J.; Sumpter, J. P. and Tyler, C. R., (2001). Exposure of juvenile roach (Rutilus rutilus) to treated sewage effluent induces dose-dependent and persistent disruption in gonadal duct development. *Environmental Science and Technology*, **35** 462-470.
Rodriguez-Mozaz, S.; López de Alda, M. J. and Barceló, D., (2004). Monitoring of estrogens, pesticides and bisphenol A in natural waters and drinking water treatment plants by solid-phase extraction–liquid chromatography–mass spectrometry. *Journal of Chromatography A*, **1045** (1-2): 85–92.
Rossiter, H. M. A., (2008). Personal communication, Arsenic speciation in Pine Hill groundwater.
Routledge, E. J.; Sheahan, D. A.; Desbrow, C.; Brighty, G. C.; Waldock, M. and Sumpter, J. P., (1998). Identification of estrogenic chemicals in STW effluent. 2. In vivo responses in trout and roach. *Environmental Science and Technology*, **32** (11): 1559-1565.
Sadrzadeh, M.; Razmi, A. and Mohammadi, T., (2007). Separation of different ions from wastewater at various operating conditions using electrodialysis. *Separation and Purification Technology*, **54** (2): 147-156.
Sadrzadeh, M. and Mohammadi, T., (2008). Sea water desalination using electrodialysis. *Desalination*, **221** (1-3): 440-447.
Samoilov, O. Y., (1953). Hydration of ions in aqueous solution. *Russian Chemical Bulletin*, **2** (2): 219-225.
Sata, T.; Yamaguchi, T. and Matsusaki, K., (1995). Effect of hydrophobicity of ion exchange groups of anion exchange membranes on permselectivity between two anions. *Journal of Physical Chemistry*, **99** (34): 12875-12882.
Sata, T.; Teshima, K. and Yamaguchi, T., (1996). Permselectivity between two

anions in anion exchange membranes crosslinked with various diamines in electrodialysis. *Journal of Polymer Science Part A: Polymer Chemistry*, **34** (8): 1475-1482.

Sata, T.; Yamaguchi, T.; Kawamura, K. and Matsusaki, K., (1997). Transport numbers of various anions relative to chloride ions in modified anion exchange membranes during electrodialysis. *Journal of the Chemical Society, Faraday Transactions*, **93** (3): 457-462.

Sata, T., (2000). Studies on anion exchange membranes having permselectivity for specific anions in electrodialysis - effect of hydrophilicity of anion exchange membranes on permselectivity of anions. *Journal of Membrane Science*, **167** (1): 1-31.

Sata, T.; Sata, T. and Yang, W., (2002). Studies on cation-exchange membranes having permselectivity between cations in electrodialysis. *Journal of Membrane Science*, **206** (1-2): 31-60.

Savari, S.; Sachdeva, S. and Kumar, A., (2008). Electrolysis of sodium chloride using composite poly(styrene-co-divinylbenzene) cation exchange membranes. *Journal of Membrane Science*, **310** (1-2): 246-261.

Schäfer, A. I., (2001). *Natural organics removal using membranes: principles, performance and cost*. CRC Press, Boca Raton, USA.

Schäfer, A. I.; Mastrup, M. and Lund Jensen, R., (2002). Particle interactions and removal of trace contaminants from water and wastewaters. *Desalination*, **147** (1-3): 243-250.

Schäfer, A. I.; Nghiem, L. D. and Waite, T. D., (2003). Removal of the natural hormone estrone from aqueous solutions using nanofiltration and reverse osmosis. *Environmental Science and Technology*, **37** (1): 182-188.

Schäfer, A. I.; Andritsos, N.; Karabelas, A. J.; Hoek, E. M. V.; Scheider, R. and Nyström, M., (2004). Fouling in nanofiltration, In: Schäfer, A. I.; Waite, D. T. and Fane, A. G., (Eds), *Nanofiltration: Principles and applications*, Elsevier, Oxford, UK.

Schäfer, A. I.; Broeckmann, A. and Richards, B. S., (2007). Renewable Energy Powered Membrane Technology. 1. Development and Characterization of Photovoltaic Hybrid Membrane System. *Environmental Science and Technology*, **41** (3): 998-1003.

Schäfer, A. I.; Broeckmann, A. and Richards, B. S., (2007). Renewable energy powered membrane technology. 1. Development and characterization of a photovoltaic hybrid membrane system. *Environmental Science and Technology*, **41** (3): 998-1003.

Schausberger, P.; Mustafa, G. M.; Leslie, G. and Friedl, A., (2009). Scaling prediction based on thermodynamic equilibrium calculation-scopes and limitations. *Desalination*, **244** (1-3): 31-47.

Schlautman, M. A. and Morgan, J. J., (1993). Effects of aqueous chemistry on the binding of polycyclic aromatic hydrocarbons by dissolved humic materials. *Environmental Science and Technology*, **27** (5): 961-969.

Schmidt, W. F.; Hapeman, C. J.; Fettinger, J. C.; Rice, C. P. and Bilboulian, S., (1997). Structure and asymmetry in the isomeric conversion of beta- to alpha-endosulfan. *Journal of Agricultural and Food Chemistry*, **45** (4): 1023-1026.

Schmidt, W. F.; Bilboulian, S.; Rice, C. P.; Fettinger, J. C.; McConnell, L. L. and Hapeman, C. J., (2001). Thermodynamic, Spectroscopic, and Computational

Evidence for the Irreversible Conversion of β- to α-Endosulfan. *Journal of Agricultural and Food Chemistry*, **49** (11): 5372-5376.

Schmitt-Kopplin, P.; Hertkorn, N.; Garrison, A. W.; Freitag, D. and Kettrup, A., (1998). Influence of Borate Buffers on the Electrophoretic Behavior of Humic Substances in Capillary Zone Electrophoresis. *Analytical Chemistry*, **70** (18): 3798-3808.

Schoeman, J. J., (2008). Evaluation of electrodialysis for the treatment of a hazardous leachate *Desalination*, **224** (1-3): 178-182.

Schreinemachers, D. D., (2003). Birth malformations and other adverse perinatal outcomes in four US wheat-producing states. *Environmental Health Perspectives*, **111** (9): 1259-1264.

Schulten, H. R., (1994). A chemical structure for Humic Acid. Pyrolysis-gas chromatography/mass spectrometry and pyrolysis-soft ionization mass spectrometry evidence, In: Senesi, N. and Miano, T. M., (Eds), *Humic substances in the global environment and implications on human health*, Elsevier Science, pp. 43-56.

Schulten, H. R. and Schnitzer, M., (1995). Three-dimensional models for humic acids and soil organic matter. *Naturwissenschaften*, **82**, 487-498.

Schwarzenbach, R. P.; Gschwend, P. M. and Imboden, D. M., (2003). *Environmental organic chemistry*. 2nd ed.; John Wiley & Sons, Hobeken, USA.

Seidel, A. and Elimelech, M., (2002). Coupling between chemical and physical interactions in natural organic matter (NOM) fouling in nanofiltration membranes: implications for fouling control. *Journal of Membrane Science*, **203** (1-2): 245-255.

Senesi, N. and Testini, C., (1980). Adsorption of some nitrogenated herbicides by soil humic acids. *Soil Science*, **130** (6): 314-320.

Senesi, N.; Testini, C. and Miano, T. M., (1987). Interaction mechanisms between humic acids of different origin and nature and electron donor herbicides: a comparative IR and ESR study. *Organic Geochemistry*, **11** (1): 25-30.

Senesi, N., (1992). Binding mechanisms of pesticides to soil humic substances. *Science of the Total Environment*, **123/124**, 63-75.

Shaposhnik, V. A.; Zubets, N. N.; Strygina, I. P. and Mill, B. E., (2002). High demineralization of drinking water by electrodialysis without scaling on the membranes. *Desalination*, **145** (1-3): 329-332.

Sharpe, R. M. and Skakkebaek, N. E., (1993). Are oestrogens involved in falling sperm counts and disorders of the male reproductive tract? *The Lancet*, **341** (8857): 1392-1396.

Shih, W. Y.; Rahardianto, A.; Lee, R. W. and Cohen, Y., (2005). Morphometric characterization of calcium sulfate dihydrate (gypsum) scale on reverse osmosis membranes *Journal of Membrane Science*, **252** (1-2): 253-263.

Shin, H. S.; Monsallier, J. M. and Choppin, G. R., (1999). Spectroscopic and chemical characterizations of molecular size fractionated humic acid. *Talanta*, **50** (4): 641.

Shivaramaiah, H. M.; Sanchez-Bayo, F.; Al-Rifai, J. and Kennedy, I. R., (2005). The fate of endosulfan in water. *Journal of Environmental Science and Health Part B*, **40**, 711-720.

Shutava, T. and Prouty, M., (2005). pH responsive decomposable layer-by-layer nanofilms and capsules on the basis of tannic acid. *Macromolecules*, **38** (7):

2850-2858.
Siang, H. Y.; Yee, L. M. and Seng, C. T., (2007). Acute toxicity of organochlorine insecticide endosulfan and its effect on behaviour and some hematological parameters of Asian swamp eel (*Monopterus albus*, Zuiew). *Pesticide Biochemistry and Physiology*, **89** (1): 46–53.
Simpson, A. J., (2002). Determining the molecular weight, aggregation, structures and interactions of natural organic matter using diffusion ordered spectroscopy. *Magnetic Resonance in Chemistry*, **40** (13): S72-82.
Singh, N. C.; Dasgupta, T. P.; Roberts, E. V. and Mansingh, A., (1991). Dynamics of pesticides in tropical conditions. Kinetic studies of volatilization, hydrolysis and photolysis of dieldrin, and α- and β-endosulfan. *Journal of Agricultural and Food Chemistry*, **39** (3): 575-579.
SIS, (2009). ChemIDplus Advanced. http://chem.sis.nlm.nih.gov/chemidplus/chemidheavy.jsp
Smith, G., (2004). *Basic Chemical Thermodynamics*. Imperial College Press, London, UK.
Snyder, S. A.; Adham, S.; Redding, A. M.; Cannon, F. S.; DeCarolis, J.; Oppenheimer, J.; Wert, E. C. and Yoon, Y., (2007). Role of membranes and activated carbon in the removal of endocrine disruptors and pharmaceuticals. *Desalination*, **202** (1-3): 156-181.
Solvay S.A, http://www.solvay.com/.
Spyres, G.; Nimmo, M.; Worsfold, P. J.; Achterberg, E. P. and Miller, A. E. J., (2000). Determination of dissolved organic carbon in seawater using high temperature catalytic oxidation techniques *TrAC Trends in Analytical Chemistry*, **19** (8): 498-506.
Squire, D., (2000). Reverse osmosis concentrate disposal in the UK. *Desalination*, **132** (1-3): 47-54.
Strathmann, H., (2004). *Ion-exchange membrane separation processes*. Elsevier, Amsterdam, Netherlands.
Sumpter, J. P. and Johnson, A. C., (2005). Lessons from endocrine disruption and their application to other issues concerning trace organics in the aquatic environment. *Environmental Science and Technology*, **39** (12): 4321-4332.
Sutherland, T. D.; Horne, I.; Lacey, M. J.; Harcourt, R. L.; Russell, R. J. and Oakeshott, J. G., (2000). Enrichment of an Endosulfan-Degrading Mixed Bacterial Culture. *Applied and Environmental Microbiology*, **66** (7): 2822–2828.
Sybron Chemicals Inc, http://www.sybronchemicals.com/.
Syracuse Research Corporation, (2009). Interactive LogKow (KowWin) Demo. http://www.syrres.com/eSc/kowwin.htm
Szpyrkowicz, L.; Juzzolino, C. and Kaul, S. N., (2001). A Comparative study on oxidation of disperse dyes by electrochemical process, ozone, hypochlorite and fenton reagent. *Water Research*, **35** (9): 2129-2136.
Takahashi, H.; Ohba, K. and Kikuchi, K. I., (2003). Sorption of mono-carboyxylic acids by an anion-exchange membrane. *Biochemical Engineering Journal*, **16** (3): 311-315.
Tamer, N.; Köroğlu, B. K.; Arslan, C.; Akdoğan, M.; Köroğlu, M.; Çam, H. and Yildiz, M., (2007). Osteosclerosis due to endemic fluorosis. *Science of the Total Environment*, **373** (1): 43-48.

Tanaka, S.; Nakata, Y.; Kuramitz, H. and Kawasaki, M., (1999). Electrochemical Decomposition of Bisphenol A and Nonylphenol Using a Pt/Ti Electrode. *Chemistry Letters*, **28** (9): 943-944.

Tanaka, S.; Ehara, R.; Itoi, S. and Goto, T., (2003). Ion-exchange membrane electrodialytic salt production using brine discharged from a reverse osmosis seawater desalination plant. *Journal of Membrane Science*, **222** (1-2): 71-86.

Tanaka, Y., (2003). Mass transport and energy consumption in ion-exchange membrane electrodialysis of seawater. *Journal of Membrane Science*, **215** (1-2): 265-279.

Tanaka, Y., (2004). Concentration polarization in ion-exchange membrane electrodialysis. The events arising in an unforced flowing solution in a desalting cell. *Journal of Membrane Science*, **244** (1-2): 1-16.

Tanaka, Y., (2005). Limiting current densitynext term of an ion-exchange membrane and of an electrodialyzer. *Journal of Membrane Science*, **266** (1-2): 6-17.

Tang, C. Y.; Kwon, Y. N. and Leckie, J. O., (2007). Characterization of humic acid fouled reverse osmosis and nanofiltration membranes by transmission electron microscopy and streaming potential measurements. *Environmental Science and Technology*, **41** (3): 942-949.

Tansel, B.; Sager, J.; Rector, T.; Garland, J.; Strayer, R. F.; Levine, L.; Roberts, M.; Hummerick, M. and Bauer, J., (2006). Significance of hydrated radius and hydration shells on ionic permeability during nanofiltration in dead end cross flow modes. *Separation and Purification Technology*, **51** (1): 40-47.

Ternes, T. A., (2001). Analytical methods for the determination of pharmaceuticals in aqueous environmental samples. *Trends in Analytical Chemistry*, **20** (8): 419-434.

Ternes, T. A.; Stumpf, M. and Mueller, J., (1999a). Behavior and occurrence of estrogens in municipal sewage treatment plants - II. Aerobic batch experiments with activated sludge. *Science of the Total Environment*, **225** (1-2): 91-99.

Ternes, T. A.; Stumpf, M.; Mueller, J.; Haberer, K.; Wilken, R. D. and Servos, M., (1999b). Behavior and occurrence of estrogens in municipal sewage treatment plants - I. Investigations in Germany, Canada and Brazil. *Science of the Total Environment*, **225** (1-2): 81-90.

Thayalakumaran, T.; Bristow, K. L.; Charlesworth, P. B. and Fass, T., (2008). Geochemical conditions in groundwater systems: Implications for the attenuation of agricultural nitrate. *Agricultural Water Management*, **95** (2): 103-115.

Thorpe, K. L.; Hutchinson, T. H.; Hetheridge, M. J.; Scholze, M.; Sumpter, J. P. and Tyler, C. R., (2001). Assessing the biological potency of binary mixtures of environmental estrogens using vitellogenin induction in juvenile rainbow trout (Oncorhynchus mykiss). *Environmental Science and Technology*, **35** 2476-2481.

Thorpe, K. L.; Cumming, R. I.; Hutchinson, T. H.; Scholze, M.; Sumpter, J. P. and Tyler, C. R., (2003). Relative potencies and combination effects of steroidal estrogens in fish. *Environmental Science and Technology*, **37** (6): 1142-1149.

Tinggi, U., (2003). Essentiality and toxicity of selenium and its status in Australia: a review. *Toxicology Letters*, **137** (1-2): 103-110.

Tipping, E., (2002). *Cation Binding by Humic Substances*. Cambridge University Press, Cambridge, UK.

Topp, E. and Smith, W., (1992). Sorption of the herbicides atrazine and metolachlor to selected plastics and silicone rubber *Journal of Environmental Quality*, **21** (3): 316-317.

Turek, M. and Dydo, P., (2003). Electrodialysis reversal of calcium sulphate and calcium carbonate supersaturated solution. *Desalination*, **158** (1-3): 91-94.

Turek, M.; Dydo, P.; Ciba, J.; Trojanowska, J. and Kluczka, J. P.-K., B., (2005). Electrodialytic treatment of boron-containing wastewater with univalent permselective membranes. *Desalination*, **185** (1-3): 139-145.

Turek, M.; Dydo, P.; Trojanowska, J. and Bandura, B., (2007a). Electrodialytic treatment of boron-containing wastewater. *Desalination*, **205** (1-3): 185-191.

Turek, M.; Dydo, P. and Was, J., (2007b). High efficiency electrodialysis reversal of concentrated calcium sulfate and calcium carbonate solutions. *Desalination*, **205** (1-3): 62-66.

Turek, M. and Dydo, P., (2008). Comprehensive utilization of brackish water in ED-thermal system. *Desalination*, **221** (1-3): 455-461.

Urase, T. and Kikuta, T., (2005). Separate estimation of adsorption and degradation of pharmaceutical substances and estrogens in the activated sludge process. *Water Research*, **39** (7): 1289-1300.

Van der Bruggen, B.; Schaep, J.; Maes, W.; Wilms, D. and Vandecasteele, C., (1998). Nanofiltration as a treatment method for the removal of pesticides from ground waters. *Desalination*, **117** (1-3): 139-147.

Van der Bruggen, B.; Everaert, K.; Wilms, W. and Vandecasteele, C., (2001). Application of nanofiltration for removal of pesticides, nitrate and hardness from ground water: rejection properties and economic evaluation. *Journal of Membrane Science*, **193** (2): 239-248.

Van der Bruggen, B.; Koninckx, A. and Vandecasteele, C., (2004). Separation of monovalent and divalent ions from aqueous solution by electrodialysis and nanofiltration. *Water Research*, **38** (5): 1347-1353.

Verliefde, A.; Cornelissen, E.; Amy, G.; Van der Bruggen, B. and van Dijk, H., (2007). Priority organic micropollutants in water sources in Flanders and the Netherlands and assessment of removal possibilities with nanofiltration. *Environmental Pollution*, **146** (1): 281-289.

Veza, J. M., (2001). Desalination in the Canary Islands: an update. *Desalination*, **133** (3): 259-270.

Voice, T. C. and Weber Jr, W. J., (1985). Sorbent concentration effects in liquid/solid partitioning. *Environmental Science and Technology*, **19** (9): 789-796.

Volkov, A. G.; Paula, S. and Deamer, D. W., (1997). Two mechanisms of permeation of small neutral molecules and hydrated ions across phospholipid bilayers. *Bioelectrochemistry and Bioenergetics*, **42** (2): 153-160.

Vuik, J.; van der Poll, J. M.; Vink, R. and de Vos, R. H., (1990). Adsorption experiments of etridiazole and oxamyl on polyethylene sheets and poly(vinyl chloride) tubing used in horticulture. *Journal of Agricultural and Food Chemistry*, **38** (1): 328-330.

Walse, S. S.; Shimizu, K. D. and Ferry, J. L., (2002). Surface-catalyzed transformations of aqueous endosulfan. *Environmental Science and Technology*, **36** (22): 4846-4853.

Walse, S. S.; Scott, G. I. and Ferry, J. L., (2003). Stereoselective degradation of

aqueous endosulfan in modular estuarine mesocosms: formation of endosulfan γ-hydroxycarboxylate. *Journal of Environmental Monitoring*, **5** (3): 373-3797.

Wang, G. S. and Hsieh, S. T., (2001). Monitoring natural organic matter in water with scanning spectrophotometer. *Environment International*, **26** (4): 205-212.

Wentworth, W. E. and Chen, E. C. M., (1981). Theory of electron capture, In: Zlatkis, A. and Poole, C. F., (Eds), *Electron Capture: Theory and Practice in Chromatography*, Elsevier, New York, USA.

Wenzel, A.; Müller, J. and Ternes, T. A., (2000). *Study on endocrine disruptors in drinking water*, Fraunhofer Institute for Molecular Biology and Applied Ecology (IME), ESWE Institute for Water Research and Water Technology, Schmallenberg and Wiesbaden, Germany.

Werner, M. and Schäfer, A. I., (2007). Social aspects of a solar-powered desalination unit for remote Australian communities. *Desalination*, **203** (1-3): 375-393.

WHO, (2003). *Endosulfan in drinking-water. Background document for preparation of WHO Guidelines for drinking-water quality*, World Health Organization, Geneva, Switzerland.

WHO, (2006). *Guidelines for Drinking Water Quality*, World Health Organization, Geneva, Switzerland.

WHO, (2009). *Calcium and Magnesium in Drinking-water: Public health significance*. World Health Organization, Geneva, Switzerland.

Williams, M. E.; Hestekin, J. A.; Smothers, C. N. and Bhattacharyya, D., (1999). Separation of organic pollutants by reverse osmosis and nanofiltration membranes: mathematical models and experimental verification. *Industrial and Engineering Chemistry Research*, **38** (10): 3683-3695.

Williams, R. J.; Johnson, A. C.; Smith, J. J. L. and Kanda, R., (2003). Steroid estrogens profiles along river stretches arising from sewage treatment works discharges. *Environmental Science and Technology*, **37** (9): 1744-1750.

Williamson, R.; Klamut, J. and Hopkins, J., (2008). Surface water quality, In: Harter, T. and Rollins, L., (Eds), *Watersheds, groundwater and drinking water: A practical guide,* University of California Agriculture and Natural Resources, Oakland, USA.

Witorsch, R. J., (2002). Endocrine disruptors: Can biological effects and environmental risks be predicted? *Regulatory Toxicology and Pharmacology*, **36** (1): 118-130.

Xie, X.; Ellis, A.; Wang, Y.; Xie, Z.; Duan, M. and Su, C., (2009). Geochemistry of redox-sensitive elements and sulfur isotopes in the high arsenic groundwater system of Datong Basin, China. *Science of the Total Environment*, **407** (12): 3823-3835.

Xu, T., (2005). Ion exchange membranes: State of their development and perspective. *Journal of Membrane Science*, **263** (1-2): 1-29.

Yamamoto, H. and Liljestrand, H. M., (2003). The fate of estrogenic compounds in the aquatic environment: Sorption onto organic colloids. *Water Science and Technology*, **47** (9): 77-84.

Yan, W. L. and Bai, R., (2005). Adsorption of lead and humic acid on chitosan hydrogel beads. *Water Research*, **39** (4): 688-398.

Yazicigil, Z. and Oztekin, Y., (2006). Boron removal by electrodialysis with anion-exchange membranes. *Desalination*, **190** (1-3): 71-78.

Ying, G. G. and Kookana, R. S., (2003). Degradation of five selected endocrine-

disrupting chemicals in seawater and marine Sediment. *Environmental Science and Technology*, **37** (7): 1256-1260.

Yoon, Y.; Westerhoff, P.; Snyder, S. A. and Esparza, M., (2003). HPLC-fluorescence detection and adsorption of bisphenol A, 17β-estradiol, and 17α-ethynyl estradiol on powdered activated carbon. *Water Research*, **37** (14): 3530–3537.

Yoon, Y.; Westerhoff, P.; Yoon, J. and Snyder, S. A., (2004). Removal of 17□ estradiol and fluoranthene by nanofiltration and ultrafiltration. *Journal of Environmental Engineering* **130** (12): 1460-1467.

Yoon, Y.; Westerhoff, P.; Snyder, J. C. and Wert, E. C., (2006). Nanofiltration and ultrafiltration of endocrine disrupting compounds, pharmaceuticals and personal care products *Journal of Membrane Science*, **270** (1-2): 88-100.

You, S. J.; Yin, Y. and Allen, H. E., (1999). Partitioning of organic matter in soils: effects of pH and water/soil ratio. *Science of the Total Environment*, **227** (2-3): 155-160.

Zagorodni, A. A., (2006). *Ion Exchange Materials: Properties and Applications*. Elsevier, Amsterdam, Netherlands.

Zanoni, M. V. B.; Sene, J. J. and Anderson, M. A., (2003). Photoelectrocatalytic degradation of Remazol Brilliant Orange 3R on titanium dioxide thin-film electrodes *Journal of Photochemistry and Photobiology A: Chemistry*, **157** (1): 55-63.

Zeni, M.; Riveros, R.; Melo, K.; Primieri, R. and Lorenzini, S., (2005). Study on fluoride reduction in artesian well-water from electrodialysis process. *Desalination*, **185** (1-3): 241.

Zhang, W.; Wahlgren, M. and Sivik, B., (1989). Membrane characterization by the contact angle technique : II. Characterization of UF-membranes and comparison between the captive bubble and sessile drop as methods to obtain water contact angles. *Desalination*, **72** (3): 263-273.

Zhang, Y.; Van der Bruggen, B.; Pinoy, L. and Meesschaert, B., (2009). Separation of nutrient ions and organic compounds from salts in RO concentrates by standard and monovalent selective ion-exchange membranes used in electrodialysis. *Journal of Membrane Science*, **332** (1-2): 104-112.

Zhou, J.; Lu, X.; Wang, Y. and Shi, J., (2002). Molecular dynamics study on ionic hydration. *Fluid Phase Equilibria*, **194-197** (1): 257-270